Seismic Behaviour and Analysis of Continuous Reinforced Concrete Bridges

by

Payam Tehrani

Supervisor:

Professor Denis Mitchell

Department of Civil Engineering and Applied Mechanics,

McGill University

Montreal, Quebec, Canada

April 2012

A manuscript-based thesis submitted to McGill University in partial fulfillment of the requirements of the degree of Doctor of Philosophy

© Payam Tehrani, 2012

Abstract

This study focuses on the seismic analysis and behaviour of continuous 4-span bridges. Different methods of analyses including linear multi-mode analysis, inelastic time history analysis and incremental dynamic analysis (IDA) are used for the seismic evaluations of bridges in this study.

This thesis includes two main parts. In the first part the seismic behaviour of bridges with different column heights (i.e., irregularity due to different column stiffnesses) is studied. The seismic evaluations are carried out in the transverse and longitudinal directions of bridges to recognize the important aspects which influence the seismic behaviour. Parametric studies were carried out for a number of bridges in the transverse and the longitudinal directions. To perform a large number of designs and analyses, a computer program was developed to design the bridges, perform the modelling and extract and evaluate the analysis results. The effects of different column heights, different column diameters, different superstructure mass and stiffness, as well as different abutment conditions on the seismic response of bridges were studied using elastic and inelastic analyses. The results from the elastic and inelastic analyses were compared to demonstrate the limitations of the linear analyses for the seismic design and evaluation of irregular bridges. The effects of including nonlinear abutment models with different stiffness and strengths were also studied in the longitudinal response of the bridges. Seismic ductility demands and concentration of ductility demands were evaluated and the maximum demand to capacity ratios were predicted for a wide range of bridges studied.

The use of different regularity indices to predict the seismic response of bridges was also investigated.

In the second part of the thesis, the use of incremental dynamic analysis for seismic evaluation of bridges is studied. The influence of different record selection methodologies including the UHS-based, CMS-based and epsilon-based methods on the predictions of the IDA results is investigated. In addition, the effects of different earthquake types including crustal, subduction interface and subduction inslab earthquakes on the IDA results are studied.

Three large record sets were selected for three earthquake types and a fast algorithm was developed for the incremental dynamic analysis to evaluate the collapse capacity of different bridge configurations subjected to different earthquake types. The IDA results were also predicted for different subsets of records with specific characteristics. The effects of spectral shapes and epsilon values were also considered using seismic hazard deaggregation results.

Résumé

Cette étude se concentre sur l'analyse sismique et sur le comportement des ponts à 4 portées continues. Différentes méthodes d'analyse, telles que la méthode multimode linéaire, la méthode temporelle non linéaire et la méthode d'analyse dynamique incrémentale (ADI), sont utilisées pour l'évaluation sismique de ponts.

Cette thèse se divise en deux parties principales. Dans la première partie, le comportement sismique des ponts composés de colonnes de différentes hauteurs (c'est-à-dire, irrégularité causée par différentes raideurs de colonne) est étudié. Les évaluations sismiques sont réalisées dans les directions transversal et longitudinal des ponts afin de considérer les aspects importants qui influencent le comportement sismique. Des études paramétriques furent réalisées pour un certain nombre de ponts (c'est-à-dire 648 ponts dans la direction transversale et plus de 2500 cas dans la direction longitudinale). Afin d'effectuer un grand nombre de dimensionnements et d'analyses, un programme informatique fut développé pour dimensionner des ponts, effectuer la modélisation et extraire et évaluer les résultats d'analyse. Les effets de différentes hauteurs de colonne, de différents diamètres de colonne, de différentes masses et raideurs de la superstructure, et de différentes conditions de butée sur la réponse sismique des ponts furent étudiés en utilisant des analyses élastiques et inélastiques. Les résultats des analyses élastiques et inélastiques furent comparés afin de démontrer les limitations des analyses linéaires pour le dimensionnement et l'évaluation sismique des ponts irréguliers. Les effets sur la réponse longitudinale des ponts de modèles de butée non linéaires considérant différentes résistances et raideurs (incluant différentes longueurs d'espace de joint et différents nombres de piles) furent également étudiés. Les demandes sismiques en ductilité et la concentration des demandes en ductilité furent évaluées et la demande maximale des ratios en capacité fut prédite pour un large éventail de ponts étudiés. L'utilisation de différents indices de régularité pour prédire la réponse sismique des ponts fut aussi examinée.

Dans la seconde partie de la thèse, l'utilisation de l'ADI pour l'évaluation sismique des ponts est étudiée. L'influence de différentes méthodes de sélection d'enregistrement (incluant les méthodes basées sur l'aléa sismique, le spectre moyen conditionnel et

l’epsilon) sur les prédictions obtenues avec l’ADI est examinée. De plus, l’effet de considérer différents types de tremblement de terre (incluant des tremblements de terre de surface et de subduction) sur les résultats de l’ADI est étudié. Présentement, seulement les tremblements de terre de surface sont utilisés pour l’évaluation de la performance sismique des structures. Les procédures actuelles ne sont pas nécessairement appropriées pour les régions soumises à des tremblements de terre de subduction. Trois ensembles d’enregistrement furent sélectionnés pour trois types de tremblement de terre (c’est-à-dire un total de 3 x 78 = 234 enregistrements). Un algorithme à calcul rapide fut développé pour l’ADI afin d’évaluer la capacité à l’effondrement de différentes configurations de pont soumises à différents types de tremblement de terre. Les résultats de l’ADI furent également prédits pour différents sous-ensembles d’enregistrements ayant des caractéristiques spécifiques (c’est-à-dire des valeurs d’epsilon positives, des faibles facteurs d’échelle, etc.). Les effets des spectres de réponse et des valeurs d’epsilon furent aussi considérés en utilisant les résultats de désagrégation du risque sismique.

Preface

I would like to express my deep and sincere gratitude to my supervisor, Professor Denis Mitchell, for his guidance and patience during my PhD study and for providing me with freedom on my research. His nice personality and his friendly and inspiring treatment during my study are greatly appreciated.

The financial support provided by the Natural Sciences and Engineering Research Council of Canada (NSERC) for the Canadian Seismic Research Network is gratefully acknowledged. The International Doctoral Award (MIDAs) provided by the McGill University is also appreciated.

I would like to thank Dr. William Cook for installing the computer equipments and the remote control connections which expedited performing the large volume of the computer analyses in this research.

I also thank Dr. Alejandro de la Puente for providing his program “Ruaumoko helper” which inspired the development of the computer programs in this research.

I would like to also thank the anonymous reviewers of the manuscripts for their comments which helped the improvement the papers.

I would like to thank the European Laboratory for Structural Assessment (ELSA) for providing the test data which was used to validate the numerical models, as presented in Appendix A of this thesis.

I would like to thank the following professors/scholars for their responses to my short questions on different subjects, through emails, and/or for providing me with the requested papers and references: Jack Baker, Matej Fischinger, Nigel Priestley, Athol

Carr, Dimitrios Vamvatsikos, Yuk Hon Chai, Amr Elnashai, Kazuhiko Kawashima, Kent A. Fogleman , Saiid Saiidi and Murat Saatcioglu.

I also thank the entire Staff of the Department of Civil Engineering and Applied Mechanics, who helped solving those little problems that students have.

I would like to thank my friends Ali Ghafari Oskoei and Hossein Azimi who helped me the most during my first days in Canada and also thank all of my office colleagues and friends, especially Hamed Layssi and Farshad Habibi for making my Ph.D. study an enjoyable experience. I also thank my friend Iman Ghorbani for the mutual scientific discussions we had together.

Last, but certainly not least, I would like to express my special gratitude to my family in Iran, especially my beloved spouse Solmaz and my parents for their endless patience, love, encouragement and support during my studies.

“Contributions of Authors”

I would like to express my sincere thanks to Prof. Katsu Goda for providing the raw seismic hazard data for Vancouver and Montreal and information for the Japanese earthquakes which was used in this research (in Chapters 5 and 6). His support on the seismological subjects are also gratefully acknowledged. I would like to also thank Prof. Gail Atkinson and Prof. Luc Chouinard for reviewing the manuscript in Chapter 5 and providing me with constructive comments.

Dedicated to my parents, dear Hossein and Shohreh, to my wife, Solmaz and to my brothers, Pouya and Peyman.

Table of Contents

List of Tables

List of Figures

1 Introduction and Literature Review

1.1 Introduction

Earthquake-resistant bridges should be designed to have regular configurations where possible to ensure that the seismic behaviour is simple and predictable and above all, inelastic energy dissipation is distributed almost uniformly in yielding components such as columns. In regular structures the seismic demand does not tend to concentrate in a few elements and all of the columns and/or fuse elements contribute to the seismic response of the structure. However this ideal situation is often not achievable in bridge construction due to irregularities imposed by site topography and required bridge geometry (e.g., ramps).

It is recognised that in practice, bridges with certain configurations are more vulnerable to earthquakes than others. Experience indicates that a bridge is most likely to be vulnerable if (1) excessive deformation demands occur in a few brittle elements, (2) the structural configuration is complex, or (3) a bridge lacks redundancy (Chen and Duan, 2000).

A common form of irregularity arises when a bridge traverses a basin or a valley requiring columns with different lengths. Bridges with different column lengths can have undesirable seismic behaviour in earthquake events. Stiffness irregularities in this type of bridges results in considerable concentration of seismic forces in the shorter columns which are usually the stiffer parts of the lateral resisting system. As a result very high shear and moment forces arise in these columns.

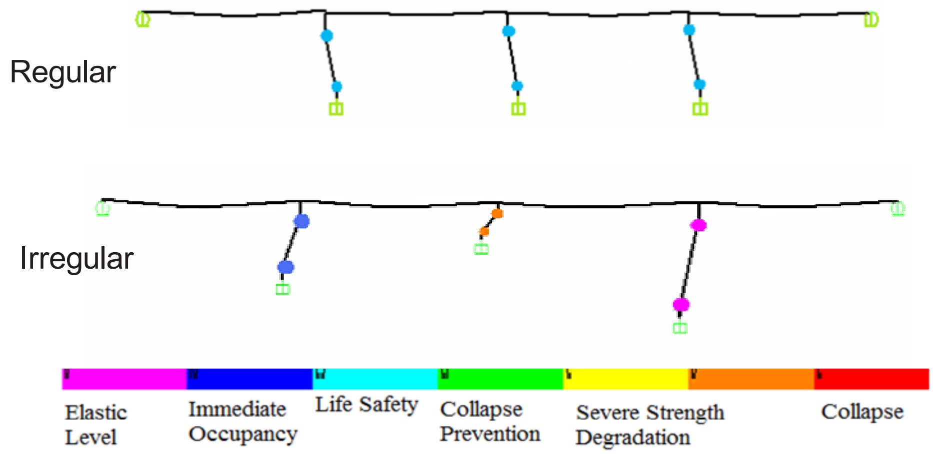

Fig. 1.1.An example of the concentration of the ductility demands in the stiffest column (bridge at the bottom). The results obtained using a pushover analysis in SAP2000. The columns in the regular bridge (bridge at the top) have uniform ductility demands.

Although the response of the superstructure in such irregular bridges may be relatively uniform, the deformation demands on the individual substructure piers can be highly irregular; with the largest strains imposed on the shortest columns. In some cases, the deformation demands on the stiffer columns can induce their failure before longer, more flexible columns can fully participate (e.g., Fig.1.1). The effects identified above can be exacerbated in long-span bridges due to spatial and temporal variations in the ground motions and out of phase displacements of the adjacent frames with different dynamic characteristics which induce large relative displacements between adjacent bridge columns (Chen and Duan, 2000).

Another problem arises in analysis of these irregular bridges where the sequential yielding of ductile members may result in substantial deviations of the results from linear analyses performed with the assumption of a global force reduction factor R from those of the nonlinear response of the bridge structure. This problem is due to the fact that the plastic hinges which appear first usually develop the maximum inelastic strains, which may lead to concentration of unacceptably high ductility demands in these hinges. Furthermore, following the formation of the first plastic hinges (normally in the stiffer members) the distribution of stiffness and hence of forces may change from that predicted by the equivalent linear analysis. This may lead to a substantial change in the assumed pattern of plastic hinges (CEN, 2005). One may try to solve the problem by reducing the value of the force modification factor, R, in which case it is certainly possible to reduce the ductility demand in the stiffer piers, but the resulting overall design may be very costly. Differentiated behavioural factors could then be proposed as a function of bridge geometry (Calvi et al., 1994).

To improve the seismic performance of the bridges with varying column length several methods such as the use of foundation sleeves for piers with appropriate depths to equalize the effective length and stiffness of the columns (Priestly et al., 1996) , the use of isolation devices (such as elastomeric and sliding bearings) with appropriate stiffness to adjust the stiffness distribution and to improve the damping level (Calvi and Pavese,1997) and the use of in-span hinges and abutments with sacrificial shear keys (Saiidi et al. , 2001) can be beneficial.

In the past, earthquake damage to these types of bridges (e.g., failure of the shorter columns), has been reported (Mitchell et al., 1995; Broderick and Elnashai, 1995 and Chen and Duan, 2000). Due to the vulnerability of irregular bridges and lack of research on this subject, research is needed to investigate the seismic behaviour and methods of analysis of bridges with varying column stiffnesses.

The application of incremental dynamic analysis (IDA) for bridge structures is another important issue which will be studied in this research. The use of different record selection methodologies in IDA for the seismic evaluation of bridge structures is an important issue which will be studied. In addition, the influence of considering different earthquake types on the seismic evaluation of bridge structures using IDA is also studied. Currently very limited research is available on these subjects which clearly require more attention. More details and background information regarding incremental dynamic analysis and different record selection methods are provided in Chapter 2. More details and background information regarding different earthquake types are available in Appendix F.

1.2 Research objectives

The main objectives of this research are:

- To study the effects of different column heights and column stiffnesses on the seismic response, and safety of bridges designed according to the 2006 Canadian Highway Bridge Design Code provisions.

- To investigate the use of the elastic multi-mode method for the seismic analysis of the irregular bridges with different column and superstructure stiffnesses.

- To evaluate the effects of different abutment conditions and abutment modeling on the seismic response of bridges.

- To evaluate the seismic performance of bridges using Incremental Dynamic Analysis (IDA) considering the spectral shapes and epsilon effects.

- To investigate the effects of using different record selection methodologies on the seismic assessment of the bridges using IDA.

- To compare the effects of including different earthquake types (i.e., subduction interface and inslab earthquakes) on the seismic performance assessment of bridges.

1.3 Thesis organization

This thesis is organized in seven chapters:

Chapter 1: “Introduction and literature review” presents an introduction to the problems associated with irregular bridges with different column stiffnesses as well as an outline of the thesis and a literature review of the previous studies concerning irregular bridges.

Chapter 2: provides background information and a literature review of the use of incremental dynamic analysis (IDA) for seismic evaluation of structures, the use of different record selection methods in IDA, different methods for prediction of the capacity at different damage states, the development of fragility curves and seismic risk assessment using IDA results. Chapter 2 has been summarized into a book chapter : Tehrani, P. and Mitchell, D. “Incremental Dynamic Analysis Applied to Seismic Performance and Risk Assessment of RC Bridges” in the publication “Seismic Risk Analysis and Management of Civil Infrastructure Systems, Edited by Tesfamariam, S. (UBC, Canada) and Goda, K. (Bristol, UK), Woodhead Publishing Limited, submitted in March 2012.

Chapter 3 : This chapter includes the paper: Tehrani, P. and Mitchell, D. “Effects of Column and Superstructure Stiffness on the Seismic Response of Bridges in the Transverse Direction”, accepted for publication in the Canadian Journal of Civil Engineering, Manuscript 2011-0516, This chapter presents the study of the transverse seismic response of bridges with column stiffness irregularity. The important parameters affecting the seismic behaviour of bridges in this direction, including column stiffnesses, abutment conditions and super structure stiffness have been studied. The use of different regularity indices to determine the irregularity of bridges has been also studied.

Chapter 4: This chapter includes the paper: Tehrani, P. and Mitchell, D. ”Effects of Column Stiffness Irregularity on the Seismic Response of Bridges in the Longitudinal Direction”, submitted in March, 2012 to the Canadian Journal of Civil Engineering (Manuscript 2012-0091),. This chapter presents the study of the seismic response of bridges with column stiffness irregularity in the longitudinal direction. The effects of abutment conditions on the seismic response of bridges are also presented in this chapter.

Chapter 5: This chapter includes the paper: Tehrani, P., Goda, K., Mitchell, D., Atkinson, G.M. and Chouinard, L.E. "Effects of Different Record Selection Methods and Earthquake Types on the Transverse Response of Bridges", submitted in December 2011 to the Journal of Earthquake Engineering and Structural Dynamics (Manuscript EQE-11-0079, revised version),. This chapter presents the use of incremental dynamic analyses for the seismic assessment of bridges. The effects of using different record selection methods and different earthquake types on the IDA results are studied.

Chapter 6: This chapter includes the paper: Tehrani, P. and Mitchell, D."Seismic Response of Bridges Subjected to Different Earthquake Types using IDA", submitted in January 2012 to the Journal of Earthquake Engineering (Manuscript UEQE-2012-1345). In this chapter the incremental dynamic analysis has been used to evaluate the seismic response of different bridge configuration using a large set of records including 234 ground motion records from three different earthquake types. The effects of including different earthquake types and using different subsets of records in the seismic assessments of bridges are studied.

Chapter 7: "Conclusions" summarizes the main conclusions from this study and provides some recommendations for future studies.

Appendices:

Appendix A: provides more details regarding structural modelling, the validation of computer models and preliminary results.

Appendix B: provides details regarding the computer program developed for design and modelling of the bridges and extracting and processing the analyses results.

Appendix C: provides more information regarding the seismic hazard deaggregation and presents more details regarding the computer program developed to compute the seismic deaggregation results from the seismic hazard data. The seismic deaggregation results for

Vancouver are also given in some tables for different deaggregation methods and different ground motion prediction equations.

Appendix D: provides more details regarding the computer program developed for record selection and prediction of the conditional mean spectrum (CMS).

Appendix E: provides information regarding a program developed to monitor the details of the analysis results from RUAUMOKO program.

Appendix F: provides more information regarding the subduction (i.e., interface and inslab) earthquakes.

Appendix G: provides the list and detailed information regarding the ground motion records selected for different earthquake types in Chapter 6.

Appendix H: provides a pushover analysis of the bridge studied in Chapter 5.

Appendix I: provides some analysis results for some bridges studied in Chapter 5 and 6.

1.4 Background and literature review

1.4.1 Bridges with column stiffness irregularity

Existing research on bridges with different column stiffnesses is limited, particularly in North America, and most of the available studies have been carried out in Europe based on the Eurocode provisions which are different from the North America provisions.

The first attempt in this regard was made by Calvi et al., (1994) and Calvi and Pinto (1996). A simple, multi-degree-of-freedom, nonlinear dynamic model was used, after some verification of the reliability of the results in comparison with more refined simulations. The pier reinforcement was designed according to EC8/2, with some modifications of the minimum longitudinal reinforcement percentage (assumed as low as 0.25% as commonly adopted for standard structural design rather than 1 %). The maximum concrete compressive strain was assumed equal to 0.6%, with a parabolic/constant stress-strain curve; the steel stress-strain curve was assumed bilinear, with no maximum elongation capacity. The model used in the parametric simulations assumes that each pier is hinged at the top and fixed at the base, with a bilinear global force-displacement curve, resulting from a plastic hinge lumped at the base. The numerical analyses indicated that the EC8/2 design approach may result in lower than expected safety levels, or higher than expected ductility demands, when stiff piers are coupled with flexible piers.

A first attempt to define a “parameter of regularity”, was made in this study which is a measure of the difference between the mode shape of the whole bridge and of the deck alone. The regularity parameter is expressed in Eq. 1.1.

[1.1] $$R_1 = \sqrt{\frac{\sum_{j=1}^{n} (\Phi_i^B M \Phi_j^D)^2}{n}}$$

$$[1.2] \qquad R_2 = 1 - \frac{\sum_{i=1}^{n}\sum_{j=1}^{n}[(1-\delta_{ij})\left|\Phi_i^B\, M\, \Phi_j^D\right|]}{n}$$

A new index, R_2 (given in Eq. 1.2), was then proposed by subtracting the norm of the products of the off-diagonal terms to increase the sensitivity of the index. Where in Eqs. 1.1 and 1.2, Φ_i^B , Φ_j^D and M are the modal shapes of the bridge and the modal shapes and the mass matrix of the deck alone, respectively. A summary of different indices of regularity are given by Maalek et al. (2009):

1- Use of Modal Assurance Criterion-MAC (Ewins, 2000):

$$[1.3a] \qquad MAC_i(D,B) = \frac{\left|\left\{\Phi_i^D\right\}^T\left\{\Phi_i^B\right\}\right|^2}{\left(\left\{\Phi_i^D\right\}^T\left\{\Phi_i^D\right\}\right)\left(\left\{\Phi_i^B\right\}^T\left\{\Phi_i^B\right\}\right)}$$

$$[1.3b] \qquad MAC(D,B,n) = \sqrt{\frac{\sum_{i=1}^{n}(MAC_i(D,B))^2}{n}}$$

2- Use of Modal Scale Factor-MSF (Ewins, 2000):

$$[1.4a] \qquad MSF_i = \frac{\left|\left\{\Phi^D\right\}^T\left\{\Phi^B\right\}\right|_i}{\left(\left\{\Phi^D\right\}^T\left\{\Phi^D\right\}\right)_i}$$

$$[1.4b] \qquad MSF(D,B,n) = \sqrt{\frac{\sum_{i=1}^{n}(MSF_i(D,B))^2}{n}}$$

3-Difference Ratio of Mode Shapes-DRMS (Fischinger and Isakovic, 2003; Mackie and Stojadinovic, 2003 and Maalek et al., 2009):

$$[1.5a] \qquad DRMS_i(D,B) = \frac{\left|\Phi^D - \Phi^B\right|}{\left|\Phi^D\right|} = \frac{\sum\left|d^D - d^B\right|}{\sum\left|d_i^D\right|} = \frac{\left|S_D - S_B\right|}{\left|S_D\right|}$$

$$DRMS(D,B,n)=\sqrt{\frac{\sum_{i=1}^{n}(DRMS_i(D,B))^2}{n}} \quad [1.5b]$$

To improve the seismic performance of irregular bridges some design approaches for the use of isolation systems have been proposed namely the "*equal (minimum) strength approach"* and the *"maximum strength approach"* (Calvi and Pavese, 1997). In the equal strength design approach the design will be based on the strength of the weakest column, while in the maximum strength method different strength and stiffness will be assigned to isolation systems considering the strength of each column and based on the maximisation of a proposed regularity index given in Eq. [1.6a]. To account for the strengths of the piers in the index, a more efficient (but complex) regularity index was proposed which was based on the measure of the difference between a vector containing the product of modal mass and spectral amplification and a vector containing the coefficients producing the target deformed shape.

$$R_3=1-\frac{1}{2}\left(\frac{\sqrt{\sum_{i=1}^{m}(y_i-z_i)^2}}{\sqrt{\sum_{i=1}^{m}(y_i)^2}+\sqrt{\sum_{i=1}^{m}(z_i)^2}}+\frac{\sqrt{\sum_{i=1}^{n}(V_i-k_{ei}\Delta_{ei})^2}}{\sqrt{\sum_{j=1}^{n}V_j^2}}\right) \quad [1.6a]$$

$$y_i=\frac{\Phi_i^T M\nu}{\Phi_i^T M\Phi_i} \quad [1.6b]$$

$$\nu=\sum_{i=1}^{m}y_i\Phi_i \quad [1.6c]$$

Where $z_i=\beta_i S_{di}$, β_i are the modal participating factors, ν is the vector of the imposed displacements, Φ_i are the eigenvectors of the whole bridge, and S_{di} are the spectral displacements, V_i are the yield strengths of the piers (or of the isolators, if present, i.e., 85% of the critical strength of the, corresponding pier), k_{ei} are the elastic stiffness of the isolators and Δ_{ei} are the yielding displacements of the isolators.

Four reinforced concrete bridge models (1:2.5 scale) have been tested in the European Laboratory for Structural Assessment (ELSA) using the pseudo-dynamic test method (Pinto et al., 1996). Two bridge configurations were considered including a regular (bridge B232) and another irregular bridge which included three alternative design solutions (bridges B213A, B213B and B213C). In the case (B213B), the reinforcement percentage of the shortest pier was increased (from 0.92% to 1.69%), with the aim to reduce the high ductility demand which was anticipated in the analysis. In the other case (B213C), the strength of the taller piers was increased (from 0.50% to 1.15%), so that the forces attracted by the shortest pier can, in principle, be reduced.

Results showed that the absorbed energy in the regular bridge was almost equally shared between the three piers while in the irregular bridge it was concentrated in the short middle pier, which dissipated more than 70% of the total energy. Furthermore, safety against collapse of the irregular bridges was quite low compared to the safety of the regular bridge. In fact, despite the comparable demands obtained for the design earthquake, the regular bridge was able to withstand twice the design loads without loss of capacity and with a homogenous damage pattern. On the other hand, the irregular bridges, tested with an input signal 1.2 times the design earthquake, suffered quite important damage concentrated in the short central pier. Therefore a minor variation in the peak ground acceleration may result in significant damage or high probability of failure.

A comparison between the test results obtained for the three irregular bridges confirmed that the strategy adopted for the design of the bridge B213B, which corresponds to the use of a lower modification factor, results in performance that is not as bad as the other bridges and may lead to a suitable design approach for these bridges with larger amounts of longitudinal reinforcement in the short column. The short pier of bridge B213C, containing less reinforced pier showed essentially flexural cracking while the pier from bridge B213B had inclined shear cracking.

1.4.2 Modal pushover analysis (MPA)

Elastic analysis cannot predict the failure mechanisms or the redistribution of forces that follow plastic hinge development, while pushover analysis identifies the locations of structural inelasticity and failure mechanisms. Nonlinear static (pushover) analysis is a popular tool for the seismic assessment of buildings. Although it is simpler compared to nonlinear dynamic time-history analysis, its application is restricted to structures wherein the response is governed by a single mode. To eliminate this limitation, pushover analyses to consider higher modes effects have recently been developed for the case of building structures. However little research has been focused on bridges in which the higher modes effects are even more pronounced in the seismic response of the structure.

In an early work (Sasaki et al., 1998), the multi-mode pushover procedure was used to identify the effects of higher modes in pushover analysis of buildings and separate pushover curves were derived for each significant mode, however no attempt was made to combine modal responses. In addition to MPA ,as another improved pushover method, ‘adaptive’ multi-mode pushover analysis method was developed (Bracci et al., 1997; Gupta and Kunnath ,2000 and Antoniou et al., 2002) involving updating the loading pattern, according to the current displaced shape of the structure at each step, which is determined by modal combination rules at each stage of the response.

Modal pushover analysis (MPA), proposed by Chopra and Goel (2002), and subsequently improved by them (Chopra and Goel, 2004), is a method in which the pushover analyses are carried out separately for each significant mode, and the modal components (displacements, drifts, etc.) are combined using an appropriate combination rule. Considering inelastic time history analysis (ITHA) as a benchmark, errors in MPA are typically smaller than in the case of superposition at the level of loading (with fixed loading pattern), as recommended in the FEMA356 Guidelines, for example (FEMA 356, 2000).

Modal pushover analysis has been extended for application to bridge structures (Kappos et al., 2004; Fischinger et al., 2004; Pinho et al., 2005; Paraskeva et al., 2006; Isakovic and Fischinger, 2006 and Isakovic et al., 2008). On the basis of the results obtained for the long curved irregular bridge studied by Paraskeva et al. (2006), MPA seems to be a promising approach that yields more accurate results compared to the 'standard' pushover analysis, without requiring the higher modelling effort and computational cost, as well as the other problems involved in ITHA and above all this method, unlike the adaptive analyses, can be easily implemented using available standard software tools. Some common computer programs such as SAP2000 are capable of performing modal pushover analysis. The application of this method in bridge codes is then expected in the near future after further confirmation of this method for a wide range of bridge structures. It is thus concluded that more research is required, to further investigate the application of the MPA to bridge structures with different configurations, degree of irregularity, and dynamic characteristics (e.g., in terms of higher mode significance), since MPA is expected to be even more valuable for the assessment of the seismic behaviour of bridges with contribution of higher modes (Paraskeva et al., 2006).

1.4.3 Analysis of bridges with different column stiffnesses

The use of different elastic and inelastic analysis methods such as single mode (SM), multi mode (MM) and inelastic time history analysis (ITHA) to predict the response of regular and irregular bridges were investigated by Fischinger et al., (1997) on a few four-span viaducts with different abutment conditions. The results indicated that the elastic single mode procedure completely failed to identify the critical elements of many of the viaducts that were analyzed and sometimes yielded qualitatively different results than the MM and time history analyses. In addition, elastic analysis failed completely to predict the displacement shape of some of the analyzed irregular viaducts. It was also concluded that the results were sensitive to the ratio of torsional to translational stiffness r_k = (K_t / K_y), where K_t and K_y are defined in Eqs. [1.7a] and [1.7b], respectively. The strength of the columns was another important factor affecting the results.

[1.7a] $K_t = (\sum K_{ci} x_i) / r^2$

[1.7b] $K_y = \sum K_{ci}$

where K_{ci}, x_i and r are the flexural stiffness of pier i, the distance of pier i from the centre of mass and the radius of inertia respectively. K_t is a measure of the sensitivity of the structure to rotations in the horizontal plane. The influence of higher modes was not important in the case of a symmetric viaduct or when the ratio of the maximum column stiffness to the deck stiffness, r_k, was less than approximately 15. The complex behaviour with important contribution of several response modes was typical in the situations when the deck is relatively flexible in the transverse direction in comparison with piers, the ratio of the quasi-torsional to translational stiffness of the structure is small, the supports at the abutments are free in the transverse direction and the end cantilevers are long and the viaduct is asymmetric. In the case of free supports at the abutments, the results of the MM and SM methods differed even much more than in the case of pinned abutments.

Fischinger and Isakovic (2003) have proposed an irregularity index as a global numerical measure to help designers decide about the suitability of the single-mode pushover analysis for bridges. This index represents relative differences between the areas bounded by the normalized displacement lines of the first and second iteration of the single-mode pushover method. For the first iteration a uniform load pattern is used to perform the pushover analysis. The resulting displaced pattern of the bridge from the first iteration will then be used as a new load pattern for the second iteration of pushover. It was roughly estimated that bridges with an irregularity index, IRI, less than 5% could be analysed with the simpler analysis procedures such as single-mode pushover method.

[1.8] $IRI = \dfrac{\sum |\phi_{i,1} - \phi_{i,2}| \Delta x_i}{\sum |\phi_{i,1}| \Delta x_i} .100 = \dfrac{\sum_{i=1}^{n-1} |\phi_{i,1} - \phi_{i,2}|}{\sum_{i=1}^{n-1} |\phi_{i,1}|} .100$

Where $\phi_{i,1}$ is the normalised displacements obtained within the first iteration of the pushover method, $\phi_{i,2}$ is the normalised displacements obtained within the second iteration of the pushover method and Δx_i is the distance between two points where displacements were calculated. A similar IRI has been also proposed by Mackie and Stojadinovic (2003) in which mode shapes of the bridge and the deck alone are used instead of the first and the second iteration of the pushover method, respectively.

Based on the results from the previous works on a few simple 4-span bridges, it can be found that the elastic analysis and simple pushover method should be used with care for the following cases (Fischinger and Isakovic, 2003):

a) Viaducts with great eccentricity, defined as a distance between the center of stiffness of the supporting elements and the center of mass.
b) Torsionally flexible viaducts (due to the abrupt changes in the dynamic properties of the bridge once the columns yield).
c) Viaducts with a relatively flexible deck in comparison with stiff and strong columns.
d) Viaducts with a very stiff central pier. This situation is more pronounced for viaducts with roller supports at the abutments. These effects depend also on the relative stiffness of the central columns in comparison with the deck.
e) For viaducts with very stiff and relatively strong end columns the influence of higher modes can be expected even if they are symmetric.

In a study by Isacovic and Fischinger (2006), the influence of the higher modes and their consideration in the pushover analysis of 6 four-span reinforced concrete single column bent viaducts was investigated. Typical multimode pushover-based methods (modal pushover analysis, modal adaptive non-linear static procedure and incremental response spectrum analysis) are addressed and compared with a single mode procedure and inelastic time history analysis for three types of viaducts including regular, slightly irregular, and highly irregular viaducts. Based on the results from this study in most cases, all the analysed multimode pushover-based methods have given results comparable with those obtained from time history analysis, with exception of the cases where the torsional sensitivity varied during the response.

According to this study, if the substructure is flexible in comparison with the superstructure in the transverse direction, the influence of the higher modes will be small. It was confirmed that the level of irregularity and contribution of the higher modes in the response are considerably influenced by the position of stiff columns (particularly when they are positioned close to the centre of the bridge), since certain configuration of stiff columns enlarge the torsional sensitivity of the viaduct. Thus, for the analysis of irregular bridges having short and slightly damaged columns, the multimode methods are needed. The results also showed that for the case of a lower ductility demand, the pushover procedures underestimate the response while in the region of higher ductility demand or at higher earthquake intensity, in which plastic hinges develop in all columns, they yield similar results as the ITHA.

The applicability of a typical single-mode pushover method and two typical multi-mode pushover methods (the modal pushover analysis (MPA) and incremental response spectrum analysis (IRSA) methods (Aydinoglu, 2004)) for the analysis of single column bent viaducts in the transverse direction was then studied considering some longer viaducts with more bents (Isacovic et al., 2008). According to the results the single-mode pushover method is accurate enough for bridges where the effective modal mass of the fundamental mode is at least 80% of the total mass. In the case of the moderately irregular long viaducts the MPA method performed well.

The results from a study by Pinho et al. (2007) indicate that the use of single-run pushover analysis might still be feasible even for irregular bridge configurations, provided that a displacement-based adaptive version of the method is employed.

Research by Kappos et al. (2002) on an irregular bridge showed that soil-structure interaction (SSI) had small effects on the response of the bridge and even smaller displacements and less reinforcement were obtained when soil-structure interaction (SSI) was considered in the models.

A comparison between the modelling using fibre cross-sections and beam elements in the analyses was carried out in some studies. Although the beam model with lumped plasticity was simple, it yielded results which were quite in good agreement with more detailed models (Calvi et al., 1994 and Fischinger and Isakovic, 2003).

A comparison of the results from elastic response spectra and inelastic time history analyses for an existing irregular bridge in a study by Jones et al., (2001) showed that the effects of velocity pulses, especially when the structure is located in sufficient proximity to faults to experience near-field effects from a fault rupture, can substantially change the bridge response. They also recommended that a drift limit may be a useful preliminary design tool, because when drifts exceeded certain limits then the results from the elastic and inelastic analyses were not consistent.

1.5 Code provisions

1.5.1 Caltrans (2006) and AASHTO Guidelines (2009)

The requirements in Caltrans (2006) and the AASHTO Guidelines (2009) compare the ductility demands with the ductility capacities in the energy dissipating members (displacement-based design) instead of using an overall modification factor for design (force-based design). Although the problem of different ductility demands of columns in irregular bridges can be better addressed using this method, the ductility demands which are based on the linear analysis methods such as response spectrum analysis (which is permitted for design of irregular bridges) usually underestimate the ductility demands in critical members and can lead to unsafe designs. Some conservative limitations are recommended in Caltrans and the AASHTO Guidelines for the ratio of the column stiffnesses in a frame or bent to balance the bent or pier stiffness along the bridge. For any two bents or any two columns within a bent this stiffness ratio is recommended be greater than 0.5. For adjacent bents or adjacent columns within a bent this ratio is recommended to be less than 0.75. Some of the consequences of not meeting these relative stiffness indicators include increased damage in the stiffer elements and an unbalanced distribution of inelastic response throughout the structure.

If project constraints make it impractical to satisfy the stiffness requirements, a careful evaluation of the local ductility demands and capacities shall be required for bridges in regions of high seismicity.

1.5.2 Eurocode

In the Eurocode (EN 1998-2, 2005) a force-based design approach is used for the design of bridges. The reduction factor, q (similar to the modification factor R), for reinforced concrete columns depends on the shear span to depth ratio and on whether the member is inclined or vertical. The q factor will then be modified in the cases of high axial loads and irregular seismic behaviour of the bridge. In this regard the local force reduction factor r_i associated with member i is defined as:

[1.9a] $$r_i = q\,(M_{Ed,i} / M_{Rd,i})$$

[1.9b] $$\rho = r_{max} / r_{min} \leq \rho_o$$

[1.9c] $$q_r = q\,(\rho_o / \rho) \geq 1.0$$

where $M_{Ed,i}$ and $M_{Rd,i}$ are the maximum values of design moment at the intended plastic hinge location of ductile member i from the seismic analysis and the design flexural resistance of the section with the actual reinforcement, respectively. The bridge is considered to have regular seismic behaviour when Eq. 1.9b is satisfied. Where r_{max} and r_{min} are the maximum and minimum values of r_i, respectively and ρ_o is a limit value selected so as to ensure that sequential yielding of the ductile members will not cause unacceptably high ductility demands on the member. The recommended value for ρ_o is 2.0. The force reduction factor is then reduced to q_r for the irregular seismic behaviour according to Eq. 1.9c. To capture the actual seismic behaviour of an irregular bridge where the ductility demands concentrate in a few elements and the distribution of the forces deviate from that predicted by the linear analysis, a combination of an equivalent linear analysis with a non-linear static analysis is recommended.

1.5.3 CSA-S6-06 and AASHTO-04

The seismic design provisions in the Canadian Highway Bridge Design Code (CHBDC) (CSA 2006) are based on the AASHTO Specifications (AASHTO 2004). S6 uses a force modification factor, R, and an importance factor, I, of 1.0, 1.5 and 3.0 for “other”, “emergency-route” and “lifeline” bridges, respectively. The AASHTO Specifications combine the force modification factor for “ductility” with the importance factor to give one force modification factor for “other”, “essential” and “critical” bridges. Nevertheless, the resulting design forces are similar. The CHBDC requires that the MM (multi-mode spectral method and also referred as response spectrum analysis in this paper) be used for the analysis of irregular bridges, even in seismic performance zone 4. However for irregular lifeline bridges, time-history analysis is required in zones 3 and 4. Concerning the column stiffness ratios for regular bridges, the 2004 AASHTO and the 2006 CHBDC specifications indicate that the maximum bent or pier stiffness ratio from span to span should not exceed 4.0 for bridges up to 4 spans, 3.0 for 5 spans and 2.0 for 6 span bridges. These stiffness limits are for bridges with a continuous superstructure or multiple simple spans with longitudinal restrainers and transverse restraint at each support or a continuous deck slab, otherwise this ratio shall not exceed 1.25.

The modification factors, R, are taken conservatively and lower than the expected displacement ductility capacities, since the procedure is intended to apply to a wide variety of bridge geometries. Where possible, pier stiffnesses should be adjusted to attempt to achieve uniform yield displacements and ductility demands on individual piers. In cases where attempts to “regularize” the structure are impractical, suitable analyses need to be developed to account for localized, rather than simultaneous, yielding of piers. In some cases, it may be possible to use “stiff” piers with energy dissipating bearings to alleviate the problem as discussed in the CHBDC Commentary (CSA, 2006).

1.5.4 Performance objectives for bridges

Based on the CHBDC provisions, bridges are classified into three importance categories including lifeline bridges, emergency-route bridges and other bridges.
Emergency-route bridges are generally those that carry or cross over routes that should, at a minimum, be open to emergency vehicles and for security/defence purposes immediately after the design earthquake (CHBDC, 2006).

The Seismic Subcommittee of the CHBDC has proposed the following performance criteria as presented in Table 1.1 for the next version of the CHBDC. According to Table 1 the emergency-route bridges should be repairable after the occurrence of an earthquake with 10% probability of exceedance in 50 years. However, all bridges should not collapse when subjected to earthquakes with 2% probability of exceedance in 50 years.

Table 1.1. Proposed seismic design performance criteria by the Seismic Subcommittee of the CHBDC

Seismic Ground motion Probability of Exceedance (return period)	Service Level	Damage Level
Lifeline Bridges		
2% in 50 years (2475 years)	Possible loss of service	Significant (No collapse)
5% in 50 years (975 years)	Limited	Repairable
10% in 50 years (475 years)	Immediate	Minimal
Emergency-Route Bridges		
2% in 50 years (2475 years)	Possible loss of service	Significant (No collapse)
10% in 50 years (475 years)	Limited	Repairable
Other Bridges		
2% in 50 years (2475 years)	Possible loss of service	No collapse

1.6 Problems associated with the force-based design approach

The forced-based design method involves some underlying assumptions which may not be valid particularly for certain types of structures. Some problems associated with irregular bridges are due to some unrealistic assumptions made in the force-based design method.

In addition, the degree of protection provided against damage under a given seismic intensity is non-uniform from structure to structure, when the force-based design approach is used. Thus, the concept of "uniform risk" which is implicit in the formulation of current seismic design codes is not achieved in the structural design. Using displacement-based approaches, such as the Direct Displacement-Based Design (DDBD) method (Priestley et al., 2007), a more rational and realistic design is achieved. The main problems associated with the use of the force-based design approach have been summarized by Priestley (Priestley et al., 2007). Some of these problems which are related to the subject of this research are summarized below:

1.6.1 Interdependency of strength and stiffness and relationship between Strength and ductility demand

In force-based design the member stiffness is traditionally assumed to be independent of strength, for a given member section. The flexural rigidity can be estimated from the moment curvature relationship in accordance with the beam equation as $EI = M_n / \Phi_y$. Where M_n is the nominal moment capacity and Φ_y is the yield curvature based on the equivalent bi-linear representation of the moment-curvature curve. The assumption of constant member stiffness implies that the yield curvature is directly proportional to flexural strength. Detailed analyses and experimental evidence show that this assumption is invalid in that stiffness is essentially proportional to strength, and the yield curvature is essentially independent of strength, for a given section (Priestley et al., 2007).

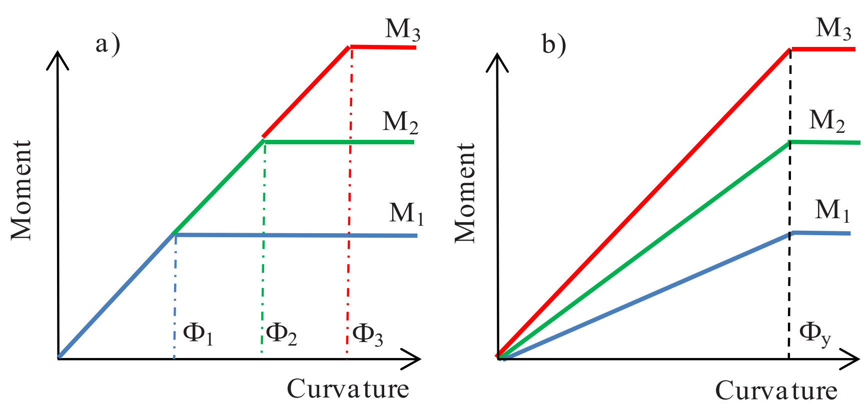

Fig. 1.2. Influence of strength on moment-curvature diagram: a) design assumption (constant stiffness); b) realistic condition (constant yield curvature) (adapted from Priestley et al., (2007))

Furthermore, according to the common force-based assumption that stiffness is independent of strength, increasing the strength of a structure by reducing the force-reduction factor improves its safety. However, experimental and analytical results indicate that the displacement capacity decreases as the strength increases (Priestley et al., 2007).

1.6.2 Structures with unequal column heights

The ductility capacity of a cantilever bridge column, μ_Δ, can be calculated using Eqs. 1.10a to 1.10c.

[1.10a] $$\Delta_y = \Phi_y H^2 / 3$$

[1.10b] $$\Delta_P = \Phi_p L_p H$$

[1.10c] $$\mu_\Delta = \frac{\Delta_y + \Delta_p}{\Delta_y} = 1 + 3\frac{\Phi_p L_p}{\Phi_y H}$$

Where Φ_y and Φ_p are the yield and plastic curvature, Δ_y and Δ_p are the yield and plastic displacement of the column, L_p is the plastic hinge length and H is the height of the column. Therefore based on Eq.1.10c, the displacement ductility capacity reduces as the height increases (Priestley et al., 2007). Thus the concept of uniform displacement ductility capacity, and hence of a constant force-reduction factor may not be appropriate even for this very simple class of structure in that the influence of structural geometry on displacement capacity of columns with identical cross-sections, axial loads and reinforcement details is not considered.

In conventional force-based design a force-reduction factor, reflecting the assumed ductility capacity is applied to determine the seismic design lateral force, which is then distributed to the piers in proportion to their stiffness. Implicit in this approach is the assumption of equal displacement ductility demand for all columns. If the columns have the same cross section dimensions, as is likely to be the case for architectural reasons, the design shear forces in the columns will be in inverse proportion to H_i^3, since the stiffness of column *i* is given by $K_i = \frac{C_1 E I_{i.e}}{H_i^3}$,where $I_{i.e}$ is the effective cracked-section stiffness of column *i*.. The consequence of this design approach is that the design moment at the base of the piers will be $M_{Bi} = C_2 V_i H_i = \frac{C_1 C_2 EI_{i.e}}{H_i^2}$ that is, in inverse proportion to the square of the column heights. C_1 *and* C_2 are constants dependent on the degree of fixity at the pier top. Consequently the shortest piers will be allocated much higher flexural reinforcement contents than the longer piers. This has three undesirable effects. First, allocating more flexural strength to the short piers will increase their elastic flexural stiffness, $EI_{i.e}$, even further with respect to the more lightly reinforced longer piers. Second, allocating a large proportion of the total seismic design force to the short piers increases their vulnerability to shear failure. Third, the displacement capacity of the short piers will clearly be less than that of the longer piers, since the displacement capacity of heavily reinforced columns is reduced as the longitudinal reinforcement ratio increases and hence the force-based design approach will tend to reduce the displacement capacity (Priestley et al., 2007).

In DDBD approach in which the stiffness of the pier is based on the effective secant stiffness at the maximum displacement, the distributed seismic forces are inversely proportional to the height of the columns (see Eq. [1.11b]) assuming that the columns have equal reinforcement ratios (Kowalsky, 1997).

[1.11a] $$K_{eff} = \frac{K_{cr}}{\mu} = \frac{3EI_{cr}}{H^3}\frac{\Delta_y}{\Delta_m} = \frac{EI_{cr}\Phi_y}{H\Delta_m}$$

[1.11b] $$F = K_{eff}\Delta_m = \frac{EI_{cr}\Phi_y}{H} \Rightarrow F_i = \frac{\frac{1}{H_i}}{\sum\frac{1}{H_i}}$$

where F_i is the shear force in column i, I_{cr} is the column cracked section moment of inertia, Δ_m is the maximum displacement of the column and μ is the displacement ductility demand in the column. The other parameters are defined before. The use of a force-reduction factor which does not reflect the different ductility demands and capacities clearly result in structures having different safety levels (Priestley et al., 2007).

1.6.3 Structures with dual (Elastic and Inelastic) load paths

In case of bridges with fixed abutments subjected to transverse seismic excitation, the primary seismic resistance is provided by bending of the piers, which are designed for inelastic response. However, since the abutments are restrained against the transverse movements, another load path is also developed by the elastic bending of the superstructure. As a result, the application of a force-reduction factor for design is not rational, since part of the loads is carried by elastic action in the superstructure (Priestley et al., 2007). Determination of the correct design solution for the transverse response of bridges is considerably more onerous than for longitudinal design (Priestley et al., 2007).

1.7 Introduction to direct displacement-based design method

Damage can be directly related to deformation. Hence designing structures to achieve a specified displacement limit implies designing for a specified risk of damage, which is compatible with the concept of uniform risk applied to determining the design level of seismic excitation. Therefore different structures designed with this approach will (ideally) have the same risk of damage, rather than a variable risk associated with current design approaches. Using state-of-the-art detailing/deformation relationships, structures with uniform risk of collapse, as well as of damage can theoretically be achieved. The fundamental difference from force-based design is that the Direct Displacement Design (DDBD) characterizes the structure to be designed by a single-degree-of-freedom (SDOF) representation of performance at peak displacement response, rather than by its initial elastic characteristics (Priestley et al., 2007). This procedure was initially proposed by Priestley (1993), with the objective of designing a structure which would achieve, rather than be bounded by, a given performance limit state under a given seismic intensity (Priestley, 1993; Kowalsky, 1997, Priestley et al., 2007). The method utilizes the Substitute Structure approach (Gulkan and Sozen, 1974) to model the inelastic structure as an equivalent elastic single-degree-of-freedom (SDOF) system. Calvi and Kingsley (1995) extended this methodology to multiple degree of freedom bridge structures.

Dwairi and Kowalsky (2006) investigated the displacement patterns of bridges subjected to transverse seismic excitations using nonlinear time-history analysis. The variables considered in this study included the bridge geometry, the superstructure stiffness, the substructure strength and the stiffness and abutment support conditions. A series of three inelastic displacement patterns were identified: (1) a rigid body translation (2) a rigid body translation with rotation and (3) a flexible pattern. A relative stiffness index, RS (Eq. [1.12]), that is a function of the superstructure and substructure stiffness was shown to be a key variable in determining the type of displacement pattern a bridge is likely to follow.

[1.12] $$RS = \frac{K_s}{\sum_{i=1}^{n} K_{c_i}} = \frac{\dfrac{32 I_s}{5 L_s^3}}{\sum_{i=1}^{n} \dfrac{I_{c_i}}{h_{c_i}^3}}$$

where n is the number of piers, index i refers to the pier number, I_c is the pier cracked section moment of inertia, h_c is the pier height, I_s is the deck gross moment of inertia, and L_s is the deck total length. Based on the analyses results, a rigid body translation pattern was identified for symmetric bridges with free abutments. In addition, a rigid body translation with rotation was identified for asymmetric bridges with free abutments. The majority of bridges with abutment restraint in the transverse direction had flexible displacement patterns. The DDBD procedure was then evaluated for some multi-span bridge design cases. The evaluation process showed that all of the four and five-span asymmetric bridge cases had displacements less than the target displacements and the target displacement profile was accurately predicted. However the target displacements were exceeded in more than 50% of the design cases for 6, 7 and 8 span bridges for symmetric and asymmetric bridge configurations. In a limited number of cases with very irregular configurations and flexible superstructures, the design procedure failed to predict the target-displacement profile. The failure is attributed to the inability of the effective mode shapes to estimate the target-displacement profile of a highly irregular MDOF structure.

In some studies at the ROSE School (Botero, 2004 and Restrepo, 2006), the displacement-based procedure has been used to design different series of bridge configurations with restrained abutments. The resulting designs were subjected to acceleration time histories to assess the accuracy of the method in terms of reaching the target design objectives, represented by target displacements. Satisfactory results were in general obtained from the assessment of the procedure using inelastic time-history analyses. Good results were also obtained for irregular Bridge configurations which showed that the implementation of the DDBD method to more complex structures is fully feasible. Nevertheless, there are still some problems associated with the displacement pattern of very stiff bridge configurations, like those with very short central pier (or piers) and taller exterior piers .In those types of bridges generally the first elastic and inelastic mode shapes significantly differ and clearly more studies should be focused on these types of bridges.

2 Incremental dynamic analysis applied to seismic performance and risk assessment of RC bridges

P. Tehrani and D. Mitchell, McGill University, Canada

2.1 Introduction

In Chapter 1 the problems associated with the bridges with different column stiffnesses were explained. This thesis also focuses on the use of incremental dynamic analyses for the seismic evaluation of bridges. This chapter provides an introduction to the incremental dynamic analysis (IDA) method, different methods for record selection, concepts of epsilon and spectral shape, different ground motion prediction equations and the application of IDA method for development of fragility curves and risk assessments. The use of different theoretical and experimental models to estimate the capacity of bridge columns is also explained. The concepts and background information presented in this chapter are used in Chapters 5 and 6 to study the use of IDA for the seismic assessment of bridges.

Chapter 2 was summarized into a book chapter : Tehrani, P. and Mitchell, D. “Incremental Dynamic Analysis Applied to Seismic Performance and Risk Assessment of RC Bridges”, and has been submitted in March 2012 to the publication “Seismic Risk Analysis and Management of Civil Infrastructure Systems, Editors: Tesfamariam, S. (UBC, Canada) and Goda, K. (Bristol, UK), Woodhead Publishing Limited.
The authors are permitted to use the material from the book chapter in this thesis for non-commercial purposes, with acknowledgement to the original source.

2.2 Incremental dynamic analysis

2.2.1 Introduction

IDA, developed by Vamvatsikos and Cornell (2002), is an analysis method which can be used for more detailed seismic performance predictions of structures subjected to different seismic excitation levels. IDA involves numerous inelastic time history analyses performed using one or a set of ground motion record(s), each scaled (up or down) to study different seismic intensity levels.

The IDA procedure has been adopted by some guidelines including the ATC-63 provisions (ATC-63, 2008) to determine the seismic performance, collapse capacity and fragility assessment of buildings. Some of the main objectives of the multi-purpose IDA analysis can be summarized as follows (Vamvatsikos and Cornell, 2002) :

1. To provide a thorough evaluation of the seismic responses (seismic demands) for a wide range of seismic intensity levels,
2. To provide a better understanding of the seismic response of structures due to rare and more severe ground motions at ultimate performance levels, including collapse,
3. To provide valuable insight into the changes in the structural response as the intensity of the ground motion changes
4. To provide estimates of the dynamic capacity of the structural systems, also known as the collapse capacity of the structure, defined as the point of global dynamic instability,
5. To compare the seismic responses due to different possible ground motion records and to provide estimates of the variability (uncertainty) in the seismic responses, when a set of records with different characteristics are used,
6- To provide information regarding possible structural responses, required for the probabilistic seismic performance assessment of structures and seismic risk analysis (e.g., development of fragility curves and prediction of the annual rate of collapse).

2.2.2 Damage measures and intensity measures

The IDA results are commonly presented using an intensity measure (IM) versus a damage measure (DM) of interest. IM is a non-negative scalable scalar, which is a function of the unscaled accelerogram, and is monotonically increased with a scale factor (Vamvatsikos and Cornell, 2002). Many quantities are available to characterize the intensity of a ground motion record; however such quantities are often treated as non-scalable parameters. Examples of such quantities include the moment magnitude, duration, or Modified Mercalli Intensity. Examples of scalable IMs which are commonly used in the IDA include the Peak Ground Acceleration (PGA), Peak Ground Velocity, and the 5% damped Spectral Acceleration at the structure's first-mode period (Sa (T_1,5%)). The use of the Sa(T_1,5%) quantity as the IM is often recommended and used in different research studies and guidelines [e.g., ATC-63 (2008), and Vamvatsikos and Cornell (2002)].

The damage measure, DM, is defined as a non-negative scalar quantity that characterizes the response of the structure to seismic excitations and can be deduced from the output of the nonlinear dynamic analysis. A wide range of such quantities are available and can be selected as a DM. Selecting an appropriate DM depends on the objective of the analyses and the characteristics of the structure. Some of the common choices include the maximum base shear, maximum columns ductility demands, various proposed damage indices (e.g., global cumulative hysteretic energy), and maximum column drift ratio). For bridges the maximum drift ratio of the critical columns or the maximum ductility demand is typically used for the DM parameter.

2.2.3 IDA Curves

The results of an IDA for a structure is often presented in the form of one or more IDA curves each representing the IDA results performed for each ground motion record. An IDA curve is the plot of the damage measure (DM) variable versus one or more intensity measure (IM) parameter(s). These curves demonstrate the state of the DM parameters at different intensity levels of the input records. This enables the study of the seismic demand parameters from low seismic intensity levels prior to yielding of the structure up to ultimate performance levels such as dynamic instability of the structure (i.e., collapse), buckling or fracture of the steel bars, shear failure, etc. Each non-linear dynamic analysis performed at each seismic intensity level is presented by a point in the IDA curve. This point demonstrates the maximum seismic demand (in terms of the DM parameter) obtained at the corresponding intensity level of the ground motion record. The full IDA curve then can be developed by fitting a curve through the points computed for different intensity levels (IM). The interpolation between the points is often used for this purpose. An example of an IDA curve is shown in Fig. 2.1 in which the spectral acceleration at the fundamental period, $S_a(T_1)$, and the maximum drift ratio of columns are used as IM and DM parameters, respectively.

The various types of IDA responses that may be observed are discussed by Vamvatsikos and Cornell (2002). Such responses may include hardening behaviour, softening behaviour, waving behaviour, and structural resurrection. Increasing the ground motion intensity in IDA does not always necessarily result in higher damage predictions. In fact the details of the ground motion records will also influence of the IDA results. For example a higher intensity of ground motion records may result in an earlier yielding of the structure. This in turn can change the effective period of the structure and the amount of dissipated energy due to inelastic deformations. So that the resulting maximum displacement of the structure may be even smaller than that obtained for a lower intensity.

Once the nonlinear dynamic analyses performed at certain ground motion intensities and the corresponding DM values are obtained, it is possible to use interpolation to approximate the entire IDA curve without performing additional analyses. The interpolations are typically performed either using basic piecewise linear approximation, or the spline interpolation (Vamvatsikos and Cornell, 2004). However to use interpolation the nonlinear dynamic analyses should be performed at a sufficient number of intensity levels to make sure that this approximation is acceptable. The use of spline interpolation has the advantage that it is more precise and the interpolations can be performed using smaller number of points (see Vamvatsikos and Cornell (2004) for more details). However the use of the linear interpolation is more straightforward for practical purposes, provided that a sufficient number of points is available at closely spaced IM values to approximate the full IDA curves.

Other methods to approximate the IDA curves and to determine the statistics of the IDA curves include the parametric methods such as the two-parameter, power-law model $\theta_{max}=\alpha\ [S_a(T_1)]^{\beta}$ introduced by Shome and Cornell (1999). Such parametric methods often provide a simple yet powerful description of the curves, although they lack the flexibility to accurately capture each IDA curve (Vamvatsikos and Cornell, 2002).

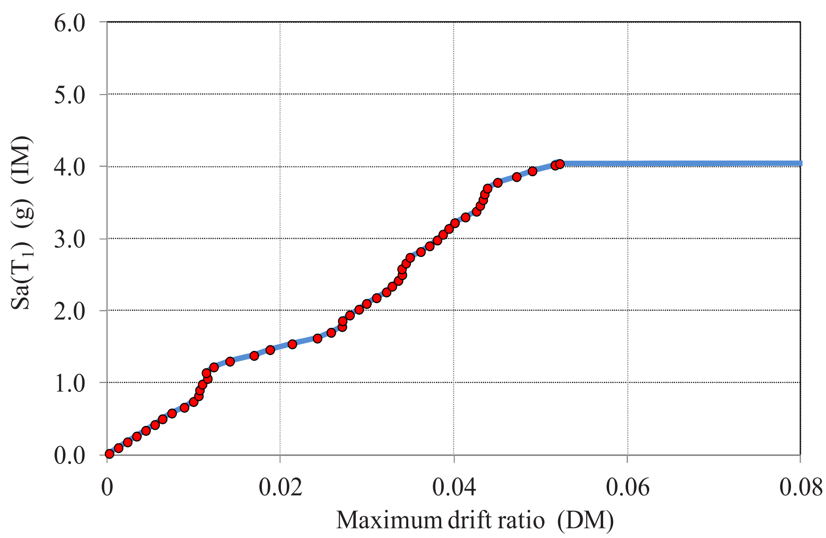

Fig. 2.1. An example of an IDA curve developed using $Sa(T_1)$ as IM and maximum drift ratio as DM. The results of nonlinear dynamic analysis for each IM are shown by dots and linear interpolation is used to fit a curve though these points. The last point of the IDA curve corresponds to an infinite drift ratio (i.e., dynamic instability).

2.2.4 Summarizing IDA results

Different ground motion records in IDA often result in different response predictions which are quite dissimilar, due to a wide range of behaviour and large record-to- record variability. Hence it is difficult to choose one particular response prediction to represent the behaviour of the structure. Therefore it is essential to summarize such large amount of data obtained through all IDA curves to quantify the randomness introduced by the records. Appropriate summarization techniques should be used to reduce this data to the distribution of *DM* given *IM* and to the probability of exceeding any specific limit-state given the *IM* level. There are several methods to summarize the IDA curves, but the use of percentiles (fractiles) are the most appropriate approach, since at the point of dynamic instability, introduced by flatlines in the IDA curves, the DM values are infinite and therefore the use of mean values or similar parameters is not possible (Vamvatsikos and Cornell, 2002).

In order to evaluate the IDA results often the median responses are determined along with the predicted dispersion of the results from different ground motion records. The IDA results thus can be summarized in percentiles, including median (50% percentile), 16% and 84% percentiles. With the assumption of a lognormal distribution of maximum drift ratio as a function of $S_a(T_1)$, the median (i.e., 50% percentile) is the natural 'central value' and the 84%, 16% percentiles correspond to the median times $e^{\pm \text{dispersion}}$, where 'dispersion' is the standard deviation of the logarithms of the values (Jalayer and Cornell, 2003). These percentile curves are much smoother than the individual IDA curves and can better represent the overall behaviour of a structure.

For example if 44 records are used in IDA, for each arbitrary IM value 44 values of DM are obtained (i.e., DM given IM values). By summarizing the DM values into their 16%, 50%, and 84% percentiles the percentile values of DM given IM are obtained for the arbitrary IM value considered. This procedure can then be repeated for a number of different IM values (preferably spaced at equal intervals) and the corresponding percentiles of DM values can be obtained. By interpolating the points obtained for each

DM fractile, the percentile IDA curves can be generated and the IDA results can be summarized into 16%, 50%, and 84% percentile IDA curves, as shown in Fig. 2.2.

A summary of the IDA curves can be expressed, either by the values of DM given IM or the values of IM given DM can be used. The first method provides the distribution of demand (i.e., DM) in the structure at a given intensity level, IM, while the second approach provides the distribution of intensities, IM, that cause a given level of damage, DM, in the structure. It has been shown that when percentiles are used to summarize the IDA results, the 16%, 50%, and 84% percentiles given *IM* **(**e.g., $Sa(T_1)$**)** almost perfectly match the 84%, 50%, and 16% percentiles, respectively, given DM (e.g., maximum drift ratio). In another word the line connecting the x% percentiles of DM given IM is the same as the one connecting the (100−x)% percentiles of IM given DM (Vamvatsikos and Cornell, 2004).

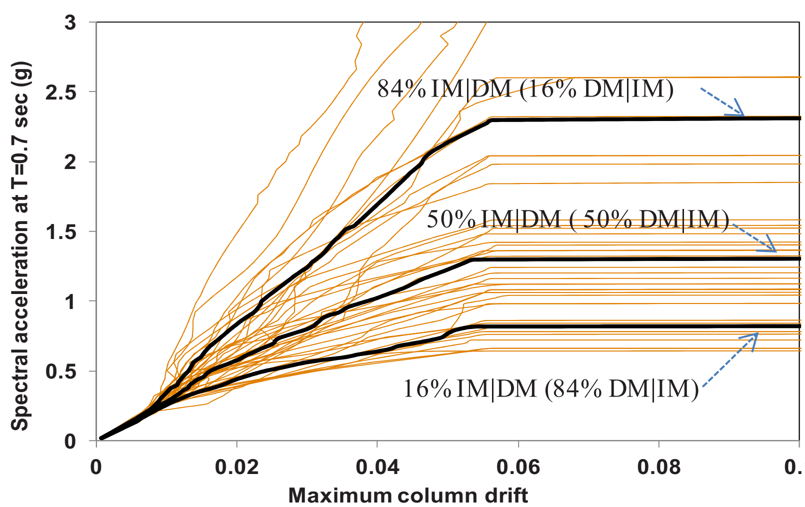

Fig. 2.2. An example of IDA curves developed using 44 crustal records for a 4-span bridge (percentile 16%, 50% and 84% IDA curves are shown by heavy lines) (Adapted from Tehrani et al. (2012))

Typically the median IDA curves exhibit similar trends and they include distinct segments which are influenced by the capacity boundary curves (i.e., the back-bone response curve) of the structural components. Based on such observations the capacity boundary of the structures may be used to predict the median IDA curves using simpler analyses. The idea is to obtain the capacity boundary curve of the structure by means of a simple pushover analysis and then use this curve as a back-bone curve of a single degree of freedom system for nonlinear dynamic analyses (e.g., see Vamvatsikos and Cornell, (2006)).

2.2.5 Characteristics of median IDA curves

Individual IDA curves for single ground motion records are typically very sensitive to dynamic interaction between the properties of the system and the characteristics of the ground motion such as the frequency content and the duration of the records. Fractile IDA curves (16th, 50th and 84th percentiles), however, are much more stable and provide better information on the central value (i.e., median) and variability (i.e., dispersion) of the response. In general, median IDA curves exhibit the following characteristics as shown in Fig. 2.3 (ATC-62, 2008):

- An initial linear segment is observed which corresponds to linear-elastic behaviour of the structural model prior to yielding in which the lateral deformation is proportional to the ground motion intensity. However in some systems, the initial linear segment may be extended beyond the yielding point into the inelastic deformation range as shown in Fig. 2.3. In this pseudo-linear segment, lateral deformation demand is approximately proportional to ground motion intensity, which is consistent with the familiar equal-displacement approximation for estimating inelastic displacements. The range of lateral deformation demands over which the equal-displacement approximation is applicable depends on the characteristics of the force-displacement capacity boundary and the period of vibration of the structure.

- A second segment on the median IDA curve corresponds to inelastic behaviour of the structure in which lateral deformation (DM) is no longer proportional to ground motion intensity (IM). As intensity increases, lateral deformation demands increase at a faster rate. This segment corresponds to softening of the system, or reduction in stiffness of the structure (reduction in the slope of the IDA curve). In this segment, the system "transitions" from linear behaviour to eventual dynamic instability. Although a curvilinear segment is always present, in some cases the transition can be relatively long and gradual, while in other cases it can be very short and abrupt. Typically structures with higher redundancy exhibit a longer transition segment, due to redistribution of the inelastic deformation demands.

- A final linear segment that is horizontal, or nearly horizontal, in which infinitely large lateral deformation demands occur at small increments in ground motion intensity. This segment corresponds to the point at which a system becomes unstable (lateral dynamic instability) and corresponds to the collapse capacity of the structure.

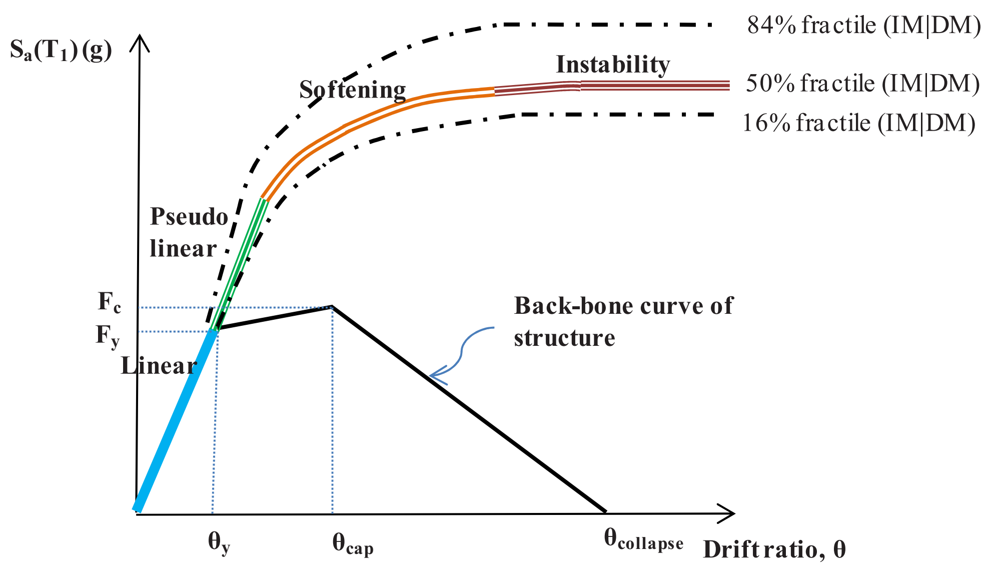

Fig. 2.3. Characteristics of median IDA curves (adapted from ATC-62, 2008)

2.2.6 Defining limit-States on IDA curves

For performance-based seismic assessments, the limit-states should be defined on the IDA curves. Such limit states are often defined in terms of engineering demand parameters such as drift ratios, plastic rotations, ductility demands, etc. Generally, exceeding a structural limit-sate on the IDA curves can be identified by means of either

DM-based or IM-based rules (Vamvatsikos and Cornell, 2002). The DM-based rule states that if the DM value exceeds a certain limit (e.g., the drift capacity at different limit states such as serviceability, damage control, etc.) then the limit state is exceeded. This rule is on the basis of the fact that DM is a measure of structural damage and when it exceeds a certain limit the structure fails to satisfy the corresponding limit-state (i.e., the expected structural damage is higher than that acceptable for the limit-state). Such limits on DM values for different limit-states can be obtained through experiments, theory, or judgment. An example of such limits is the drift limits recommended by Dutta and Mander (1998) for bridge columns at different damage states which are mainly based on engineering experience and judgement. Such capacity limits may not be deterministic, but be defined using a probability distribution function which are typically reported in terms of the central values and dispersions. An example of this case is the empirical equations developed by Berry and Eberhard (2007) to predict the median and standard deviation of the drift capacities of bridge columns at different damage states. When the DM-based rule is used to define the limit states, in some cases multiple points on the IDA curve may be found that satisfy a limit state. Such cases mainly occur, when the IDA curve exhibits the weaving or hardening behaviour. In these cases often the point with the lowest IM value that satisfies the limit sate is selected as the capacity point (e.g., see Fig. 2.4). The use of the DM-based rules is simple and is recommended for the limit states other than collapse. In the case of collapse, where the IDA curves flatten and the DM values become infinite, the application of the DM-based approach is not often possible. This is because in this case a wide range of DM values may correspond to only a small range of IM values.

By generating the IDA curve for each record and defining the limit state capacities for each IDA curve, the IM given DM value (set as the DM value at the limit state capacity) can be obtained for each curve. The limit-state capacities can then be summarized into central values (e.g., the mean or the median) and a measure of dispersion (e.g., the standard deviation, or the difference between two fractiles).

The IM-based rule is used mainly for the prediction of the collapse capacity. For this purpose the minimum IM value at which dynamic instability occurs is determined from the IDA curves and is defined as the collapse capacity of the structure. However in this case each IDA curve should be treated individually, since each IDA curve exhibit a distinct collapse capacity .This is contrary to the DM-based rule that a single drift limit (or any other DM parameter) is defined for all IDA curves at each limit-state.

Other limit states have also been used to determine the state of collapse. An example is the FEMA-350 (2000), 20% tangent slope approach in which the last point on the curve with a tangent slope equal to 20% of the elastic slope is determined to be the capacity point. The idea is that the flattening of the IDA curve is an indicator of impending dynamic instability with the DM increasing at higher rates and approaching infinity (Vamvatsikos and Cornell, 2002). This limit state is also determined using an IM-based rule. An example of defining different limit-state points (e.g., serviceability, damage control, and collapse) on the IDA curves is shown in Fig. 2.4. The predicted drift capacities are only specific for the case considered here.

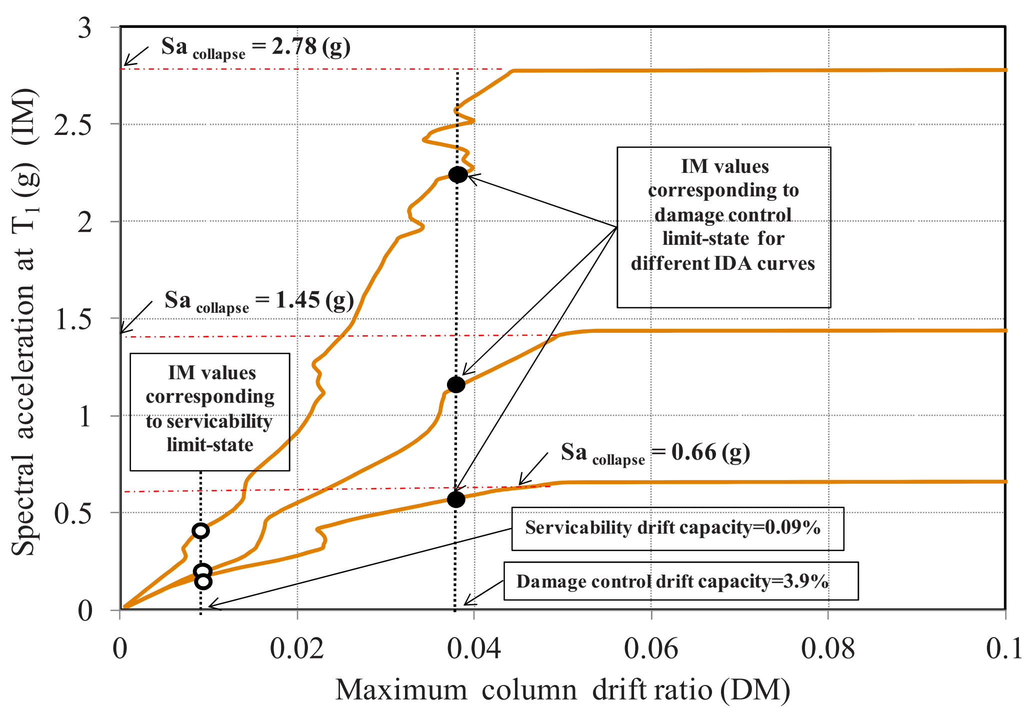

Fig. 2.4. Prediction of different limit states on IDA curves

2.3 Different IDA procedures and algorithms

Depending on the purpose of structural analyses several algorithms can be used to perform IDA. Since the application of IDA often involves numerous inelastic dynamic analyses for each record, such analyses are often time-consuming and can take several hours to several days depending on the structure under analysis and the available computational resources. Therefore the use of time-efficient algorithms to perform IDA can be very beneficial and significantly decrease the computation time. The following algorithms are often used to run IDA analyses:

2.3.1 Regular IDA algorithms

The simplest way to perform the IDA is to scale the records incrementally at uniform steps. For this purpose the analysis for each record starts with a small IM value and ends when the maximum IM value of interest is reached. For each step the IM value will be increased by a fixed value, Δ_{IM}. The value of Δ_{IM} should be chosen such that a sufficient number of points can be obtained for the developments of the IDA curves. If the Δ_{IM} is large, the analysis can be performed faster, but the IDA curves may not be interpolated with acceptable precisions. An optimum Δ_{IM} should be chosen to have a balance between the required precisions in the prediction of the structural responses and the computation time. Another important issue is the estimation of the maximum IM values which can significantly affect the computation time. For example, if the objective of the IDA is the prediction of the collapse capacity of structure for each record, a large value should be assigned to the maximum IM to make sure that the ultimate collapse capacity for each record can be determined. As a result, for all ground motion records the analyses should be carried out up to the maximum IM value, while for many of them the structural collapse occurs in much smaller IM values. This results in many redundant and unnecessary analyses which increase the computation time.

2.3.2 Time-efficient algorithms

Time-efficient algorithms can be developed to significantly reduce the computation time and to increase the precisions in the prediction of the seismic responses. For example the analyses can start with larger increments of IM and the size of the increments can be adjusted in the subsequent steps based on the results obtained in the previous steps. The IM increments, Δ_{IM}, can be significantly decreased at the IM values near collapse. Accordingly the analyses for each record can stop when the structural collapse occurs or when the ultimate damage measures of interest are determined. The use of such advanced algorithms, such as the "hunt & fill" algorithm (Vamvatsikos and Cornell 2002), ensures that the record scaling levels are appropriately selected to minimize the number of required runs and the required precisions in prediction of the seismic responses are attained at the lowest computation costs. The extra efforts required in developing the more complex time-efficient algorithm will be paid back with significantly lower computation time, especially when a large number of records (especially when the duration of records are also long) are used in IDA, or when a large number of structures needs to be evaluated using IDA.

2.3.3 ATC-63 procedure

In the ATC-63 provisions only the median collapse capacity of the structure should be determined and thus the computation of the full IDA curves is not necessary. For this purpose first the records are normalized by their respective peak ground velocities (to remove unwarranted variability due to different characteristics of records such as magnitude, distance, and soil type) and then all the records are collectively scaled up or down until 50% of the records cause structural collapse. The spectral acceleration, at which 50% of the records cause collapse, is the median collapse capacity of the structure and then will be used to compute the collapse margin ratios for the seismic performance assessment of the structure.

In the ATC-63 procedure the collapse capacity of the structure for each of the 44 records is unknown (i.e., at least 50% of the records causing dynamic instability) and only the median collapse capacity of the record set is determined. Thus a direct evaluation of the variability in collapse prediction is not possible using this method. In fact, the ATC-63 provisions use a presumed value of the logarithmic standard deviation of 0.4 to reflect the record-to-record variability. It must be noted that often the record-to-record variability is simply estimated using the elastic response spectra of the records (e.g., ATC63 provisions). Although this may provide a simple and rough estimate of the actual variability in the prediction of the collapse capacities, it does not take into account problems associated with the duration of the records, strength and stiffness degradation and associated period elongation, and other important aspects that can only be considered through performing nonlinear dynamic analyses.

2.3.4 Fast IDA procedures

Other algorithms to perform IDA can also be developed, based on the objectives of the structural analyses. Often the most important outcome of the IDA is the prediction of the median collapse capacity which will be used in the probabilistic performance based assessment of the structures. Therefore for prediction of collapse capacities the structural analyses can be started at higher intensities in which structural collapse is expected. The initial estimates can be predicted using a pushover analysis or can be chosen based on judgement. A good prediction of the initial estimate of the median collapse capacity will minimize the computation time of the IDA. Such algorithms are especially helpful when the records with long durations (e.g., subduction interface and inslab ground motion records) or a large number of records are used in the IDA. However for such fast IDA algorithms the full IDA curves are not available, since the analyses are performed only at high ground motion intensities that can cause structural collapse. If the prediction of the standard deviation of the results is also required, the collapse capacity of the structure for each record are predicted using the fast IDA algorithm and the median and the dispersion of the results can be estimated.

Such fast algorithms can be performed even faster if the prediction of the dispersion of the results is not required. An example is the method recommended by the ATC-63 provisions which only requires the prediction of the median collapse capacity, while a presumed value of 0.4 is used as the logarithmic standard deviation of the results due to record-to-record variability. For such cases the use of all records in all steps will not be required. For example if a record cause structural collapse at a certain intensity level, it can be assumed that it will cause structural collapse at a higher intensity level as well (i.e., it is assumed that structural resurrection or other bizarre cases in IDA is not applicable). Similarly if a record does not cause structural collapse at a certain intensity level, it will not cause collapse at lower intensity levels. Therefore such records can be removed from the IDA in the subsequent steps and IDA can be performed much faster.

2.4 Structural modelling for IDA

In IDA the intensity of the ground motion records are increased until they cause structural instability which is referred to as structural collapse. Therefore the structural models in the IDA should be capable of simulating structural collapse and should directly or indirectly consider all significant deterioration modes that contribute to collapse including the stiffness, strength, and inelastic deformations under reversed cyclic loading. The most important structural parameters that influence the IDA predictions include the plastic deformation capacity, θ_{cap}, and the post-capping rotation capacity, θ_{pc} (Ibarra et al., 2005). These parameters are used to define a component backbone curve, as shown in Fig. 2.5.

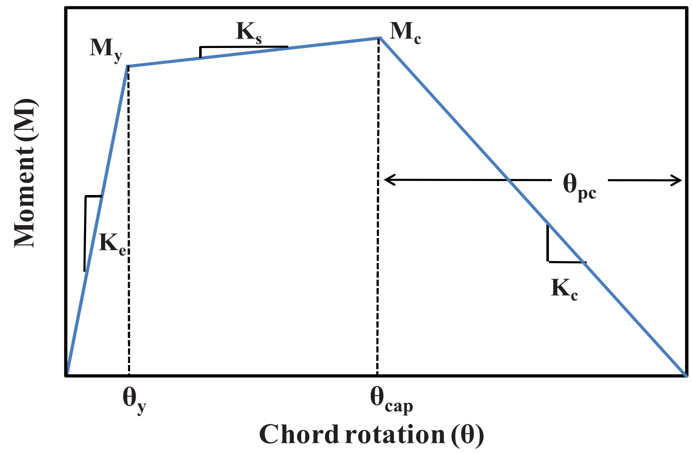

Fig. 2.5. Backbone curve parameters (adapted from ATC-63 (2008))

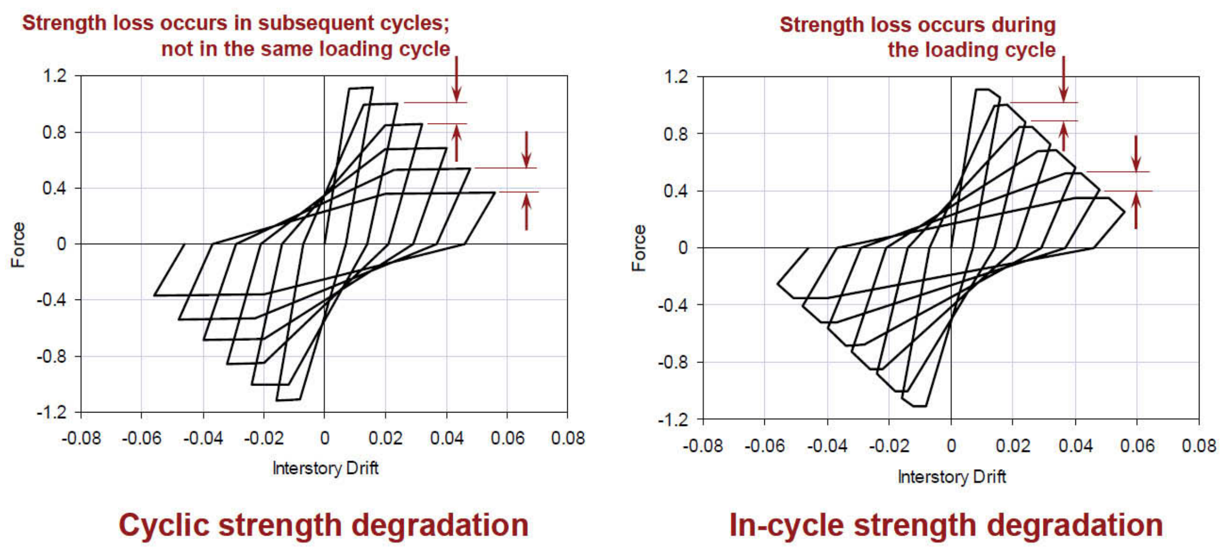

Fig. 2.6. Differences between cyclic and in-cycle strength degradation (from FEMA P440A (ATC-62), 2008).

In combination with stiffness degradation, structural components and systems may experience in-cycle strength degradation (Fig. 2.6). In-cycle strength degradation is characterized by a loss of strength within the same cycle in which yielding occurs. As additional lateral deformation is imposed, a smaller lateral resistance is developed. This results in a negative post-yield stiffness within a given cycle. In-cycle strength degradation can occur as a result of geometric nonlinearities (P-delta effects), material nonlinearities, or a combination of these. In reinforced concrete components, material nonlinearities that can lead to in-cycle strength degradation include concrete crushing, shear failure, buckling or fracture of longitudinal reinforcement, and splice failures (FEMA P440A (ATC-62), 2008).

The distinction between cyclic and in-cycle degradation, as shown in Fig. 2.6, is important because the consequences of each are vastly different. Dynamic response of systems with cyclic strength degradation is generally stable, while in-cycle strength degradation can lead to lateral dynamic instability (i.e., collapse). In modelling for IDA the in-cycle strength degradation is very important for prediction of the collapse capacity and the global dynamic instability of the structures and is often considered by the negative post capping stiffness defined in the component back-bone curves. (e.g., see Fig. 2.5).

Modern bridges are designed and detailed to meet the seismic code requirements for ductile response, including capacity design concepts and adequate support lengths at the abutments. The ductile columns contain code-compliant spiral reinforcement to confine the concrete, avoid shear failure and to control buckling of the vertical reinforcing bars. For continuous bridges, with all other failure modes avoided, the flexural response governs the response of the bridge and sidesway collapse is the governing collapse mechanism. While the columns will undergo a ductile inelastic response during a major event, the bridge superstructure is designed to remain elastic and is typically modelled using elastic elements.

When structures with poor detailing are studied or when other collapse modes are probable, such degrading collapse modes should be either considered directly in the structural models or be treated indirectly through non-simulated component limit state criteria. Such degrading modes may include shear failure or failure due to degradation of shear capacity at high ductility levels (e.g., interaction of shear and flexure which is referred as to shear-flexure or ductile shear failure). Including code-conforming confinement reinforcement in the plastic hinge region of bridge columns will prevent such undesirable failure modes. Where such collapse modes cannot be included directly in the models, often they are considered indirectly by imposing some drift limits corresponding to such collapse modes. That is, after performing the IDA, the collapse capacities can be modified for other collapse modes such that the corresponding IM values to the non-simulated collapse modes (in terms of DM) will be considered as the collapse capacity of the structure. However this simplification in modelling through application of the non-simulated component limit state criteria should be accounted for by increasing the modelling uncertainty in the overall seismic performance assessment of the structure. The model proposed by Elwood (2004) is an example of the models that can predict the drift corresponding to shear failure and axial failure of columns with insufficient transverse reinforcement.

The influence of the abutments on the seismic response of the bridges can be included in structural modelling. However the effects of abutments may be conservatively neglected, if they do not significantly influence the seismic response. An alternative approach may be analyzing the bridges for two cases of restrained and unrestrained movements at the abutments to evaluate the seismic response of the structure and to recognize the controlling case. For example in the transverse response often shear keys are used to restrain the transverse movements of the superstructure at the abutments. The shear keys may either be designed based on the capacity design concepts so that they will survive under high ground motion intensities or they can be designed as fuses to fail at low ground motion intensity levels to prevent damage in the abutments and piles. Therefore according to the design philosophy for such elements different modelling approaches may be accepted. The most direct approach would be to include the degrading behaviour and failure of shear keys in the structural models. The shear key models by Megally et al. (2003) can provide the required information for this purpose. The spring abutment model developed by Aviram et al. (2008) can be used when the effects of abutments are directly considered in modelling. In this abutment model the effects of all important abutment parameters such as strength and stiffness due to back-fill soil, abutment wing wall and back wall, piles, bearing pads, shear keys and gaps are considered in the response.

The effects of expansion joints can be considered using gap elements in the structural models. For example for the case of the continuous bridges, the expansion joints are typically situated at the end abutments and can be considered by means of gap elements in the abutment models. If cap beams are present then the cap beams and beam-column joints are designed as capacity protected elements (design to transmit the probable resistance of the columns) and therefore are modelled as elastic elements. However this is not applicable for the case of the single column bridges studied in this research which are assumed to be hinged at the top and fixed at the base.

2.5 Scaling of records in IDA

Due to the limited number of strong records available that can cause significant damage (or collapse) in modern structures, the use of scaled records in IDA and nonlinear dynamic analyses of structures is often inevitable and is widely used in practice and research. However, concern is often expressed about the validity of structural analysis results obtained using scaled ground motion records.

The use of an excessive scaling factor (e.g., factor of 10 or greater) could induce significant bias in the predicted structural responses (Luco and Bazzurro, 2007). There is a large growing body of literature concerning questions related to scaling of ground motions, so that it is difficult to provide a simple answer in this regard. However it can be concluded that in general the legitimacy of the scaling procedure depends on the structure, the choice of the DM, and the choice of the IM (Vamvatsikos and Cornell, 2002).

The similarity of the response spectral shape of a record to the target response spectrum has been shown to be an important criterion in selecting records which result in unbiased response predictions. For moderate period structures with maximum drift ratio taken as the DM and $S_a(T_1)$ as the IM and for a general class of records (moderate to large magnitudes, M) the use of scaling typically results in similar predictions with those obtained using un-scaled records. On the other hand where the response of the structure is dominated by the first mode, the use of PGA as the IM can result in biased structural response predictions, since the average ratio of $S_a(T_1)$ to PGA changes with magnitude and therefore the spectral shape effects cannot be well captured when PGA is used as the IM. In fact if the IM has been chosen such that the regression of DM jointly on IM, M and R is found to be effectively independent of magnitude and distance (in the range of interest), scaling of records will provide good estimates of the distribution of DM given IM (Vamvatsikos and Cornell,2002). It has been demonstrated that the use of scaling in cases where the records are selected based on methodologies that account for the spectral shape effects (such as the epsilon-based method and CMS-based method), result in unbiased predictions similar to those obtained using un-scaled records (Baker and Cornell, 2005 and 2006a).

2.6 Prediction of damage states

In order to determine the capacity of a structure (e.g., in terms of IM parameters) at different limit states, some criteria are needed to determine the state of damage (i.e., onset of spalling, bar buckling, etc.) at different DM values. Such criteria may not be determined deterministically, but be reported as random variables (i.e., the median drift capacity and a standard deviation). Such models are also referred as the capacity models which predict the probability of exceeding a damage state given DM. For example if the maximum drift ratio of columns is used as DM, some criteria on drift limits should be determined to predict the state of damage in the structural elements at various drift ratios (i.e., drift capacity corresponding to cover-spalling, or drift capacity corresponding to bar buckling, etc.). Such models can be developed either empirically (e.g., experiments, experience, etc.) or theoretically (e.g., using cross-sectional analysis). Such data are usually provided in terms of engineering demand parameters (such as tensile and compressive strain limits, ductility capacity, drift capacity, etc.) for different damage states (e.g., yielding, cover spalling, bar buckling, bar fracture, and collapse). Such information is also required in structural modelling to define the back-bone curves of the response of structural elements (e.g., to determine deformation capacity, θ_{cap}, post-capping rotation capacity, θ_{pc} ,etc.) as shown in Fig. 2.5. Such information is available from several experimental and theoretical studies as discussed below.

2.6.1 Study by Dutta and Mander (1998)

Dutta and Mander (1998) recommended some simple drift limits for bridge columns at different damage states consistent with those defined in HAZUS (1999). These limits are given for two cases of seismically and non-seismically designed bridges. Such estimates of the structural damage at different drift limits provide good information for the preliminary evaluation of bridges. However the use of such constant drift limits for a large variety of bridge columns with different geometric and mechanical characteristics may not be appropriate where more precise seismic evaluations are carried out. The ultimate drift capacity of columns in such cases should be defined explicitly as a function of important parameters that influence the deformation capacity. The recommended drift limits along with the expected damage at each damage state are summarized in Table 2.1.

Table 2.1. The recommended drift limits by Dutta and Mander (1998) at different damage states

Damage State	Description of Bridge Damage States (HAZUS 99)	Drift Limits (non-seismically designed)	Drift Limits (seismically designed)
No	No damage to a bridge	0.005	0.008
Minor/ Slight	Minor cracking and spalling to abutments, hinges, columns or minor cracking to the deck	0.007	0.01
Moderate	Any column experiencing moderate cracking and spalling (column structurally still sound), any connection having cracked shear keys or bent bolts, or moderate settlement of the approach	0.015	0.025
Major/Extensive	Any column degrading without collapse (column structurally unsafe), any connection losing some bearing support, or major settlement of the approach	0.025	0.05
Complete Collapse	Any column collapsing and connection losing all bearing support, which may lead to imminent deck collapse	0.05	0.075

2.6.2 Theoretical method by Priestley et al. (2007)

Structural damage can be defined as a function of the maximum compression strain in the confined core concrete and the maximum tension strain in the reinforcing bars. The strain limits then can be converted for simplicity to displacements, drifts, and rotations, which are widely used by the engineers, using appropriate relationships between strain, curvature and displacement assuming an appropriate plastic hinge length in yielding elements.

Serviceability limit state is usually exceeded when the concrete cover outside the confined core starts spalling or crack widths are larger than allowable limits. The spalling state is determined according to the maximum compression strain in unconfined concrete cover which is usually limited to a value in a range of 0.003 to 0.004. To control the crack widths, the maximum strains in the reinforcing bars should not exceed an appropriate limit. In ordinary environments a crack width of 1.0 mm is typically appropriate and the corresponding maximum tension strain to this crack width is around 0.015 for column or wall elements (Priestley et al., 2007).

The ultimate compression strain in the confined core is mainly a function of degree of confinement and the quality of detailing in the plastic hinge regions. Several empirical equations are available in the literature to estimate the ultimate compression strain in the confined concrete core, among them is the widely used Mander equation (Mander et al., 1988). The Mander et al. equation is based on equal energy principles in which the ultimate compression strain corresponds to the fracture of hoops. Beyond this level, crushing of the concrete, buckling, and fracture of the steel bars are unavoidable and the structural elements must be usually replaced, since repairing is not economical. Experimental studies however indicate that he ultimate strains predicted by Mander equation are conservative in which the actual ultimate strains exceed the predicted values by a factor of about 1.3 to 1.6. This conservatism in the Mander et al. equation is mainly due to ignoring the combined effect of axial compression and flexure while the original Mander et al. model was derived based on the assumption of pure axial compression of the members such as foundations or columns. To account for this, Priestley et al. (2007) recommend using the ultimate strains based on this equation for damage control limit state for which this degree of conservatism is deemed to be appropriate. However for the Life Safety (LS) limit state the predicted values from Mander et al. equation may be increased by 50% to correspond to the experimental results.

For the damage control tension strain limit, the ultimate strain in steel bars, ε_{su}, from the monotonic tests cannot be used directly for moment curvature analysis and the calculation of the ultimate curvature. Due to the possibility of buckling of the bars when subjected to reversed loading and considering low-cycle fatigue of the reinforcing bars in addition to slip between the reinforcing steel and the concrete, the ultimate tension strain from the monotonic tests must be modified. The level of this strain will depend on the volumetric ratio and longitudinal spacing of the transverse reinforcement. Usually a strain level of 0.6 to 0.7 times the ultimate strain of the steel bars in monotonic tests is recommended for calculating the ultimate curvature of the section which should not be taken larger than 0.05 (Priestly et al., 1996 and 2007). In order to attain this level of strain, the spacing of the transverse reinforcement must be code conforming. For the life safety performance level the value of 0.9 times the ultimate strain of steel bars, 0.9 ε_{su}, is recommended by Priestley et al. and this value should not be larger than 0.08 (Priestly et al., 2007). The strain limits for different damage states are summarized in Table 2.2.

Table 2.2. Maximum strain in concrete and steel at different damage states (Priestley et al., 2007)

Damage state	Rebar tension strain (ε_s)	Concrete comp. strain (ε_c)
Yielding	0.002	0.002
Serviceability	0.015	0.004
Damage Control	$0.6\varepsilon_{su}$ ($\leq$0.05)	$\varepsilon_c <$ Mander eq.
Life Safety	$0.9\varepsilon_{su}$ ($\leq$0.08)	$\varepsilon_c <$ 1.5*Mander eq.

2.6.3 Equations by Berry and Eberhard (2007)

A study by Berry and Eberhard (2007), based on experimental data from the PEER Structural Performance Database (Berry et al., 2004), provides some empirical equations to estimate the engineering demand parameters (EDP) including drift ratio, plastic rotation, and strain in the longitudinal bars for circular bridge columns based on the properties of columns including the longitudinal and transverse steel ratio, the axial load ratio, and the geometry. Such equations are provided for different damage states including spalling, reinforcing bar buckling, and bar fracture. The equations given for different damage states as a function of different EDP are summarized in Table 2.3. The bar buckling state can represent the point at which strength degradation starts to define capacity of the columns. Few test results are available to calibrate the post-capping stiffness of the columns. Mackie and Stojadinovic (2007) provide an equation for estimation of the drift at failure, using the same test data used by Berry and Eberhard. The equations by Berry and Eberhard for spalling, bar buckling, and bar fracture damage states along with the equation by Makie and Stojadinovic (2007) to predict the drift at failure are summarized in Table 3. In Table 3, $\rho_{eff} = f_{ys}\, \rho_{s,trans} / f'_c$, is the effective confinement ratio, $\rho_{s,trans}$ is the volumetric transverse reinforcement ratio, f_{ys} is the yield stress of the transverse reinforcement f'_c is the concrete compressive strength, d_b is the diameter of the longitudinal reinforcement, D is the column diameter, P is the axial load, A_g is the gross area of the cross section, and L is the distance from the column base to the point of contraflexure.

Table 2.3. Summary of the equations by Berry and Eberhard (2007) for cover-spalling, bar buckling, and bar failure, and equation by Mackie and Stojadinovic (2007) to estimate drift at failure

			Measured/Calculated	
Damage State	EDP	Equation	mean	coefficient of variation
Cover Spalling	Δ_{sp}/L (%)	$1.6\,(1-P/A_g f'_c)\,(1+L/10D)$	1.07	0.35
	$\theta_{p\text{-}sp}$	1.2	0.98	0.34
	ε_{sp}	0.008	0.99	0.45
Bar Buckling	Δ_{bb}/L (%)	$3.25\,(1+150\rho_{eff}\, d_b / D)(1 - P / A_g f'_c)(1 + L / 10D)$	1.01	0.25
	$\theta_{p\text{-}bb}$	$2.75\,(1+150\rho_{eff}\, d_b / D)(1 - P / A_g f'_c)(1 + L / 10D)$	1.01	0.24
	ε_{bb}	$0.045+0.25\rho_{eff} \le 0.15$	1.00	0.24
Bar Fracture	Δ_{bf}/L (%)	$3.5\,(1+150\rho_{eff}\, d_b / D)(1 - P / A_g f'_c)(1 + L / 10D)$	0.97	0.20
	$\theta_{p\text{-}bf}$	$3.0\,(1+150\rho_{eff}\, d_b / D)(1 - P / A_g f'_c)(1 + L / 10D)$	0.97	0.20
	ε_{bf}	$0.045+0.30\rho_{eff} \le 0.15$	0.96	0.21
Failure	Δ_{ff}/L (%)	$16 + 0.71\,L - 15D - 3.8e^{-5} f'_c - 2.8e^{-5} f_y + 1.7\rho_{s,long} + 1.9\rho_{s,trans} - 12P/A_g f'_c$	-	0.35

2.6.4 Study by Fardis and Biskinis (2003)

Panagiotakos and Fardis (2001) have provided some empirical equations to estimate the yield and ultimate deformations of reinforced concrete members with rectangular cross-sections. Fardis and Biskinis (2003) then provided a more complete set of equations for different structural elements such as columns (with rectangular and circular sections) and walls. Such equations are given for the case of different collapse modes such as flexure and shear-flexure failure modes and for different loading types including monotonic and reversed cyclic loadings. The ultimate deformation in these equations was considered as the point with 20% strength degradation. Therefore these equations may be more appropriate for the case of conventional seismic evaluations based on the seismic codes where such definitions for the ultimate displacements have been used. However, for the purpose of structural modelling in IDA, where the prediction of the cap point (i.e., point where strength degradation begins) is required, some back calculations may be required. Such calculations may not be straightforward since the post-capping stiffness is not given in these studies. Nevertheless such equations provide an excellent source of information for structural modelling and evaluation.

2.6.5 Study by Haselton et al. (2007)

Haselton et al. (2007) provide a comprehensive set of equations for the purpose of modelling and evaluation of the reinforced concrete structural members. This study provides equations to define the important modelling parameters in the backbone curves (e.g., the capping deformation and post capping stiffness, etc.) as a function of the geometric and mechanical characteristics of the structural members. These equations were primarily provided for the purpose of structural modelling in IDA and were also included in the ATC-63 provisions. Furthermore, equations are given to predict the hysteresis parameters based on a sophisticated hysteresis model by Ibarra et al. (2005). This study provides all the necessary information for structural modelling in IDA. However the application of such equations for the case of circular bridge columns may not be appropriate, since only the experimental data from the members with rectangular cross-sections were used to derive the equations.

2.7 Treatment of uncertainties in IDA

2.7.1 Types of variability

Each source of variability in general can be classified into *aleatory* (randomness) and *epistemic* (uncertainty) types of variability. The random nature of ground motions (known as record-to-record variability) is considered as aleatory variability. The epistemic variability in the prediction of collapse capacity is primarily due to lack of knowledge about the ground motion hazard model and the structural model. Accurate estimation of the epistemic uncertainties (including the modelling uncertainty) is often time-consuming and involves extensive application of Monte Carlo simulations or the FOSM (First Order Second Moment) method (Liel et al., 2009, and Zareian and Krawinkler, 2007). The ATC-63 provisions provide a simplified judgmental method to estimate total uncertainty in prediction of the collapse capacity which may be used when such information is not available.

To de-convolve the effects of *epistemic* and *aleatory* uncertainties on the collapse probability, it is usually assumed that the median collapse capacity is a random variable and the dispersion due to record-to-record variability is independent of the dispersion due to *epistemic* uncertainty in the structural model. Based on this assumption, collapse capacity predictions can be carried out using the ground motion records applied to the structural mathematical model with the properties of elements set to their median values. Using such an approach provides the collapse fragility curve with median value of the collapse capacity, η_c, and the dispersion due to record to record variability, β_{RTR} (randomness in collapse capacity). In order to incorporate the effect of *epistemic* uncertainty, it is assumed that the median of the collapse capacity, η_c, is a random variable which is lognormally distributed with median (median estimate of median of collapse capacity) $\overline{\eta}_c$ and dispersion of $\beta_{epistemic}$ (Zareian and Krawinkler, 2007).

Combining the effects of different sources of uncertainty can be carried out using different approaches, including the confidence interval approach and the mean estimate approach. The use of the confidence interval method results in predictions that are highly dependent on the confidence interval chosen. Therefore the use of the mean estimate approach is preferred, since it provides a more practical and consistent approach for this purpose (see Liel et al., (2009), and Zareian and Krawinkler (2007) for more details). When aleatory (record-to-record) uncertainties only are considered, the structural response is well-described by a lognormal distribution (Cornell et al., 2002), with median, η_c, and logarithmic standard deviation (β_{RTR}). In the mean estimates approach, it is assumed that the epistemic (e.g., modeling) uncertainty describes uncertainty in the median collapse capacity (η_c), and that this random variable is also lognormally distributed with median value of $\overline{\eta}_c$ and lognormal standard deviation of $\beta_{epistemic}$. The random variables associated with epistemic and aleatory uncertainty are assumed to be independent. It can be shown that when these two distributions are combined the resulting distribution is also lognormal with the median value of $\overline{\eta}_c$ and a logarithmic variance that is the sum of the two logarithmic variances (i.e. $\beta_{TOT} = \sqrt{\beta_{RTR}^2 + \beta_{epistemic}^2}$) (Benjamin and Cornell, 1970). Thus, when the mean estimates approach is used, the median is unchanged when modeling uncertainties are incorporated, but the variance increases. The results derived from this approach are not sensitive to whether individual uncertainties are classified as aleatory or epistemic, which is helpful when the classification of a particular uncertainty is not obvious.

2.7.2 Sources of uncertainty and combining uncertainties

Many sources of uncertainty contribute to total variability in collapse capacities predicted using IDA. The main sources of uncertainty include (ATC-63, 2008):

1-Record-to-Record (RTR) Uncertainty. This uncertainty is due to variablity in the sesmic response of structures to different ground motion records. The variability in response is mainly due to different frequency content and dynamic characterstics of the records, variablity in the hazard characterization of the ground motions records, and different duration of records used in the IDA.

2- Design Requirements-Related (DR) Uncertainty. Such uncertainty is associated with the quality of the design requirements.

3- Test Data-Related (TD) Uncertainty. This type of uncertainty is related to the quality of the test data used to define the structural system.

4- Modelling (MDL) Uncertainty. This uncertainty is associated with the quality and robustness of the nonlinear structural models and the ability to accurately simulate the nonlinear behaviour of the structural elements subjected to seismic excitations.

The total uncertainty can be predicted by combining RTR, DR, TD, and MDL uncertainties. The collapse fragility of the structure can be estimated by multiplying the predicted median collapse capacity from IDA, to a random lognormal variable such as λ_{TOT} with a median value of unity and a lognormal standard deviation of β_{TOT}. This lognormal random variable, λ_{TOT}, in turn consists of four independent lognormal random variables such that, $\lambda_{TOT}= \lambda_{RTR}\, \lambda_{DR}\, \lambda_{TD}\, \lambda_{MDL}$, where λ_{RTR}, λ_{DR}, λ_{TD}, and λ_{MDL} are lognormal random variables with a median value of unity and a lognormal standard deviation of β_{RTR}, β_{DR}, β_{TD}, and β_{MDL} respectively. Since these random variables are assumed to be statistically independent, the total uncertainty in prediction of the collapse capacity, β_{TOT}, described in terms of lognormal standard deviation can be computed using Eq.[2.1].

[2.1] $$\beta_{TOT} = \sqrt{\beta_{RTR}^2 + \beta_{DR}^2 + \beta_{TD}^2 + \beta_{MDL}^2}$$

Based on the ATC-63 provisions the uncertainty due to record-to-record variability is taken as β_{RTR} = 0.40 in all cases. However this is based on the period range of building structures and considering only crustal earthquakes. For bridges or other structures β_{RTR} can be directly estimated from the IDA results. Quality ratings for design requirements, test data, and nonlinear modeling are translated into quantitative values of uncertainty based on the following scale: (A) Superior, β = 0.20; (B) Good, β = 0.30; (C) Fair, β = 0.45; and (D) Poor, β = 0.65 (ATC-63, 2008). More details concerning the criteria to determine the quality ratings for different sources of uncertainty are available in ATC-63 (2008). Other studies have also used similar values for uncertainty. For example in a study by Mander et al. (2007) the uncertainty due to modelling and predicting the capacity of the bridge columns were considered as 0.25 and 0.2 respectively.

2.8 Development of fragility curves using IDA results

IDA results are used for the development of the fragility curves of structures for different limit-states. The fragility curve gives the conditional probability that a certain limit-state be exceeded (i.e., probability of failure) at a given IM value.

Fractile IDA curves can be used to draw fragility curves. For example if the fragility curves for the collapse state needs to be developed, at each level of IM the number of IDA curves with flat-lines (i.e., indicator of the global dynamic instability) can be counted and the corresponding probability of collapse can be simply calculated as the ratio of the number of IDA curves with flat-lines to the total number of IDA curves (i.e., the number of records caused collapse at intensities lower than chosen IM divided by the total number of records used in IDA).

For example in Fig. 2.7 the corresponding probability of failure at different IM levels (i.e., $S_a(T_1)$ is used as IM) are derived from the IDA results shown in Fig. 2.2. The fragility curves were developed for collapse and cover-spalling damage states. The cover-spalling state was defined as exceeding the drift ratio of 1.85% determined using the equations by Berry and Eberhard (2007). The fragility curves developed using IDA data are shown by dots, in which each dot represents the number of records that caused failure to the total number of records at different IM levels. In Fig. 2.7 the cumulative lognormal distribution curves developed using the median and standard deviation of the IDA results at collapse and cover-spalling limit states are also shown. As can be seen the fragility curves using IDA data can be well estimated using such curves.

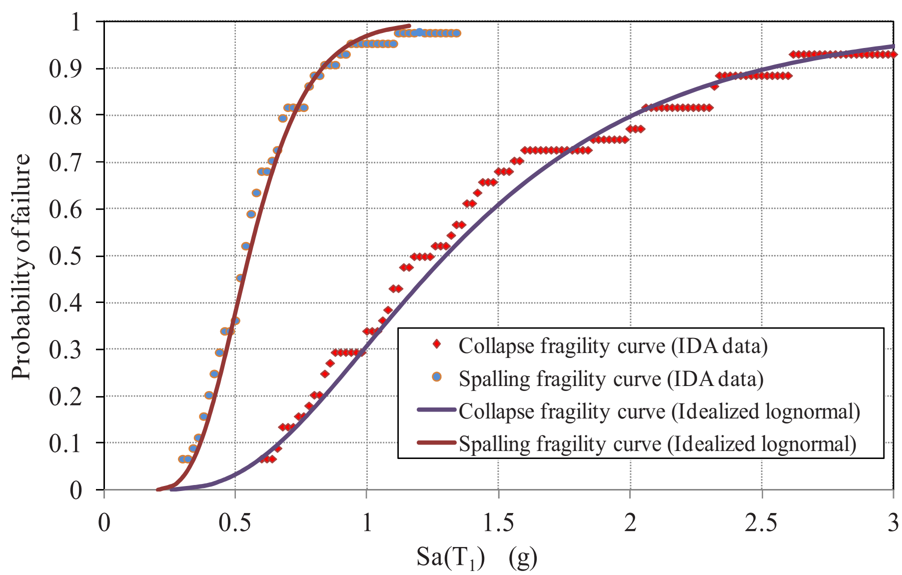

Fig. 2.7. Development of fragility curves for different limit states using IDA results

Therefore assuming that the data is lognormally distributed, it is possible to develop the fragility curves at collapse (or any other limit-state) by computing only the median collapse capacity and logarithmic standard deviation of the IDA results at collapse. The fragility curves then can be analytically computed using Eq.[2.2]:

$$[2.2] \quad P(failure \mid S_a = x) = \Phi\left(\frac{\ln(x) - \ln(Sa^{C}_{50\%})}{\beta_{RTR}}\right)$$

where $\Phi(.)$ is the cumulative normal distribution function, $S_a{}^{C}{}_{50\%}$ is the median capacity determined from IDA, and β_{RTR} is the record to record variability in the IDA results. In the IDA results only the uncertainty due to record-to-record variability has been considered. Therefore it is necessary to modify the fragility curves developed using the

IDA results to include the uncertainty due to other sources of uncertainty as discussed before (i.e, β_{DR}, β_{TD}, and β_{MDL}). Hence it is possible to inflate the fragility curves using the mean estimate approach (as discussed above) to include the total uncertainty in predictions. The modified fragility curve then can be computed using the following equation:

[2.3] $$P(failure \mid S_a = x) = \Phi\left(\frac{\ln(x) - \ln(Sa^{C}_{50\%})}{\beta_{TOT}}\right)$$

where β_{TOT} is the total uncertainty as defined by Eq. [2.1]. Uncertainty influences the shape of a fragility curve plotted from the results of IDA. Fig. 2.8 shows collapse fragility curves reflecting different levels of uncertainty (i.e., β_{TOT} = 0.4, 0.65, and 0.9). As indicated in the figure, additional uncertainty has the effect of "flattening" the curve. While the median collapse intensity is unchanged, additional uncertainty causes a large increase in the probability of collapse at the lower IM levels such as the IM level corresponding to the maximum considered earthquake (MCE).

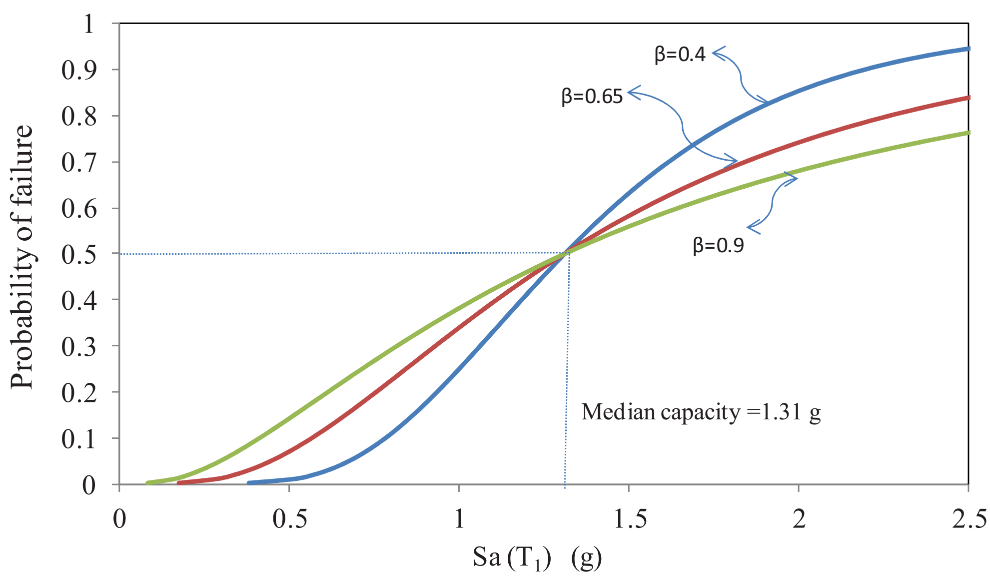

Fig. 2.8. Effect of uncertainty on the shape of fragility curves

2.9 Seismic risk assessment

Seismic risk can be expressed as the potential economic, social and environmental consequences of seismic events that may occur in a specified period of time. In order to quantify the seismic risk associated with a certain structure, one needs to combine two important elements of seismic hazard and seismic fragility analyses. Seismic hazard is in fact a description of the severity of the environment, in terms of the probability that a certain limit of seismic intensity measure, IM, is exceeded in a certain period of time, T. The determination of the seismic hazard is accomplished through using conventional probabilistic seismic hazard analysis (PSHA). An example of a seismic hazard curve in terms of mean annual frequency of exceedance developed for Vancouver (site class C) at T= 1 sec. using the updated seismic hazard data provided by Goda et al. (2010) is shown in Fig. 2.9.

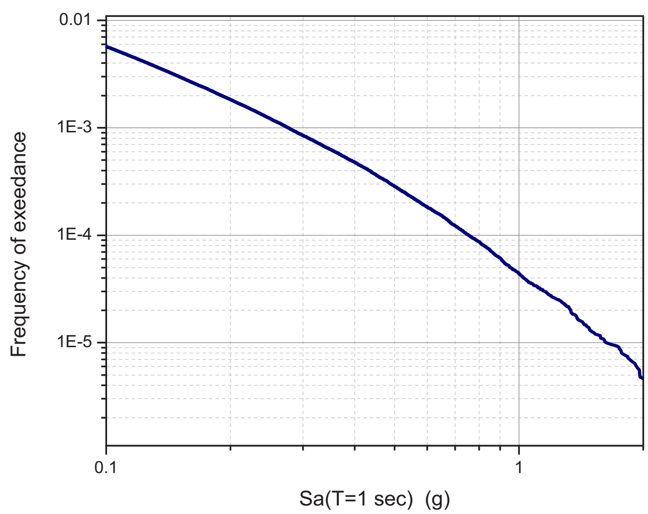

Fig. 2.9. Hazard curve for Vancouver at T=1 sec. using the updated seismic hazard data by Goda et al. (2010)

In addition to seismic hazard, the influence of the occurrence of seismic events with certain intensities on the structures should also be known. Fragility is in fact a conditional probability of exceeding a limit state, given a level of seismic hazard. The fragility analysis can be carried out either empirically using experimental studies or field observations, or analytically through nonlinear dynamic analysis (such as IDA) of the structural models. The result of the fragility analysis is often presented using fragility curves which present the probability of exceeding a certain a limit state (such as collapse, bar buckling, fracture of hoops, shear failure, etc.) as a function of the seismic intensity, IM (e.g., $S_a(T_1,5\%)$).

Once quantified, the hazard and fragility functions are combined to produce the probability of failure in a period of time, T. This is done by using the Total Probability Theorem (Benjamin and Cornell 1970), which states that, if $\{B_1,..., B_n\}$ is a set of mutually exclusive and collectively exhaustive events and A is any other event, then the probability of A can be calculated using Eq. [2.4].

$$[2.4] \quad P[A]=\sum_{i=1}^{n} P[A \mid B_i]\; P[B_i]$$

To use this result for seismic risk assessments, the seismic intensity, IM, is discretized into n distinct levels, say I_1, ..., I_n and the events A and B_i in Eq. [2.4] are taken as A =“The structure fails at least once in T” (i.e., “The structure exceeds the limit state at least once in T”) and B_i = ”IM= I_i”. Exceeding a certain limit state (which is in turn expressed as exceeding a certain damage measure, DM) is referred to as failure here. It is often reasonable to assume that the structure of interest survives in T if it does not fail under the highest seismic intensity, IM, experienced during that period of time, T (Veneziano, 2005). Under such assumption, the probability of failure in T is obtained from Eq. [2.4] as:

$$[2.5] \quad P[at\ least\ one\ failure\ in\ T]=\sum_{i=1}^{n} P[failure \mid IM = I_i]\; P[IM = I_i]$$

Eq. [2.5] shows how the hazard (probabilities P[IM= I_i]) and the fragility (the probabilities P[failure| IM= I_i]) are combined in the assessment of seismic risk. The IDA results can be used to develop the fragility curves which in turn will be used for seismic risk assessment of the structures.

In some cases, one is not interested in the physical damage to a facility, but in the consequences that such damage might have on the exposed population or the environment. The risk should in this case be measured through the probability that a consequence C (e.g., number of fatalities, repair cost, or down time) exceeds a certain level c* in T years (Veneziano, 2005). The probability that C > c* at least once in T years then can be evaluated through a second application of the total probability theorem, as follows :

$$[2.6] \quad P[C > c^*] = \sum_{j=1}^{m} P[C > c^* \mid D = d_j] P[D = d_j]$$

where d_1,..., d_m are m discretized levels of damage D. The probabilities $P[D = d_j]$ are evaluated through repeated application of Eq. [2.5], each time defining “failure” as the event $D = d_j$, this will result in Eq. [2.7].

$$[2.7] \quad P[C > c^*] = \sum_{j=1}^{m} \sum_{i=1}^{n} P[C > c^* \mid D = d_j] \; P[D = d_j \mid IM = I_i] \;\; P[IM = I_i]$$

Whereas the probabilities $P[C > c^* | D = d_j]$ are the result of a consequence model. This is also known as the loss or performance model and the parameter C is also known as the decision variable, DV, in the framing equation adopted by the Pacific Earthquake Engineering Center (Cornell and Krawinkler, 2000) as will be discussed later.

In case the level of damage, d_j, is expressed in terms of drift ratios, the (annual) probability of exceeding a drift level d_j, $\lambda (d_j)$, can be calculated using Eq. [2.8]. $\lambda (d_j)$ is also known as the drift hazard curve (or demand hazard curves in general).

$$[2.8] \quad \lambda(d_j) = \sum_{i=1}^{n} P[D > d_j \mid IM = I_i] \; P[IM = I_i]$$

In continuous, integral form Eq. [2.8] is expressed as :

$$[2.9] \quad \lambda(d) = \int_{IM=0}^{IM=+\infty} P[D > d \mid IM] \; |d\lambda(IM)|$$

To compute P_{PL} , the (annual) probability of the performance level not being met (e.g., the annual probability of collapse), P[C > c*|D = d_j] in Eq. [2.7] will be the probability that the drift capacity at limit state, D^c, is less than some level of D, which can be expressed by P[D≥D^c|D=d_j]. The term P[D ≥ D^c| D = d_j] can to a first approximation be assumed to be independent of the information about the drift level itself (Cornell et al. 2002), so that this term can be written as P[D ≥ D^c |D = d_j]= P[d_j ≥ D^c]. Therefore to determine P_{PL}, Eq. [2.7] can be rewritten as Eq.[2.10]:

$$[2.10] \quad P_{PL} = \sum_{j=1}^{m}\sum_{i=1}^{n} P[d_j \geq D^C] \; P[D = d_j \mid IM = I_i] \; P[IM = I_i]$$

From Eq. [2.8] we have $P[D = d_j \mid IM = I_i] \; P[IM = I_i] = \left|\lambda(d_j) - \lambda(d_{j-1})\right|$ and therefore:

$$[2.11] \quad P_{PL} = \sum_{j=1}^{m}\sum_{i=1}^{n} P[\mathrm{d_j} \geq D^C] \; \left|\lambda(d_j) - \lambda(d_{j-1})\right|$$

In continuous, integral form Eq. [2.11] is expressed as:

$$[2.12\,] \quad P_{PL} = \int_{d=0}^{d=+\infty} P[d \geq D^C] \; |d\lambda(d)|$$

2.10 Framework for performance-based earthquake engineering (PBEE)

The power of IDA as an analysis method is put to use well in a probabilistic framework, where the estimation of the annual likelihood of the event that the demand exceeds the limit-state or capacity is required. This is the likelihood of exceeding a certain limit-state, or of failing a performance level, within a given period of time. The concepts and equations presented before can be generalized in a framing equation adopted by the Pacific Earthquake Engineering Center (Cornell and Krawinkler, 2000), given in Eq. [2.13].

[2.13] $$\lambda(DV) = \int\int G(DV \mid DM)\, |dG(DM \mid IM)|\; |d\lambda(IM)|$$

Where in this equation IM, DM and DV are vectors of intensity measures, damage measures and "decision variables" (such as the annual earthquake loss and/or the exceedance of one or more limit states), respectively. G(DV|DM) is the probability that the (vector of) decision variable(s) exceed specified values given that the engineering damage measures are equal to particular values. This term is in fact equivalent to the term $P[C > c^* | D = d_j]$ in Eq. [2.7]. λ (IM) is the conventional hazard curve (i.e. the mean annual frequency of IM exceeding a certain value) and $d\lambda$ (IM) is equivalent to $P[IM= I_i]$ in Eq. [2.7] presented before. Further, G(DM|IM) is the probability that the Damage Measure(s) exceed certain values (corresponding to certain limit states) given that the Intensity Measure(s) equal particular values .Therefore dG(DM|IM) is the differential of the complementary cumulative distribution function (CCDF) of DM given IM. This term is equivalent to the term $P[D=d_j| IM= I_i]$ in Eq. [2.7].

Examples of G(DV|DM) when the DV is a binary damage state indicator variable (i.e., the decision variable is simply a scalar "indicator variable": DV=1 if the limit-state is exceeded and zero otherwise) are various "fragility curves" and λ(DV) is the expected annual loss in this case .

The term |dG(DM|IM) | is in fact obtained from the statistical characterization of the IDA curves. Therefore the IDA produces precisely the information needed both for PBEE demand characterization and for global collapse capacity characterization (Vamvatsikos and Cornell, 2002).

When DV is an indicator variable, λ(DV) in Eq. [2.13] is simply the mean annual frequency of exceeding a limit state (i.e., annual loss). Generally the prediction of λ(DV) can be carried out using either a DM-based approach or IM-based approach. In the DM-based approach an intermediate variable DM is used (e.g., in Eq. [2.13]) so that the total annual loss can be de-coupled into different damage state terms (Jalayer and Cornell, 2003). It is convenient to express the extent of damage and the associated financial loss in terms of DM, which makes the use of DM as an intermediate variable in Eq. [2.13] very useful. For example, where the predictions of the total financial loss are required, such predictions can be provided for different damage states separately and the total financial risk associated to the structure can then be estimated by summing the financial losses for all damage states. For instance, the recommended loss ratios by Dhakal and Mander (2006) for different damage states (DS) as defined by HAZUS (1999) are presented in Table 2.4. The loss ratio is defined as the ratio of the cost of repair or retrofit/strengthening needed to restore the functionality of the bridge to the total replacement cost.

Table 2.4. Loss ratio for different damage states (Dhakal and Mander, 2006)

Damage state	DS1	DS2	DS3	DS4	DS5
Assumed	0	0.1	0.3	1	1
Range	0	0.05-0.15	0.2-0.4	1.0-1.2	1

If the intermediate variable DM is integrated out, Eq. [2.13] can be rewritten as Eq. [2.14] in an IM-based format.

[2.14] $$\lambda(DV) = \int G(DV \mid IM) \, | d\lambda(IM) |$$

For example in the case that DV is an indicator variable, the mean annual frequency of exceeding a limit state λ_{LS} can be computed from Eq. [2.15] as:

$$[2.15] \qquad \lambda_{LS} = \lambda(DV = 1) = \int G(IM > IM^{C} \mid IM) \, |d\lambda(IM)|$$

where DV=1 when the demand IM exceed capacity in terms of IM, IM^C. The first term in Eq. [2.15] is in fact the probability that the capacity IM^C is less than some level of IM, which is equal to CDF of IM^C (i.e., $F(IM^C|IM)$). Eq. [2.15] can then be rewritten as:

$$[2.16] \quad \lambda_{LS} = \int_{IM=0}^{IM=+\infty} F(IM^{C} \mid IM) \left| \frac{d\lambda(IM)}{dIM} \right| dIM$$

$F(IM^C|IM)$ is in fact the fragility curve developed for the capacity of the structure in terms of IM corresponding to a certain limit-state. For example in the case of the collapse limit state, the IM^C for each IDA curve is the collapse capacity, which is defined as the IM at which the curves become flat (i.e., global dynamic instability of the structure). Therefore $F(IM^C|IM)$ function can be predicted using IDA results, which is exactly the percentile IDA curves developed in terms of IM. An example of the fragility curves developed for collapse and spalling damage states are presented in Fig. 2.7.

Using integration by parts it can be shown that Eq. [2.16] can also be rewritten as Eq. [2.17]:

$$[2.17] \quad \lambda_{LS} = \int_{IM=0}^{IM=+\infty} f(IM^{C} \mid IM) \lambda(IM) dIM$$

where $f(IM^C|IM)$ is the probability density function of capacity in terms of IM and $\lambda(IM)$ is the conventional hazard curve. This can be numerically computed by Eq. [2.18] using the fragility and hazard curves. Where in Eq. [2.18], F_R is the fragility function developed for a damage state (e.g., cover-spalling, or collapse) and spectral acceleration, S_a, is used as intensity measure, IM.

$$\lambda_{LS} = \sum_{All\ S_{a_i}} [F_R(S_{a_i}) - F_R(S_{a_{i-1}})]\lambda(S_{a_i}) \qquad [2.18]$$

On the other hand, if some reasonable approximations can be made, Eq. [2.16] can be analytically integrated (Shome and Cornell 1999, Cornell et al. 2002). It is only needed to assume that the IM-values of capacity are lognormally distributed and that the IM-hazard curve can be approximated by fitting a straight line in the log-log space, $\lambda\ (\mathrm{IM}) = k_0 \mathrm{IM}^{-k}$, either by a global regression, same for all limit-states, or by a local fit at the median IM-capacity for each limit-state (Vamvatsikos and Cornell 2004). Based on these assumptions the integration in Eq. [2.16] will result in Eq. [2.19]:

$$\lambda_{LS} = \lambda(IM^{C}_{50\%}).\exp\left(\frac{1}{2}(k\ S_{\ln IM^C})^2\right) \qquad [2.19]$$

where $S_{\ln IM^C} = (\ln IM^C_{50\%} - \ln IM^C_{16\%})$ is (approximately) the standard deviation of the natural logarithm of the IM-capacity and $IM^C_{x\%}$ is the x% percentile of the capacity (in terms of IM) derived from the fractile IDA curves.

2.11 Ground motion prediction equations

A ground motion prediction equation (GMPE) (also known as the attenuation function) is referred to a statistical model which estimates the mean and variance of ground shaking with distance from an earthquake source. Such equations are often developed separately for different tectonic regions (e.g., shallow crustal regions, subduction zones, etc.).

Different GMPEs may require different parameter to estimate the ground motion intensity at a site of interest. Such parameters basically include earthquake magnitude, distance and site condition (e.g., rock, soft soil). The soil type is considered more explicitly using the average shear wave velocity, V_{s30}, in modern GMPEs. More sophisticated GMPEs require more complex and detailed parameters including the fault type and mechanisms, different measures for distance (such as Joyner-Boore distance ,R_{jb}, closest distance from the site to the ruptured area, R_{rup}, etc.), aftershock or main shock, site on hanging wall or foot wall, fault rupture width and length, hypocentral depth, etc. For crustal earthquakes such information for different records are available from the PEER-NGA database at http://peer.berkeley.edu/nga/flatfile.html. Such data can be used to estimate the mean and variance of the ground motion intensity of the records at a site with a specific distance and soil condition using the selected GMPEs. These mean and variance values are also used to predict the epsilon, ε, parameter. Epsilon is an important characteristic of a ground motion which is used in the record selection and prediction of the spectral shapes.

The list of GMPEs used by the Geological Survey of Canada (GSC) and the updated model by Goda et al.(2010) are given by Atkinson and Goda (2011) which is summarized in Table 2.5. More details about the seismic hazard results and the program developed to extract the deaggregation of the seismic hazard are discussed in Appendix C.

Table 2.5. Summary of the adopted ground motion prediction equations (GMPE) (Table adapted from Atkinson and Goda, 2011)

Earthquake type	Source	Variable	Seismic hazard model implementation: Weight
Shallow crustal earthquakes in eastern Canada	***AB95*** : Atkinson and Boore (1995)	**M**, r_{hypo}, NEHRP site class A	GSC 1995 model: [***AB95*** (1.0)]
	SGD02 : Silva *et al*. (2002)	**M**, r_{jb}, NEHRP	Updated model: [***SDG02*** (0.2) , ***C03*** (0.3), ***AB06*** (0.4) , ***A08*** (0.1)]
	C03 : Campbell (2003)	**M**, r_{rup}, NEHRP site class A	
	AB06 : Atkinson and Boore (2006)	**M**, r_{rup}, V_{s30}, stress drop	
	A08 : Atkinson (2008)	**M**, r_{jb}, V_{s30}	
Shallow crustal earthquakes in western Canada	***BJF97*** : Boore *et al*. (1997)	**M**, r_{jb}, V_{s30}	GSC 1995 model: [***BJF97*** (1.0)]
	A05 : Atkinson (2005)	**M**, r_{rup}, V_{s30}	Updated model: [***A05*** (0.25), ***HG07*** (0.25), ***BA08*** (0.5)]
	HG07 : Hong and Goda (2007)	**M**, r_{jb}, V_{s30}	
	BA08 : Boore and Atkinson (2008)	**M**, r_{jb}, V_{s30}	
Inslab earthquakes in the Cascadia subduction zone	***YCSH97*** : Youngs *et al*. (1997)	**M**, r_{rup}, H, NEHRP site class	GSC 1995 model: [***YCSH97*** (1.0)]
	AB03 : Atkinson and Boore (2003)	**M**, r_{rup}, H, V_{s30}	Updated model: [***AB03*** (0.6) , ***Z06*** (0.2), ***GA09*** (0.2)]
	Z06 : Zhao *et al*. (2006)	**M**, r_{rup}, H, V_{s30}	
	GA09 : Goda and Atkinson (2009)	**M**, r_{rup}, H, V_{s30}	
Interface earthquakes in the Cascadia subduction zone	***YCSH97*** : Youngs *et al*. (1997)	**M**, r_{rup}, H, NEHRP site class	GSC 1995 model: [***YCSH97*** (1.0)]
	GSWY02 : Gregor *et al*. (2002)	**M**, r_{rup}, NEHRP site class C or D	Updated model: [***GSWY02*** (0.25), ***AB03*** (0.25) , ***Z06*** (0.25), ***AM09*** (0.25)]
	AB03 : Atkinson and Boore (2003)	**M**, r_{rup}, H, V_{s30}	
	Z06 : Zhao *et al*. (2006)	**M**, r_{rup}, H, V_{s30}	
	AM09 : Atkinson and Macias (2009)	**M**, r_{rup}, V_{s30}	

2.12 Record selection for IDA

2.12.1 Spectral shapes of the records and epsilon values

The spectral shapes of the records are especially important for collapse assessments which can change the calculated collapse capacity of the structures by 70% (Baker and Cornell 2006a, Haselton and Baker 2006, Zareian 2006). Therefore neglecting the influence of the spectral shapes in collapse assessment of the structures using IDA can result in very conservative and biased predictions.

It has been shown that $\varepsilon(T_1)$ (i.e., epsilon value of the ground motion record at the fundamental period) is a proxy of spectral shape (Baker and Cornell, 2006a). As the epsilon value increases, the spectral shapes tend to be more peaked (e.g., see Fig. 2.11). Epsilon, ε, is computed by subtracting the mean predicted ln $S_a(T)$, from the record's ln $S_a(T)$, and dividing by the logarithmic standard deviation (as estimated by the ground motion prediction equation). This is given by Eq. [2.20]:

$$[2.20] \quad \varepsilon(T) = \frac{\ln S_a(T) - \mu_{\ln S_a}(M, R, T)}{\sigma_{\ln S_a}(T)}$$

where $\mu_{\ln Sa}(M,R,T)$ and $\sigma_{\ln S_a}(T)$ are the predicted mean and standard deviation, respectively, of ln S_a at given period and ln $S_a(T)$ is the log of the spectral acceleration of interest. The first two parameters are computed using ground motion prediction equations (GMPE) which are also known as attenuation models. An example of the epsilon values computed for the case of the Imperial Valley (1979) record is shown in Fig. 2.10.

Rare ground motions that can cause modern structures to collapse have peaked spectral shapes that can be represented by positive epsilon values at the fundamental period , $\varepsilon(T_1)$. This peaked spectral shape is much different than a standard uniform hazard spectral shape and accounting for this has been shown to increase the computed collapse capacity significantly. The values of spectral acceleration at the longer periods are important, because the effective period of the structure increases as the structure undergoes inelastic deformation. This is even more important for the modern structures that have high ductility capacities and are designed for high inelastic demands. Similarly the values of spectral acceleration at shorter periods are also important especially for structures with significant contributions of higher modes in the seismic response.

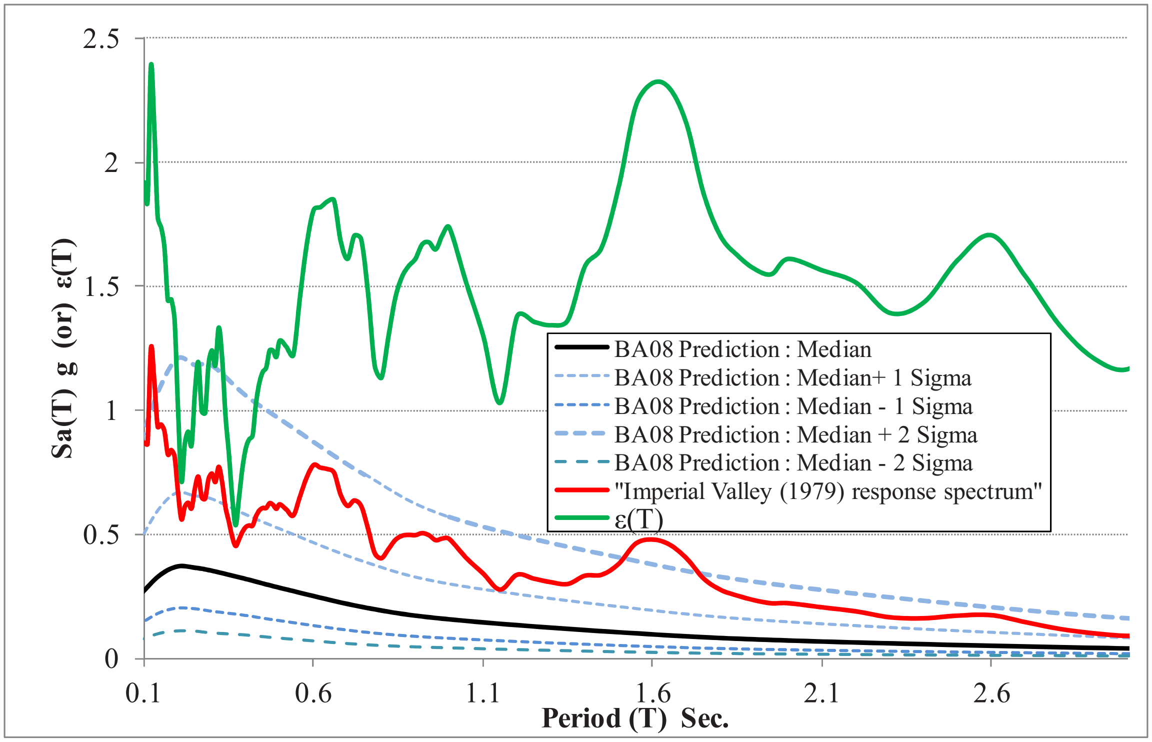

Fig. 2.10. An example of ε values computed for the case of Imperial Valley (1979) record using BA08 GMPE

The most direct approach to account for spectral shape in structural analysis is to select ground motions with $\varepsilon(T_1)$ values similar to ε values obtained from seismic hazard deaggregation analysis for the site and hazard level of interest. An alternative approach is to use an intensity measure (IM) other than $S_a(T_1)$ that accounts for spectral shape, if epsilon values are not considered in the record selection and analysis. Such intensity measures include inelastic spectral displacement or S_a values averaged over a period range (Backer and Cornell 2006 and 2008). However the use of these intensity measures are not common, while $S_a(T_1)$ intensity measure is widely used to describe the seismic hazard.

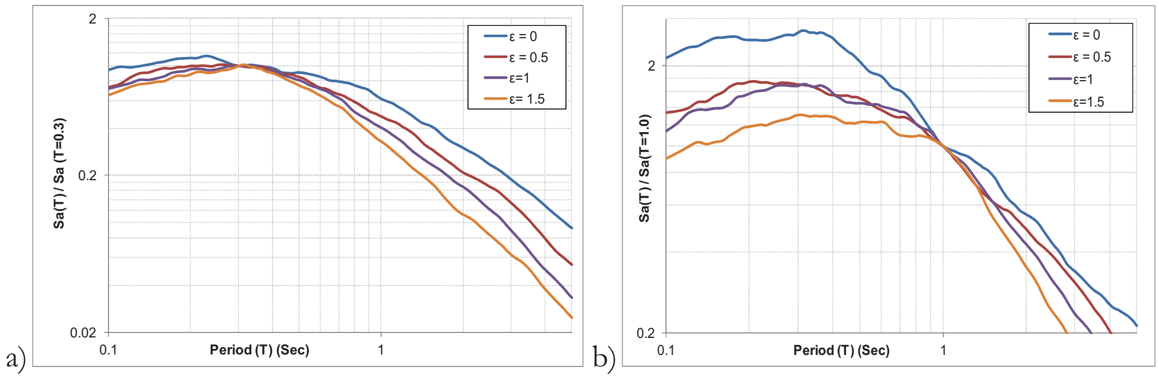

Fig. 2.11. The normalized average response spectra of crustal ground motion records for different ε values at a) T=0.3 sec and b) T=1 sec.

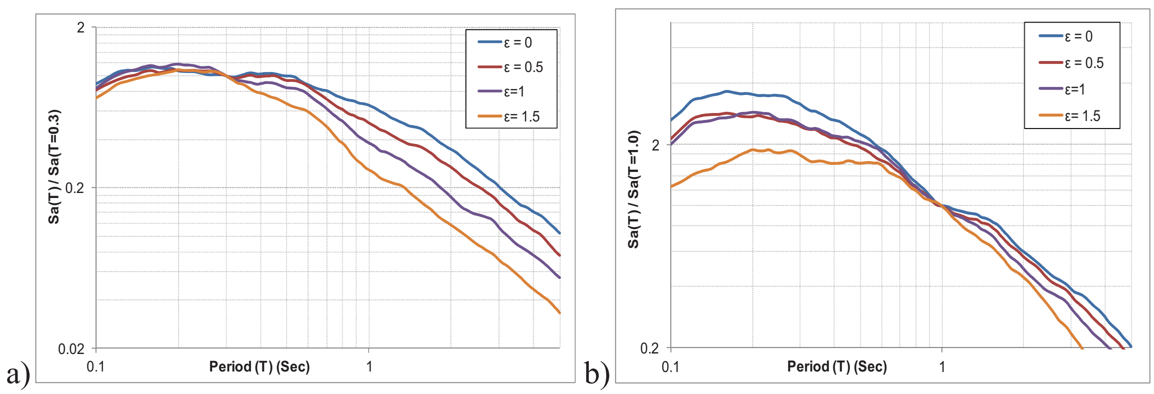

Fig. 2.12. The normalized average response spectra of interface ground motion records for different ε values at a) T=0.3 sec and b) T=1 sec.

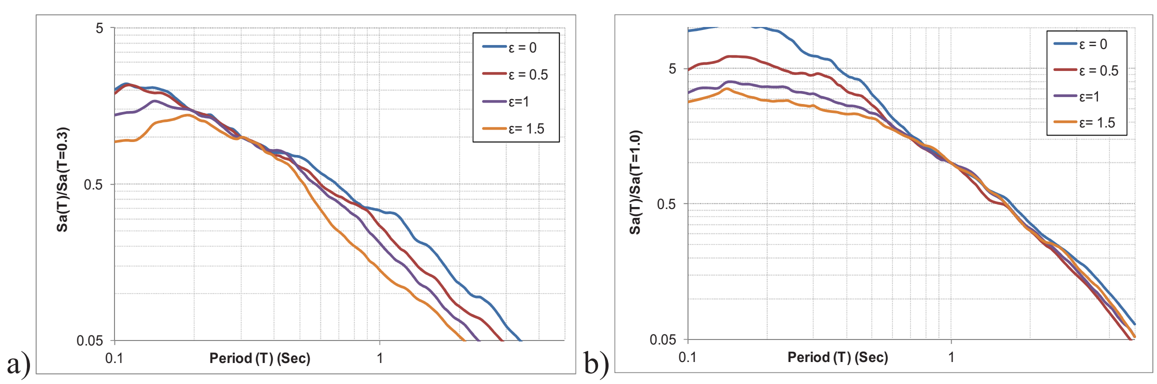

Fig. 2.13. The normalized average response spectra of inslab ground motion records for different ε values at a) T=0.3 sec and b) T=1 sec.

In Fig. 2.11 to 2.14 the influence of the ε values on the average spectral shape of the records are demonstrated. The average geometric mean response spectra of 50 ground motion records (22 records for the case of inslab events) with average $\varepsilon(T_1)$ values similar to the target epsilon values were used to develop these graphs. Such curves are presented for two different periods of T=0.3 sec and T=1 sec. As can be seen, as the ε values increase the resulting average response spectra of the records become more peaked. For crustal and interface events this issue is observed for both cases of T=0.3 sec and T=1 sec. However in the case of inslab events it was found that in longer periods the spectral shapes are insensitive to the epsilon values, as can be seen in Fig. 2.13b. This may be primarily due to weak frequency content of such events in longer periods.

2.12.2 Record selection strategies

Record selection for inelastic time history analysis is a critical issue and many different methods have been developed and used for this purpose. This subject is even more important for the case of Incremental Dynamic Analysis (IDA) and collapse capacity evaluation of structures. It has been demonstrated that the record selection methodology has an important influence on the IDA results (Tehrani et al., 2012).

A realistic record selection strategy should take into account important characteristics of the ground motion records which influence the structural response. Such important aspects of records mainly include the magnitude, M, distance, R, ε, and site conditions. Due to the limited number of natural records available, selecting ground motions with similar M, R, and ε values to match target values obtained through seismic deaggregation is very difficult, if not impossible. Therefore usually one or two of these parameters are chosen as key parameters for record selection. Accordingly different potential record selection methodologies may be utilized.

1-UHS-Based approach:

The simplest method for record selection is to choose the records such that their response spectra match a target uniform hazard spectrum (UHS) over a range of periods. The seed records used in this method can be either artificial, natural, or manipulated natural records. Artificial records can be generated using some available software to match a UHS. Alternatively, natural records can be manipulated by changing the frequency content, so that the response spectra of the records match a target UHS. Scaled natural records that are matched to a target UHS over a range of periods are often recommended by some codes. This range must include the important modes of the structure as well as the effects of period elongation due to inelastic deformation of the structure. A period range of $0.2T_1$ to $2T_1$ (where T_1 is the fundamental vibration period of a structure) is usually recommended and used for this purpose. This range is similar to the $0.2T_1$ to $1.5T_1$ range specified by ASCE 7-05 (ASCE, 2005), but statistical studies suggest that nonlinear structures are often sensitive to response spectra at periods longer than $1.5T_1$ (Baker and Cornell 2008, Haselton and Baker 2006, and Vamvatsikos and Cornell 2005).

Although conceptually simple, these methods for record selection are deemed to be conservative, particularly when ultimate performance limits of a structure (such as bar buckling, fracture, collapse, etc.) are the primary objective of the analysis. This is because the response spectra of the records are forced to match a target UHS, such as that specified in the National Building Code of Canada (NBCC, 2010). The UHS is a composite of predicted responses at different periods, and may not be representative of individual ground motion spectra. Furthermore, the UHS tends to be dominated at any individual period by motions above the median, whereas individual spectra are unlikely to be equally above-median at all periods. That is, often no natural record can be found to match the UHS over a wide period range and hence the analysis results using UHS-matched records may be conservatively unrealistic and biased. To solve these problems, the use of the Conditional Mean Spectrum (CMS) in lieu of the UHS has been recommended in recent years (Baker, 2011).

2-MR-based record selection:

In this method the records with the closest magnitude, M, and distance, R, to the mean magnitude and mean distance obtained from the seismic deaggregations are chosen. A difference of one unit in magnitude may be treated as equivalent to a difference of 40 km in distance (Baker and Cornell, 2006a). For the records selected based on magnitude and distance, it has been shown that inclusion of the parameter ε in a vector IM results in reduced estimates of structural response relative to the estimates obtained with the scalar IM $S_a(T_1)$.This indicates that response predictions obtained using the MR-based record selection approach are biased when $S_a(T_1)$ is used as IM.

3-Epsilon-based record selection:
The record property ε at the fundamental period of the structure, $\varepsilon(T_1)$, is an important property to match when selecting ground motions for analysis, where the ground motion intensity is measured using $S_a(T_1)$. The value of $\varepsilon(T_1)$ is in fact a proxy for spectral shape, and it has been demonstrated that selecting records with similar epsilon values to mean epsilon values obtained from the seismic hazard deaggregation can result in a more realistic prediction of seismic responses, especially at ultimate performance levels including collapse where the spectral shape effects are more prominent.

4-CMS-based record selection:
The CMS-based record selection strategy is the only method that can take into account the influence of all three ground motion parameters (i.e., M, R, and ε) in record selection. The idea is to predict the expected spectral shape of the records with magnitude, distance and ε values equal to the target values obtained from the seismic deaggregation. After predicting the target spectral shape, the records with similar spectral shape over a range of period of interest (usually $0.2T_1$ to $2T_1$) will be selected, while no strict criteria on M, R and ε are imposed. In another words, the records with spectral shapes matching the CMS for a given M, R and ε will be accurate predictors of structural response, regardless of their actual M, R, and ε values (Baker and Cornell, 2006a). This method will be discussed more in the next section.

A study by Baker and Cornell (2005) suggests that the records selected based on ε or CMS can also be scaled without resulting in biased predictions, unlike other methods such as UHS-based or M-R-based record selection. These observations can be explained by the idea that spectral shape (i.e., spectral acceleration values at other periods, given S_a

at T_1) is the record property that directly affects seismic response of structures, whereas magnitude, distance and ε are proxies for spectral shape (and ε is a more important proxy) (Backer and Cornell, 2006).

2.12.3 Conditional mean spectrum (CMS)

The CMS provides the expected response spectrum, conditioned on occurrence of a target spectral acceleration value at the period of interest. It has been found that the CMS can be used as an appropriate target response spectrum for selecting ground motions as input for dynamic analysis (Baker, 2011). In the development of a CMS, some important aspect of records including magnitude (M), distance (R), and epsilon (epsilon, ε, is defined as the number of logarithmic standard deviations of a target ground motion from a median ground motion prediction equation (GMPE) for a given M and R) will be considered from the deaggregation of the seismic hazard. Baker (2011) proposed a method for calculating the CMS, given by Eq. [2.21]:

[2.21] $$\mu_{\ln S_a(T_i)|\ln S_a(T_n)} = \mu_{\ln S_a}(\overline{M},\overline{R},T_i) + \rho(T_i,T_n)\overline{\varepsilon}(T_n)\sigma_{\ln S_a}(T_i)$$

where an appropriate ground motion prediction equation (GMPE) must be used to evaluate the mean and standard deviation of the natural logarithm of the spectral acceleration at the vibration period T_i denoted by $\mu_{\ln S_a}(\overline{M},\overline{R},T_i)$ and $\sigma_{\ln S_a}(T_i)$, respectively, in which $\overline{M}$, $\overline{R}$, and $\overline{\varepsilon}(T_n)$ are the mean magnitude, mean distance and mean value of epsilon at the considered period T_n, respectively. These mean values are calculated from the seismic hazard deaggregation and $\rho(T_i,T_n)$ is the inter-period correlation of spectral accelerations at vibration periods T_i and T_n. The equation proposed by Baker and Cornell (2006b), Eq.[2.22], is used to calculate this inter-period correlation.

$$[2.22] \quad \rho(T_{n1},T_{n2}) = 1-\cos\left(\frac{\pi}{2}-\left[0.359+0.163\ I_{T_{min<0.189}} \ln\frac{T_{min}}{0.189}\right]\ln\frac{T_{max}}{T_{min}}\right.$$

Where T_{max} and T_{min} are the larger and the smaller of T_{n1} and T_{n2}, respectively, and $I_{T_{min<0.189}}$ is an indicator function that equals one if T_{min} is less than 0.189 sec and equals zero otherwise.

For measuring the match with the target spectrum sum of squared errors (SSE) between the logarithms of the ground motion's spectrum and the target spectrum (Eq. [2.23]) is used as recommended by Baker (2011).

$$[2.23] \quad SSE = \sum_{j=1}^{n} (\ln Sa(T_j) - \ln Sa_{CMS}(T_j))^2$$

Where ln $S_a(T_j)$ is the log spectral acceleration of the ground motion at period T_j and ln $S_{aCMS}(T_j)$ is the log CMS value at period T_j . Therefore the values of SSE will be computed for all records considered and the records with the smallest SSE values will be selected. This approach is more effective if ground motion scaling is also allowed. To scale the ground motions, Baker (2011) recommends scaling each ground motion so that its spectral acceleration at the considered period, $S_a(T_1)$, matches the target spectral acceleration from the CMS, $S_{aCMS}(T_1)$. Although the concept of scaling the records is sometimes questioned, it has been observed that ground motions selected and scaled to match the CMS produce displacements that are comparable to displacements produced by unscaled ground motions, unlike scaling procedures using other methods (Baker and Cornell, 2005 and Luco and Bazzurro, 2007). Thus the scaling procedure outlined by Baker (2011) is not expected to adversely impact the resulting structural responses.

A complicated aspect in constructing a CMS for a site in south-western British Columbia, in comparison with a site in California, is that three earthquake types, having distinctly different characteristics, contribute to the overall seismic hazard. Therefore, three CMS must be constructed for record selection (Goda and Atkinson, 2011), "CMS-Crustal", “CMS-Interface”, and “CMS-Inslab”. In order to account for these events, two sets of CMS can be considered as proposed by Goda and Atkinson (2011). The first approach is the CMS-Event-based procedure which is based on the weighted average of the CMS that are computed by using applicable GMPEs and the corresponding scenarios for the three earthquake types, in proportion to the relative influences of the scenarios (i.e., the number of records from each event type is proportional to the percentage of contribution of that event type in seismic hazard). The second approach is the “CMS-All-based” which is the weighted average of “CMS-Crustal”, “CMS-Interface”, and “CMS-Inslab” by considering relative influences of the individual earthquake types without considering different earthquake type records in the selection procedure. In fact “CMS-All-based” is the simplified version of CMS-Event-based in which different event types are considered in the construction of the CMS, but in selecting the records the relative influences of the scenarios are not considered. This results in variability of the seismic response based on the “CMS-All-based” approach being smaller than that based on the “CMS-Event-based” approach. However, it must be noted that for each earthquake type, the variability of the selected records in general tends to be underestimated for CMS-based or UHS-based approaches, since a close match to a target response spectrum is imposed (Baker, 2011). Nevertheless, the “CMS-Event-based” approach can account for the variability of the CMS among different event types more reasonably than does the “CMS-All-based” approach.

2.12.4 Simplified method to include the spectral shape effects

The direct use of the epsilon-based method to account for the spectral shape of the ground motion records is often time-consuming and complicated in practice. A simplified method has been developed by Haselton et al. (2011) to modify the collapse capacity predictions for the effects of epsilon and spectral shapes. For this purpose, a fixed set of records can be used to perform the incremental dynamic analyses. The predicted capacities obtained using the IDA will then be modified for the effects of spectral shapes using a spectral shape factor (SSF). To compute the SSF a regression analysis needs to be carried out to derive a relationship between the natural logarithm of the collapse capacities versus the epsilon (T_1) values for each record. The result of such a regression analysis can be presented in the form of $\ln[S_C] = \beta_0 + \beta_1\varepsilon$. Where the S_C is the collapse capacity (at the fundamental period) , β_0 is the average collapse capacity when $\varepsilon = 0$, and β_1 indicates how sensitive the collapse capacity (S_C) is to changes in the ε value. The SSF is then calculated using Eq. [2.24].

$$[2.24] \quad SSF = \exp[\beta_1(\bar{\varepsilon}_0(T) - \bar{\varepsilon}(T)_{records})]$$

where $\bar{\varepsilon}(T)_{records}$ is the mean epsilon of the records and $\bar{\varepsilon}_0(T)$ is the mean epsilon value from the seismic deaggregation. The probability of exceedance of 0.5% in 50 years is recommended by ATC-63 to calculate mean epsilon values for ductile structures. As an example the β_1 factor was computed as 0.317 for a case study using a linear regression analysis as shown in Fig. 2.14.

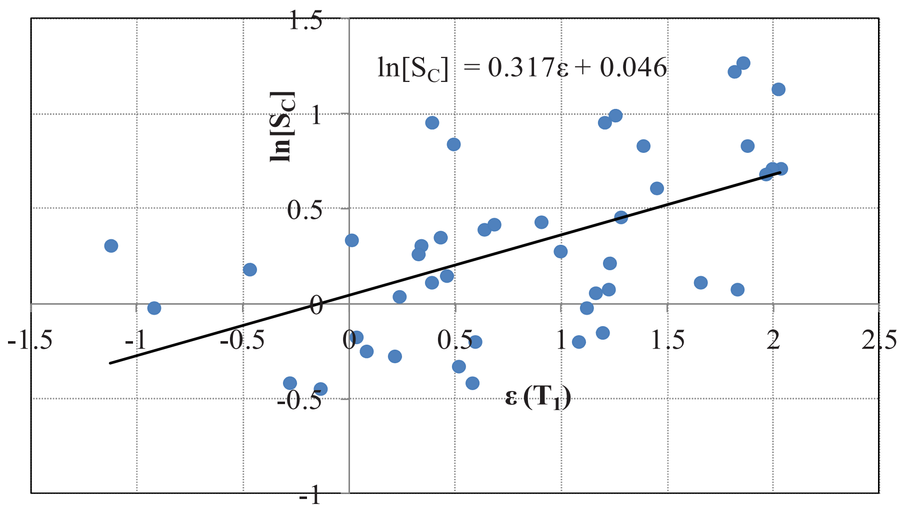

Fig. 2.14. An example of the regression analysis to determine the β_1 factor

2.13 Evaluation of the seismic performance

The IDA results can be used to evaluate the seismic performance of structures. In the ATC-63 provisions the probability of collapse at the maximum considered earthquake level (MCE) is used for this purpose. The probability of collapse at MCE level, which usually corresponds to 2% probability of exceedance in 50 years, should be reasonably low. The probability of collapse at this seismic excitation level is typically limited to 10% (and to 20% for a few cases) (ATC, 2008). These limits are currently based on judgement and accordingly different limits on the maximum probability of collapse may be accepted for different types of structures and the importance of the structure.

Eq.[2.3] can be used to estimate the probability of collapse at MCE level. Replacing x in Eq.[2.3] by the spectral acceleration at the fundamental period of the structure at the MCE level, Sa_{MCE}, the probability of collapse can be estimated using Eq. [2.25].

$$[2.25] \quad P(failure \mid Sa = Sa_{MCE}) = \Phi\left(\frac{\ln(Sa_{MCE}) - \ln(Sa_{50\%}^{C})}{\beta_{TOT}}\right) = \Phi\left(\frac{-\ln(\frac{Sa_{50\%}^{C}}{Sa_{MCE}})}{\beta_{TOT}}\right)$$

The ratio of the median collapse capacity of the structure (in terms of spectral acceleration at the fundamental period of the structure), $Sa_{50\%}^{C}$, to the spectral acceleration at MCE level (i.e., Sa (T_1) for 2% probability of exceedance in 50 years given by seismic design codes), Sa_{MCE}, is defined as the collapse margin ratio (CMR). Therefore using the values of CMR and β_{TOT}, which are determined from the IDA results, the probability of collapse at MCE level can be estimated using Eq.[2.26]. The seismic performance of a structure is satisfactory if the estimated probability of collapse is acceptable (e.g., typically less than about 10%).

$$[2.26] \quad \mathrm{P}(collapse\ at\ MCE\ level) = \Phi\left(\frac{-\ln(CMR)}{\beta_{TOT}}\right) \qquad (CMR = \frac{Sa_{50\%}^{C}}{Sa_{MCE}})$$

The fragility curves derived from the IDA results can also be combined with the seismic hazard analysis to predict the seismic risk and the total probability of collapse (i.e., mean annual rate of collapse) as discussed before.

References:

Please see the last section

3 Effects of Column and Superstructure Stiffness on the Seismic Response of Bridges in the Transverse Direction

Payam Tehrani[1] **and Denis Mitchell**[1]

3.1 Preface

The significance and problems regarding bridges with different column heights and stiffnesses are discussed in Chapter 1 and Appendix A. This chapter describes a parametric study on a wide range of bridges with different column and superstructure properties to investigate the safety of bridges designed based on the CHBDC provisions and to investigate whether the use of linear analysis methods is appropriate for the prediction of the seismic response of bridges with different column stiffnesses. Verification of the computer models and preliminary results and other modelling details are presented in Appendix A. The computer program developed for the parametric studies is discussed in Appendix B.

This chapter was summarized into a manuscript: Tehrani, P. and Mitchell, D. " Effects of Column and Superstructure Stiffness on the Seismic Response of Bridges in the Transverse Direction", Canadian Journal of Civil Engineering, Manuscript 2011-0516, accepted in March 2012.

Some parts of the manuscript including the introduction, literature review and the definition of some regularity indices were also presented in Chapter 1. However these parts were not removed from the manuscript to maintain its integrity and consistency.

---

[1] McGill University, Department of Civil Engineering, 817 Sherbrooke St. West, Montreal QC H3A 2K6

According to the NRC Research Press policies, the authors retain the right to "reuse all or part of their manuscript in other works created by them for non-commercial purposes". (http://www.nrcresearchpress.com/page/authors/information/rights)

3.2 Abstract

The transverse seismic responses of continuous 4-span bridges designed based on the 2006 Canadian Highway Bridge Design Code were studied using inelastic time history analyses. A total of 648 bridge configurations were considered in which the column heights, column diameters, superstructure stiffness and mass as well as abutment restraint conditions were studied. The maximum ductility demands obtained using elastic and inelastic analyses were compared to study the influence of the degree of irregularity. The effects of column stiffness ratios and superstructure to substructure stiffness ratios on the maximum ductility demands and concentration of ductility demands were investigated. A number of different regularity indices were compared to determine the suitability of these different indices in predicting the influence of irregularity. This study demonstrates the conservative nature of the 2006 Canadian Highway Bridge Design Code and provides some guidance on factors for determining the degree of irregularity and suitable regularity indices when carrying out non-linear dynamic analyses of bridges.

Key words: Irregular bridges, Inelastic time history analysis, Regularity index, CHBDC 2006, NBCC 2010, Seismic response

3.3 Introduction

The seismic response of bridges becomes more complex, when geometrical properties such as the number of spans, the ratio of adjacent span lengths, subtended angle for curved bridges, and the span-to-span bent or pier stiffness ratio exceed criteria typically defined by seismic design provisions. For such cases, simple linear analysis methods typically fail to predict the seismic response and therefore the use of more sophisticated analysis methods is necessary. Bridges with complex seismic behaviour are classified as irregular bridges in seismic design codes. This study focuses on the effects of different column and superstructure stiffnesses on the seismic response of straight bridges. A bridge becomes more irregular as the difference between the column stiffnesses increases, leading to greater differences between the results of elastic and inelastic analyses, and concentration of ductility demands in a few stiffer elements.

For bridges with regular configurations (i.e., having columns with similar stiffnesses), subjected to significant ground motions, the inelastic energy dissipation does not tend to concentrate in a few ductile elements and it is expected that all of the plastic hinges will contribute to the seismic response of the structure. However it is not possible to always have regular configurations due to the need for different column heights for valley crossings and ramps. Experience indicates that a bridge is more likely to be vulnerable if: (1) excessive deformation demands occur in a few elements, (2) the structural configuration is complex, or (3) a bridge lacks redundancy (Chen and Duan, 2000).

Bridges with significantly different column heights result in considerable concentration of shears and moments in the stiffer shorter columns. In some cases, the deformation demands on the short columns can cause failure before the longer, more flexible adjacent columns can fully participate. In addition, the sequential yielding of the ductile members may result in substantial deviations of the nonlinear response predictions from linear analyses performed with the assumption of a global force reduction factor, R. This difference is due to the formation of plastic hinges which appear first in the stiffer columns and may lead to a concentration of unacceptably high ductility demands in these hinges. Following the formation of the first plastic hinges, the distribution of stiffness and hence of forces may change from that predicted by linear analysis. This may lead to a substantial change in the assumed sequence of plastic hinges (CEN, 2005). One may try to solve the problem by reducing the value of the R factor, in which case it is certainly possible to reduce the ductility demand in the stiffer piers, but the resulting overall design may be very costly. Calvi et al., (1994) proposed that different modification factors could be used as a function of bridge geometry.

Examples of earthquake damage to irregular bridges with different column heights as well as poorly designed and detailed bridges have been reported (Broderick and Elnashai, 1995; Mitchell et al., 1995; Chen and Duan, 2000). Some studies have been conducted on irregular bridges designed using the Eurocode provisions (Calvi and Pinto, 1996; Pinto et al., 1996; Fischinger et al., 1997; Isacovic and Fischinger, 2006 and Isacovic et al., 2008). There is little research on this subject especially for bridges designed using American and Canadian provisions. Currently the use of elastic analysis is permitted in these codes for bridges with significant irregularity features, while the use of elastic analysis may not be appropriate for some irregular bridges. Due to the vulnerability of irregular bridges, more research is needed to investigate the seismic behaviour and suitable methods of analysis for such bridges.

3.4 Regularity and irregularity indices

The purpose of a regularity index is to determine the degree of regularity or irregularity of a bridge as a function of key structural parameters. The first attempt to provide a regularity index was made by Calvi et al., (1994 and 1996). They proposed an index of regularity, IR, which is a measure of the difference between the mode shape of the whole bridge with deck and columns and the mode shape of the deck without columns, given by Eq. 3.1.

$$[3.1] \quad IR = \sqrt{\frac{\sum_{j=1}^{n} (\Phi_i^B M \Phi_j^D)^2}{n}} \qquad [3.2] \quad IMR = 1 - \frac{\sum_{i=1}^{n}\sum_{j=1}^{n} [(1-\delta_{ij})\left|\Phi_i^B M \Phi_j^D\right|]}{n}$$

Following this study a new index, IMR (Eq. 3.2), was then proposed by subtracting the norm of the products of the off-diagonal terms to increase the sensitivity of the index. Where Φ_{Bi} , Φ_{Dj} and M are the mode shapes of the bridge and the mode shapes of the deck alone and the mass matrix, respectively and n is the number of modes considered. In Eq. 3.2, δ_{ij} is the Kronecker delta which is equal to 1 if i=j and 0 otherwise. In these equations Φ_{Di} is a measure of the inelastic mode shapes by neglecting the stiffness of columns. When Φ_{Bi} and Φ_{Dj} are similar, the predicted response of the structure using the elastic and inelastic analysis methods are generally in good agreement.

A number of other indices for assessing regularity have been proposed, including:

1- Use of Modal Assurance Criterion-MAC (Ewins, 2000):

[3.3-a] $$MAC_i(D,B) = \frac{\left|\left\{\Phi_i^D\right\}^T \left\{\Phi_i^B\right\}\right|^2}{\left(\left\{\Phi_i^D\right\}^T \left\{\Phi_i^D\right\}\right)\left(\left\{\Phi_i^B\right\}^T \left\{\Phi_i^B\right\}\right)}$$ [3.3-b] $$MAC(D,B,n) = \sqrt{\frac{\sum_{i=1}^{n}(MAC_i(D,B))^2}{n}}$$

2- Use of Modal Scale Factor-MSF (Ewins, 2000):

[3.4-a] $$MSF_i = \frac{\left|\left\{\Phi^D\right\}^T \left\{\Phi^B\right\}\right|_i}{\left(\left\{\Phi^D\right\}^T \left\{\Phi^D\right\}\right)_i}$$ [3.4-b] $$MSF(D,B,n) = \sqrt{\frac{\sum_{i=1}^{n}(MSF_i(D,B))^2}{n}}$$

3-Difference Ratio of Mode Shapes-DRMS (Fischinger et al., 2003 and Maalek et al., 2009):

[3.5-a] $$DRMS_i(D,B) = \frac{\left|\Phi^D - \Phi^B\right|}{\left|\Phi^D\right|} = \frac{\left|S_D - S_B\right|}{\left|S_D\right|}$$ [3.5-b] $$DRMS(D,B,n) = \sqrt{\frac{\sum_{i=1}^{n}(DRMS_i(D,B))^2}{n}}$$

In Eq. 3.5-a S_D and S_B are the area under the mode shapes Φ_D and Φ_B, respectively. It must be noted that contrary to the other indices described above, the DRMS index is 0 for regular bridges and it increases with the degree of irregularity. A summary of different indices for regularity are given by Maalek et al., (2009). These indices were derived for bridges with transverse restraint at the abutments.

3.5 Code Provisions

3.5.1 Caltrans (2006) and AASHTO Guidelines (2009)

The requirements in Caltrans (2006) and the AASHTO Guidelines (2009) compare the ductility demands with the ductility capacities in the energy dissipating members (displacement-based design) instead of using an overall modification factor for design (force-based design). Although the problem of different ductility demands of columns in irregular bridges can be better addressed using this method, the ductility demands which are based on the linear analysis methods such as response spectrum analysis (which is permitted for design of irregular bridges) usually underestimate the ductility demands in critical members and can lead to unsafe designs. Some conservative limitations are recommended in Caltrans and the AASHTO Guidelines for the ratio of the column stiffnesses in a frame or bent to balance the bent or pier stiffness along the bridge. For any two bents or any two columns within a bent this stiffness ratio is recommended be greater than 0.5. For adjacent bents or adjacent columns within a bent this ratio is recommended to be less than 0.75. Some of the consequences of not meeting these relative stiffness indicators include increased damage in the stiffer elements and an unbalanced distribution of inelastic response throughout the structure.

If project constraints make it impractical to satisfy the stiffness requirements, a careful evaluation of the local ductility demands and capacities shall be required for bridges in regions of high seismicity.

3.5.2 Eurocode

In the Eurocode (CEN, 2005) a force-based design approach is used for the design of bridges. The reduction factor, q (similar to the modification factor R), for reinforced concrete columns depends on the shear span to depth ratio and on whether the member is inclined or vertical. The q factor will then be modified in the cases of high axial loads and irregular seismic behaviour of the bridge. In this regard the local force reduction factor r_i associated with member i is defined as:

[3.6-a] $r_i = q\ (M_{Ed,i} / M_{Rd,i})$

[3.6-b] $\rho = r_{max} / r_{min} \leq \rho_o$

[3.6-c] $q_r = q\ (\rho_o / \rho) \geq 1.0$

where $M_{Ed,i}$ and $M_{Rd,i}$ are the maximum values of design moment at the intended plastic hinge location of ductile member i from the seismic analysis and the design flexural resistance of the section with the actual reinforcement, respectively. The bridge is considered to have regular seismic behaviour when Eq. 3.6-b is satisfied. Where r_{max} and r_{min} are the maximum and minimum values of r_i, respectively and ρ_o is a limit value selected so as to ensure that sequential yielding of the ductile members will not cause unacceptably high ductility demands on the member. The recommended value for ρ_o is 2.0. The force reduction factor, is then reduced to q_r for the irregular seismic behaviour according to Eq. 3.6-c. To capture the actual seismic behaviour of an irregular bridge where the ductility demands concentrate in a few elements and the distribution of the forces deviate from that predicted by the linear analysis, a combination of an equivalent linear analysis with a non-linear static analysis is recommended.

3.5.3 CSA-S6-06 and AASHTO-04

The seismic design provisions in the Canadian Highway Bridge Design Code (CHBDC) (CSA, 2006) are based on the AASHTO Specifications (AASHTO, 2004). S6 uses a force modification factor, R, and an importance factor, I, of 1.0, 1.5 and 3.0 for "other", "emergency-route" and "lifeline" bridges, respectively. The AASHTO Specifications combine the force modification factor for "ductility" with the importance factor to give one force modification factor for "other", "essential" and "critical" bridges. Nevertheless, the resulting design forces are similar. The CHBDC requires that the MM (multi-mode spectral method and also referred as response spectrum analysis in this paper) be used for the analysis of irregular bridges, even in seismic performance zone 4. However for irregular lifeline bridges, time-history analysis is required in zones 3 and 4. Concerning the column stiffness ratios for regular bridges, the 2004 AASHTO and the 2006 CHBDC specifications indicate that the maximum bent or pier stiffness ratio from span to span should not exceed 4.0 for bridges up to 4 spans, 3.0 for 5 spans and 2.0 for 6 span bridges. These stiffness limits are for bridges with a continuous superstructure or multiple simple spans with longitudinal restrainers and transverse restraint at each support or a continuous deck slab, otherwise this ratio shall not exceed 1.25.

The modification factors, R, are taken conservatively and lower than the expected displacement ductility capacities, since the procedure is intended to apply to a wide variety of bridge geometries. Where possible, pier stiffnesses should be adjusted to attempt to achieve uniform yield displacements and ductility demands on individual piers. In cases where attempts to "regularize" the structure are impractical, suitable analyses need to be developed to account for localized, rather than simultaneous, yielding of piers. In some cases, it may be possible to use "stiff" piers with energy dissipating bearings to alleviate the problem as discussed in the CHBDC Commentary (CSA, 2006).

3.6 Methods to improve the seismic behaviour of irregular bridges

Several methods could be used to improve the seismic performance of bridges with varying column heights. These methods include the use of foundation sleeves for piers with appropriate depths to equalize the effective length and stiffness of the columns (i.e., lower footings and isolation casing), the use of isolation devices (such as elastomeric and sliding bearings) with appropriate stiffness to adjust the stiffness distribution and to improve the damping level (Priestley et al., 1996) and the use of in-span hinges and abutments with sacrificial shear keys (Saiidi et al., 2001).

Caltrans (2006) recommends some techniques to alleviate problems associated with stiffness irregularities including using oversized pile shafts, using modified end fixities, reducing and/or redistributing superstructure mass, varying the column cross section and longitudinal reinforcement ratios, adding or relocating columns and modifying the hinge/expansion joint layout.

A bridge memo for designers (Caltrans, 2011), gives some recommendations for the design of columns that may be useful for the case of irregular bridges with different column heights. These include pinning the columns at footings in multi-column bents, pinning the base of the column adjacent to abutments in single-column bents, the use of broader sections for taller columns and the use of pile shafts in lieu of footings.

3.7 Modelling and evaluation of the bridges

3.7.1 Limit states and corresponding strain limits

Emergency-route bridges must be repairable after the occurrence of a design earthquake with 10% probability of exceedance in 50 years (CSA, 2006). This performance level requires damage control, in which the damage in the structural elements should not exceed some acceptable limits which are usually defined as a maximum compression strain in the confined core concrete and a maximum tensile strain in the reinforcing bars. After occurrence of a maximum considered earthquake (MCE) with 2% probability of exceedance in 50 years, significant damage is expected but collapse should be prevented. Several approaches are available to estimate the ultimate compression strain in the confined concrete core (Mander et al., 1988; Paultre and Légeron, 2008). The Mander et al. equation is based on equal energy principles in which the ultimate compression strain corresponds to the fracture of the hoops. Beyond this level, crushing of the concrete, buckling and fracture of steel bars can occur. Experimental studies indicate that the ultimate strains predicted by the Mander equation are conservative with the actual ultimate strains exceeding the predicted values by a factor of about 1.3 to 1.6 (Priestley et al., 2007). This conservatism is mainly due to the presence of combined axial compression and flexure while the original Mander model was derived for pure axial compression and it also does not take into account the additional confinement provided by connecting members such as foundations or cap beams. To account for this, Priestley et al., (2007) recommended using conservative ultimate strains based on the Mander equation for damage control. However for the Life Safety (LS) limit state (i.e., no collapse), they recommended that the predicted values from the Mander equation be increased by 50% as suggested by the experimental results.

Due to the possibility of buckling of the bars when subjected to reversed cyclic loading and considering low-cycle fatigue of the reinforcing bars in addition to slip between the reinforcing steel and the concrete, the ultimate tensile strain, ε_{su}, from the monotonic tests must be modified to predict the ultimate curvature. The level of this strain will depend on the volumetric ratio and spacing of the transverse reinforcement. For the damage control limit state, a strain level of 0.6 to 0.7 times the ultimate strain of steel bars in monotonic tests is recommended for calculating the ultimate curvature of the section which should not be taken larger than 0.05 (Priestley et al., 1996 and 2007). In order to attain this level of strain, the spacing of the transverse reinforcement must be code conforming. For the life safety performance level a strain of 0.9 times the ultimate strain of steel bars, 0.9 ε_{su}, is recommended and this value should not be larger than 0.08 (Priestley et al., 2007).

Based on the degree of confinement either steel strains or concrete strains may control the ultimate curvature of a section. However, considering the relatively high percentage of transverse reinforcement based on current seismic design codes, the ultimate strain in the steel often controls the ultimate curvature of the section. A study by Berry and Eberhard (2007) provides some empirical equations to estimate the drift ratio, plastic rotation, and longitudinal strain for circular bridge columns based on the longitudinal and transverse steel ratio, axial load ratio, and geometric properties of the column. For example as shown in Table 3.1-a the predicted ultimate drift at damage control for the circular bridge column described is 3.9%, while the equations proposed by Berry and Eberhard (2007) result in a predicted ultimate drift capacity of 5.3% corresponding to the bar buckling damage state (see Table 3.1-b). This indicates that the prediction for the drift limit for the damage control state is about 35% lower (i.e., more conservative) than that predicted by the experimentally derived equations for this case. The predicted ultimate drift capacity at the life safety limit state of 5.69% is in good agreement with that predicted using the empirical equations (i.e., 5.30% for bar buckling and 5.74% for bar fracture).

For the emergency-route bridges studied, the ultimate tensile strain in the steel bars corresponding to bar buckling given by Berry and Eberhard (2007) was used to compute the ultimate ductility of the columns.

Table 3.1. Deformations at different damage states for a column with D=1.5m, H=5m, ρs=2.0%, and ρv =1.2% a) Using moment-curvature analyses (Priestley et al., 2007); b) Using experimentally derived equations (Berry and Eberhard, 2007)

a)

Damage state	Drift	Strain	Curvature ductility	Disp. ductility
Yielding	0.59%		1	1
Serviceability	0.93%	ε_c=0.004 or ε_s=0.015	2.7	1.6
Damage Control	3.91%	ε_c< Mander eq.or $\varepsilon_s=0.6\varepsilon_{su} < 0.05$	15.9	6.2
Life Safety	5.69%	ε_c< 1.5*Mander eq. or $\varepsilon_s=0.9\varepsilon_{su}< 0.08$	25.6	9.6

b)

Damage state	Drift	Strain
Cover Spalling	1.85%	0.008
Bar Buckling	5.30%	0.075
Bar Fracture	5.74%	0.081

3.7.2 Calculating ductility capacities and modelling assumptions

Moment-curvature analyses were performed to determine the curvatures corresponding to the strain levels in the steel and the concrete for different damage states. The corresponding displacement, drift, curvature ductility, and displacement ductility can be computed for each performance level. A computer program was developed (Tehrani, 2012) to design the columns and carry out the moment-curvature analyses to compute the curvature at different steel and concrete strains. The confinement effects in the concrete core were considered using the Mander equation (Mander et al., 1988) in the moment-curvature analysis assuming confinement reinforcement in accordance with the provisions of the CHBDC (CSA, 2006).

The effective curvature at yield can be either estimated from available experimental data or from moment-curvature analysis. For circular sections Eq. 3.7 proposed by Priestley et al., (2007) provides a good estimate for the yield curvature, Φ_y, given by :

[3.7] $$\Phi_y=2.25\ \varepsilon_y / D$$

In which ε_y is the yield strain of the flexural reinforcement and D is the diameter of the column cross section. In this study the yield curvature was computed for each cross-section using moment-curvature analysis, although the results were generally close to the estimates using Eq. 3.7. The bilinear idealization of the moment-curvature responses were carried out using the procedure describe by Priestley et al., (2007). For this purpose the first yield is defined as the point on the moment-curvature response when the extreme tension reinforcement first attains the yield strain, or when the extreme concrete compression fibre reaches a strain of 0.002, whichever occurs first. The moment and curvature at first yield are denoted by M_y and Φ'_y respectively. The line defining the elastic stiffness is extended up to the nominal moment capacity, M_n, and corresponding curvature, Φ_y. M_n is the moment resistance corresponding to an extreme fibre compression strain of 0.004 in the concrete or an extreme tension strain of 0.015 in the steel bars, whichever occurs first. The corresponding curvature is defined as the nominal yield curvature Φ_y for the idealized response. The plastic branch then can be defined by connecting the nominal yield point to the ultimate point of the curve. The elastic stiffness of the section (also known as the effective stiffness) then can be calculated using Eq. 3.8.

[3.8] $$EI_{eff} = M_y / \Phi'_y = M_n / \Phi_y$$

It is well known that the curvature distribution cannot simply be integrated along the column height for estimating the displacements since this ignores some deformations including shear deformation and strain penetration due to bar anchorage. A simplified approach is often used which involves the concept of a "plastic hinge" of length L_p over which the curvature is assumed to be constant and equal to the maximum value at the column base. For a column fixed at the base and pinned at the top, the curvature distribution is considered to be linear at other parts of the column. The plastic hinge length includes a strain penetration length, L_{sp}, to account for anchorage deformation due to strain penetration over a length equal to development length of the steel bars. The strain penetration length may be computed using Eq. 3.9 proposed by Priestley et al., (1996 and 2007):

[3.9] $L_{sp}=0.022\, f_y\, d_{bl}$ (f_y in MPa)

where f_y and d_{bl} are the yield strength and diameter of the longitudinal reinforcement, respectively. The plastic hinge length, L_p, can then be calculated using Eq. 3.10.

[3.10] $L_p = k\, L_c + L_{sp} \geq 2\, L_{sp}$

where L_c is length from the critical section to the point of contraflexure in the member and the k factor is mainly a function of the ratio of the ultimate tensile strength to yield strength of the flexural reinforcement (k = 0.08 was used in this study). The force versus displacement relationship can then be calculated using the moment-curvature response. For a cantilever column of height H, the displacement at yield, Δ_y, and displacement at ultimate, Δ_u, can be calculated using Eq. 3.11 and 3.12.

[3.11] $\Delta_y = \Phi_y\, (H + L_{sp})^2 / 3$

[3.12] $\Delta_u = \Delta_y + (\Phi_u - \Phi_y)\, L_p H$

The modified Takeda hysteresis model (Otani, 1981) was used in this study to model the behaviour of the RC columns using Ruaumoko software (Carr, 2009). This model has two main parameters, alpha and beta, which control the unloading and the reloading stiffness, respectively (see Fig. 3.1). Alpha is usually in the range of 0 to 0.5 and beta varies between 0 and 0.6. Increasing the alpha parameter decreases the unloading stiffness and increasing the beta parameter increases the reloading stiffness. For bridge columns Priestley et al., (1996 and 2007) recommend using an alpha value of 0.5 and a beta value of zero which was used in this study.

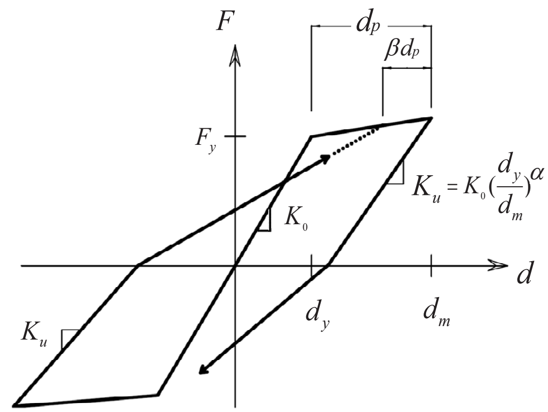

Fig. 3.1. Modified Takeda hysteresis loop (adapted from Carr (2009))

3.7.3 Range of parameters studied

The seismic responses in the transverse direction of 4-span continuous bridge structures were studied. According to Priestley et al., (2007), the longitudinal and transverse behaviour can be considered independently for straight bridges, such as those considered in this study. The bridge structures shown in Fig. 3.2 were designed according to the Canadian Highway Bridge Design Code (CSA, 2006) using a force modification factor, R, of 3 and an importance factor of 1.5 (i.e., I = 1.5 for emergency-route bridges). The bridges were designed for Vancouver assuming a site class C (i.e., $360 \leq V_{s30} \leq 760$ m/sec).

To investigate the effects of parameters such as column heights and diameters, superstructure stiffness and mass, a parametric study was carried out. Column heights were considered as 7, 14, and 21 m and column diameters were 1.5, 2.0, and 2.5 m. It must be noted that in each configuration the three columns all have the same diameters (see Fig. 3.2). The minimum and maximum longitudinal reinforcement ratios were 0.8% and 6.0%, respectively. The transverse steel ratios were determined based on the CHBDC 2006 provisions to satisfy the requirements for maximum factored shear forces, confinement in the plastic hinge regions, and the capacity design philosophy. However in most cases the spiral confinement reinforcement ratio of 1.2% controlled.

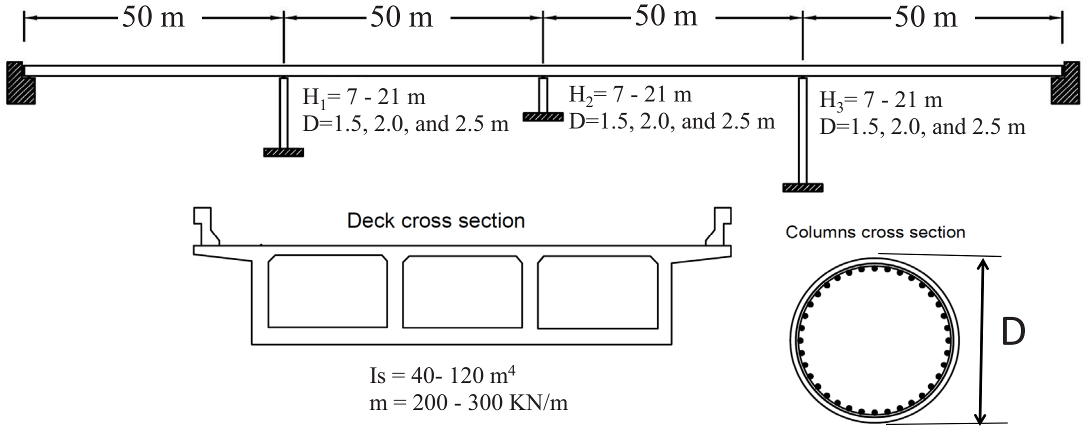

Fig. 3.2. Bridge configurations studied with different column heights

The superstructure lateral stiffness is also an important parameter in the seismic response which is proportional to the moment of inertia of the superstructure cross-section relative to the vertical axis. The superstructure moment of inertia of box-girder bridges usually varies between 40 to 150 m^4 (Dwary and Kowalski, 2006), hence values of 40, 80 and 120 m^4 were chosen for the parametric study. The superstructure mass was considered as a uniformly distributed load of 200 kN/m and 300 kN/m. The concrete compressive strength and the yield stress of the reinforcing bars were taken as 40 and 400 MPa, respectively. These combinations of column heights (i.e., 3 different heights for three columns), diameters (i.e., 3 different diameters), superstructure stiffness (i.e., 3 different values of I_s), and masses (i.e., 2 different values) resulted in 324 bridges with different configurations. In addition, the study was carried out for two cases of restrained and unrestrained movements in the transverse direction at the abutments, so that a total of 648 bridges were studied.

For inelastic time history analyses 7 spectrum matched records were used. These artificial records were generated using the SIMQKE software (Vanmarcke and Gasparini, 1979; Carr, 2009). For the nonlinear analyses of the bridges, the records were matched to the design spectra given by the National Building Code of Canada (NBCC) (2010). These spectra correspond to 2% probability of exceedance in 50 years, while the design spectrum given in the CHBDC (CSA, 2006) corresponds to 10% probability of exceedance in 50 years. The 2010 NBCC spectrum with the hazard level of 2% in 50 years, which will be used in the next edition of the CHBDC, was used to evaluate the seismic behaviour of the bridges. The effects of irregularity on the seismic response are expected to be more pronounced at higher seismic intensity levels. The ductility demands in the columns should not exceed the ductility capacities computed based on the life safety limit state (i.e., no collapse). The resulting average response spectrum of the seven records used along with design spectra for Vancouver based on the CHBDC (2006) and NBCC (2010) are shown in Fig. 3.3. The average displacement for each bridge was determined using the averaging procedure proposed by Priestley et al., (2007) which considered the maximum positive and maximum negative displacements predicted for each input record.

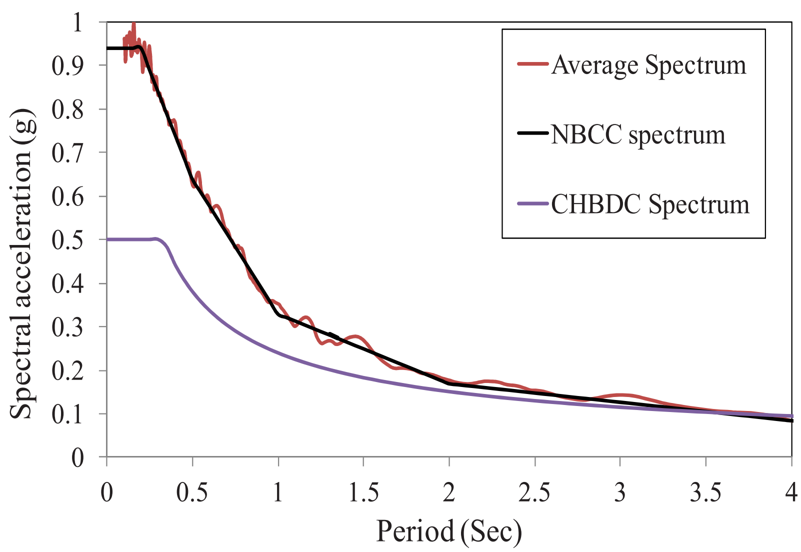

Fig. 3.3. Average response spectrum of 7 records used for inelastic time history analysis matching the 2010 NBCC spectrum (2% in 50 years)

3.8 Predicted response of bridges with restrained abutments

In this section the results obtained for the case of bridges with restrained transverse movements at the abutments are presented.

3.8.1 Effect of column stiffness ratios

Fig. 3.4 illustrates the influence of the maximum column stiffness ratio (stiffness of the stiffest column divided by the stiffness of the most flexible column) on the ductility demand. As can be seen the maximum ductility demands obtained are less than 3. However when the stiffness ratios are more than about 8 the maximum ductility demands exceed 2.5 with minimum ductility demands of around 1.7. For more regular bridges (small column stiffness ratio) the minimum range of the ductility demands are smaller (e.g., about 0.5 for stiffness ratio around 1). However it must be noted that in general it cannot be concluded that ductility demands in more irregular structures are always higher than those of regular structures. Some other parameters such as strength of columns and the overall stiffness of the structure play an important role in controlling the maximum ductility demand on columns. For example, regular bridges often require lower column strengths, compared to irregular structures, due to the uniform distribution of seismic demands in regular bridges. This may increase the ductility demands on a regular bridge, while an irregular bridge with larger column strengths may have even lower seismic demands at the design earthquake level. Similarly, stiffer substructures attract more seismic forces which result in higher ductility demands. Thus a stiff regular structure may have higher ductility demands than a more flexible irregular structure. While the maximum ductility demand may not be an appropriate parameter to identify the degree of irregularity of a bridge, the maximum to minimum ductility demand ratio provides a better parameter for this purpose.

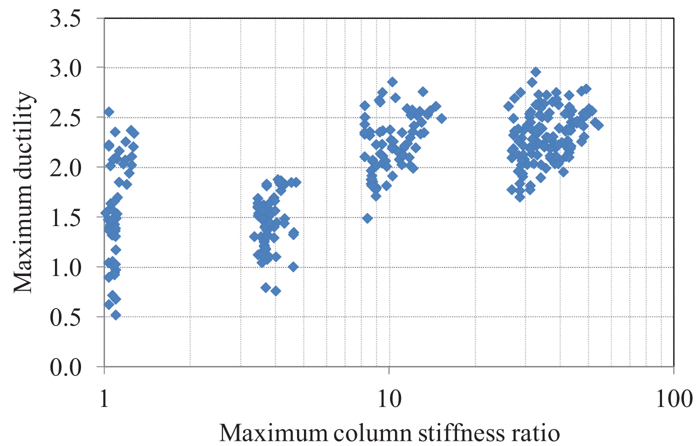

Fig. 3.4. Effect of column stiffness ratio on maximum ductility demand for bridges with various configurations

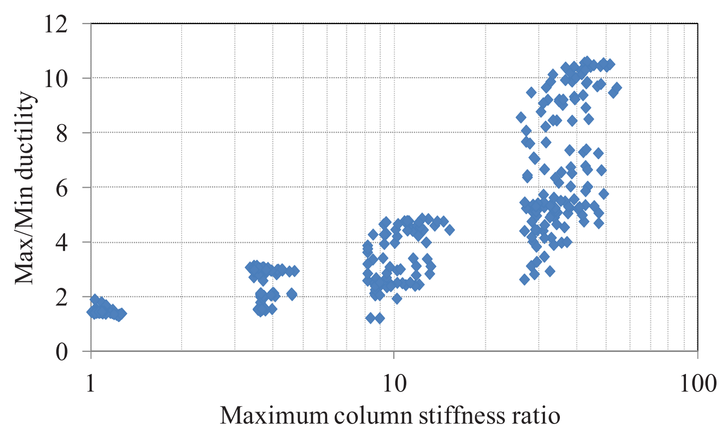

Fig. 3.5. Effect of column stiffness ratio on maximum to minimum ductility ratio

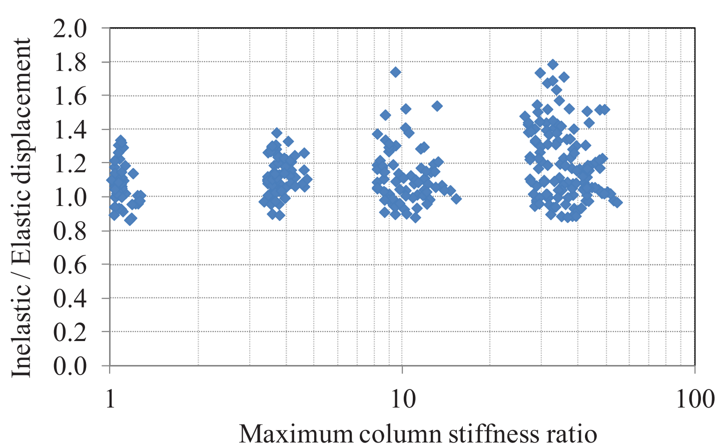

Fig. 3.6. Effect of column stiffness ratio on the ratio of the displacements obtained using elastic and inelastic analysis

Fig. 3.5 shows that the column stiffness ratios influence the maximum to minimum ductility demand ratios. This ratio indicates how structural components participate in the seismic behaviour. A large value of the max/min ductility ratio indicates that the seismic demands are concentrated in a few elements. This figure also shows that when the maximum column stiffness ratios are more than about 10, the max/min ductility ratios increase significantly with values as high as 10 being predicted. Maintaining a maximum column stiffness ratio of about 4 (regularity limit according to CHBDC for 4 span bridges) limited the max/min ductility to about 3.0. Fig. 3.6 indicates that the ratio of displacements obtained from inelastic analysis to those obtained from elastic analysis can be more than 1.4, when the maximum column stiffness ratios are more than about 5. For some irregular configurations, there are significant deviations of the displacement envelopes determined using elastic and inelastic analysis. An example of such a configuration is the irregular bridge with column heights of 7, 14 and 21 m, column diameters of 2.5 m and a flexible superstructure with $I_s = 40\ m^4$. As shown in Fig. 3.7, the displacement envelopes determined from elastic and inelastic analysis are significantly different for this configuration. For the irregular bridge the displacement of the critical central short column is underestimated using the elastic response spectrum analysis (multi-mode spectral method). This can lead to an unsafe design. However, due to the conservative design approach in the 2006 CHBDC, with an R factor of 3.0 and an importance factor of 1.5, the maximum ductility demands in such critical cases did not exceed the ductility capacity of these ductile columns. The 2006 CHBDC permits the use of elastic multi-modal analysis for irregular bridges and therefore would not provide realistic designs for some irregular configurations.

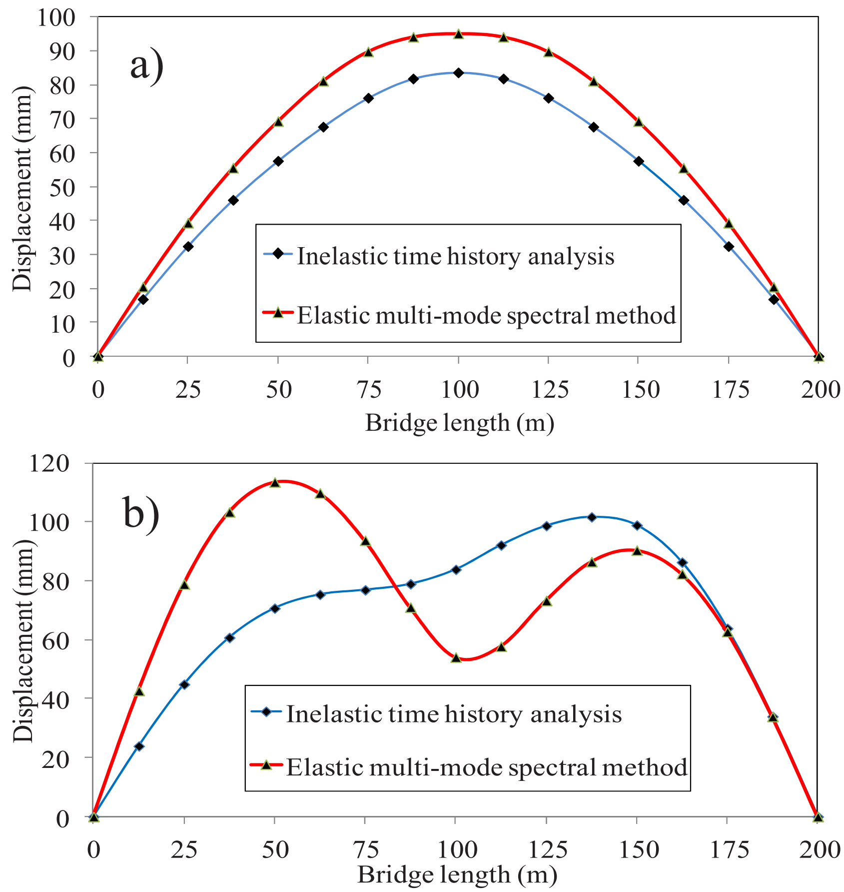

Fig. 3.7. Comparison of the displacement envelopes obtained using elastic and inelastic analysis for a) a regular bridge and b) an irregular bridge

3.8.2 Effect of superstructure to substructure stiffness ratio

Another parameter which is known to be very important in the seismic response of a bridge in the transverse direction is the superstructure to substructure stiffness ratio, RS. This ratio was calculated using Eq. 3.13.

[3.13] $$RS = \frac{K_s}{K_c} = \frac{\frac{32I_s}{5L_s^3}}{\frac{3I_c}{h_c^3}}$$

where I_c is the moment of inertia of the stiffest column with cracked section properties, h_c is the column height, I_s is the gross moment of inertia of the deck, and L_s is the deck total length. It is noted that in this study the substructure stiffness, K_c, was taken as the stiffness of the stiffest column, since it was found that this provided a better prediction parameter than the sum of the stiffness of all columns.

As can be seen in Fig. 3.8, when the superstructure to substructure stiffness ratio is less than 1.0, higher ductility demands are observed and more importantly the maximum to minimum ductility demands can be drastically increased. In addition the same trend is observed in the ratio of displacements obtained from elastic response spectrum analysis and inelastic time history analysis. When the superstructure to substructure stiffness is less than 0.3, the displacement ratio from elastic and inelastic analysis can exceed 1.4 as can be seen in Fig. 3.9.

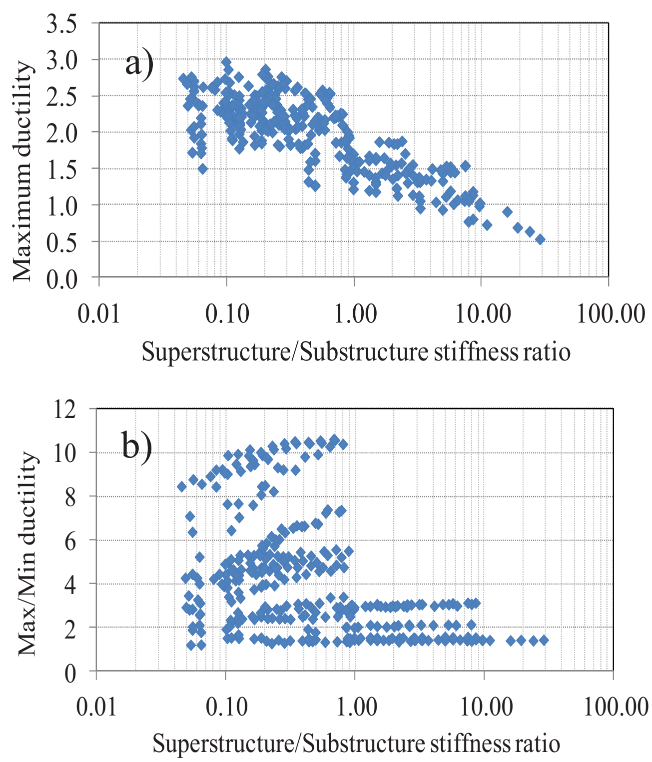

Fig. 3.8. Effect of superstructure to substructure stiffness on a) maximum ductility demand and b) maximum to minimum ductility demand

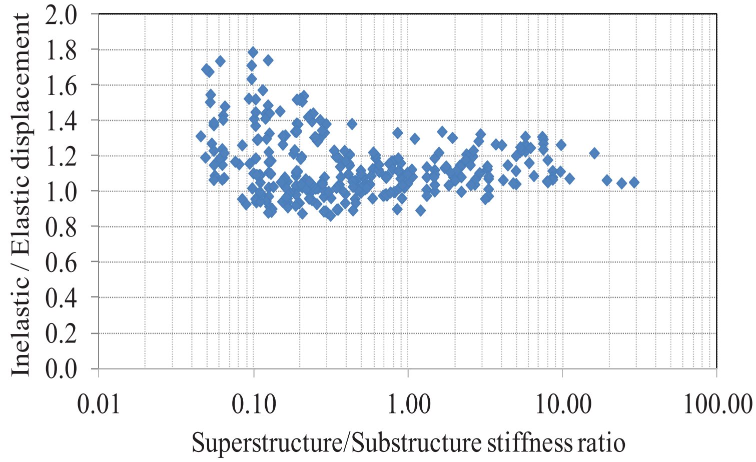

Fig. 3.9. Effect of superstructure/substructure stiffness on the results from elastic and inelastic analysis

3.8.3 Prediction of regularity indices

Several regularity indices have been proposed in the past that are used to estimate the degree of irregularity of a bridge structure and determine if linear analysis can be used to predict the maximum displacements of a structure. In Figs. 3.10 to 3.12 different regularity indices are compared using several response parameters such as maximum ductility demands, max/min ductility ratios, and the deviation of results from elastic and inelastic analysis. This enables a comparison of the suitability of these indices. The results from IR and MSF regularity indices were similar and thus only the results obtained for the IR index are presented.

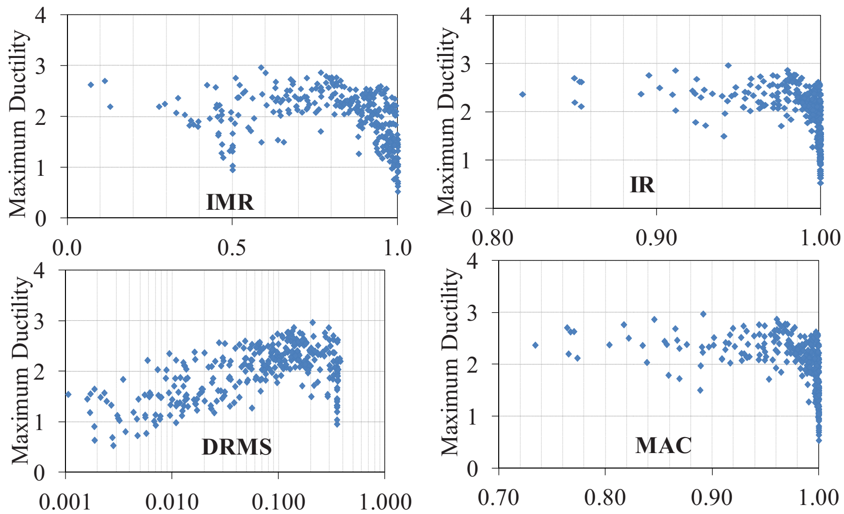

Fig. 3.10. Different regularity indices versus maximum ductility demand

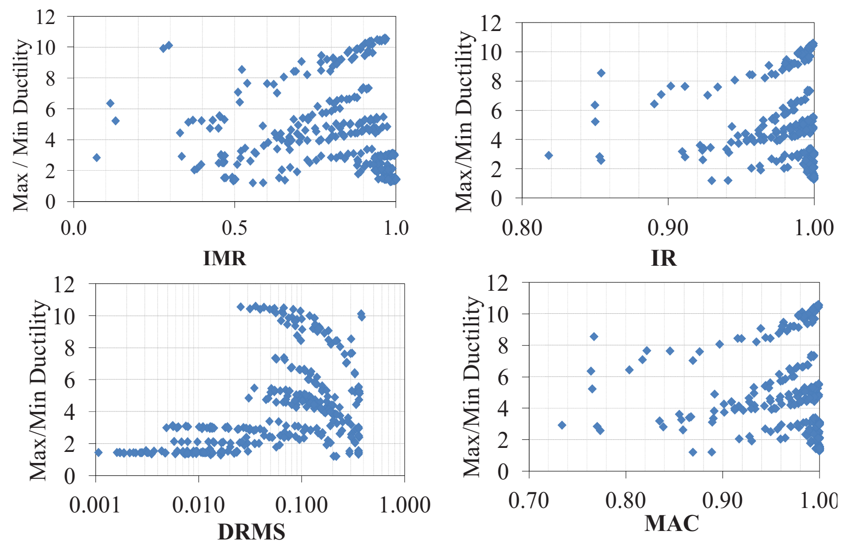

Fig. 3.11. Different regularity indices versus maximum to minimum ductility demand ratio

Fig. 3.10 shows the regularity indices versus the maximum displacement ductility demands obtained from the inelastic time history analysis. It is clear that the sensitivity of the IR and MAC regularity indices are quite low. For example, for the variety of the configurations considered the value of IR and MAC indices obtained were in the range of 0.8 to 1.0 and 0.7 to 1.0, respectively. In addition there is no obvious trend between the value of these indices and the predicted maximum ductility demands. However, it can be seen that the structures with IR index of less than 0.99 and MAC index of less than 0.98

have higher ductility demands in general. The sensitivity of the IMR index is better than those of IR and MAC and it can be seen that the bridges with IMR index of less than 0.9 generally have a higher ductility demand. However there are cases with small IMR index values that have lower ductility demands than those with higher IMR index values. The DRMS index seems to provide a better indicator for maximum ductility demands and a trend can be seen that with increases in the DRMS index the ductility demands increase in general. The bridge configurations studied had DRMS values between 0 and 0.4.

In Fig. 3.11, the maximum to minimum ductility demands, which are an indication of the concentration of demand in a few elements, are shown versus different regularity indices. As can be seen the IR, IMR, and MAC indices show no clear trend in predicting this parameter. On the other hand, the DRMS index predicts the trend of this parameter and as can be seen the bridges with the DRMS index of less than 0.025 have lower concentration of ductility demands and thus this value may be used as a criterion to avoid problems with the concentration of ductility demands.

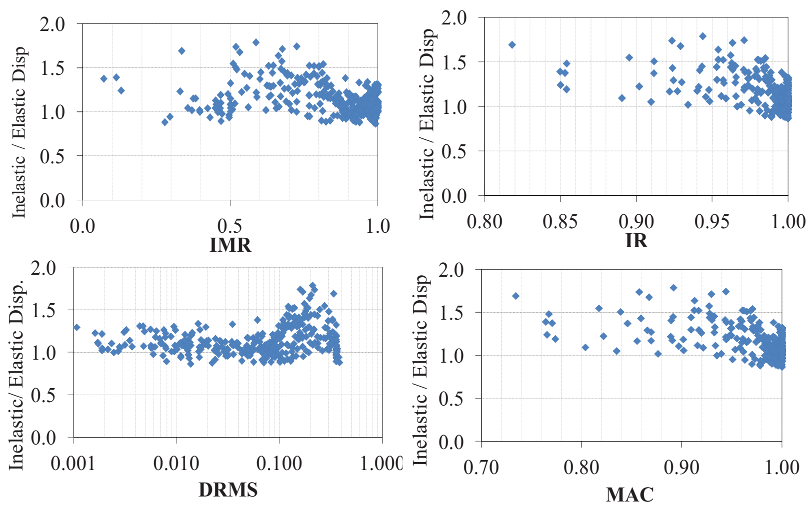

Fig. 3.12. Different regularity indices versus the ratio of the displacements obtained using inelastic and elastic analysis

The IR, IMR, and MAC indices are primarily aimed at identifying structures that would give rise to poor correlation between their seismic response using elastic and inelastic analyses. Fig. 3.12, illustrates that these indices are relatively successful in providing such an indicator. For example, based on the results obtained the response of structures with the IMR index of more than 0.85, IR index of more than about 0.95, or MAC index of more than 0.9 can be predicted using elastic analysis otherwise care must be taken to adopt an appropriate method of analysis. The DRMS index provides a good indicator, with DRMS index values of less than 0.08 resulting in good agreement between elastic and inelastic analysis.

A comparison of the regularity indices in Figs. 3.10 to 3.12, indicates that the DRMS index is the most useful indicator of regularity and therefore the DRMS index is recommended for determining an appropriate method of analysis.

3.9 Predictions of responses of Bridges with unrestrained abutment conditions

In this section the results obtained for the case of bridges with free abutment conditions at the ends (i.e., unrestrained transverse movements) are presented.

3.9.1 Effect of maximum column stiffness ratios

A similar trend is observed in the case of unrestrained abutment conditions. As can be seen in Fig. 3.13, when the maximum column stiffness ratio exceeds 5.0, the ductility demands concentrate in a few elements so that only a few columns contribute to the seismic response. For cases having a maximum column stiffness ratio exceeding 8.0, the results from the elastic analysis may not be representative of the actual response.

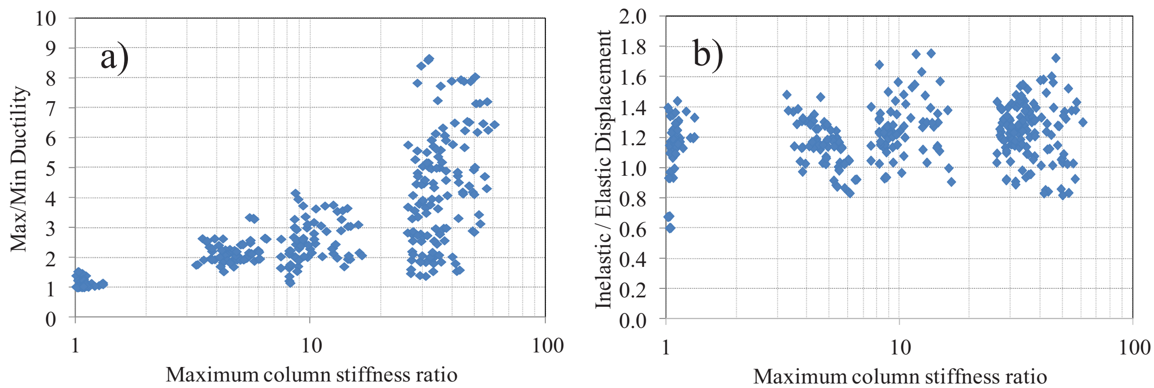

Fig. 3.13. Influence of column stiffness ratios on a) maximum to minimum ductility demands and b) results obtained from elastic and inelastic analyses (Bridges with unrestrained abutment conditions)

3.9.2 Effect of superstructure to substructure stiffness ratios

Fig. 3.14 illustrates the importance of the superstructure to substructure stiffness ratio on the seismic response of the bridge structures in the transverse direction. When this value is less than 0.8, the variations in the column stiffnesses can result in uneven distribution of seismic demands and can increase the maximum ductility demands. In addition, when this stiffness ratio is less than 0.8, the results from elastic analysis may substantially deviate from those obtained using inelastic analyses.

No general trend was found between the modal participation mass ratio of the first mode, $M_{1,}$ and the parameters studied. However it was seen that typically structures with M_1 of more than 96% had lower maximum ductility demands and in addition the results from elastic and inelastic analysis in such structures were in good agreement.

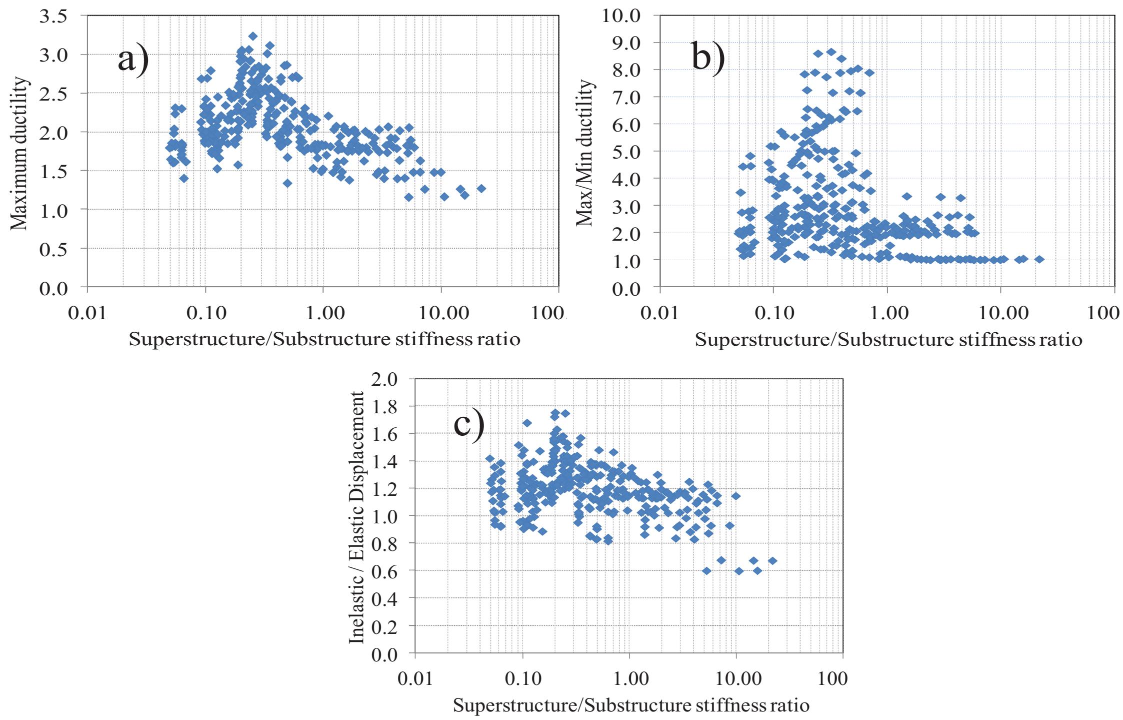

Fig. 3.14. Effect of supersructure to substructure stiffness ratio on a) maximum ductility demands, b) maximum to minimum ductility demands ratio, and c) results obtained from elastic and inelastic analyses

3.10 Displacements from elastic versus inelastic analysis

The inelastic-to-elastic displacement ratio for each bridge was determined as the maximum of the ratios of the predicted inelastic to elastic displacements for all bridge columns. The difference between the inelastic and elastic responses is due to:

1- Inelastic analysis accounts for the concentration of inelasticity in critical elements.

2- Research has shown that considering the stiffness or strength degradation in the hysteretic models typically results in higher predictions of the maximum displacements than elastic analysis relying on the equal displacement concept (Priestley et al., 2007).

3- In this study conservative values were used for the hysteretic parameters controlling the reloading and unloading stiffness in RC columns based on the recommendations by Priestley et al., (1996 and 2007) that can result in slightly higher displacement predictions than those obtained from elastic analysis.

4- There are two different load paths in the transverse direction (one via elastic deformation of superstructure and one via inelastic deformation of the columns) which results in different predictions of displacements when compared with the displacements from the elastic analysis.

3.11 Demand to capacity ratios

To evaluate the safety of the bridges the maximum demand to capacity ratios were computed for the 648 cases studied. In each case the capacities of the columns were computed using a moment curvature analysis considering the confinement effects from the spiral reinforcement. The displacement ductility capacity is a function of several factors including the longitudinal and transverse reinforcement ratios, the column heights and the column diameters, resulting in different ductility capacities for each design configuration.

As shown in Fig. 3.15 the ductility demand to ductility capacity ratios are typically less than 0.5 for both cases of restrained and unrestrained abutment conditions. For bridges with restrained abutment conditions this ratio varies from 0.1 to 0.45 while for bridges with unrestrained abutment conditions this ratio varies between about 0.2 and 0.5. The results indicate that the safety margins are not uniform for bridges with different configurations and structures designed using the force-based CHBDC (2006) provisions have different levels of safety. This non uniform level of safety is expected when the force-based design philosophy is used. Displacement-based design approaches are often recommended to resolve this problem (Priestley et al., 2007).

It is noted that the longitudinal responses of the bridges were also studied (Tehrani, 2012) indicating similar conservatism in the design using the CHBDC (2006).

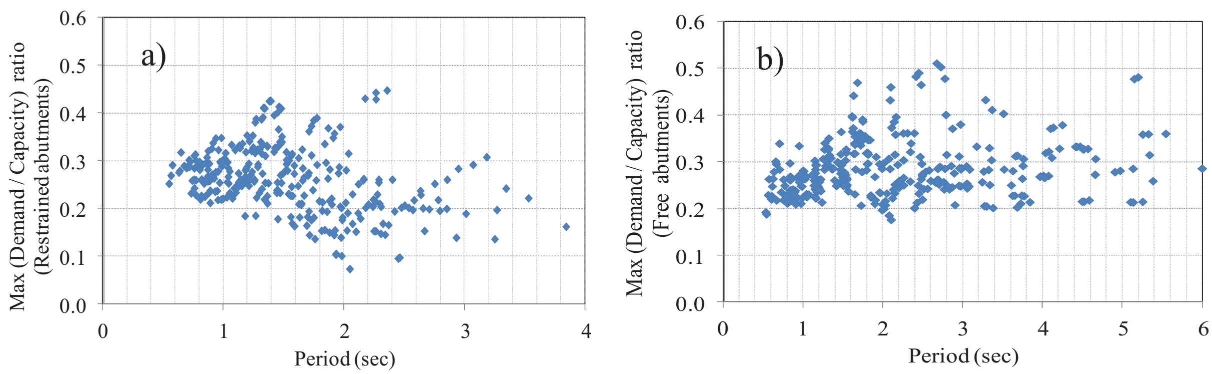

Fig. 3.15. The maximum capacity to demand ratios for a) restrained abutments and b) unrestrained abutments

3.12 Summary and Conclusions

Six hundred and forty-eight bridges with different configurations and with restrained and unrestrained abutment conditions were designed based on the 2006 Canadian Highway Bridge Design Code (CHBDC). Non-linear time history analyses were used to predict the responses of these bridges using 7 spectrum-matched records. The conclusions from this study on four-span reinforced concrete bridges located in Vancouver are summarized as follows:

(1) The force-based design procedures of the 2006 CHBDC gives overly conservative designs due to the combined use of low R factors and the use of importance factors, even for some irregular bridges. In addition, the records used for the predicting the responses matched the 2% in 50 year spectrum of the 2010 National Building Code of Canada, whereas the CHBDC design spectrum is based on accelerations with a probability of exceedance of 10% in 50 years.

(2) The different approaches to predict damage states for different performance levels used in this study provide useful guidance for the next edition of the CHBDC that will be based on performance requirements.

(3) The maximum ductility demands obtained were typically less than 3.0. Based on current seismic design practice and the high percentage of confinement reinforcement in the columns, much higher ductility capacities are expected. The ductility capacities in the range of 6.5 to 8.5 were obtained in the life safety limit state (i.e., no collapse) for the range of columns with different properties (i.e., height, diameter, and reinforcement ratios) studied.

(4) It is noted that conservative hysteretic parameters were used in this study along with spectrum-matched records which are known to be conservative (since they have high frequency content over a wide period range which is not observed in natural records). Therefore, considering less conservative approaches can result in predictions of even lower seismic demands.

(5) The transverse responses of the bridges are reported in this paper, because the behaviour of irregular bridges in the transverse direction is more prone to irregularities than in the longitudinal direction. This is because the response in the transverse direction is governed by a multi-degree of freedom system (displacements are different at different columns), while in the longitudinal direction the response is typically governed by a single degree of freedom system (displacements are the same for all columns). In addition, in the transverse direction, contrary to that in the longitudinal direction, the seismic behaviour is also affected by the position of columns along the length of the bridge and the superstructure stiffness properties. Such parameters are not currently considered in the definition of irregularity in the seismic codes. A study of these bridges in the longitudinal direction (Tehrani and Mitchell, 2012c) indicated similar conservatism in the design using the CHBDC (2006).

(6) It was shown that exceeding a maximum column stiffness ratio of about 5 to 8 can cause significant concentration of ductility demand as well as deviation of the predicted non-linear response from the predicted elastic response.

(7) A superstructure to substructure stiffness ratio, RS, of less than 0.3 in the case of restrained movements at the abutments, and 0.8 in the case of free movements at the abutments may result in incorrect response predictions using elastic multi-mode analysis. Bridges with RS ratios greater than 1.0 typically had more uniform ductility demands in the columns, while bridges with RS values less than 1.0 may exhibit concentrations of seismic ductility demand in a few elements.

(8) The effects of column stiffness ratio and superstructure to substructure stiffness ratio were important for both cases of restrained and unrestrained movements at the abutments. The concentration of ductility demands were slightly larger in the case of restrained abutment condition, while the maximum ductility demands obtained were larger on average for the case of bridges with unrestrained abutments. In the case of unrestrained abutments, the difference between elastic and inelastic analyses was more sensitive to the superstructure to substructure stiffness ratio.

(9) While the column stiffness ratios and the superstructure to substructure stiffness ratios provide simple, practical means of identifying regularity, the DRMS index can also be used to choose an appropriate method of analysis. For bridges with restrained abutment conditions and with DRMS index values of less than 0.08 the results from the elastic and inelastic analyses were in good agreement.

(10) Based on the results obtained, for some configurations, the displacement envelopes were significantly different from the elastic and inelastic analysis; however due to high conservatism in the current CHBDC this did not lead to an unsafe design at least for the cases considered in this study. This problem may be more important if less conservative design approaches are used and when higher earthquake levels are considered. It is recommended that the CHBDC be changed to exclude the use of elastic analysis for irregular emergency-route and lifeline bridges that do not satisfy the criteria obtained in this study.

Acknowledgements

The financial support provided by the Natural Sciences and Engineering Research Council of Canada for the Canadian Seismic Research Network is gratefully acknowledged.

References

Please see the last section.

4 Effects of Column Stiffness Irregularity on the Seismic Response of Bridges in the Longitudinal Direction

Payam Tehrani[2] and Denis Mitchell[1]

4.1 Preface

The effects of different column stiffness irregularity and other important parameters which influence the seismic response of bridges in the transverse direction are presented in Chapter 3. It was concluded that for some cases the use of elastic multi-mode method underestimates the maximum seismic demands in the bridge columns. This chapter describes a study that investigates if the use of elastic analysis is appropriate for predicting the seismic response of irregular bridges in the longitudinal direction.

This chapter focuses on the effects of column stiffness irregularity in the longitudinal direction. Contrary to the transverse direction, the superstructure stiffness in the longitudinal direction is very large and the response of the continuous bridges in the longitudinal direction is similar to a single degree of freedom system. Therefore the main parameters influencing the seismic response in the longitudinal direction include the stiffness of columns and the abutment properties. The influences of the abutments are also studied in the longitudinal direction of the bridges. The results obtained in Chapter 3 for the transverse direction can be combined with the results obtained in the longitudinal direction of bridges to estimate the overall demand to capacity ratios. Similar modelling assumptions, as discussed in Chapter 3 and Appendix A, were used for modelling of

[2] McGill University, Department of Civil Engineering, 817 Sherbrooke St. West, Montreal QC H3A 2K6

bridges in Chapter 4. The computer program developed for the parametric studies is discussed in Appendix B

This chapter was included into a manuscript: Tehrani, P. and Mitchell, D. ”Effects of Column Stiffness Irregularity on the Seismic Response of Bridges in the Longitudinal Direction”, Canadian Journal of Civil Engineering, Manuscript 2012-0091, submitted March, 2012.

According to the NRC Research Press policies, the authors retain the right to “reuse all or part of their manuscript in other works created by them for noncommercial purposes”. (http://www.nrcresearchpress.com/page/authors/information/rights)

4.2 Abstract

The longitudinal seismic responses of 4-span continuous bridges designed based on the 2006 Canadian Highway Bridge Design Code were studied using elastic response spectrum and inelastic time-history analyses. The seismic response of more than 2900 bridges were studied to determine the effects of different design and modelling parameters including the effects of different column heights, column diameters, and superstructure mass as well as different abutment stiffnesses. The bridges were designed using two different force modification factors of 3 and 5. The effects of column stiffness ratios on the elastic and inelastic analysis results, maximum ductility demands, concentration of ductility demands, and demand to capacity ratios were investigated. The results indicate that the seismic response and maximum ductility demands in the longitudinal direction are influenced by important parameters such as the total stiffness of the substructure, the column stiffness ratio and the aspect ratio of the columns.

Key words: Irregular bridges, Column stiffness, Bridge abutment, Inelastic time history analysis, CHBDC 2006, NBCC 2010, Seismic response.

4.3 Introduction

Bridges with significantly different column heights result in considerable concentration of seismic demands in the stiffer, shorter columns. In some cases, the deformation demands on the short columns can cause failure before the longer, more flexible columns can fully participate. In addition, the sequential yielding of the ductile members may result in substantial deviations of the nonlinear response predictions from the linear response predictions made with the assumption of a global force reduction factor, R. This difference is due to the fact that plastic hinges, which appear first in the stiffer columns, may lead to concentrations of unacceptably high ductility demands in these columns. Where possible, the stiffness of piers should be adjusted to attempt to achieve uniform yield displacements and ductility demands on individual piers. A summary of the methods to improve the seismic performance of such bridges is discussed by Tehrani and Mitchell (2012a).

Examples of earthquake damage to irregular bridges with different column heights (e.g., failure of the shorter columns), has been reported (Broderick and Elnashai, 1995; Mitchell et al., 1995; Chen and Duan, 2000). The transverse response of bridges with different column heights and different superstructure stiffnesses was studied by Tehrani and Mitchell (2012a) which demonstrated that irregularities due to different column stiffnesses have significant effects on the seismic behaviour of bridges. Research is needed to investigate if these effects are also important in the longitudinal direction and to evaluate the seismic safety of bridges with column stiffness irregularities. In this paper, the effects of different column stiffnesses and stiffness ratios on the longitudinal responses of bridges are presented. In addition, the influence of the abutments on the seismic response of bridges is investigated. The main parameters in this study include the column heights and diameters, different force modification factors, abutment stiffness and strength, and the hysteresis stiffness degradation parameters used in the nonlinear analyses. The influence of such parameters on the maximum ductility demands, maximum drift ratios, concentrations of ductility demands, ductility demand to capacity ratios, as well as comparisons of predictions from the elastic and inelastic analyses, are presented.

4.4 Modelling and analysis of the bridges

A computer program was developed (Tehrani, 2012) to design the columns and to carry out moment-curvature analyses to compute the curvatures corresponding to different steel and concrete strains used as damage indicators. The displacements, drifts, curvature ductilities, and displacement ductility capacities then can be computed for different performance levels. The confinement effects in the concrete core were considered using the Mander equation (Mander et al., 1988) in the moment-curvature analysis assuming that spiral confinement reinforcement was provided in accordance with the provisions of the Canadian Highway Bridge Design Code (CHBDC) (CSA, 2006).

The bilinear idealization of the moment curvature curves and the determination of the effective curvature at yield, plastic hinge lengths and strain penetration depths for the vertical bars were included in the analyses based on the recommendations by Priestley et al., (1996 and 2007). More details are given by Tehrani and Mitchell (2012a).

The modified Takeda hysteresis model (Otani, 1981) was used in this study to represent the behaviour of the RC columns using Ruaumoko software (Carr, 2009). This model has two main parameters, α and β, which control the unloading and the reloading stiffness, respectively (see Fig. 4.1). The parameter α is usually in the range of 0 to 0.5 and β varies between 0 and 0.6. Increasing the parameter α decreases the unloading stiffness and increasing the parameter β increases the reloading stiffness. For bridge columns, Priestley et al., (1996 and 2007) recommend using the conservative values of α= 0.5 and β =0.

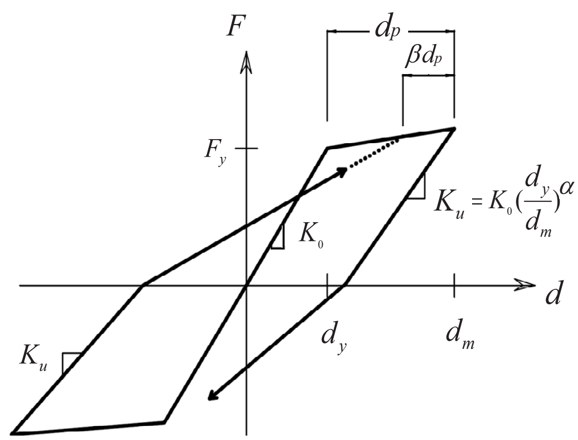

Fig. 4.1. Modified Takeda hysteresis loop (adapted from Carr (2009))

4.5 Range of parameters studied

The seismic responses in the longitudinal direction of 4-span continuous straight bridge structures were studied (see Fig. 4.2). According to Priestley et al., (2007), the longitudinal and transverse behaviour may be studied independently for straight bridges, such as those considered in this study.

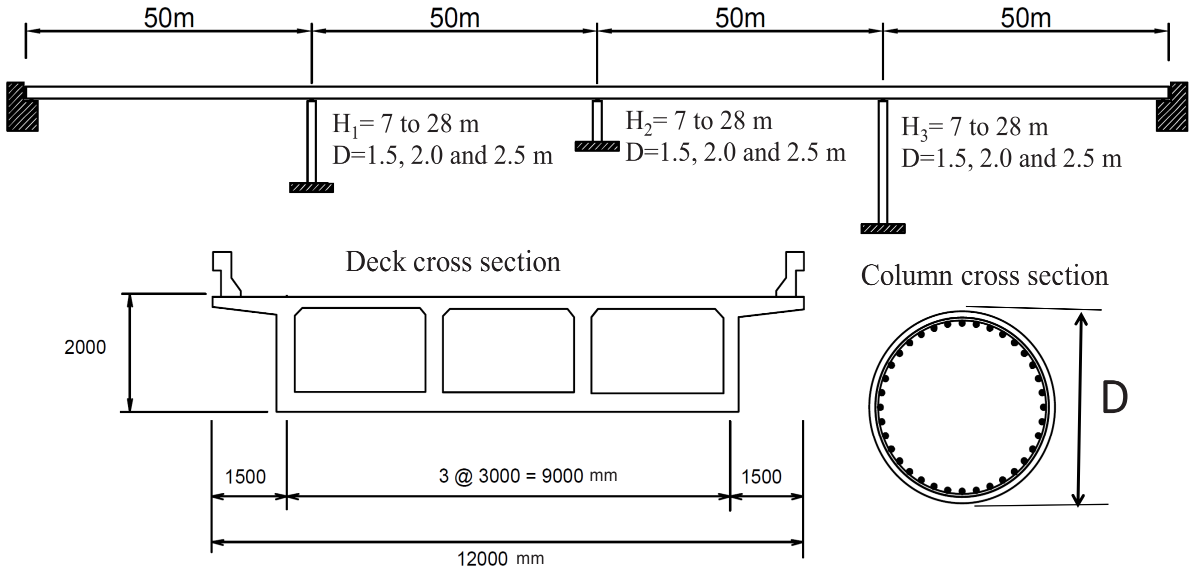

Fig. 4.2. Bridge properties

The bridge structures were designed according to the CHBDC (CSA, 2006) using a force modification factor, R, of 3 and 5 in the longitudinal direction and an importance factor of 1.5 (i.e., I = 1.5 for emergency-route bridges). The bridges were designed for Vancouver assuming a site class C (i.e., $360 \leq V_{s30} \leq 760$ m/sec).

To investigate the effects of different column heights, different diameters and varying column stiffness ratios on the seismic response, a parametric study was carried out. Column heights were varied from 7 to 28 m with increments of 3.5 m (i.e., 7 different heights for each column). The column diameters were 1.5, 2.0, and 2.5 m and in each configuration the three columns all had the same diameters (see Fig. 4.2). These combinations of column heights and diameters resulted in 252 bridges with different column arrangements (i.e., it was assumed that the position of columns along the bridge has no effects on the seismic response in the longitudinal direction). The superstructure mass was considered as a uniformly distributed load of 200 kN/m. The effect of increasing the superstructure mass to 300 kN/m on the seismic response was also investigated for some cases. The bridges were designed and evaluated for two different R values of 3 and 5. Further, different hysteresis parameters, α and β, were used in the structural modelling. In addition, the effects of abutment stiffness and capacity on the seismic response of bridges were also considered for different number of piles and different gap lengths between the superstructure and the abutment. The significance of the P-Delta effects was also studied. Considering all of the parameters, more than 2900 bridge structures with different geometries, designs and modelling parameters were studied. A schematic view of the structural models is shown in Fig. 4.3.

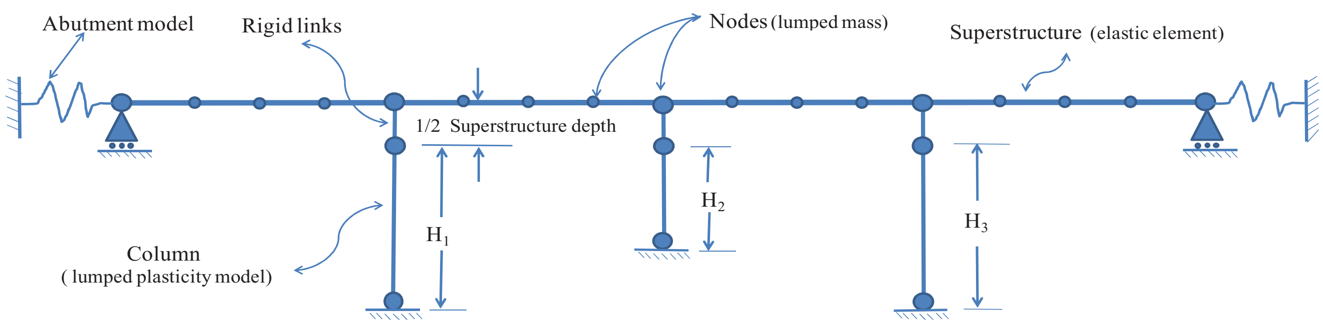

Fig. 4.3. Structural modelling of the bridges

The minimum and maximum longitudinal reinforcement ratios in bridge columns were 0.8% and 6.0%, respectively. The transverse steel ratios were determined based on the CHBDC 2006 provisions to satisfy the requirements for confinement in the plastic hinge regions and to provide factored shear resistances corresponding to the capacity design philosophy. However in most cases the spiral confinement reinforcement ratio of 1.2% controlled. The concrete compressive strength and the yield stress of the reinforcing bars were taken as 40 and 400 MPa, respectively.

For the inelastic time history analyses, 7 spectrum matched records were used. These artificial records were generated using the SIMQKE software (Vanmarcke and Gasparini, 1979 and Carr, 2009). For the nonlinear analyses of the bridges, the records were matched to the design spectra given in the National Building Code of Canada (NBCC) (NRCC, 2010). These spectra correspond to 2% probability of exceedance in 50 years, while the design spectrum given in the CHBDC (CSA, 2006) corresponds to 10% probability of exceedance in 50 years. The 2010 NBCC spectrum with the hazard level of 2% in 50 years, which will be used in the next edition of the CHBDC, was used to evaluate the seismic behaviour of the bridges. For this more appropriate probability of occurrence the effects of irregularity on the seismic response are expected to be more pronounced. The bridges should not collapse at this seismic hazard level.

The resulting average response spectrum of the seven records used along with the design spectra for Vancouver based on the CHBDC (CSA, 2006) and the NBCC (NRCC, 2010) are shown in Fig. 4.4. The average displacement for each bridge was determined using the averaging procedure proposed by Priestley et al. (2007) which considered the maximum positive and maximum negative displacements predicted for each input record.

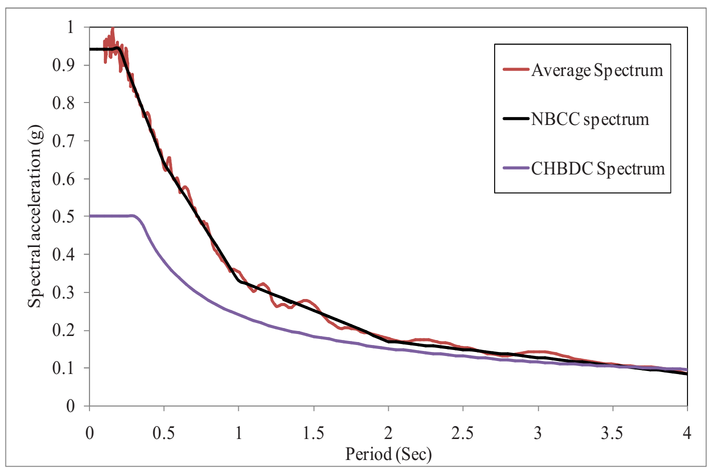

Fig. 4.4. Average response spectrum for 7 records used for inelastic time history analysis matching the 2010 NBCC spectrum (2% in 50 years)

The capacity of the columns were determined assuming that the maximum strains in steel bars attained the bar buckling strain limits given by Berry and Eberhard (2007) and the maximum concrete compression strain predicted by the Mander equation modified based on the recommendations by Priestley et al., (2007) for the life safety limit state. More details concerning the evaluation of ductility capacity of columns using different methods are available in Tehrani and Mitchell (2012a).

4.6 Modelling the abutments

Fig. 4.5 shows the abutment details, with a gap between the backwall and the superstructure which is supported on bearing pads. The simplified abutment model developed by Mackie and Stojadinovic (2003) and Aviram et al. (2008), as shown in Fig. 4.6, was used to study the influence of the abutments on the seismic response of the bridges in the longitudinal direction. The longitudinal response is a function of the system response including the elastomeric bearing pads, the gap, the abutment backwall, the abutment piles, and the soil backfill material. Prior to impact due to gap closure, the superstructure forces are transmitted through the elastomeric bearing pads to the abutment, and subsequently to the piles and backfill, in a series system. After gap closure, the superstructure bears directly on the abutment backwall and mobilizes the full passive backfill pressure (Aviram et al., 2008). In the simplified model used the effects of the bearing pads on the responses are ignored. However, it has been shown that the results from the simplified abutment models in the longitudinal direction are in good agreement with those obtained using more detailed models (Aviram et al., 2008).

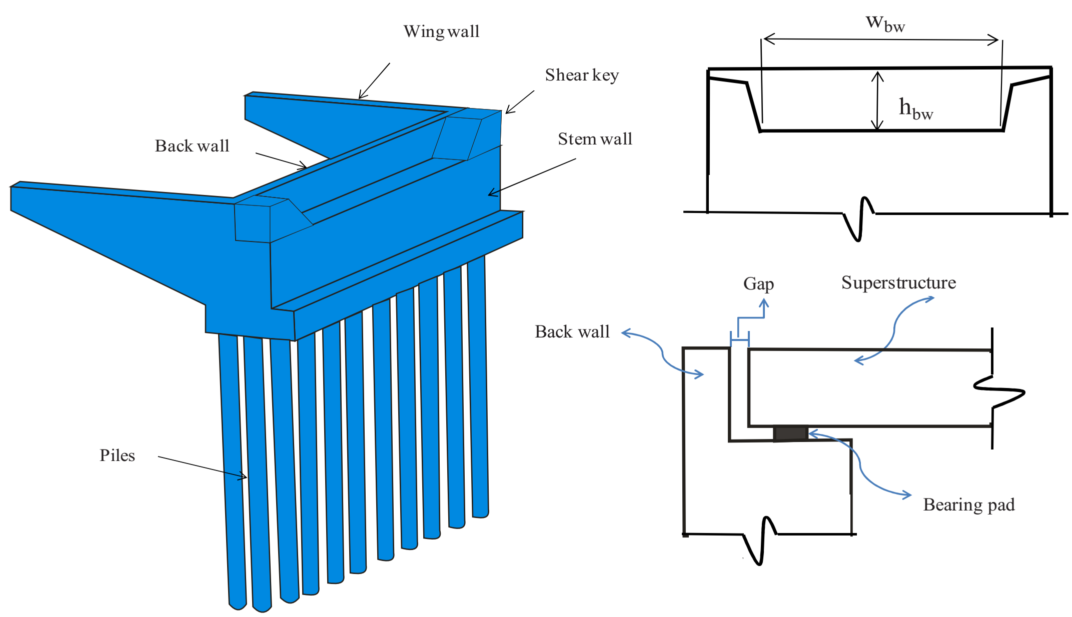

Fig. 4.5. Schematic view of the seat-type abutment and its components

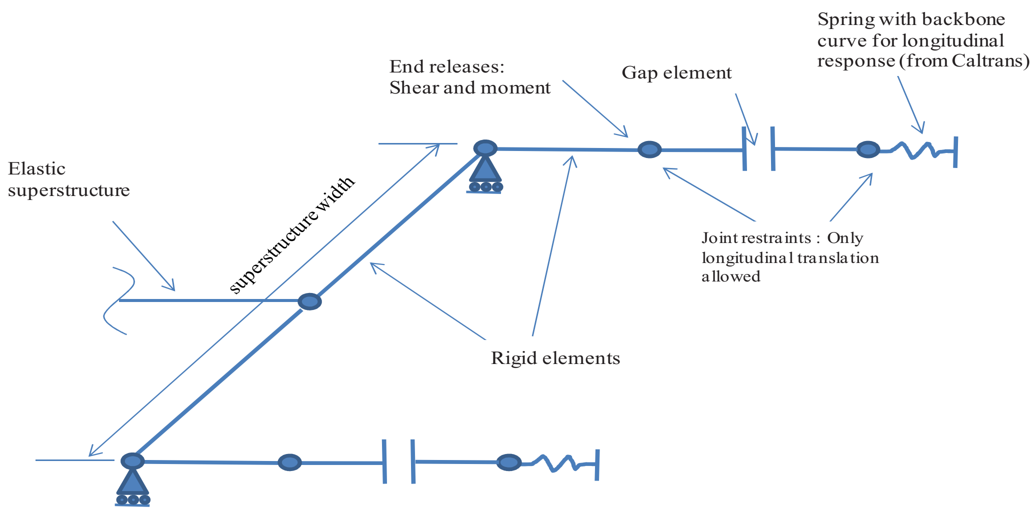

Fig. 4.6. Simplified abutment model for the longitudinal response

The abutment response in the longitudinal direction is accounted for by two zero-length elements at the extreme locations of rigid elements connected to the superstructure, as shown in Fig. 4.6. The abutment stiffness, K_{abt}, and its ultimate strength, P_{bw}, are obtained from Eq. [4.1] and [4.2] from Caltrans (2006) which are based on a study by Maroney and Chai (1994).

$$[4.1] \quad K_{abt}=K_i\, w_{bw}\, (h_{bw}/1.7)$$

$$[4.2] \quad P_{bw}= p\, A_e\, (h_{bw}/1.7)$$

$$[4.3] \quad A_e= h_{bw}\, w_{bw}$$

where K_i is the initial embankment fill stiffness and is taken as 11500 kN/m/m, p is the passive soil pressure taken as 239 kPa and A_e is the effective abutment area, defined as the area which is effective for mobilizing the backfill. The effective backwall area is given by Eq. [4.3] (Caltrans, 2006), with h_{bw} and w_{bw} defined in Fig. 4.5. In this study h_{bw} and w_{bw} were taken as 2.0 m and 9.0 m, respectively based on the superstructure geometry.

To model the abutments the bilinear hysteresis loop model with "slackness" (Carr, 2009), as shown in Fig. 4.7a, was used in the RUAUMOKO software (Carr, 2009). This hysteresis model includes a gap and a spring in series which can be used to model the initial gap and the resulting stiffness and strength associated with the abutments. An example of the hysteretic behaviour of such an element obtained in the analyses is demonstrated in Fig. 4.7b. As shown, the abutment elements only resist compression forces.

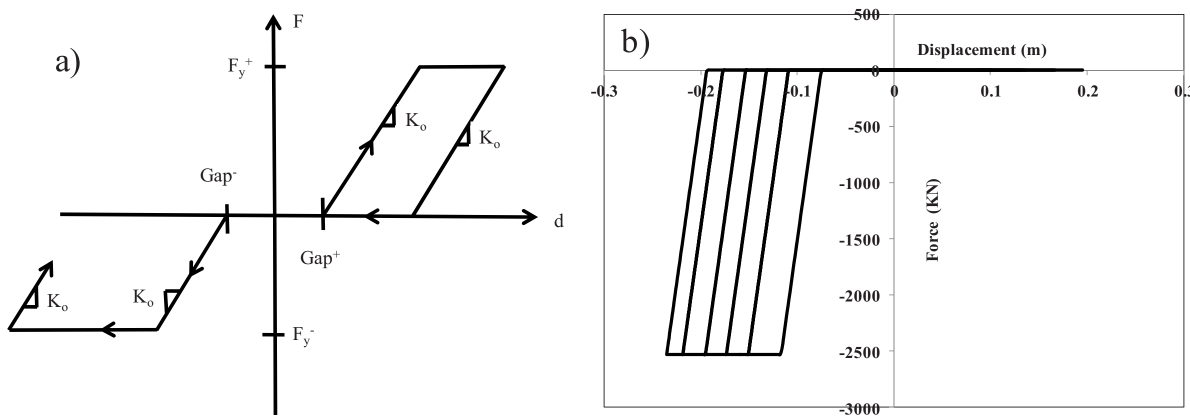

Fig. 4.7. a) Hysteresis model with gap and nonlinear spring used to model abutment response (Carr, 2009) b) typical nonlinear response from analysis

Different abutment stiffnesses and strengths were considered in the structural modelling to study the seismic response of bridges in the longitudinal direction including cases with (see Fig. 4.5) and without piles. To estimate the stiffness and strength of the piles the empirical pile resistant equations given by Goel and Chopra (1997) (see Eqs. [] and []) were used. These equations provide an ultimate strength that is assumed to occur at 1 in. (25 mm) displacement. The maximum displacement of the piles was taken as 2.4 in. (60 mm). The stiffness of the piles was conservatively neglected when deformations exceeded this value, since the abutments and back walls are expected to be damaged at deformations higher than this level (Goel and Chopra, 1997). The combined response of the backfill and piles is determined by the combined response predicted by Eqs. [4.1] to [4.5].

$$[4.4] \quad R_{pile} = 40 \text{ kips / pile} \quad = 178 \text{ KN/pile}$$

$$[4.5] \quad K_{pile} = 40 \text{ kips /in.} \quad = 7000 \text{ KN/m}$$

Four different gap lengths (i.e., 25, 50, 75, and 150 mm) along with three different pile configurations (i.e., 0, 10, and 20 piles) were considered for modelling the influence of the abutments. In addition, to study the influence of the abutments on different bridge configurations, the column heights were varied from 7 to 28 m for each column with increments of 7 m. This resulted in more than 720 bridge models.

The addition of the backfill contribution without piles provided a significant decrease in the ductility demand. The seismic responses were only slightly improved when piles were added to the abutments, however the effects of increasing the number of piles were more pronounced for the case of smaller gap lengths and for more flexible bridges.

The reductions of ductility demand in the bridge columns are shown in Fig. 4.8b as a function of the ratio of the total stiffness of the columns, K_{cols}, and the abutment effective stiffness, $K_{eff\text{-}abt.}$ The abutment effective stiffness, $K_{eff\text{-}abt}$, accounting for the gap closure is defined in Fig. 4.8a. As this ratio, K_{cols} / $K_{eff\text{-}abt}$, decreases the influence of the abutments in the seismic response becomes more pronounced with up to 80% reduction in the ductility demands. This indicates that the seismic response of bridges with flexible columns will be affected more significantly by including the abutments in the structural modelling.

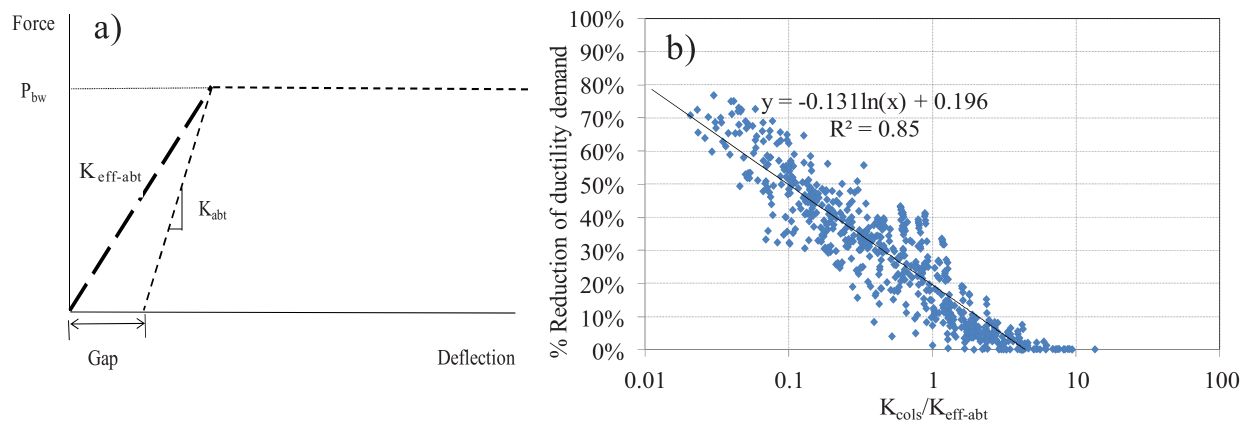

Fig. 4.8. Influence of abutment stiffness: a) effective abutment stiffness (Caltrans, 2006); b) the influence of the ratio of the total stiffness of columns to effective abutment stiffness on the maximum ductility demands

4.7 Evaluation of maximum ductility demands

An important outcome of the nonlinear dynamic analyses is the maximum column ductility demands which will be used to assess the seismic performance. The effects of column stiffness irregularities on the maximum displacement ductility demands were investigated. For each bridge the ductility demand in the most critical column is reported as the maximum ductility demand in the bridge. The results are based on the average responses obtained by means of inelastic time history analysis using 7 spectrum matched records.

The effects of the total stiffness of the columns on the maximum ductility demands obtained from nonlinear dynamic analyses are presented in Fig. 4.9. As expected the stiffer structures typically attract higher ductility demands in the columns. Another important parameter which will influence the maximum column ductility demand is the maximum stiffness ratio of the columns (i.e., maximum column stiffness divided by minimum column stiffness). Larger column stiffness ratios typically result in a concentration of ductility demand in the stiffest column which in turn imposes higher ductility demands on this element. The impact of the maximum column stiffness ratio on the maximum ductility demand of columns is depicted in Fig. 4.10. Since both the total stiffness of the columns and the maximum stiffness ratio of columns affect the maximum ductility demands, another parameter has been defined as the product of these two variables (i.e., total stiffness of columns times maximum stiffness ratio of columns). As presented in Fig. 4.11, this new parameter shows an improved correlation with the maximum ductility demands in the columns. The results are presented for two different force modification factors of 3 and 5 used in design. As the force modification factor, R, increases, the scatter in the maximum predicted ductility demands increases and the maximum ductility demands become more sensitive to the product of the total stiffness of the columns and the maximum stiffness ratio, as indicated by the slope of the regression lines in Fig. 4.9 to Fig. 4.11.

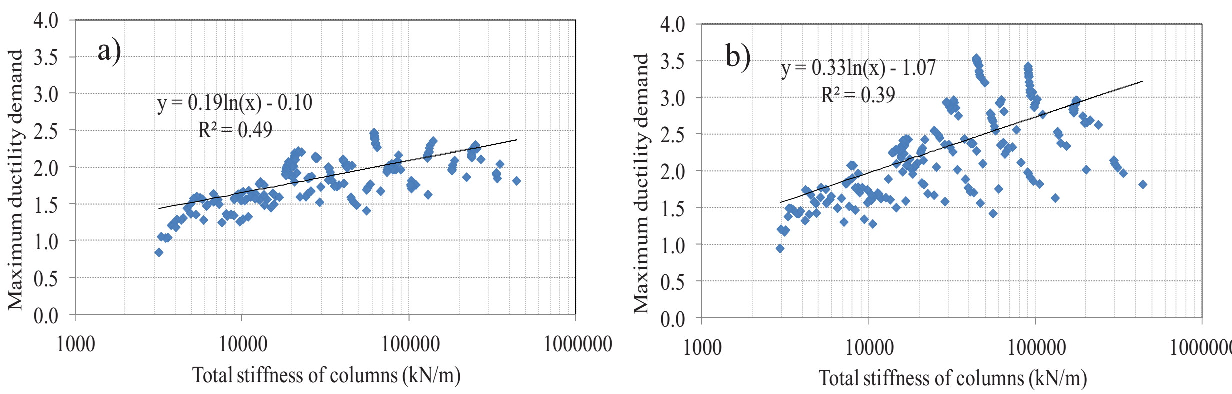

Fig. 4.9. Effects of total stiffness of columns on the maximum displacement ductility demands: a) R=3, α=0.5 and β=0; b) R=5, α=0.5 and β=0

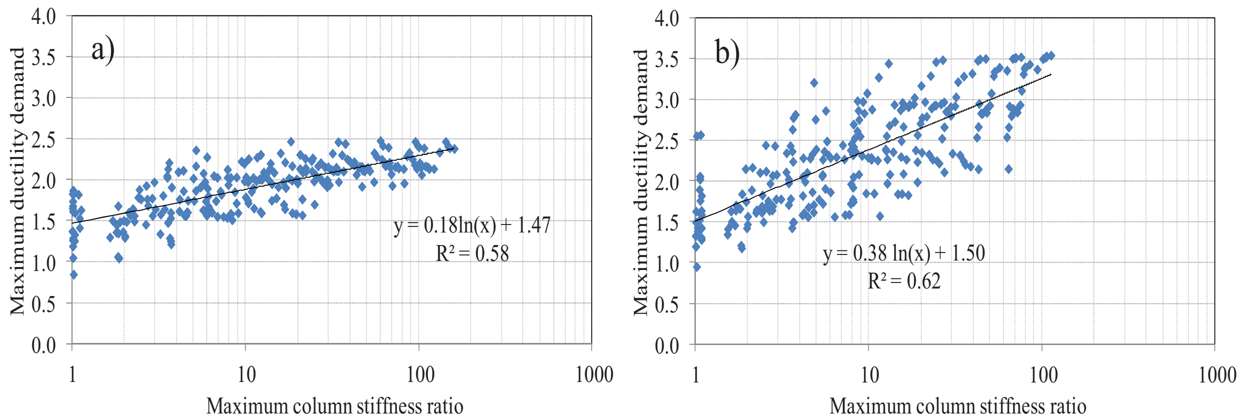

Fig. 4.10. Effects of maximum column stiffness ratio on the maximum displacement ductility demands: a) R=3, α=0.5 and β=0; b) R=5, α=0.5 and β=0.

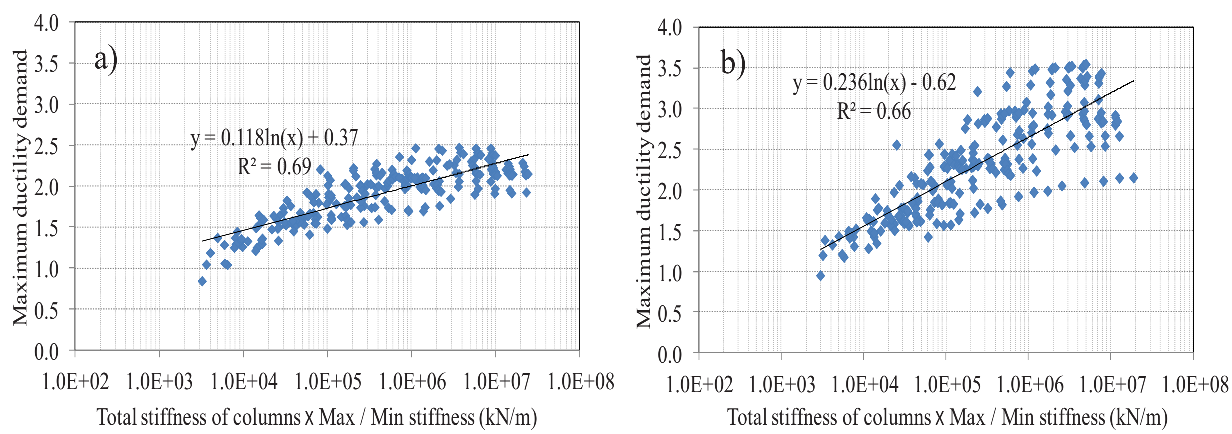

Fig. 4.11. Effects of "columns total stiffness times max stiffness ratio" on the maximum displacement ductility demands: a) R=3, α=0.5 and β=0; b) R=5, α=0.5 and β=0.

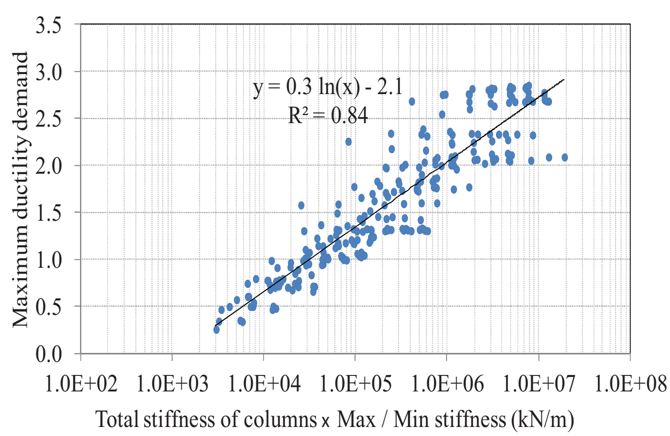

Fig. 4.12. Effects of "columns total stiffness times max stiffness ratio" on the maximum displacement ductility demands considering the influence of abutments (Gap=50 mm, R=5, α=0.5 and β=0)

The correlation between the maximum ductility demand and the product of the total stiffness of columns and maximum stiffness ratio is even better, as shown in Fig. 4.12, when the influence of the abutments was included. This is probably due to the fact that the inclusion of the abutments in the structural modelling significantly reduces the nonlinear geometric effects due to P-Delta effects.

The results presented in Figs. Fig. 4.9 to Fig. 4.11 were derived assuming the unloading and reloading hysteresis parameters of α=0.5 and β=0 in the modified Takeda hysteresis model. The analysis results using hysteresis parameters of α=0 and β=0.6 (i.e., lower bound values) and also α=0.3 and β=0.3 (i.e., close to the average values from tests) are demonstrated in Figs. Fig. 4.13a and Fig. 4.13b, respectively. The maximum ductility demands for these cases are about 3.0 and 3.2, respectively, while in the case of α=0.5 and β=0 (i.e., upper bound values) the maximum ductility demands were about 3.5. The influence of the hysteresis parameters was larger for the bridges with higher values of the parameter "total stiffness of columns times the max stiffness ratio". However, in general, the influence of the hysteresis parameters on the seismic response was not very significant. These effects were even smaller when a force modification factor of R=3 was used in design, due to the smaller nonlinear deformations in the columns.

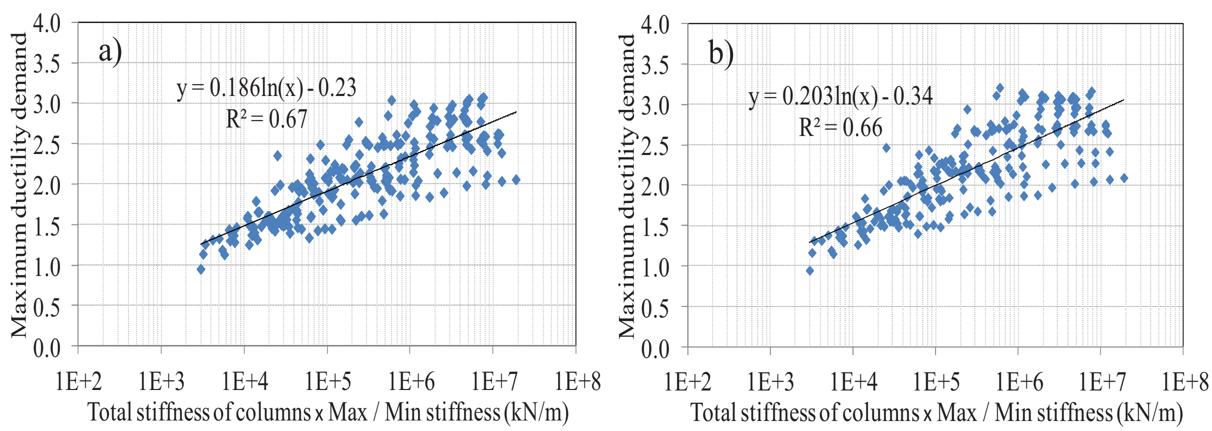

Fig. 4.13. Effects of hysteresis parameters, α and β, on the maximum displacement ductility demands for R=5 and: a) α=0 and β=0.6; b) α=0.3 and β=0.3

4.7.1 P-Delta effects

To investigate the importance of P-Delta effects, the bridges previously designed with these effects were also designed neglecting P-Delta effects (i.e., using a first-order analysis) and an R factor of 5. The maximum ductility demands versus the average aspect ratio (i.e., H_{ave}/D) of the bridge columns for this case are shown in Fig. 4.14. Where the average aspect ratios were more than about 9 (corresponding to an average slenderness ratio of 72), the P-Delta effects were more important and the bridges were susceptible to instability due to P-Delta effects when subjected to ground motions corresponding to 2% probability of exceedance in 50 years. This slenderness limit may be smaller for bridges with larger dead loads. As shown in Fig. 4.14, the extremely large ductility demands (i.e., larger than 10) obtained for average slenderness ratios greater than 72 are due to structural instability. It is noted that, for these slender cases, the inclusion of the stiffness and strength of the bearing pads and abutments resulted in stable seismic responses.

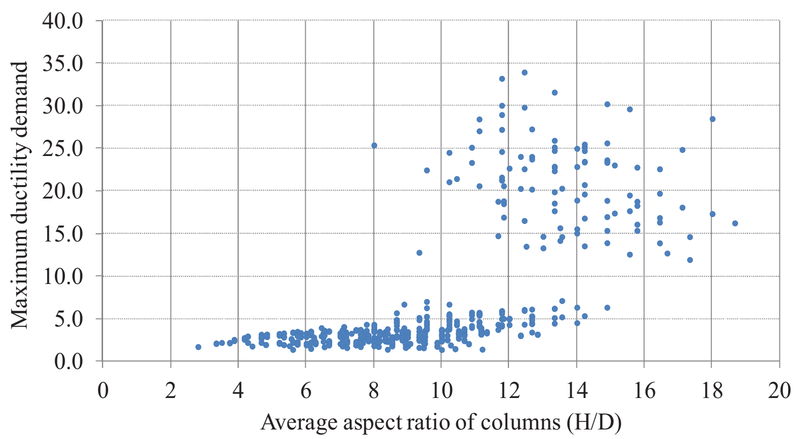

Fig. 4.14. Possible instability due to P-Delta effects for bridges that were designed neglecting P-Delta effects.

4.8 Predictions from inelastic versus elastic analysis

A study by Tehrani and Mitchell (2012a) demonstrated that column stiffness irregularities can result in significant deviations of the elastic multi-mode analysis results from the inelastic dynamic analysis when the transverse response of bridges were studied.

As shown in Fig. 4.15 the differences in the maximum displacement predictions using the elastic and inelastic analyses were typically small for response in the longitudinal direction. The differences were generally less than 20% with higher differences when the total stiffness of columns was quite low. This is probably due to P-Delta effects and the higher dispersions of the response spectra of the ground motion records in the longer period range. However, for the bridges with lower total column stiffness the maximum ductility demands are typically small (e.g., see Fig. 4.9). The ratio of the displacements obtained from the inelastic and elastic analyses were not significantly affected by the maximum stiffness ratio of the columns. The use of R=3 in design also led to similar results obtained for the case of R=5.

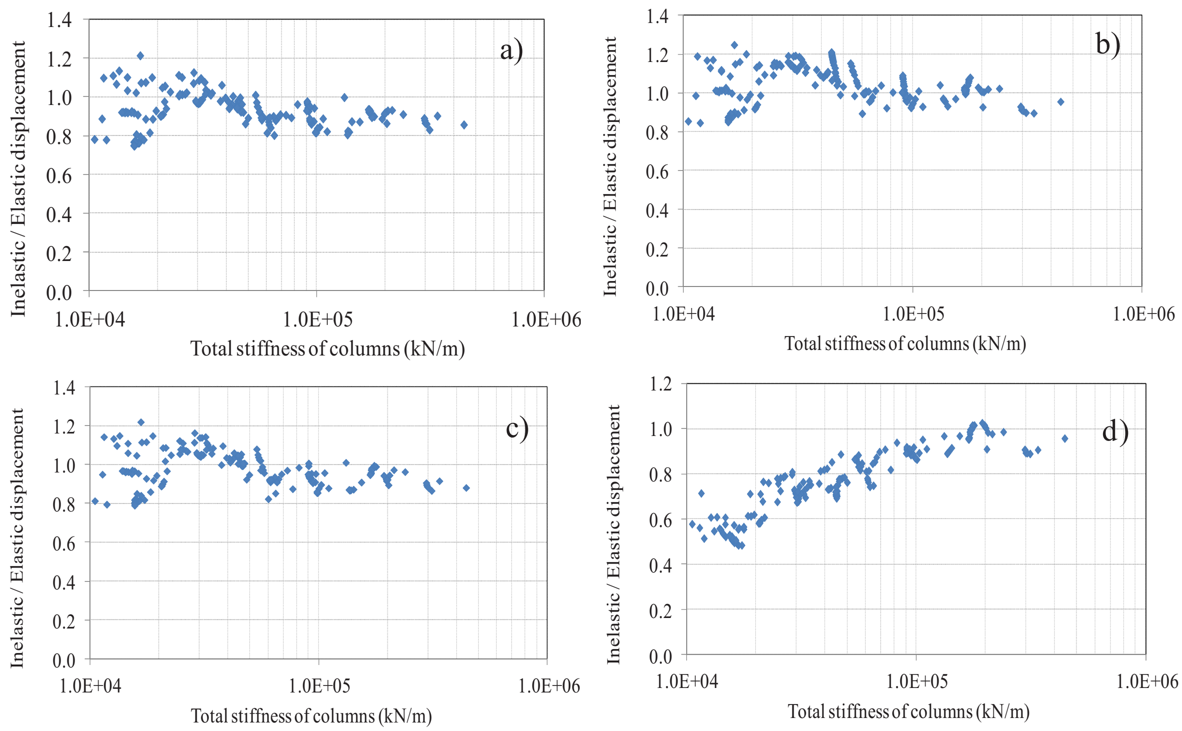

Fig. 4.15. Effects of total stiffness of columns on the ratio of the displacements obtained using inelastic and elastic analysis for R=5 and: a) α=0 and β=0.6; b) α=0.5 and β=0; c) α=0.3 and β=0.3; d) considering the influence of the abutments on seismic response (no piles, gap=50 mm, α=0.5 and β=0)

The ratios of the maximum displacement demands obtained using the inelastic and elastic analyses are presented in Fig. 4.15a-c for different hysteresis loop parameters. The Takeda hysteresis loop model with $\alpha=0$ and $\beta=0.6$ represents no unloading stiffness degradation and small reloading stiffness degradation (i.e., lower bound values), while the choice of $\alpha=0.5$ and $\beta=0$ overestimates the unloading and reloading stiffness degradation (i.e., upper bound values). Nevertheless, the effects of using different hysteresis parameters are not significant and the differences between the inelastic and elastic results are typically small, as shown in Fig. 4.15a -c. It should be noted that the equal displacement concept is based on bi-linear hysteresis models with no stiffness degradation. When stiffness degradation is considered in the nonlinear response, somewhat different predictions may be obtained.

For the cases where the effects of the abutments are included in the nonlinear analysis the resulting displacements for the flexible structures will be much smaller (see Fig. 4.15d) than those predicted with the assumption of free longitudinal movements at the ends (see Fig. 4.15b). The elastic responses were computed assuming free movement at the abutments in the longitudinal direction (i.e., roller supports), an assumption typically made in practice for design and analysis. Such an assumption is conservative, as is evident by comparing the results in Fig. 4.15b with those shown in Fig. 4.15d.

4.9 Concentration of seismic demands

In the longitudinal direction of continuous bridges all of the columns have almost equal displacement demands. On the other hand, in the transverse direction the columns will have different displacements depending on: a) stiffness and position of the columns; b) the superstructure transverse stiffness and c) the abutment restraint conditions.

The influence of the maximum stiffness ratio of columns on the maximum to minimum (max/min) ductility demands for response in the longitudinal direction is shown in Fig. 4.16. Increasing the maximum stiffness ratio of columns leads to higher concentrations of ductility demands in a few columns.

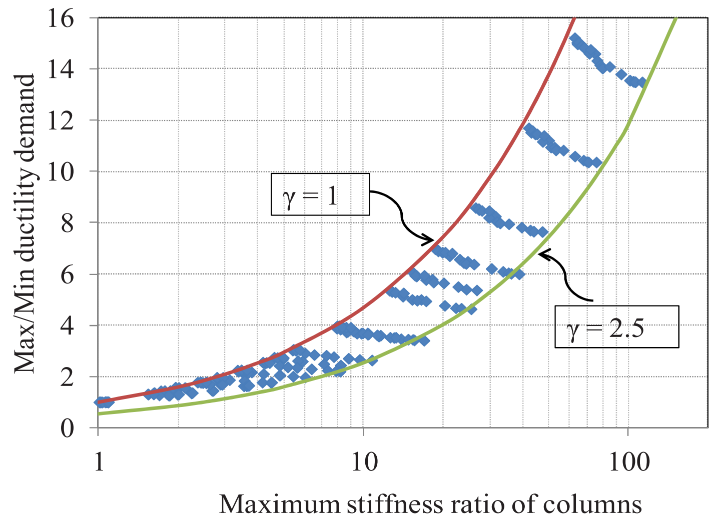

Fig. 4.16. Effects of maximum column stiffness ratio on the Max/Min ductility ratio (R=5, α=0.5 and β=0) and predictions using Eq.[4.11].

The relationship between the maximum column stiffness ratio and the maximum to minimum ductility demands can be derived, assuming that the displacement demand, Δ_d, is equal for all columns in the longitudinal direction. The maximum and minimum ductility demands can be computed using Eq. [4.6a-b], where Δ_y is the displacement at yield.

$$[4.6a] \quad \mu_{max} = \frac{\Delta_d}{(\Delta_y)_{min}} \quad \text{and} \quad [4.6b] \quad \mu_{min} = \frac{\Delta_d}{(\Delta_y)_{max}}$$

where μ_{max} and μ_{min} are the maximum and minimum displacement ductility demands in the columns.

The strain penetration depth, L_{sp}, is much smaller than the column height and can be ignored. The displacement at general yielding, Δ_y, can be approximated using Eq.[4.7a-b] for the cantilever columns.

$$[4.7a] \quad (\Delta_y)_{max} = \frac{\Phi_y H_{max}^2}{3} \quad \& \quad [4.7b] \quad (\Delta_y)_{min} = \frac{\Phi_y H_{min}^2}{3}$$

The yielding curvature, Φ_y , is mainly a function of the column diameter and the yield strain of the reinforcing bars and can be estimated using Eq. [4.8] for circular columns (Priestley et al., 2007).

$$[4.8] \quad \Phi_y = \frac{2.25\varepsilon_y}{D}$$

Since all of the columns in this study have the same diameters for each configuration, it can be assumed that the yielding curvature of the columns are almost equal and thus the maximum to minimum ductility demand ratio can be estimated using Eq. [4.9].

$$[4.9] \quad \frac{\mu_{\max}}{\mu_{\min}} = \frac{(\Delta_y)_{\max}}{(\Delta_y)_{\min}} = (\frac{H_{\max}}{H_{\min}})^2$$

For the cantilever columns considered in this study the maximum column stiffness ratio can be calculated using Eq. [4.10]:

$$[4.10] \quad \frac{K_{\max}}{K_{\min}} = \gamma(\frac{H_{\max}}{H_{\min}})^3$$

where K_{max} and K_{min} are the maximum and minimum stiffness of the columns, γ is the ratio of the effective moment of inertia (i.e., moment at general yielding of column divided by yield curvature) of the stiffest column to that of the most flexible column. Although the column diameters are equal in this study, due to different flexural strengths of the columns the effective moment of inertia of the stiffer columns which often require higher reinforcement ratios is typically higher than that of the more flexible columns assuming almost equal axial loads in the columns (since the span lengths are equal). From Eqs. [4.9] and [4.10], the max/min ductility ratio can be estimated using Eq. [4.11].

$$[4.11] \quad \frac{\mu_{\max}}{\mu_{\min}} = \gamma^{-0.67}(\frac{K_{\max}}{K_{\min}})^{0.67}$$

This expression can be adjusted for cases with different column diameters by multiplying the right hand side of Eq. [4.11] by the ratio of the column diameter of the shortest column to that of the longest column. The predicted maximum to minimum ductility demands using Eq. [4.11] are compared with the results from nonlinear analysis in Fig. 4.16. In this comparison Eq. [4.11] has been plotted with two values of γ (1 and 2.5) which represents the range of the ratios of the effective moments of inertia for the bridge columns in this study. As can be seen in Fig. 4.16, Eq. [4.11] provides a fairly accurate representation of the maximum to minimum ductility ratio, bounding the data for the range of columns studied. Eq. [4.11] can be used by designers to minimize the concentration of ductility demands by adjusting K_{max}/K_{min}.

4.10 Drift ratios

The maximum drift ratios of columns obtained using nonlinear dynamic analyses are shown in Fig. 4.17a. These maximum drift ratios are generally around 0.5% to 3.5% and typically decrease with increasing values of total stiffness of the columns. The drift ratios were relatively similar for different R values, as shown by comparing Fig. 4.17a and b. The addition of the abutments in the structural modelling decreased the maximum drift ratio by about 1.5%, as shown in Fig. 4.18, especially in the case of flexible substructures.

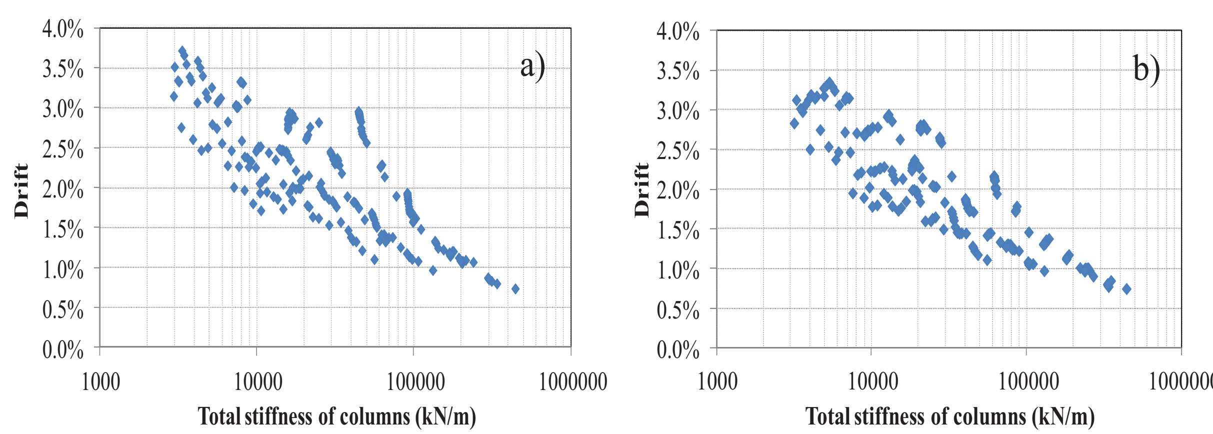

Fig. 4.17. Maximum drift ratio of columns for: a) R=5 and Takeda hysteresis model with α=0.5 and β=0; b) R=3 and Takeda hysteresis model with α=0.5 and β=0

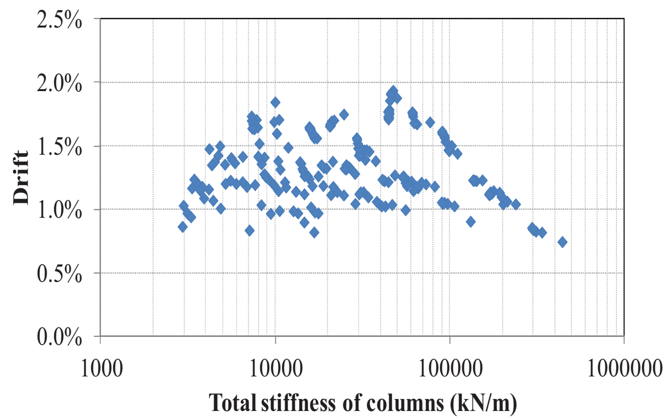

Fig. 4.18. Maximum drift ratio of columns considering the influence of the abutments in nonlinear response (no piles, gap=50 mm, R=5, α=0.5 and β=0)

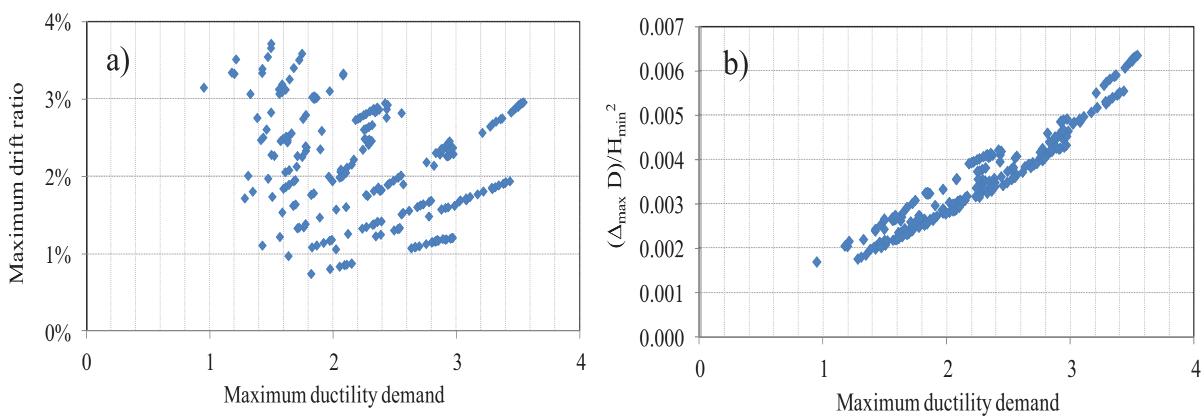

Fig. 4.19. Maximum drift ratio versus maximum ductility demand using R=5, α=0.5 and β=0 for: a) maximum drift ratio versus maximum ductility demand; b) $(\Delta\ D) / H^2$ versus maximum ductility demand

A comparison of the maximum drift ratio versus the maximum ductility demand of the columns is shown in Fig. 4.19a. Drift ratios are widely used in practice (e.g., in codes) for the assessment of structural performance. However the drift ratios may not be a good indicator of structural damage. As indicated before, the ductility was found to be proportional to $(\Delta\ D) / H^2$ (see Eq. [4.10]). In Fig. 4.19b another damage indicator is defined as $(\Delta_{max}\ D) / H_{min}^2$ (i.e., max drift ratio divided by the aspect ratio). This new parameter shows a significantly improved correlation with the column ductility demands, as shown Fig. 4.19b, compared to Fig. 4.19a. Therefore this parameter is a better indicator of damage, since the ductility demands and the corresponding structural damage are proportional to D/H^2 rather than 1/H.

4.11 Ductility demand versus ductility capacity

The maximum ductility demands obtained from the nonlinear dynamic analyses were compared to the ductility capacities of the columns to evaluate the safety margin of the columns. In Fig. 4.20 the ratio of the maximum ductility demands to the ductility capacities are shown versus the maximum stiffness ratio of the columns for various hysteresis parameters and R factors. The ductility capacity for each column is a function of the geometric properties and details of reinforcement. These ductility capacities were computed for the life safety performance level (i.e., no collapse).

The ductility demand to ductility capacity ratios from the analyses in the longitudinal direction are in the range of 0.2 to about 0.5 when a force modification factor of R=5 was used (e.g., see Fig. 4.20a). In the case of R=3 these ratios were around 0.2 to 0.4 as shown in Fig. 4.20b. Similar results were obtained when the transverse response of similar bridges were studied (Tehrani and Mitchell, 2012a). Using a lower force modification factor of R=3 did not significantly increase the safety margins as shown in Fig. 4.20c and d.

As the maximum stiffness ratio of the columns increases, the range of the maximum demand to capacity ratios obtained increases as well. For example in Fig. 4.20a when the maximum stiffness ratios are less than about 5.0 the maximum demand to capacity ratios are less than around 0.3. For maximum stiffness ratios between 5.0 to 10.0 the maximum demand to capacity ratio is around 0.4 and exceeding the stiffness ratio of 10.0 can lead to demand to capacity ratios of about 0.5.

When lower stiffness degradations were considered in the modelling (i.e., α=0.3 and β=0.3), the maximum demand to capacity ratios decreased to around 0.4 as demonstrated in Fig. 4.20c. The influence of hysteresis parameters was more pronounced for bridges with higher column stiffness ratios, possibly due to the higher nonlinear deformations and the concentration of nonlinear demands on the columns. The same trends were observed for the case of R=3 as shown in Fig. 4.20d. When the superstructure mass was increased to 300 kN/m the effects of the column stiffness ratios became even more important as shown in Fig. 4.21a and b. Including the influence of the abutments in the structural modelling reduced the maximum demand to capacity ratios to around 0.35 as shown in Fig. 4.22.

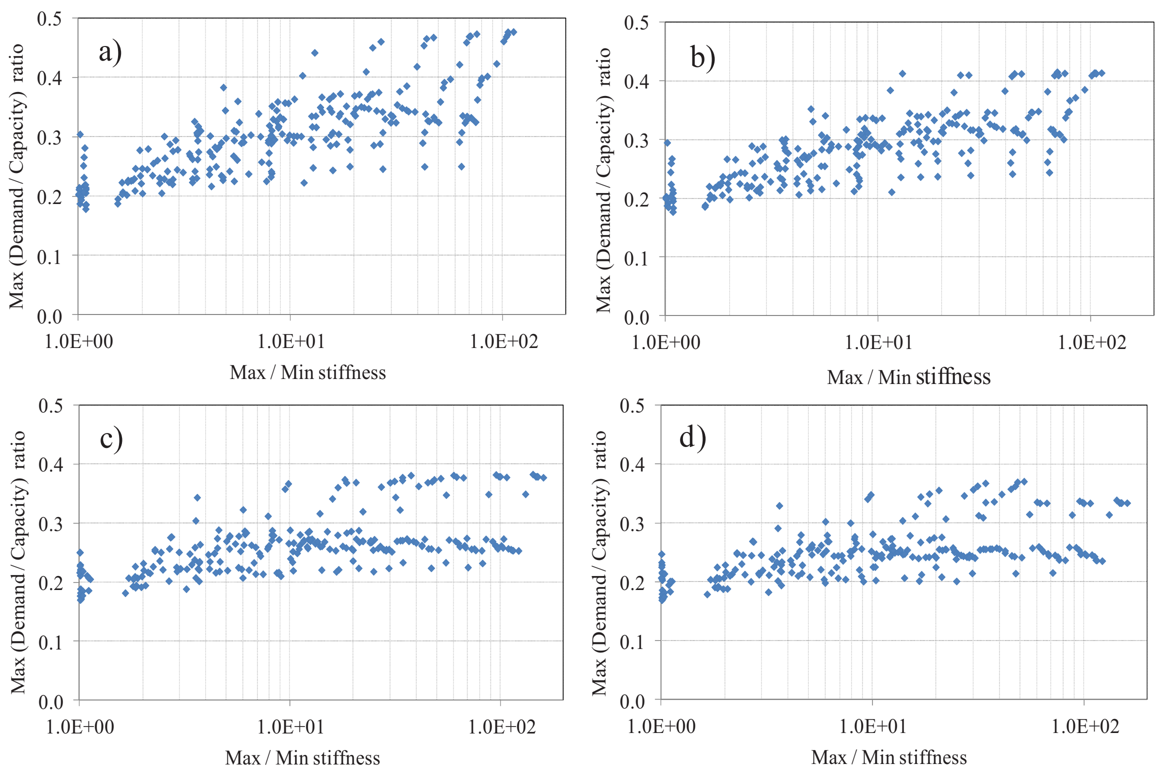

Fig. 4.20. Maximum ductility demand to ductility capacity ratios obtained for: a) R=5, α=0.5 and β=0; b) R=5, α=0.3 and β=0.3; c) R=3, α=0.5 and β=0; d) R=3, α=0.3 and β=0.3

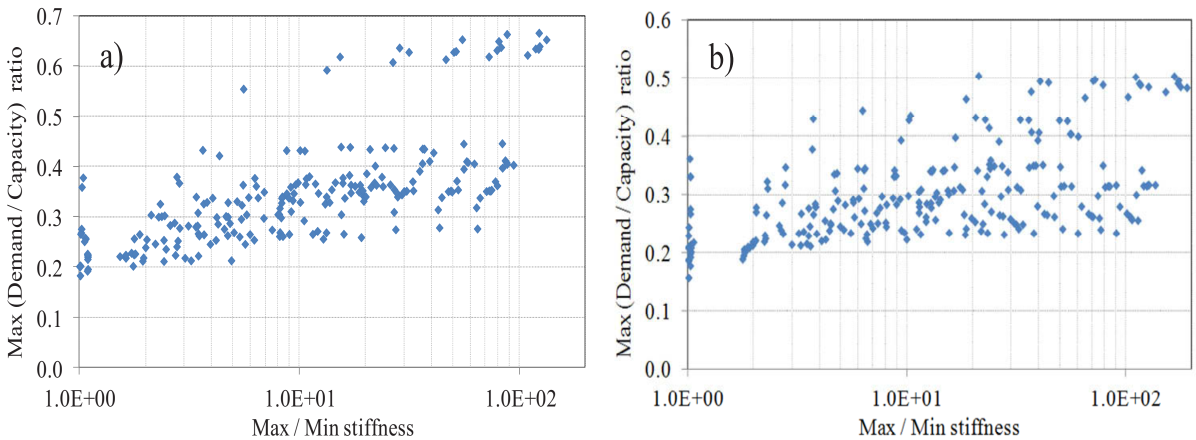

Fig. 4.21. Effects of increasing the superstructure mass to 300 KN/m on the maximum demand to capacity ratios obtained for: a) R=5, α=0.5 and β=0; b) R=3, α=0.5 and β=0

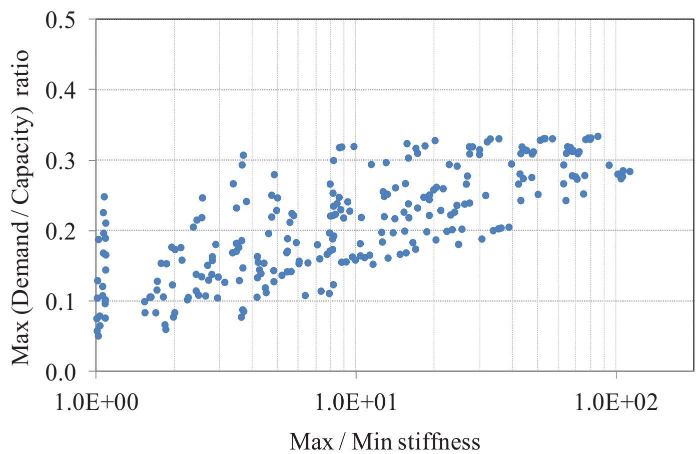

Fig. 4.22. Maximum ductility demand to ductility capacity ratios obtained when abutment effects were considered in modelling (Gap=50 mm, R=5, α=0.5 and β=0)

4.12 Normalized ductility demand

To improve the correlation between the results presented a new parameter is defined as the normalized ductility demand which is simply calculated by dividing the maximum ductility demands by the minimum aspect ratio of the columns (i.e., H_{min}/D). It was observed that the use of the average stiffness ratio of all of the columns in lieu of the maximum stiffness ratios can also slightly reduce the scatter in the results. The normalized ductility demand and normalized demand to capacity ratios are presented in Fig. 4.23a and b. As can be seen by introducing these parameters the correlation has been significantly improved compared to the results presented in Fig. 4.9 to Fig. 4.11. Hence, the overall seismic response and the maximum ductility demands in the longitudinal direction are controlled by at least three important parameters including the total stiffness of the substructure, the stiffness ratio of the columns, and the minimum aspect ratio of the columns.

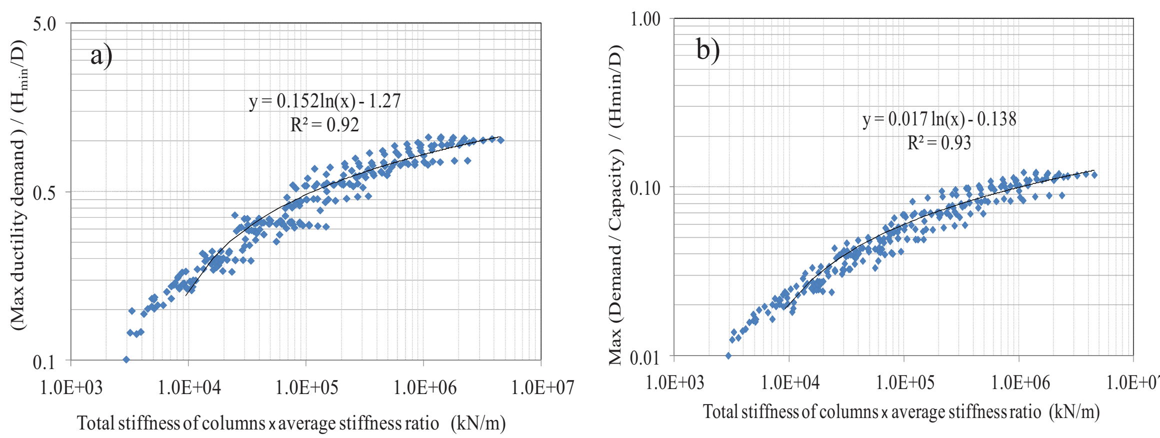

Fig. 4.23. Analysis results using R=5 and Takeda hysteresis model with α=0.5 and β=0 for: a) normalized ductility demands; b) normalized demand to capacity ratios

4.13 Demand to capacity ratios considering transverse and longitudinal responses

A combination of orthogonal seismic displacement demands are often used to approximately account for the directional uncertainty of earthquake motions and the simultaneous occurrence of earthquake effects in the two perpendicular horizontal directions. Based on the AASHTO guide specifications (AASHTO, 2009) the seismic displacements resulting from analyses in the two perpendicular directions can be combined. The seismic demand displacements can be obtained by adding 100% of the seismic displacements resulting from the analysis in one direction to 30% of the seismic displacements resulting from the analysis in the perpendicular direction and vice-versa to form two independent cases (AASHTO, 2009).

The transverse responses of similar bridges were studied by Tehrani and Mitchell (2012a). To estimate the resulting displacement ductility demands due to bidirectional ground motions the resulting displacements from the analysis in the longitudinal and transverse directions were combined using the 100% / 30% rule stated above.

The resulting displacement ductility demand to capacity ratios are shown in Fig. 4.24. The ductility capacities of the columns were computed based on the "Life Safety" performance level (i.e., collapse prevention) according to the recommendations of Priestley et al., (2007). The beneficial effects from the abutments in the longitudinal direction were conservatively neglected. The resulting demand to capacity ratios are generally less than 0.7 considering the combination of maximum ductility demands from transverse and longitudinal directions. The use of the SRSS combination rule also resulted in similar predictions with ductility demands being about 5% larger on average. As can be seen in Fig. 4.24, the demand to capacity ratios are less than 0.5 for the majority of cases. However as the maximum stiffness ratio of columns exceeds about 8.0 the demand to capacity ratios are increased by 40%.

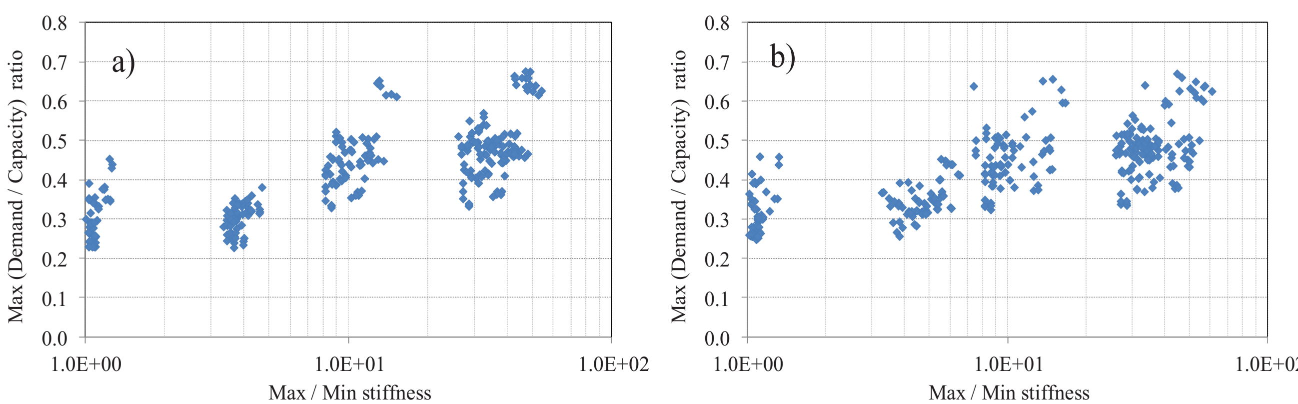

Fig. 4.24. Ductility demand to ductility capacity ratios for different bridge configurations considering transverse and longitudinal responses based on the 100%/30% rule for: a) Bridges with restrained transverse movements; b) Bridges with unrestrained transverse movements

4.14 Conclusions

Bridges with different configurations were designed based on the 2006 Canadian Highway Bridge Design Code (CHBDC). Non-linear time history analyses were used to predict the longitudinal seismic responses of these bridges using 7 spectrum-matched records. The conclusions from this study on four-span bridges located in Vancouver are summarized as follows:

(1) The seismic response and the maximum ductility demands in the longitudinal direction are controlled by the total stiffness of the substructure, the stiffness ratio of the columns, and the minimum aspect ratio of the columns. Seismic ductility demands in the longitudinal direction were correlated with the product of the total stiffness of the columns and the maximum stiffness ratio of the columns. This indicates that the ductility demands in bridge columns increase as the structural stiffness and stiffness irregularity increases.

(2) It was demonstrated that the concentration of ductility demands increases significantly with an increase in the column stiffness ratio, K_{max}/K_{min}. An equation was developed to provide a means of estimating the ratio of the maximum to minimum ductility demands. This equation is useful for designers in determining the influence of the column stiffness irregularity on the concentration of the ductility demands.

(3) The influence of the abutments on the longitudinal seismic responses of bridges was studied. Up to an 80% decrease in seismic ductility demands were observed when the abutments were considered in the structural models. The reduction of ductility demand correlates with the ratio of the total stiffness of the columns and the effective stiffness of the abutments. The influence of the abutments was more pronounced for the bridges with more flexible columns and stiffer abutments.

(4) Unlike the transverse responses, there was relatively good agreement between the displacements obtained from elastic and inelastic analyses and the

longitudinal displacements were not significantly affected by the stiffness ratio of the columns for bridges with different column heights.

(5) A dimensionless parameter was defined as $(\Delta\ D) / H^2$ (i.e., drift ratio divided by column aspect ratio) which provided an improved indicator of the structural damage compared to the conventional drift ratio (i.e., Δ / H). It was also demonstrated that normalizing the maximum ductility demands by the minimum aspect ratio of the columns significantly reduced the dispersions in the results.

(6) The predicted maximum ductility demands were generally less than 3.5 in the longitudinal direction, when a modification factor of R=5 was used in design. The predictions were even lower when the influence of the abutments was considered in the seismic response. It should be noted that the predictions are expected to be somewhat conservative, since spectrum matched records were used for the analyses.

(7) The seismic ductility demands to ductility capacity ratios were estimated for the combination of the seismic responses in the longitudinal and transverse directions. It was observed that the demand to capacity ratios were lower than 0.7 with the majority of the cases having values less than 0.5. These ratios decreased, when the influence of the abutments were considered in the seismic response. The range of demand to capacity ratios was quite high which indicate uneven safety margins for different bridges. Exceeding the maximum stiffness ratio of about 5.0 to 8.0 resulted in much larger demand to capacity ratios.

(8) CSA S6-06 requires elastic dynamic analysis for an emergency-route bridge in seismic performance zones 2 and higher if the bridge is irregular. This study indicates that the elastic dynamic analysis is appropriate for irregular bridges in the longitudinal direction. However, nonlinear dynamic analysis would be required for such irregular bridges in the transverse direction in order to accurately predict the displacement envelope and the ductility demands (Tehrani and Mitchell, 2012a).

Acknowledgements

The financial support provided by the Natural Sciences and Engineering Research Council of Canada for the Canadian Seismic Research Network is gratefully acknowledged.

References

Please see the last section.

5 Effects of Different Record Selection Methods and Earthquake Types on the Transverse Response of Bridges

Payam Tehrani[1], Katsuichiro Goda[2], Denis Mitchell[1], Gail M. Atkinson[3], and Luc E. Chouinard[1]

[1]*Department of Civil Engineering & Applied Mech., McGill University, Montreal H3A 2K6, Canada*

[2]*Department of Civil Engineering, University of Bristol, Bristol BS8 1TR, United Kingdom*

[3]*Department of Earth Sciences, University of Western Ontario, London, Ontario N6A 5B7, Canada*

5.1 Preface

The concepts of the IDA method for seismic evaluation of structures, different record selection methods, different ground motion prediction equations (GMPE) and prediction of different damage states using different methods were presented in Chapter 2.
In this chapter the IDA method has been used to evaluate the seismic response of a continuous bridge designed based on the 2006 CHBDC provisions. For this purpose a back-bone curve was defined based on different bridge specific studies for the purpose of the structural modelling for IDA. The results from the experimental and theoretical studies to define this back-bone curve were also compared.

Record selection in IDA is an important issue which can significantly affect the results. There is no research available to investigate the influence of different record selection methodologies for seismic evaluation of bridges using IDA. In this chapter the influence of using different record selection methods including the UHS-based, CMS-based and epsilon-based on the IDA results are studied. These record selection methods were explained in Chapter 2.

The bridge under study is located in Vancouver, where the seismic hazard is influenced by three different earthquake types with distinct characteristics. Little research is available to investigate the influence of considering the subduction earthquakes in the seismic assessments of bridges and currently only the records from the crustal earthquakes (e.g., the records from the PEER-NGA database) are used for seismic evaluations. Recent earthquakes in Chile (i.e., 2010 Chile earthquake) and Japan (i.e., 2011 Tohoku earthquake) demonstrated the significance of the large subduction zone earthquakes, indicating that more research is needed to focus in this subject. The records from the 2011 Tohoku earthquakes were also considered in this study.

The seismic deaggregation results for Vancouver are used to compute the CMS for different earthquake types and accordingly different CMS-based approaches are used concerning different earthquake types as will be discussed in Chapter 5.
The importance of the epsilon and spectral shapes, as explained in Chapter 2, were also included in the IDA results and the use of a simplified method to modify the results for these effects was investigated for the bridge studied. Different GMPEs were used to predict the CMS and the influence of using different GMPEs on the IDA results was investigated.

The IDA results were evaluated at different damage states and the effects of different record selection methods on the prediction of different damage states were investigated. More details regarding the prediction of different damage states using different methods and determining the these limits on the IDA curves are explained in Chapter 2.

More details regarding the automated program used for the large number of nonlinear dynamic analyses in the IDA method is available in Appendix B.

More details regarding the program developed to extract the seismic deaggregation results are available in Appendix C.

More details regarding the program developed for developing the CMS and selecting the records using different methods considering different earthquake types and different GMPEs are discussed in Appendix D.

More explanations regarding different earthquake types are given in Appendix F.

A pushover analysis of the bridge studied is also presented in Appendix H.

The detailed IDA results for the bridge studied in this chapter obtained using a large set of records (i.e., including 234 records) are also presented in Appendix I.
Chapter 5 was summarized into a manuscript: Tehrani, P., Goda, K., Mitchell, D., Atkinson, G.M. and Chouinard, L.E. "Effects of Different Record Selection Methods and Earthquake Types on the Transverse Response of Bridges", Journal of Earthquake Engineering and Structural Dynamics, Manuscript EQE-11-0079 (revised version), submitted in December 2011.

According to Wiley publication policy, the reuse of the contents of the journals is permitted for the authors (http://onlinelibrary.wiley.com/journal/10.1002/(ISSN)1096-9845/homepage/Permissions.html).

5.2 Abstract

The seismic response of a continuous 4-span bridge designed according to the current Canadian seismic provisions is investigated using Incremental Dynamic Analysis (IDA). The bridge is evaluated for two cases of restrained and unrestrained transverse movements at the abutments. Different earthquake types, including shallow crustal events, interface Cascadia subduction and deep inslab subduction, are considered in the seismic analyses. The median collapse capacities calculated using different record selection methods including CMS-based, UHS-based, and epsilon-based methods are compared. In the CMS-based method, the conditional mean spectra (CMS) for three different event types are constructed based on seismic deaggregation results. The median collapse capacities obtained considering crustal events were generally close to those obtained considering different event types. However, considering different event types in the IDA resulted in increased record-to-record variability which should be incorporated in probabilistic seismic performance assessments. The use of the epsilon-based method generally resulted in the highest collapse capacity predictions. Although the use of the CMS-based methods resulted in somewhat conservative predictions compared to those obtained using the epsilon-based method, this method was less sensitive to the number of records considered in the IDA.

KEY WORDS: Record selection, Incremental dynamic analysis, Bridges, Conditional mean spectrum, Seismic performance.

5.3 Introduction

Incremental Dynamic Analysis (IDA) (Vamvatsikos and Cornell, 2002) can be used for seismic performance assessment of structures (ATC-63, 2008). One of the most important issues in the IDA is record selection which can significantly affect the results. This study investigates the effects of different record selection methods, including different earthquake types on the seismic response of a bridge.

One of the methods that has been widely used for record selection is spectrum matching. The use of scaled natural or artificial records that are matched to a target uniform hazard spectrum (UHS) over a range of periods (referred to as the UHS-based method) is recommended by some codes. This range must include the important modes of the structure as well as the effects of period elongation due to inelastic deformation of the structure. A period range from $0.2T_1$ to $2T_1$ (where T_1 is the fundamental vibration period of a structure) is usually recommended and used for this purpose. This range is similar to the $0.2T_1$ to $1.5T_1$ range specified by ASCE 7-05 (ASCE, 2005), but statistical studies suggest that nonlinear structures are often sensitive to response spectra at periods longer than $1.5T_1$ (Baker and Cornell, 2008; Haselton and Baker, 2006; Vamvatsikos and Cornell, 2005).

Although conceptually simple, these methods for record selection are deemed to be conservative, particularly when the estimation of collapse capacity is the primary objective of the analysis. This is because the response spectra of the records are forced to match a target UHS. The UHS is a composite of predicted responses at different periods, and may not be representative of individual ground motion spectra. Furthermore, the UHS tends to be dominated at any individual period by motions above the median, whereas individual spectra are unlikely to be above-median at all periods simultaneously. No natural record can be found to match the UHS over a wide period range and hence the analysis results using UHS-matched records are often unrealistic and conservatively biased. To solve these problems, the use of the Conditional Mean Spectrum (CMS) in lieu of the UHS has been recommended in recent years (Baker, 2011). In this study selecting the records to match a CMS (conditioned on the fundamental period of the structure, T_1) is referred to as the CMS-based record selection method. This method is discussed in more detail in section 2.1.

Another method which has been used for record selection is the epsilon-based method (Baker and Cornell, 2006a). Epsilon, ε, is defined as the number of logarithmic standard deviations of a target ground motion from a median ground motion prediction equation (GMPE) for a given magnitude, M, and distance, R. Rare ground motions (large earthquake) typically have a peaked spectral shape that is much different than a standard uniform hazard spectral shape and accounting for this has been shown to increase the predicted collapse capacity significantly (increase of up to 70% (Baker and Cornell, 2006a; Haselton and Baker, 2006) . Thus neglecting the spectral shape of the records selected (e.g., in UHS-based method) for collapse assessment of the structures can result in very conservative and unrealistic predictions. The most direct approach to account for spectral shape in structural analysis is to select ground motions with epsilon (T_1) values similar to epsilon values obtained from seismic hazard deaggregation analysis for the site and hazard level of interest.

Usually only the records from crustal earthquakes have been used in seismic performance assessments (e.g., ATC-63 provisions), while for some sites such as Vancouver or Seattle subduction earthquakes with very different physical characteristics (e.g., spectral content and duration) can occur. Another important issue which is investigated in this research is the effect of considering different earthquake types (i.e., crustal, subduction interface, and inslab events) on the seismic performance evaluation of bridges located in south-western British Columbia.

5.4 Seismic hazard analysis and conditional mean spectrum

5.4.1 Conditional mean spectrum (CMS)

The CMS provides the expected response spectrum, conditioned on occurrence of a target spectral acceleration value at the period of interest. It has been found that the CMS can be used as an appropriate target response spectrum for selecting ground motions as input for dynamic analyses (Baker, 2011). In the development of a CMS, some important aspects of the records including magnitude, M, distance, R, and epsilon are considered from the deaggregation of the seismic hazard. Baker (Baker, 2011) proposed a method for calculating the CMS, and this approach was used in this study. For the development of a CMS, the mean values of spectral accelerations at different periods are computed using an appropriate GMPE. These mean values will then be modified considering the inter-period correlations, standard deviations of spectral accelerations and mean epsilon values at different periods. The resulting CMS has a peak value at the fundamental period of the structure which is equal to the corresponding spectral acceleration from the UHS.

A complicated aspect in constructing a CMS for a site in south-western British Columbia, in comparison with a site in California, is that three earthquake types, having distinctly different characteristics, contribute to the overall seismic hazard. Therefore, three CMS must be constructed for record selection, “CMS-Crustal”, “CMS-Interface”, and “CMS-Inslab” (Goda and Atkinson, 2011). In order to account for these events, two sets of CMS are considered in this study, similar to Goda and Atkinson (2011). The first approach is the CMS-Event-based procedure which is based on the weighted average of the CMS that are computed by using applicable GMPEs and the corresponding scenarios for the three earthquake types, in proportion to the relative influences of the scenarios (i.e., the number of records from each event type is proportional to the percentage of contribution of that event type in the overall seismic hazard). The second approach is the “CMS-All-based” which is the weighted average of “CMS-Crustal”, “CMS-Interface”, and “CMS-Inslab” by considering relative influences of the individual earthquake types without considering different earthquake type records in the selection procedure. In fact “CMS-All-based” is the simplified version of CMS-Event-based. This simplification in the “CMS-All-based” approach results in variability of the seismic response being smaller than that based on the “CMS-Event-based” approach. However, it must be noted that for each earthquake type, the variability of the selected records in general tends to be underestimated for CMS-based or UHS-based approaches, since a tight match to a target response spectrum is imposed (Baker, 2011). Nevertheless, the “CMS-Event-based” approach can account for the variability of the CMS among different event types more reasonably than does the “CMS-All-based” approach.

5.4.2 Preliminary record selection

Ground motion records that are used for the IDA are selected from two extensive databases, the PEER-NGA database and the K-NET/KiK-NET database. Some limitations were imposed on the minimum magnitude (M), peak ground acceleration (PGA), and peak ground velocity (PGV) of the records to consider strong ground motions available in the database. The characteristics of the records from the PEER-NGA database (179 records from 28 earthquakes) and the K-NET/KiK-NET database (189 records from 23 earthquakes) are described by Goda and Atkinson (2009). More detailed information regarding the records selected for this research and their criteria is available elsewhere (Goda and Atkinson, 2009 and 2011).

5.4.3 Seismic hazard analysis and target scenarios

Probabilistic seismic hazard analysis (PSHA) is a standard procedure for seismic hazard assessment. The results of such analysis usually include UHS and scenario events that are associated with the UHS and identified by seismic hazard deaggregation. For Canadian cities, the fourth generation of national seismic hazard maps of Canada are available (Adams and Halchuk, 2003). In this study, an updated seismic hazard model for western Canada, developed by Goda et al., (2010) will be used to take advantage of new seismic information and seismological models to improve several aspects of the current Geological Survey of Canada model.

PSHA for Vancouver was carried out using the updated seismic hazard model based on Monte Carlo simulation (Goda et al., 2010). The obtained UHS for site class C (V_{s30} = 555 m/sec, the average shear wave velocity in the top 30 m) are shown in Fig. 5.1. The assessment is based on the simulated seismic activities during 5 million years, and the considered annual non-exceedance probabilities range from 0.996 to 0.9999 (i.e., 10% to 0.5% probability of exceedance in 50 years). The UHS shown in Fig. 5.1b are mean UHS, rather than median UHS. To further investigate the characteristics of seismic events that contribute to a selected probability level, seismic hazard deaggregation for Sa(0.7) and Sa(1.3) was carried out. These two periods correspond to the fundamental periods for the bridge being considered for the restrained and unrestrained transverse movement at the abutments (restrained abutments and free abutments), respectively. Deaggregation results at different hazard levels in terms of mean magnitude M, mean distance R, and ε along with percentages of contributions of different seismic event types to the seismic hazard for different probability levels are shown in Tables 5.1 and 5.2. The deaggregation analysis is based on an "approximately equal criterion" (i.e., matching method) (Hong and Goda, 2006), where seismic events reaching a seismic intensity level between 90% and 110% of the target $Sa(T_n)$ value are used to produce deaggregation results. It was observed that the use of the exceeding method in seismic deaggregation lead to predictions with higher mean epsilon values. This can be important especially when the epsilon-based record selection method is used, potentially resulting in overestimation of the capacity of the structures.

The constructed CMS at 2% probability of exceedance in 50 years are illustrated in Figs. 5.2 and 5.3 for two vibration periods T_n = 0.7 sec and T_n = 1.3 sec, respectively. As expected, all CMS are approximately equal to the spectral acceleration values of the UHS at the target vibration periods considered (i.e.,T_n=0.7 and T_n=1.3). For the considered cases, the CMS-Crustal and CMS-All are similar. The CMS-Interface has a rich spectral content in the long vibration period range, which was found to be the most critical case for the bridge structure studied, while the CMS-Inslab has a rich spectral content in the short period range.

Table 5.1. Seismic deaggregation results for T= 0.7 sec (epsilon values using the BA08 and Z06 GMPEs)

Probability of exceedance	Percentage of contribution: [Crustal, Interface, Inslab]	Crustal events	Interface events	Inslab events
		[M , R , ε]	[M , R , ε]	[M , R , ε]
10% in 50 yr	[48%, 17%, 35%]	[6.61, 37.2, 1.27]	[8.51, 142.4, 0.20]	[6.65, 76.1, 1.19]
2% in 50 yr	[40%, 27%, 33%]	[6.78, 18.3, 1.51]	[8.63, 142.8, 1.04]	[6.82, 64.6, 1.64]
0.5% in 50 yr	[38%, 30%, 32%]	[7.03, 10.3, 1.56]	[8.69, 141.4, 1.63]	[7.00, 55.9, 1.83]

Table 5.2. Seismic deaggregation results for T= 1.3 sec (epsilon values using the BA08 and Z06 GMPEs)

Probability of exceedance	Percentage of contribution: [Crustal, Interface, Inslab]	Crustal events	Interface events	Inslab events
		[M , R , ε]	[M , R , ε]	[M , R , ε]
10% in 50 yr	[46%, 20%, 34%]	[6.74, 45.5, 1.30]	[8.49, 142.6, -0.1]	[6.78, 76.2, 1.28]
2% in 50 yr	[35%, 37%, 28%]	[6.86, 21.7, 1.51]	[8.63, 142.6, 0.79]	[6.94, 63.6, 1.77]
0.5% in 50 yr	[34%, 39%, 27%]	[7.13, 12.8, 1.67]	[8.69, 141.1, 1.34]	[7.09, 59.9, 2.10]

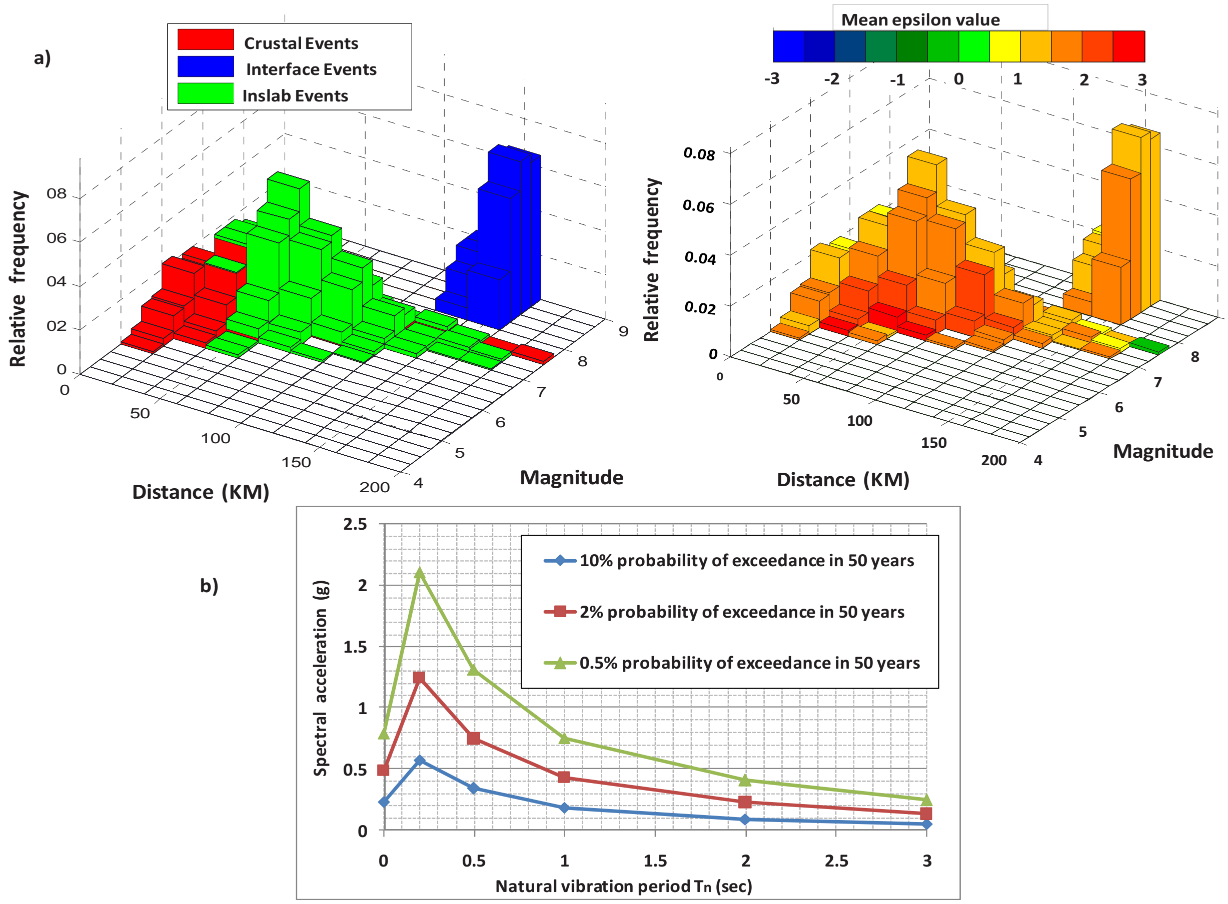

Fig. 5.1. PSHA results for Vancouver: a) Seismic hazard deaggregation for 2% probability of exceedance in 50 years at T=0.7 sec b) Uniform hazard spectra

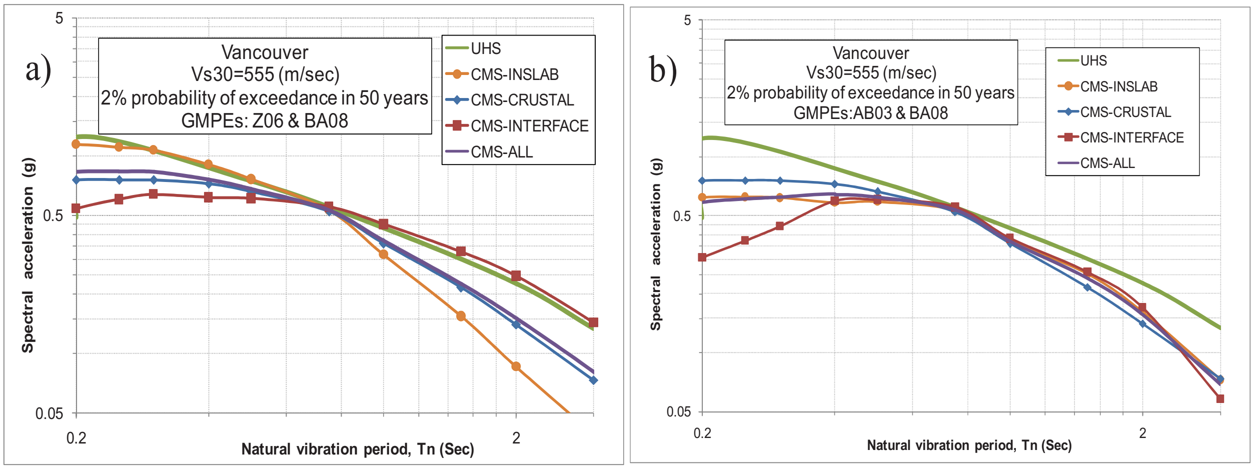

Fig. 5.2. CMS for T=0.7 sec: a) for BA08 and Z06 GMPEs, b) for BA08 and AB03 GMPEs

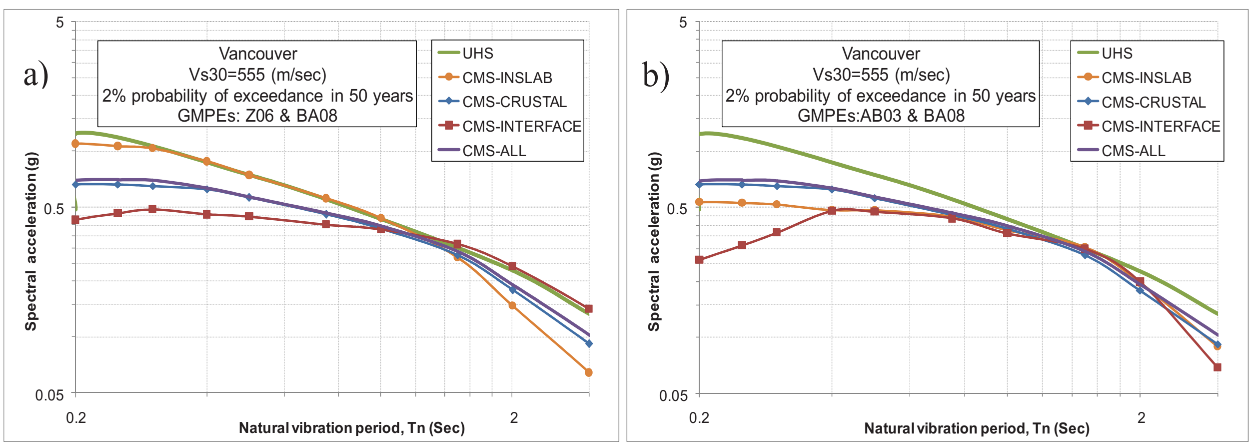

Fig. 5.3. CMS for T=1.3 sec: a) for BA08 and Z06 GMPEs, b) for BA08 and AB03 GMPEs

The adopted ground-motion prediction equations and the corresponding weighting factors used for seismic hazard analysis are provided by Atkinson and Goda (2011). For constructing a CMS however using all of the GMPEs used in PSHA may not be appropriate for practical reasons. It can be argued that contrary to conventional design using a uniform hazard spectrum where the absolute values of spectral accelerations at different periods are important, in CMS-based record selection strategy, the important aspect is the spectral shape and as long as this shape can be predicted appropriately by a limited number of GMPEs, the use of all the GMPEs may not be necessary. For the purpose of this study the newly developed PEER-NGA relationship BA08 (Boore and Atkinson, 2008) was used for crustal events. For the case of subduction events (interface and inslab) the GMPE by Zhao et al., (2006) (Z06 GMPE) and Atkinson and Boore (2003) (AB03 GMPE) were considered separately. A comparison of the constructed CMS in Figs. 5.2 and 5.3 shows that in most cases, CMS-All which is the average of all the CMS according to the percentage of contribution of each event type is very close to CMS-Crustal. This may indicate that CMS-Crustal can be a replacement for CMS-All . However this may be specific to the cases considered here and general conclusions should not be made withouth further investigations.

5.5 Bridge properties, design and modelling assumptions

5.5.1 Bridge properties

To investigate the impact of the type of records on the structural performance, a regular 4-span bridge is considered in this study. IDA (Vamvatsikos and Cornell, 2002) is used to evaluate the seismic response of the bridge at different damage states. In typical IDA analyses, records are scaled up or down until different performance levels, including collapse, are reached. At high seismic levels, bridge shear keys at the abutments are expected to fail, so that the bridge structure will be unrestrained at the ends. According to the Caltrans recommendations, the shear keys must be designed to fail in low seismic intensities to prevent damage to elements such as piles and abutments that are more expensive and difficult to inspect and repair (Caltrans, 2006). However the Canadian Highway Bridge Design Code (CHBDC) (CSA, 2006) does not recommend such a design strategy and as a result, one may not be certain whether failure of the shear keys will occur prior to the collapse of columns. Thus to consider the critical case in the seismic performance assessment, two different cases including bridges with restrained and unrestrained transverse movement at the abutments are evaluated.

The structure is a regular 4-span bridge supported by single columns with the transverse movements restrained at the abutments. The column diameter is 1.5 meters, the column height is 5 meters, the span length is 50 meters, and the superstructure consists of a box girder with a uniform dead load of 200 kN/m. (see Fig. 5.4.) The bridge was designed according to the 2006 CHBDC (CSA, 2006) with an importance factor of I =1.5 (i.e., Emergency-Route bridge). For the restrained case (effective shear keys), the first period of the structure in the transverse direction is around T_1=0.7 sec. In the case of failed shear keys, the first period of the bridge is T_1=1.3 sec. In this case, however, the second mode, T_2=0.7, has a significant contribution. The fundamental periods are computed using the effective stiffness of the columns (i.e., $K_e = M_y/\theta_y$ where M_y and θ_y are the moment and rotation at yield, respectively). In straight bridges the responses in the orthogonal directions are likely to be essentially independent (Priestley et al., 2007). The responses of the bridge in the transverse direction were chosen to assess the significance of the different ground motion types and different record selection methods.

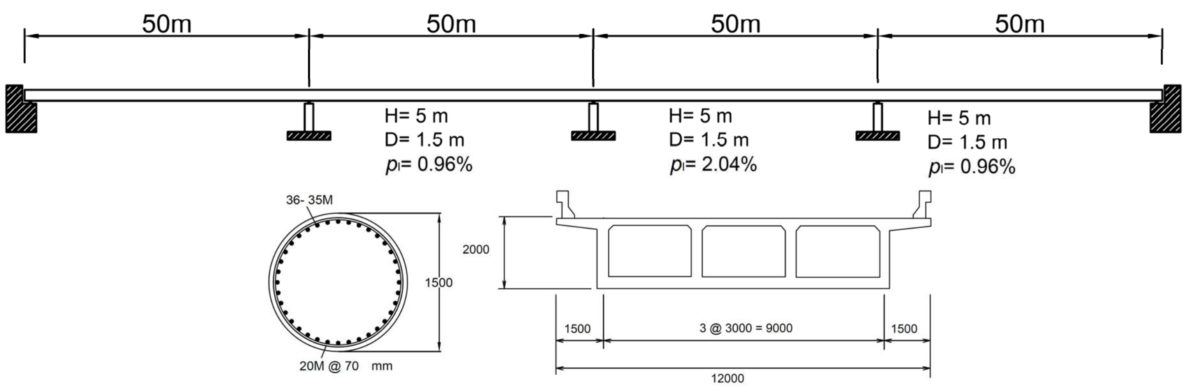

Fig. 5.4. Bridge properties

5.5.2 Incremental dynamic analysis

IDA is usually used for performance assessment and collapse evaluation of structural systems. This method involves numerous nonlinear time history analyses using a number of records in which each record is scaled incrementally until a desired performance level is reached.

One of the advantages of IDA is that one can evaluate the response of a structure at multiple performance levels, including serviceability, damage control, and life safety, according to the corresponding damage states that can be defined using appropriate engineering demand parameters such as drift, rotation, and strain. The IDA results relate statistics of a damage measure (DM) (i.e., inelastic seismic demand) with an intensity measure (IM) (usually $Sa(T_1)$ with 5% damping ratio), and can be used in the probabilistic seismic performance assessment and fragility analysis of the structure.

Figure 5.5 shows the predicted moment versus chord rotation response for the central column of the bridge. Points A, B and C represent the damage states of reinforcement yielding, cover spalling and bar buckling, respectively. The cover spalling stage is used as a serviceability limit indicator based on experimental results on bridge columns (Berry and Eberhard, 2007). Point C is used as a damage control indicator beyond which the column is not repairable and represents the maximum capacity of the column (i.e., large strains, bar buckling and concrete crushing). After the maximum capacity has been reached at point C, there is strength degradation and failure of the structure will be predicted when dynamic instability has been reached at point D which occurs with a small incremental deformation beyond point C. The strength degradation slope (C-D) was determined using a conservative approach suggested by Haselton et al. (2007), resulting in a "post-capping" chord rotation of 10% (see Figure 5.5).

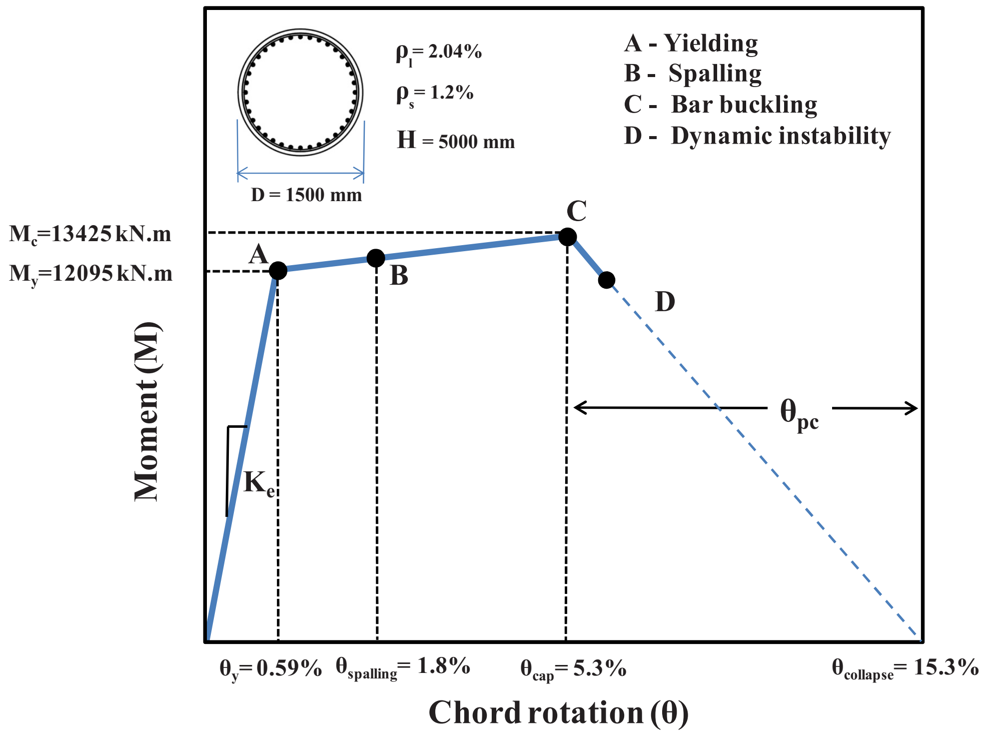

Fig. 5.5. Backbone curve parameters

5.5.3 Damage states and performance indicators

Several damage states were considered in the seismic evaluation of the bridge under study including yielding, spalling, and collapse. ATC-63 provisions provide some equations to compute the parameters of the backbone curve as shown in Fig. 5.5 for building-type elements with rectangular cross-sections. To apply this methodology to bridge structures similar back-bone curves were defined for the circular bridge columns considered in this research using the results obtained from bridge-specific studies. Generally two types of approaches (i.e., experimental and theoretical methods) can be used for this purpose.

The Mander et al. equation (Mander et al., 1988) is typically used for the theoretical prediction of the ultimate strain of concrete in the confined core. Experimental results however indicate that the ultimate strains predicted by this equation are conservative in comparison with actual ultimate strains exceeding predicted values by a factor of about

1.3 to 1.6. Usually a strain level of 0.6 to 0.7 times the ultimate strain of steel bars in monotonic tests is recommended for calculating the ultimate curvature of the section with an upper strain limit of 0.05 (Priestley et al., 1996 and 2007) for damage control assessment. In order to attain this level of strain, the amount and spacing of the transverse confinement reinforcement must be code-conforming. However, for life safety assessment, the value of 0.9 times the ultimate strain of steel bars (0.9 ε_{su}) is recommended by Priestley et al. and this value should not be taken greater than 0.08 (Priestley et al., 2007).

A study by Berry and Eberhard (2007) provides some empirical equations to estimate the engineering demand parameters including drift ratio, plastic rotation, and strain in the longitudinal bars for circular bridge columns based on the properties of columns including longitudinal and transverse steel ratio, axial load ratio, and geometry. A comparison between these approaches shows that the ultimate drifts calculated using these methods are in good agreement (e.g., the drift ratio of 5.69% corresponding to the life safety limit state using the theoretical approach is close to that obtained for the bar buckling and bar fracture damage states using the experimental equations as shown in Table 5.3a and 5.3b, respectively). In this research, the ultimate tensile strain in the steel bars corresponding to bar buckling from experimental equations is used to compute the ultimate curvature of the columns and the corresponding drift and curvature ductility is defined as the point at which strength degradation begins (i.e., θ_{cap} in Fig. 5.5).

Table 5.3. Deformations at different damage states for the central column of the bridge: a) Using the theoretical approach by Priestley et al., (2007), b) Using the experimental equations by Berry and Eberhard (2007).

a)

Damage state	Drift	Strain	Curvature ductility	Displacement ductility
Yielding (nominal)	0.59%		1	1
Serviceability	0.93%	ε_c=0.004 or ε_s=0.015	2.65	1.58
Damage Control	3.91%	ε_c< Mander eq.or ε_s=0.6ε_{su} < 0.05	15.9	6.2
Life Safety	*5.69%*	ε_c< 1.5*Mander eq. or ε_s=0.9ε_{su}< 0.08	25.6	9.6

b)

Damage state	Drift	Rotation	Strain
Cover Spalling	1.85%	0.012	0.008
Bar Buckling	5.30%	0.0451	0.075
Bar Fracture	*5.74%*	0.0492	0.081

Few test results are available to calibrate the post-capping stiffness of the columns. In ATC-63 a conservative upper limit of 0.1 is recommended for the post-capping chord rotation of columns which is controlling for most beams and columns designed according to current seismic design practice. In addition, P-Δ effects are considered directly in the analysis.

5.5.4 Bridge modelling

The modified Takeda hysteresis model (Otani, 1981) was used in this study to model the behavior of the RC columns using Ruaumoko software (Carr, 2009). This model has two main parameters, alpha and beta, which control the unloading and the reloading stiffness, respectively. Alpha is usually in the range of 0.0 to 0.5 and beta varies between 0.0 and 0.6. Increasing the alpha parameter decreases the unloading stiffness and increasing the beta parameter increases the reloading stiffness. Some researchers computed the mean values of alpha and beta for bridge columns based on experiments, as 0.26 and 0.49, respectively (Mechakhchekh, 2008). By considering the recommended values of these parameters (Priestley et al., 1996 and 2007), the values of alpha=0.3 and beta=0.3 were adopted to comply with both the recommended values in practice and the mean values from the tests. The lower value of beta was chosen to be more conservative and to account for possible defects and pinching effects in the hysteresis loops. It has been demonstrated that for a structure with ductile columns and a period in the medium-to-long range, the maximum response of the structure is relatively insensitive to the hysteretic parameters (Otani, 1981; ATC-62, 2008). It was also found that the median collapse capacity of the structure is insensitive to the stiffness degradation parameters in the Takeda model in which the differences in median collapse capacities were negligible when significantly different values of alpha and beta were considered (see Figure 5.6(b)). The structural modelling considered in this study is similar to that used by Priestley et al., (Priestley et al., 1996 and 2007), except that the backbone curve shown in Figure 5.5, including the post peak response was used.

a)
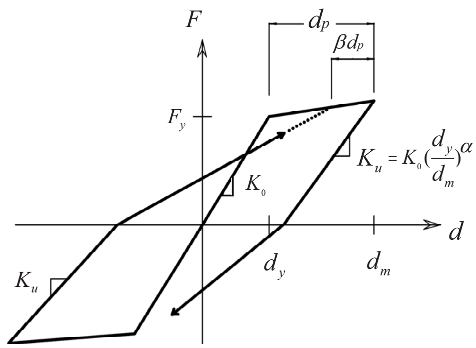

b)

	IDA result percentiles (Sa @T_1=0.7 sec)		
Parameters:	Median	16%	84%
Alpha=0.5 & Beta=0	1.26	0.80	2.27
Alpha=0.3 & Beta=0.3	1.31	0.82	2.30
Alpha=0.2 & Beta=0.5	1.34	0.84	2.30

Fig. 5.6. Effects of hysteresis parameters on the collapse capacity: a) Modified Takeda hysteresis loops; b) The collapse capacity predictions using the ATC-63 record set for different Takeda hysteresis loop parameters (alpha and beta).

5.5.5 Collapse modes and prediction of probability of collapse

The bridge under study was designed and detailed to meet the code requirements for ductile response, including capacity design concepts and adequate support lengths at the abutments, hence promoting flexural yielding and eliminating brittle failure mechanisms. The ductile columns contain code-compliant spiral reinforcement to confine the concrete, avoid shear failure and to control buckling of the vertical reinforcing bars. For this continuous bridge, with all other failure modes avoided, the flexural response governs the response of the bridge and sidesway collapse is the governing collapse mechanism. The collapse prediction is based on dynamic instability of the structure (Vamvatsikos and Cornell, 2002; ATC-63, 2008). The failure of shear keys is treated indirectly by considering two cases of restrained and unrestrained transverse movements at the abutments.

Because this research focuses on the influence of different record selection methods and earthquake types on the seismic response of bridges, a ductile bridge structure is considered with non-ductile collapse modes avoided. It is noted that poorly designed and detailed bridges would have undesirable, brittle collapse modes which would give rise to excessive variability in the predicted responses.

To evaluate the seismic performance of a structure at collapse, the median collapse capacity of the structure is computed using IDA. The probability of collapse at the maximum considered earthquake (MCE) level, which usually corresponds to 2% probability of exceedance in 50 years, should be reasonably low. The probability of collapse at this seismic excitation level is typically limited to 10% (ATC-63, 2008). To estimate the probability of collapse at the MCE level based on the computed median collapse capacity a simplified assumption is made that the cumulative probability function follows a lognormal distribution.

The collapse margin ratio, CMR, which is the ratio of the median 5%-damped spectral acceleration of the collapse level ground motions to the 5%-damped spectral acceleration of the MCE ground motions, can then be computed at the fundamental period of the structure (ATC-63, 2008).

To succinctly describe the uncertainty regarding the collapse capacity of the bridges, the standard deviation of the collapse capacities, expressed in terms of spectral acceleration, can be used. These quantities are reported in the results for individual analysis cases.

5.6 Seismic evaluation using different record selection methods

The response spectra shapes for different record selection methods provide input for the seismic evaluation of structures using IDA. The response spectra shapes can be represented by the normalized average spectral shapes; those for different record selection methods are shown in Fig. 5.7. A lower spectral value in the long period range typically results in a higher collapse capacity prediction. The spectral accelerations in the short period range are also important, if the response of the structure is influenced by higher-mode effects. The comparison between the spectral shapes obtained using the considered methodologies indicate that generally the results using "CMS-All-based" and "CMS-Event-based" methods are close and the use of the epsilon-based method usually results in the highest collapse capacity prediction.

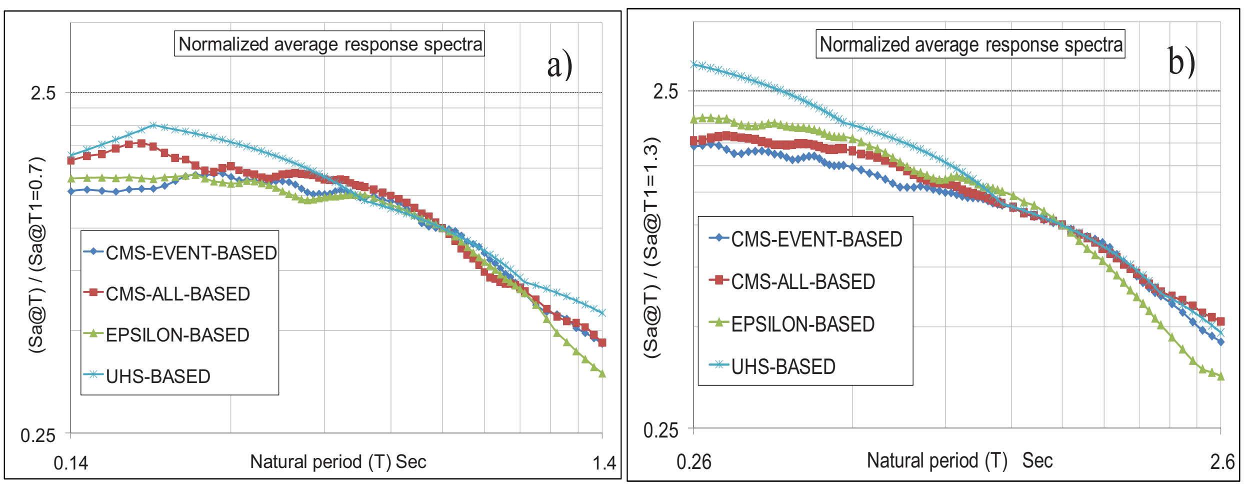

Fig. 5.7. Normalized average spectra from different methods at a) T=0.7 sec, b) T=1.3 sec

However, based on the results obtained here, one can see that the difference between the CMS-based methods and epsilon-based method is greater for the case of T_1=1.3 sec (e.g., first fundamental period of the bridge with failed shear keys) compared to the case of T_1=0.7 sec. This is because in the case of T_1=1.3 sec the beneficial effects from spectral shapes using CMS-based methods were small, while at T_1=0.7 sec the use of the CMS-based methods can result in collapse capacities similar to those obtained using the epsilon-based method. It was also found that the predicted collapse capacities using the

CMS-based methods were not as sensitive to the annual probability of exceedance as the epsilon-based methods. In the epsilon-based method, the epsilon values are computed using the BA08 GMPE for crustal events and Z06 GMPE for subduction events.

5.6.1 Seismic evaluation using crustal records

The performance of the structure is evaluated considering only crustal events in the epsilon-based method and compared to the case of using the ATC-63 fixed set of farfield records.

5.6.1.1 Bridge with restrained abutment condition (T_1=0.7 sec)

The results obtained using the epsilon-based record selection may be sensitive to the record sets used for analysis and sometimes different sets of records with similar mean epsilon values could give different results. As an example, in Fig. 5.8 the collapse capacity is about 1.84 g for records selected based on mean epsilon value of 1.56 from seismic deaggregation for 0.5% probability of exceedance in 50 years, while the collapse capacity calculated using another set of records with a similar mean epsilon was about 2.07g. The standard deviations reported in the tables reflect the logarithmic standard deviations of the collapse predictions considering all of the records studied and do not include other sources of uncertainty.

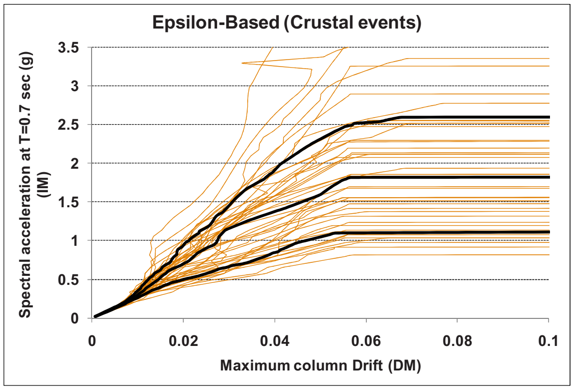

EPSILON-Based (CRUSTAL) 0.5% IN 50 YRS	IDA result percentiles (Sa @T_1=0.7)			
Damage states	Median	16%	84%	St Dev
Yielding	0.14	0.13	0.14	0.09
Cover Spalling (Exp.)	0.66	0.47	0.81	0.28
Collapse	**1.84**	1.12	2.62	0.42

Fig. 5.8. IDA results using the epsilon-based method (Crustal event,T_1=0.7 sec, CMR=3.5)

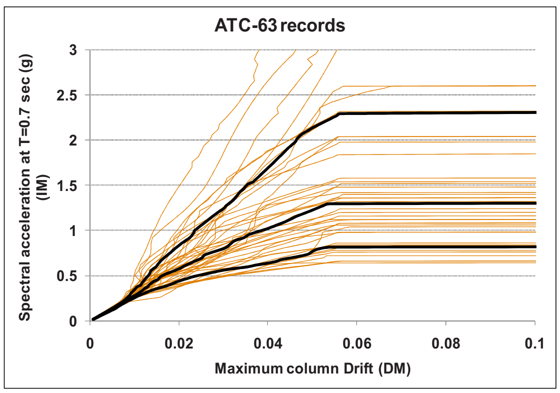

ATC-63	IDA result percentiles (Sa @T_1=0.7)			
Damage states	Median	16%	84%	St Dev
Yielding	0.15	0.14	0.15	0.05
Cover Spalling (Exp.)	0.55	0.41	0.78	0.31
Collapse	**1.31**	0.82	2.32	0.50

Fig. 5.9. IDA results using the ATC-63 record set at T_1=0.7 sec (CMR=2.53×1.26=3.2)

The IDA results based on a fixed record set recommended by the ATC-63 provisions, shown in Fig. 5.9, should be modified for the effects of epsilon which is a proxy measure for the spectral shape effects (Baker and Cornell, 2006a; ATC-63, 2008). The probability of exceedance of 0.5% in 50 years is recommended to calculate the mean epsilon values for ductile structures at collapse level (ATC-63, 2008). The regression analysis is carried out for the epsilon values of each record at the fundamental period of the structure versus the corresponding collapse capacity of each record. The result of such a regression analysis is given in a form of $\ln(Sa_{collpase}) = \beta_1\ \varepsilon + \beta_0$. The β_1 factor represents the sensitivity of the collapse capacity to a change in the epsilon value (Haselton et al., 2011). The β_1 factor which is used to modify the collapse capacity was 0.317 based on the BA08 GMPE. The β_1 value using the AS97 GMPE (Abrahamson and Silva, 1997) was found to be 0.309 showing that this value is insensitive to the GMPE used to calculate the epsilon values. This is in agreement with the values reported in the ATC-63 for ductile moment frames (i.e., 0.311). The simplified spectral shape factor, SSF, is calculated as follows (Haselton et al., 2011):

$$[5.1] \quad SSF = \exp[\beta_1(\bar{\varepsilon}_0(T) - \bar{\varepsilon}(T)_{records})]$$

where the mean epsilon of the records at T_1=0.7 sec, $\bar{\varepsilon}(T)_{records}$, is found to be 0.82 using the BA08 GMPE and the mean epsilon value from seismic deaggregation for 0.5% probability of exceedance in 50 years for crustal events, $\bar{\varepsilon}_0(T)$, is 1.56. The SSF factor then can be calculated as 1.26 (i.e. SSF=exp[0.317×(1.56-0.82)]=1.26). Thus the modified collapse capacity can be calculated as 1.26×1.31 g=1.65 g. The median collapse capacity of 1.65 g is comparable to the value of 1.84g calculated based on the epsilon-based record selection method and yet more conservative.

5.6.1.2 Bridge with free abutments (T_1=1.3)

The IDA results using the epsilon-based method for this case is shown in Fig. 5.10. The use of the epsilon-based method resulted in a collapse capacity of 1.08g and a standard deviation of 0.45.

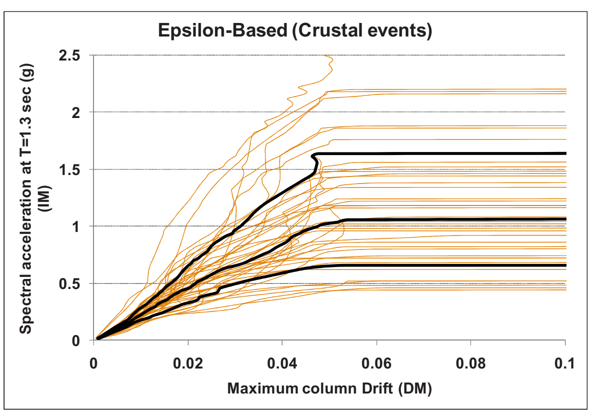

Epsilon-Based (Crustal records)	IDA result percentiles (Sa @T_1)			
Damage states	Median	16%	84%	St Dev
Yielding	0.12	0.08	0.13	0.28
Cover Spalling (Exp.)	0.42	0.30	0.56	0.34
Collapse	**1.08**	0.67	1.66	0.45

Fig. 5.10. IDA results using the epsilon-based record selection method at T_1=1.3 sec (CMR=3.8)

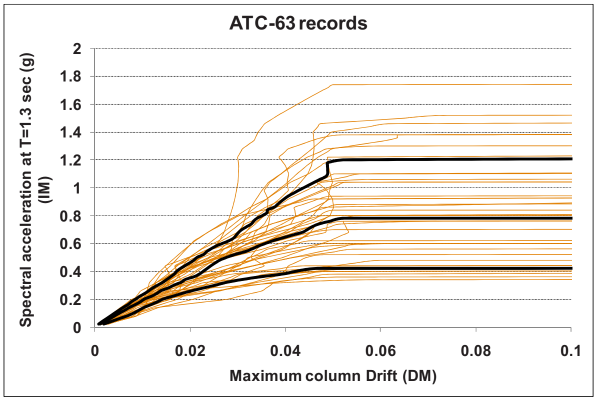

ATC-63 fixed record set	IDA result percentiles (Sa @T_1)			
Damage states	Median	16%	84%	St Dev
Yielding	0.09	0.05	0.11	0.35
Cover Spalling (Exp.)	0.32	0.24	0.41	0.28
Collapse	**0.79**	0.42	1.21	0.44

Fig. 5.11. IDA results using the ATC-63 record setat T_1=1.3 sec (CMR= 1.36 * 2.8 = 3.8)

The IDA results using the fixed record set in ATC-63, shown in Fig. 5.11, need to be modified for the effects of spectral shape. The β_1 factor in this case was equal to 0.3 based on the BA08 GMPE. The simplified spectral shape factor, SSF (Eq. [5.1]), is calculated as 1.36 and the corresponding modified collapse capacity can then be calculated as 1.36×0.79 g=1.07g. This is similar to the value of 1.08g calculated based on the epsilon-based record selection method demonstrating that the simplified method can predict collapse capacities that are in good agreement with those obtained using the epsilon-based record selection method. However a question still remains whether the epsilon-based record selection method is reliable enough for seismic evaluations. More investigations should be carried out to verify this problem.

5.6.1.3 Bridge with free abutments (T_2=0.7 Sec)

The modified collapse capacity in this case was computed as 1.35×1.36 g=1.84 g. Again the modified collapse capacity is similar to that obtained using the epsilon-based record selection method which predicts a value of 1.82g as the collapse capacity of the structure.

5.6.1.4 *Longitudinal response*

The response of the bridge in the longitudinal direction was also studied considering the effects of abutment strength and stiffness. In practice however the abutment restraints are typically neglected which leads to a conservative design. To model the abutments the spring abutment model by Aviram et al., (2008) was used. The analyses were carried out for 4 cases including neglecting the abutment stiffness and strength, and considering abutments with no piles, 10 piles and 20 piles. The stiffness and strength of the abutments, soil and piles were computed based on the recommendations by Caltrans (2006).

The gaps between the abutment and bridge deck at the ends were also considered in the abutment model. As shown in Fig. 5.12, the CMR values are higher in the longitudinal direction than in the transverse direction (see Fig. 5.11) when the influence of abutments are included in the structural model. This indicates that the transverse response of the bridge is controlling. Increasing the number of piles had minor effects on the collapse capacity.

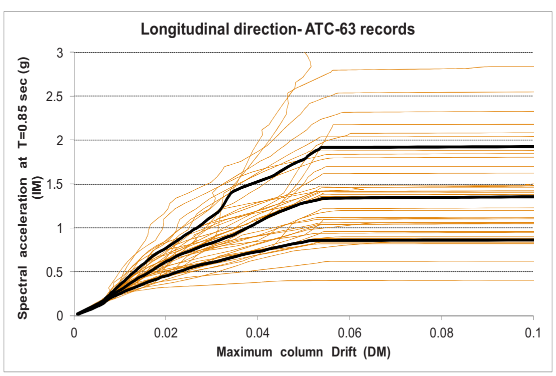

Longitudinal direction - ATC-63 record sets	IDA results Sa@T$_1$ =0.85 Sec (g)				
Case	Median	16%	84%	Modified median	Modified CMR
No abutments	0.92	0.58	1.60	1.15	2.72
Abutments with no piles	1.34	0.86	1.92	1.68	3.96
Abutments with 10 piles	1.44	0.94	1.94	1.80	4.26
Abutments with 20 piles	1.48	0.98	1.96	1.85	4.37

Fig. 5.12. IDA results in the longitudinal direction using 44 crustal records

5.6.1.5 *Three dimensional versus two dimensional analysis*

Priestley et al., (2007) concluded that the seismic responses in the orthogonal directions for straight bridges and symmetrical buildings are essentially independent and the current state-of-the-art is to model the ductility effects independently. However, a comparison of 2D and 3D nonlinear analyses was made in order to investigate the differences.

Because ground motions records are applied in pairs in three-dimensional nonlinear dynamic analyses, the resulting behaviour from each ground motion component is coupled. It has been found that the median collapse capacity resulting from three dimensional analyses is on average about 20% less than the median resulting from two-dimensional analyses (ATC-63, 2008). The application and scaling of pairs of ground motion records in IDA for three-dimensional analyses introduces a conservative bias that is not present in two-dimensional analyses (ATC-63, 2008).

It should also be noted that the comparison of the record selection methods including CMS-based and epsilon-based methods, which is the main focus of this study, requires a fundamental period to be defined for a structure so that the CMS and epsilon values at this period can be computed. The use of the 3D analysis increases the number of variables and makes the application and comparison of such methods complicated (e.g., the period to be used to compute a CMS or compute epsilon values). More research on such subjects is required.

Table 5.4. Results of IDA using a 3D analysis for different abutment stiffness and strength using 22 pairs of records applied twice at different principal directions (44 cases)

3D analysis results	IDA result percentiles at collapse (g)						
Case	Median	16%	84%	Modified median for spectral shapes	St Dev	Modified CMR for spectral shapes	Modified CMR for 3D analysis
Abutments with no piles (Fixed record set)	0.78	0.52	1.40	0.99	0.41	2.11	2.54
Abutments with no piles (Epsilon-based method)	1.06	0.64	1.58	1.06	0.52	2.27	2.72

A series of 3D analyses was carried out in which the twenty-two pairs of records were applied twice to the model, once with the ground motion records oriented along one principal direction, and then again with the records rotated 90 degrees. The predicted median collapse and percentiles using 3D analysis are reported in Table 5.4 in terms of the geometric means of the pair of ground motions at the fundamental periods (i.e., T=0.7 sec and T=0.85 sec in the transverse and longitudinal directions, respectively). While the collapse capacity of 0.99(g) was predicted using 3D analysis, the corresponding geometric mean of collapse capacities using 2D analysis for the transverse and longitudinal directions was 1.66(g) (i.e., 1.65(g) in the transverse direction and 1.68(g) in the longitudinal direction). This indicates that the predicted collapse capacity from 3D analysis is about 40% less than that obtained using 2D analysis. Applying the records in pairs may induce some conservative bias in the prediction of the collapse capacities and in the ATC-63 provisions this conservatism is accounted for by increasing the predicted median collapse capacity by 20% (i.e., the average differences). In the case of the bridge under study even higher differences (i.e., about 40%) were observed. Therefore care should be taken when treating the IDA results obtained using a 2D analysis, however the IDA results obtained from 3D analyses may be conservatively biased (ATC-63, 2008). While more research is required to study the differences between 2D and 3D analyses, this research focuses on the 2D nonlinear analysis in the transverse direction to compare the effects of different earthquake types and record selection methods.

5.6.2 Seismic evaluation considering all event types

Record sets used for the IDA should include all the probable earthquake types for the site under consideration. Contrary to the last section where crustal events only were considered in the IDA, in this section records from other event types (i.e., subduction interface and inslab events) are also considered. Several record selection methodologies are investigated for the seismic evaluation of the bridge under study using IDA. These methods include the epsilon-based and CMS-based record selection methods. The CMS-based method can be carried out in several ways such as CMS-Event-based and CMS-All-based (Goda and Atkinson, 2011). For the CMS-Event-based and epsilon-based methods, the number of records considered in the IDA from each event type is proportional to the percentage of contribution of that event type from seismic deaggregation.

5.6.2.1 Bridge with fixed abutments (T_1=0.7 Sec)

The IDA results using the CMS-based methods and considering different GMPEs are shown in Fig. 5.13 to Fig. 5.15 and Table 5.5. For the CMS-Event-based and CMS-All-based record selection methods, results are generally very similar, even using different GMPEs considered in this study (i.e., AB03 and Z06). This may be partially due to the fact that the Z06 GMPE is more conservative for interface events and less conservative for inslab events, while for the AB03 GMPE the opposite is true. Thus the considered GMPEs have counteracting effects for interface and inslab events, so that the average CMS in both cases are close to the CMS-Crustal using the BA08 GMPE. Although the median values using the CMS-Event-based and the CMS-All-based methods are similar, the standard deviations were higher in the case of the CMS-Event-based method than those obtained based on the CMS-All-based method as expected.

To investigate the sensitivity of the results from the CMS-based method to the number of the records used, the IDA was carried out using 78 records as shown in Fig. 5.15. This resulted in similar predictions using 44 records which indicates that the CMS-based methods are relatively insensitive to the number of records used in the IDA.

The IDA results using the epsilon-based method are summarized in Table 5.6 for 0.5% and 2% probability of exceedance in 50 years. It can be seen that although the median collapse capacity prediction for 0.5% probability of exceedance in 50 years is a little lower than that for 2% probability of exceedance in 50 years, the 16% and 84% percentiles are higher. This may indicate that the use of 44 records is not sufficient in this case to capture the median collapse capacity accurately. The use of 78 records in the IDA increased the median prediction by about 25% as shown in Fig. 5.16. This demonstrates that the epsilon-based method can be sensitive to the number of records used in the analysis.The median collapse capacity of 1.82 g obtained in this case is similar to that obtained before using only crustal records (e.g., see Fig. 5.8).

A comparison of the UHS-based method, shown in Fig. 5.17, with the CMS or epsilon-based methods at T=0.7 sec indicates that accounting for spectral shape and epsilon can increase the predicted collapse capacity by 40% to 75%. Similar results for the case of buildings, have been reported (Baker and Cornell, 2006a).

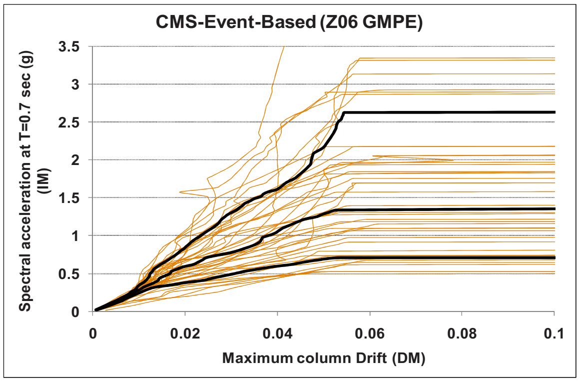

CMS-EVENT-BASED (Z06 GMPE)	IDA result percentiles (Sa @T_1)			
Damage states	Median	16%	84%	St Dev
Yielding	0.14	0.12	0.15	0.27
Cover Spalling (Exp.)	0.57	0.36	0.77	0.38
Collapse	**1.38**	0.74	2.67	0.58

Fig. 5.13. IDA results (CMS-Event based method, T_1=0.7) for Z06 GMPE (CMR=2.7)

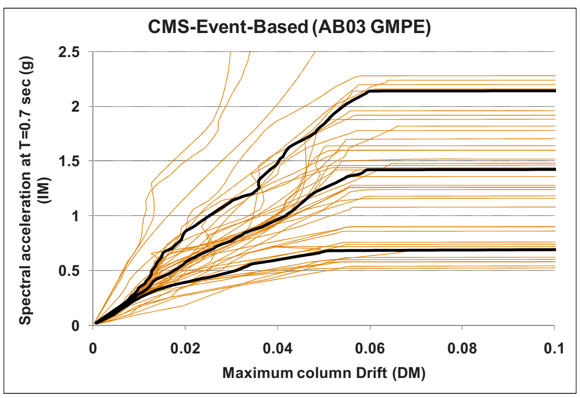

CMS-EVENT-BSD (AB03 GMPE)	IDA result percentiles (Sa @T_1)			
Damage states	Median	16%	84%	St Dev
Yielding	0.13	0.12	0.15	0.43
Cover Spalling (Exp.)	0.52	0.38	0.76	0.41
Collapse	**1.42**	0.72	2.15	0.52

Fig. 5.14. IDA results (CMS-Event-based method, T1=0.7) for AB03 GMPE (CMR=2.8)

Increasing the ductility capacity of the structure and the resulting larger period elongation can lead to even higher collapse capacities due to higher beneficial effects of spectral shapes in longer periods. Comparisons of the results obtained for yielding and spalling damage states indicate that different record selection methods had minor effects on these limit states. This is expected, as the effect of spectral shapes becomes more important at higher ductility levels. Figs. 5.13 to 5.17 indicate that typically the standard deviations are lower for the yielding and spalling states than for the collapse state. Based on the results presented it is important to note that the variability of the results are typically higher for the epsilon-based and the CMS-Event-based methods than the CMS-All-based and UHS-based methods .

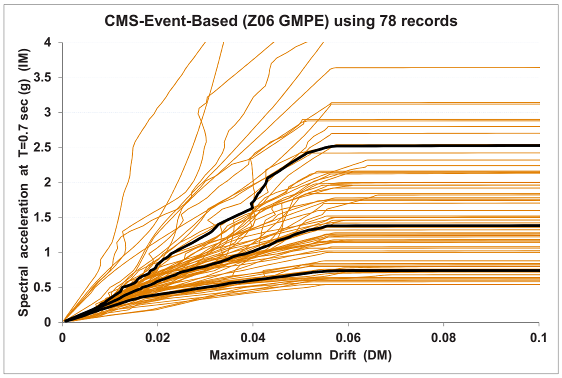

CMS-EVENT-BSD (Z06 GMPE)	IDA result percentiles (Sa @T_1)			
Damage states	Median	16%	84%	St Dev
Yielding	0.13	0.11	0.15	0.43
Cover Spalling (Exp.)	0.51	0.38	0.69	0.44
Collapse	**1.38**	0.74	2.54	0.58

Fig. 5.15. IDA results (CMS-Event based method, T_1=0.7) for Z06 GMPE using 78 records

Table 5.5. IDA results (CMS-All-based method, T_1=0.7) for a) Z06 GMPE b) AB03 GMPE

a)

CMS-ALL-BASED (Z06 GMPE)	IDA result percentiles (Sa @T_1)			
Damage states	Median	16%	84%	St Dev
Yielding	0.14	0.13	0.15	0.35
Cover Spalling (Exp.)	0.57	0.45	0.69	0.34
Collapse	**1.42**	1.06	2.25	0.44

b)

CMS-ALL-BASED (AB03 GMPE)	IDA result percentiles (Sa @T_1)			
Damage states	Median	16%	84%	St Dev
Yielding	0.15	0.14	0.16	0.28
Cover Spalling (Exp.)	0.57	0.46	0.78	0.31
Collapse	**1.45**	0.99	2.28	0.44

Table 5.6. Epsilon-based method for probability of exceedance in 50 years of a) 2% and b) 0.5% probability of exceedance in 50 years

EPSILON-BASED 2% IN 50 YRS	IDA result percentiles (Sa @T_1)			
Damage states	Median	16%	84%	St Dev
Yielding	0.13	0.11	0.15	0.41
Cover Spalling (Exp.)	0.56	0.32	0.77	0.42
Collapse	**1.47**	0.72	2.22	0.52

EPSILON-BASED 0.5% IN 50 YRS	IDA result percentiles (Sa @T_1)			
Damage states	Median	16%	84%	St Dev
Yielding	0.14	0.12	0.16	0.39
Cover Spalling (Exp.)	0.59	0.41	0.90	0.47
Collapse	**1.34**	0.91	3.02	0.60

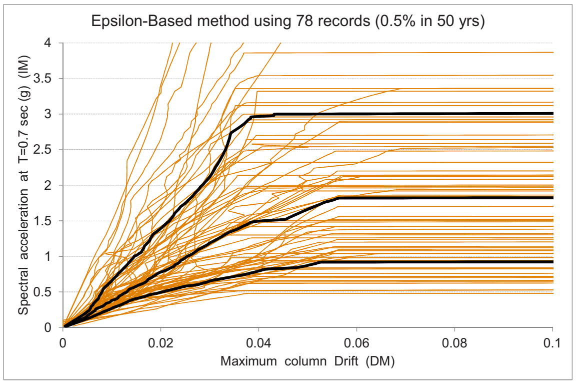

EPSILON-BASED 0.5% IN 50 YRS	IDA result percentiles (Sa @T_1)			
Damage states	Median	16%	84%	St Dev
Yielding	0.18	0.14	0.23	0.43
Cover Spalling (Exp.)	0.71	0.46	1.25	0.52
Collapse	**1.82**	0.93	3.09	0.62

Fig. 5.16. IDA results for Epsilon-based method using 78 records (CMR=3.5)

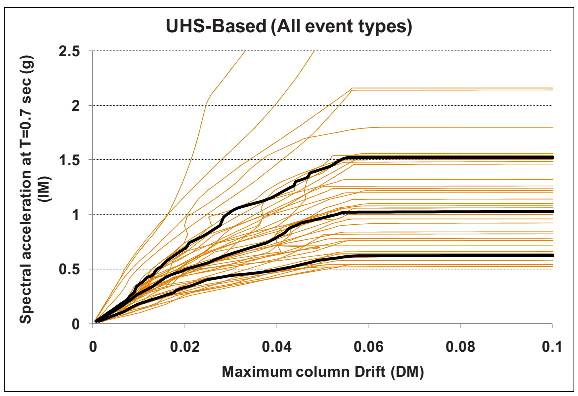

UHS-BASED	IDA result percentiles (Sa @T_1)			
Damage states	Median	16%	84%	St Dev
Yielding	0.13	0.08	0.16	0.44
Cover Spalling (Exp.)	0.47	0.31	0.64	0.38
Collapse	**1.04**	0.62	1.53	0.47

Fig. 5.17. IDA results based on the UHS-based record selection at T1=0.7 sec (CMR=2.0)

5.6.2.2 Bridge with free abutments (T_1=1.3 Sec)

The IDA results obtained using different record selection methods for the case of bridge with unrestrained abutments at the period of T_1=1.3 sec are shown in Figs. 5.18 to 5.21 and Table 5.7.

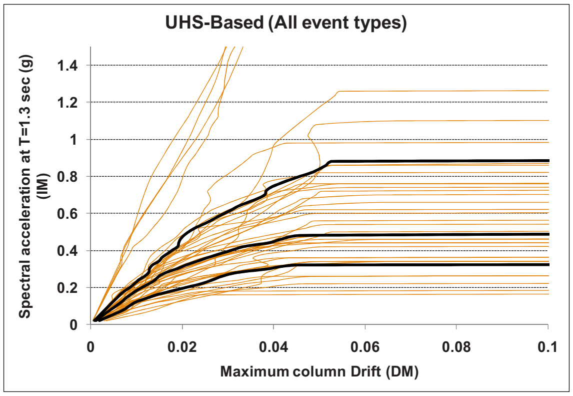

UHS-BASED	IDA result percentiles (Sa @T_1)			
Damage states	Median	16%	84%	St Dev
Yielding	0.09	0.05	0.13	0.54
Cover Spalling (Exp.)	0.29	0.18	0.40	0.49
Collapse	**0.50**	0.32	0.90	0.67

Fig. 5.18. IDA results using the UHS-based record selection method at T1=1.3 sec (CMR=1.8)

While the use of the CMS-Event-based and CMS-All-based methods again resulted in similar collapse capacity predictions, the use of the epsilon-based record selection resulted in a higher collapse capacity prediction. Increasing the number of records to 78 decreased the predicted median collapse capacity by 30% in the epsilon-based method, as shown in Fig. 5.20, while this increase in the number of records had a minor impact on the IDA results using the CMS-based method as shown in Figure 5.21 and Table 5.7. This again indicates that the IDA results using the epsilon-based record selection method can be sensitive to the number of records.

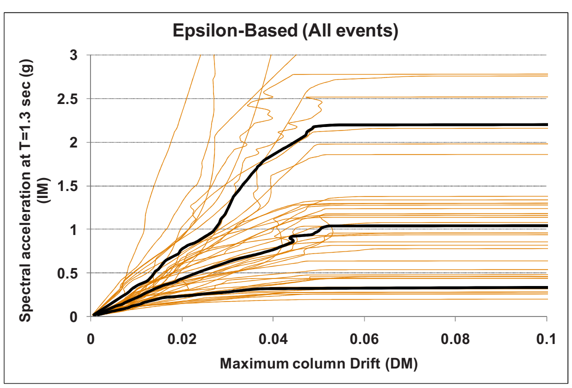

Epsilon-Based 0.5% in 50 yrs	IDA result percentiles (Sa @T_1)			
Damage states	Median	16%	84%	St Dev
Yielding	0.12	0.07	0.18	0.51
Cover Spalling (Exp.)	0.39	0.22	0.69	0.59
Collapse	**1.07**	0.34	2.25	0.83

Fig. 5.19. IDA results using epsilon-based record selection method at T_1=1.3 sec (CMR=3.8)

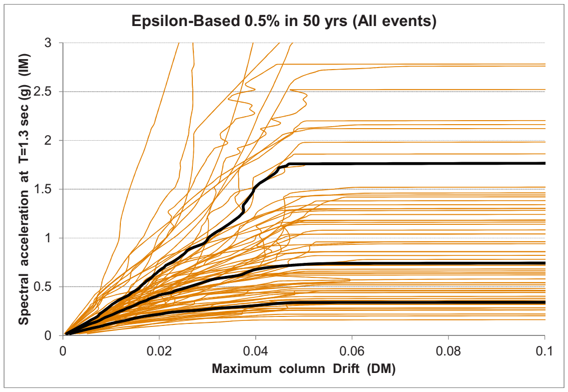

EPSILON-BASED 0.5% IN 50 YRS	IDA result percentiles (Sa @T1)			
Damage states	Median	16%	84%	St Dev
Yielding	0.11	0.07	0.13	0.56
Cover Spalling (Exp.)	0.37	0.21	0.58	0.57
Collapse	**0.74**	0.34	1.83	0.80

Fig. 5.20. IDA results for Epsilon-based method using 78 records (CMR=2.62)

The use of the CMS-based record selection in this case increased the collapse capacity prediction by about 25% compared to the results obtained based on the UHS-based method. On the other hand the use of the epsilon-based record selection method increased the predicted collapse capacity by 50%. A comparison of the results indicates that the 16% percentiles from different record selection methods are in good agreement. However the difference between the results becomes more significant for higher percentiles (see Figures 18 to 21 and Table 5.7).

Table 5.7. IDA results at T_1=1.3 sec using 44 records for a) CMS-All-based method (CMR=2.2) and b) CMS-Event-based method (CMR=2.14)

a)

CMS-ALL-BASED	IDA result percentiles (Sa @T1)			
Damage states	Median	16%	84%	St Dev
Yielding	0.09	0.08	0.12	0.30
Cover Spalling (Exp.)	0.33	0.26	0.42	0.29
Collapse	**0.62**	0.44	0.88	0.39

b)

CMS-EVENT-BASED	IDA result percentiles (Sa @T1)			
Damage states	Median	16%	84%	St Dev
Yielding	0.09	0.08	0.10	0.34
Spalling (Exprimental)	0.28	0.19	0.42	0.38
Collapse	**0.60**	0.34	0.92	0.51

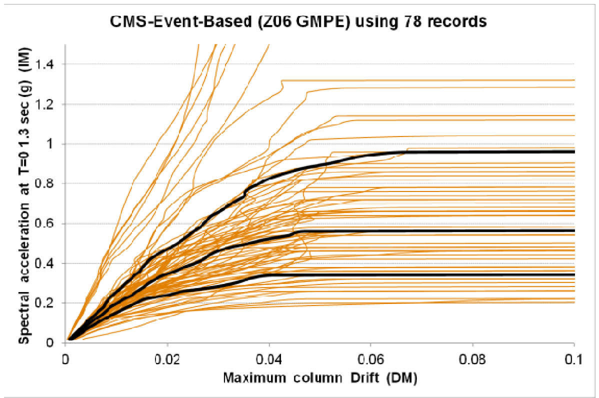

CMS-EVENT-BASED	IDA result percentiles (Sa @T_1)			
Damage states	Median	16%	84%	St Dev
Yielding	0.10	0.08	0.12	0.38
Cover Spalling (Exp.)	0.32	0.23	0.44	0.41
Collapse	**0.57**	0.35	0.97	0.60

Fig. 5.21. IDA results using CMS-Event-based method by using 78 records (CMR=2.02)

5.6.2.3 Bridge with free abutments (T_2= 0.7 Sec)

For the case of free abutments with a period of T_2=0.7 sec corresponding to the second important mode, using CMS-Event-based and CMS-All-based methods again resulted in similar collapse capacity predictions of 1.17g and 1.22g respectively. However, as noted before, the variation of the IDA results was larger for the case of CMS-Event-based (i.e., standard deviation of 0.54 versus 0.7). The collapse capacity obtained based on the epsilon-based method (i.e., 1.43g) is once again higher than those obtained using the CMS-based methods. By comparing the results obtained using the UHS-based record selection it was found that the use of the CMS-based methods can increase the predicted collapse capacity by 30% (e.g., increase from 0.9g to 1.2 g). On the other hand the increase in the collapse capacity prediction using the epsilon-based record selection method is around 60% (i.e., increase from 0.9g to 1.43g).

5.6.3 Sensitivity of the results to the number of records

To provide more rigorous results regarding the effects of the number of records and to investigate the impact of different earthquake types on the collapse capacity individually, larger record sets were considered. For this purpose 78 fixed records with the highest PGA and PGV values were selected for each earthquake type (i.e., a total of 3*78= 234 records) (Tehrani, 2012). The unmodified and modified median collapse capacities for the spectral shape effects are presented in Table 5.8. The results obtained for combining all records in proportion to the event contributions are also presented which confirmed the results obtained in sections 4.1 to 4.2. The results in Table 5.8 also indicate that the interface events can result in the lowest collapse capacity predictions for the bridge studied in this research.

Table 5.8. IDA results using 78 fixed records for each event type for a)T=0.7 sec and b)T=1.3 sec

a)

Records type	Unmodified median (g)	Modified median (g)	Modified CMR
78 Crustal records	1.37	1.63	3.20
78 Interface records	1.35	1.43	2.80
78 Inslab records	1.69	2.78	5.46
Combined results	1.44	1.84	3.61

b)

Records type	Unmodified median (g)	Modified median (g)	Modified CMR
78 Crustal records	0.75	0.93	3.24
78 Interface records	0.56	0.60	2.09
78 Inslab records	0.77	1.48	5.16
Combined results	0.71	0.88	3.07

5.7 Summary and conclusions

The seismic behavior of a 4-span bridge located in Vancouver was investigated using incremental dynamic analysis (IDA). First, the response of the bridge was evaluated by considering crustal events only. The seismic evaluation was then extended to consider all three earthquake types (i.e., shallow crustal, interface Cascadia subduction and deep inslab subduction events) that contribute significantly to overall seismic hazard in south-western British Columbia. A large pool of ground motion records was used for this purpose, compiled by combining the PEER-NGA database and the K-NET/KiK-NET database. The conclusions pertaining to the cases studied are summarized below:

(1) The median values of collapse capacities obtained in this study by considering crustal events alone were not very different from those obtained by considering the other event types. This was due to the fact that the constructed CMS-All was close to the CMS-Crustal and thus combining the effects of different seismic event types led to similar results as considering crustal events alone. Making general conclusions regarding this

matter needs more investigation, as this may be specific to the site condition and the period ranges considered here. However the uncertainty due to record to record variability was higher when different event types were considered. Thus accounting for different event types is important and should be implemented in seismic performance evaluation of bridges.

(2) The use of the UHS-based method resulted in very conservative predictions of collapse capacities which were significantly lower than those predicted using the epsilon-based method.

(3) The use of the CMS- or UHS-based methods generally underestimated the record-to-record variability, while the use of the epsilon-based record selection method resulted in larger predictions for record-to-record variability.

(4) It was found that the use of interface records in IDA resulted in the lowest capacity predictions for the bridge studied in this research. This can be attributed to the longer duration and different frequency content of the interface events compared to crustal events.

(5) It was demonstrated that the IDA results can be sensitive to the choice of the record selection method. The epsilon-based method in all of the cases resulted in the highest prediction for the capacity of the structure. However more research is required to verify the reliability of this method for seismic evaluations, as it was found that the results can be sensitive to the number of records used. Furthermore, different sets of records with comparable mean epsilon values could result in somewhat different collapse capacity predictions. Increasing the number of records used in the IDA did not influence the results obtained using the CMS-based record selection methods. The use of different GMPEs for record selection did not significantly affect the results in IDA. The influence of the record selection methods was greater on the collapse capacity prediction than on the other damage states such as yielding and spalling.

(6) The CMS and the mean epsilon values were predicted using the matching method in seismic deaggregation. The use of the exceeding method for seismic deaggregation tended to overestimate the mean epsilon values and thus the collapse capacity of the structure.

Acknowledgements

The financial support provided by the Natural Sciences and Engineering Research Council of Canada for the Canadian Seismic Research Network is gratefully acknowledged. Ground motion data for Japanese earthquakes were obtained from the K-NET and KiK-NET databases at www.k-net.bosai.go.jp and www.kik.bosai.go.jp and other crustal ground motion data obtained from the PEER-NGA database available at http://peer.berkeley.edu. The authors are grateful for the constructive and insightful comments provided by the reviewers.

References

Please see the last section.

6 Seismic Response of Bridges Subjected to Different Earthquake Types Using IDA

Payam Tehrani[1] and Denis Mitchell[1]

[1]*Department of Civil Engineering & Applied Mech., McGill University, Montreal H3A 2K6, Canada*

6.1 Preface

In Chapter 5 the IDA method was applied for the seismic evaluation of a bridge structure. The results indicated that including different earthquake types in the seismic evaluations results in a larger record to record variability, while the median collapse capacity predictions are similar to the case where only crustal events are considered. To further investigate the results obtained in Chapter 5, in Chapter 6 the IDA method is used to predict the collapse capacity of a number of bridges with different configurations and different period ranges. The bridges were also designed using different force modification factors, R.

In Chapter 5, it was also shown that when different earthquake types are considered, the IDA needs to be performed using a larger number of records, due to increased record-to-record variability in the results. For this purpose a large set of records were selected to perform the IDA. Three sets of records were selected for three different earthquake types. Each set includes 78 horizontal components (i.e., 39 pairs of ground motions). The details of the three sets of ground motion for different earthquake types are given in Appendix G.

In Chapter 5 it was demonstrated that a simplified method can be used to modify the IDA results for the effects of epsilon and spectral shapes. The results from the simplified method were in good agreement with those obtained using the direct use of the epsilon-based method. Therefore in Chapter 6 this method is used to modify the IDA results obtained using the large fixed record sets for the spectral shape effects.

Since in Chapter 6 the IDA method is applied to a number of bridges using a large number of records (i.e., 234 records for each bridge), the computation time of the analyses could be extremely long. Further, the durations of the subduction earthquake records are much longer than the crustal records, which result in the computation time of the IDA being much longer, when such earthquake types are considered in the analyses. To remove this problem, a fast IDA algorithm was developed, as discussed in Chapter 2 and will be discussed in more details in Chapter 6. In the fast IDA algorithm only the collapse capacity of the bridges will be predicted, since only the median collapse capacity and the variability in the results are needed for the seismic evaluations, as discussed in Chapter 2. It must be noted that even using the fast IDA algorithm the analyses were computationally intensive (see Appendix B for the details of the computer program). More details regarding the program developed to extract the seismic deaggregation results are available in Appendix C.

More information regarding different earthquake types are given in Appendix F.
More details of the partial results obtained are also presented in Appendix I.
A main part of Chapter 6 was included into a manuscript: Tehrani, P. and Mitchell, D. ”Seismic Response of Bridges Subjected to Different Earthquake Types using IDA”, Journal of earthquake Engineering, Manuscript UEQE-2012-1345, submitted in January 2012.

Based on the Taylor and Francis publication policy: “the authors retain the right to include an article in a thesis or dissertation that is not to be published commercially” (http://journalauthors.tandf.co.uk/preparation/copyright.asp).

6.2 Abstract

Incremental Dynamic Analysis (IDA) was used to evaluate the seismic response of straight, continuous 4-span bridges with different sub-structure configurations. Three different record sets were chosen to represent three different earthquake types which can occur for a site such as Vancouver (i.e., crustal, subduction interface, and subduction inslab earthquakes). Seventy eight records were considered in each set (i.e., a total of 234 records) and the capacities of the bridges were evaluated using a fast IDA algorithm. A simplified method to account for the effects of spectral shapes was used. Different subsets of the records with specific characteristics were also used in the IDA. The bridges were designed and evaluated for two different design force modification factors and bridges with different degrees of irregularity were studied. Comparisons of the IDA results obtained indicated that in most of the cases the interface record sets resulted in lower median collapse capacities and hence were the most critical of the ground motions studied.

Keywords Incremental Dynamic Analysis (IDA); Subduction Earthquakes; Crustal Earthquakes; Spectral Shape; Epsilon; Bridges; Regularity

6.3 Introduction

Incremental dynamic analysis (IDA) (Vamvatsikos and Cornell, 2002) is a useful tool for seismic performance assessment of structures (e.g., ATC-63 provisions (ATC-63, 2008)). The IDA results which relate statistics of a damage measure (DM) (i.e., inelastic seismic demand) with an intensity measure (IM) (usually $S_a(T_1)$) can be used in probabilistic seismic performance assessment and fragility analysis of structures.

For a realistic seismic performance assessment using IDA, appropriate records should be chosen based on the properties and location of the structure. This could result in the selection of different earthquake records for different structures. In the seismic performance assessment of a number of structures the use of different records for each structure can be very time-consuming and hence for practical reasons simplified methods can be used.

The spectral shape of the records used for seismic evaluations using IDA can significantly affect the seismic response predictions (e.g., (Baker and Cornell, 2006a). The ATC-63 provisions propose a simplified method in which a fixed set of records are used in the IDA without considering the spectral shape in the record selection. The IDA results obtained using this fixed set of records are then modified for the effects of spectral shapes based on the fundamental period and ductility capacity of each structure. This can reduce the complexity of the seismic performance evaluations. Research has shown that the results obtained from the simplified method are in good agreement with those obtained using more precise methods that directly consider the spectral shape in the record selection (e.g., (Haselton et al., 2011) and (Tehrani, 2012)). For the seismic assessment of a number of bridges with different configurations, having different degrees of irregularity, this simplified method will be used.

Usually only the records from the crustal earthquakes have been used in seismic performance assessments (e.g., ATC-63 provisions (2008)), while for some sites such as Vancouver or Seattle subduction earthquakes with very different characteristics can occur. The effects of considering different earthquake types (i.e., crustal, subduction interface, and inslab events) on the seismic performance evaluation of bridges for a site such as south-western British Columbia is the main objective of this study. The transverse responses of the bridges were chosen in this study, rather than 3D responses, to better demonstrate the influence of different earthquake types on the seismic response and to limit the variables.

6.4 Epsilon-based method and spectral shape issue

Rare ground motions (large earthquakes) typically have a peaked spectral shape that is much different than a standard uniform hazard spectral shape and accounting for this shape has been shown to increase the predicted collapse capacity significantly (increase of up to 70% (Haselton et al, 2011; Baker and Cornell, 2006; Tehrani, 2012). Thus neglecting the spectral shape of the records selected for collapse assessment of a structure can result in conservative and unrealistic predictions.

Epsilon, ε, is defined as the number of logarithmic standard deviations of a target ground motion from a median ground motion prediction equation (GMPE) for a given magnitude, M, and distance, R. The most direct approach in accounting for spectral shape in structural analysis is to select ground motions with $\varepsilon(T_1)$ values (i.e., the epsilon values at the fundamental period of the structure) similar to the epsilon values obtained from seismic hazard deaggregation analysis for the site and hazard level of interest. It has been found that the $\varepsilon(T_1)$ values are in fact a measure of the spectral shape of the records (Baker and Cornell, 2006). This approach is known as the epsilon-based record selection method. Because the direct use of this approach is often time-consuming and complicated in practice, a simplified method has been developed to modify the collapse capacity predictions for the effects of epsilon and spectral shapes (Zareian, 2006; Haselton et al., 2011). For this purpose, a fixed set of records can be used to perform the incremental dynamic analyses. The predicted capacities obtained using the IDA will then be modified for the effects of spectral shapes using a spectral shape factor (SSF). To compute the SSF a regression analysis needs to be carried out to derive a relationship between the natural logarithm of the collapse capacities versus the epsilon (T_1) values for each record. The result of such a regression analysis can be presented in the form of $\ln[S_C(T_1)] = \beta_0 + \beta_1\varepsilon$. Where the S_C is the collapse capacity, β_0 is the average collapse capacity when $\varepsilon = 0$, and β_1 indicates how sensitive the collapse capacity $(S_C(T_1))$ is to changes in the ε value. The SSF is then calculated using Eq. [6.1]

$$[6.1] \quad SSF = \exp[\beta_1(\bar{\varepsilon}_0(T) - \bar{\varepsilon}(T)_{records})]$$

where $\bar{\varepsilon}(T)_{records}$ is the mean epsilon of the records and $\bar{\varepsilon}_0(T)$ is the mean epsilon value from the seismic deaggregation. For the prediction of the epsilon values of the records, the BA08 (Boore and Atkinson, 2008) ground motion prediction equation (GMPE) was used for the crustal earthquakes and the Z06 GMPE (Zhao et al., 2006) was used for the subduction zone earthquakes (i.e., interface and inslab).

The most important issue in the simplified method which will affect the results is the prediction of the β_1 factor. In the ATC-63 provisions simplified equations are given to estimate the β_1 factor based on the ductility capacities of building structures. To develop these simplified equations to estimate the β_1 factor, a large record set including 78 crustal records was selected from the PEER-NGA database (Haselton et al., 2007) for the analyses.

The equations given in the ATC-63 provisions are specific to building structures rather than bridges and in addition, these equations may not be valid for other earthquake types (i.e., interface and inslab events). Therefore, in this study the β_1 factors are calculated directly for each bridge structure using a regression analysis. The evaluation of the β_1 factors have been carried out using the whole set of data and also using some subsets of data with specific characteristics such as positive epsilon values, lower scale factors, removal of outliers and as well as a combination of these factors. This enables an evaluation of the sensitivity of the β_1 factors and the collapse capacity estimates as a function of the characteristics of the records in the set.

The seismic evaluations based on the simplified method often involve using a fixed set of records including 22 crustal records (i.e., 44 record components) (ATC63, 2008). Since one of the important steps is the prediction of the β_1 factors for each structure, the use of 44 record components may not be adequate and more records is recommended to be used for a more precise prediction of this factor. Further some studies indicate that the use of the epsilon-based method may be sensitive to the number of records used in the IDA (Tehrani, 2012). Thus to address these issues 78 record components (39 pairs) are used for each of the three event types to evaluate the seismic response of the bridges (i.e., a total of 3*78=234 records).

6.5 Fast-IDA analysis

In a typical IDA, the analyses start with very low spectral acceleration levels and then the records are scaled up until they cause dynamic instability of the structure which indicates structural collapse. The resulting wide variation of the scale factors from small values to large values allows the determination of different performance levels (e.g., from serviceability states to structural collapse) and enables the development of the IDA curves.

For the seismic evaluations in this study, the prediction of the collapse capacities of the bridges is the primary objective and thus the full IDA curves are not required. Only the median value of spectral acceleration of the records at the fundamental period of the bridge that causes dynamic instability (collapse capacity of the structure) needs to be determined. This will significantly reduce the total number of required inelastic dynamic analyses and the computation time. It must be noted that the duration of the interface and inslab records are significantly longer than those of the crustal events and thus computation time for IDA analyses using subduction records will be significantly longer (about 4 to 6 times) than that using crustal records. In this research the variability was computed based on the predicted collapse capacities for all of the records in each set. The probability of collapse at the maximum considered earthquake (MCE) level, which usually corresponds to 2% probability of exceedance in 50 years, should be reasonably low. To estimate the probability of collapse at the MCE level based on the computed median collapse capacity a simplified assumption is often made that the cumulative probability function follows a lognormal distribution.

The ATC-63 provisions provide a simplified judgmental method to estimate the total uncertainty in the prediction of the collapse capacity. For the bridges considered in this study, the total uncertainty, expressed by β_{TOT} of 0.6 is deemed appropriate (i.e., the modelling quality and quality of test data used for the nonlinear hysteretic models were considered as “good”, and the quality of code conforming ductile design requirements was considered as “superior”).

The collapse margin ratio, CMR, which is the ratio of the median 5%-damped spectral acceleration of the collapse level ground motions to the 5%-damped spectral acceleration of the MCE ground motions, can be then computed at the fundamental period of the structure (ATC-63, 2008). The probability of collapse at the MCE level can be predicted based on the lognormal distribution model.

It should be noted that the computed median collapse capacities and CMR values are determined based on the seismic excitations applied only in the transverse direction of the bridges and thus the results do not include the effects of longitudinal seismic response. This assumption is deemed appropriate for the sake of this research, since the relative influence of considering different earthquake types on the seismic response was the main focus of this study. This simplification was made for the following reasons: to exclude further variables and uncertainty associated with bi-directional responses; problems with scaling of bi-directional excitations (Priestley et al., 2007; Baker and Cornell, 2006c); the conservative biases introduced due to the application and scaling of pairs of ground motion records in IDA (ATC-63, 2008); and the difficulty in choosing an appropriate period and scaling procedure in the epsilon-based method due to the different periods in the longitudinal and transverse directions. More research is required on these subjects.

Although a general conclusion cannot be made, studies of the longitudinal responses of similar bridges, including the influence of the abutments in the seismic response, demonstrated that the transverse response was controlling (Tehrani, 2012). The current state-of-the-art is to model the ductility effects independently and Priestley et al. (2007) concluded that the seismic responses in the orthogonal directions for straight bridges and symmetrical buildings are essentially independent. Nevertheless it is recommended that the effects of bi-directional excitations be considered when the seismic performance evaluations of the structures are carried out. More research is required on this subject.

In this research different event types and different sets of records are used and the record-to-record variability and the collapse capacity must be computed for each record set. The collapse capacities obtained for each record should be known to compute the β_1 factors and the spectral shape factors. For this purpose a time efficient algorithm was developed to compute only the spectral accelerations (at the fundamental period of the structure) that cause structural collapse for each record. For this purpose an initial estimate of collapse capacity was computed based on the expected acceptable collapse margin ratio of the structure assuming 10% probability of collapse at the maximum considered earthquake (MCE) level and that the cumulative density function follows a lognormal distribution rule (see Eq. [6.2]).

[6.2] $Sa_1(T_1)_{collapse} = Sa(T_1)_{MCE} * CMR_{acceptable}$

[6.3] $CMR_{acceptable} = 1/ \exp(\Phi^{-1}(p_{collapse}) * \beta_{TOT})$

Where, $Sa_1(T_1)_{collapse}$ is the initial estimate of the collapse capacity, $Sa(T_1)_{MCE}$ is the spectral acceleration at the fundamental period of the structure from the maximum considered earthquake spectrum, $CMR_{acceptable}$ is the acceptable collapse margin ratio, Φ^{-1} is the inverse cumulative normal distribution function, $p_{collapse}$ is the acceptable probability of collapse at the MCE level (usually taken as 10%), and β_{TOT} is the total uncertainty in predicting the collapse capacity of the structure (i.e., including uncertainties due to record-to-record variability, modelling, test data , and design requirements). Eq. [6.2] is only used to compute an initial estimate of the collapse capacity which then will be modified in several subsequent steps to compute the collapse capacity of the structure. In this study the precision in the prediction of the collapse capacities was considered as 0.02 g.

6.6 Record selection for IDA

Three fixed sets of records including 39 records (78 components) for each earthquake type (i.e., 234 records) were chosen to be used in the IDA. This large number of records was chosen to compute the β_1 values for each event type more precisely, to predict the variability in the seismic response, and to improve the capacity predictions. The records chosen in the sets are among the strongest natural records available and are deemed appropriate for the seismic performance evaluations. The criteria used for record selections are briefly discussed below.

a) Crustal record set:

For crustal earthquakes, the “basic far-field” records used by (Haselton et al., 2007) were used in this study. This set includes 39 crustal records from the PEER-NGA database. Some minimum limits on the magnitude of the events, peak ground acceleration and peak ground velocity were imposed in the record selection to be representative of strong ground motion. A limit on the maximum number of records from a single seismic event was imposed to make sure that the predictions are not biased, however a sufficient number of records must also be selected. The criteria imposed for the record selection is presented in Table 6.1.

b) Interface record set:

Since the number of available records due to subduction events is relatively small, the selection criteria used for the crustal events need to be somewhat loosened so that enough number of records can be selected. The selected records represent the strongest records available from each event in the database and an attempt was made to include at least a few records from each earthquake that roughly meets the criteria. In addition, 10 records from the destructive 2011 Tohoku earthquake were included in the set to take advantage of the latest data available for interface earthquakes.

c) Inslab record set:

Only a limited number of inslab earthquake records are available in the database, and thus the selection criteria needed to be loosened even more so that sufficient number of records can be selected. The selected records represent the strongest records available from the inslab events in the database. In addition to the inslab events from Japan, 5 records from the 2001 Nisqually earthquake in North America were included in the set. It must be noted that the shear wave velocity data, V_{S30}, for the Nisqually earthquake was not originally available by the COSMOS and USGS databases. In this study the data concerning the shear wave velocities were obtained from Caki and Walsh (2011) and Wong et al. (2011). The V_{S30} values are necessary to compute the S_a values using the corresponding GMPEs, compute the epsilon values, and to determine the soil type. Further details concerning the records used for the analyses including the list of records is available by Tehrani (2012).

Table 6.1. Criteria used for record selection for different earthquake types

Earthquake type	Magnitude	Distance (km)	Focal depth (km)	VS30 (m/sec)	PGA (g)	PGV (cm/sec)	Maximim number of records from each event	Databases
Crustal	≥ 6.5	≥ 10	-	≥180	≥ 0.2	≥ 15	6	PEER-NGA
Interface	≥ 6.7	-	< 50	≥180	≥ 0.17	≥ 13	10	K-NET and KiK-NET
Inslab	≥ 6.0	-	≥ 50	≥180	≥ 0.11	≥ 11	12	K-NET and KiK-NET and COSMOS

6.7 Bridge properties

The seismic behaviour of different bridge configurations were studied using Incremental Dynamic Analysis (IDA) considering three different earthquake types by using the 78 records for each event type. Continuous 4-span straight bridges were studied and the seismic evaluations were carried out in the transverse direction of the bridges to assess the importance of different earthquake types. It is known that the seismic response of the bridges in the transverse direction is governed by a multi-degree of freedom system which is more complex than the response in the longitudinal direction. For straight bridges the responses in the orthogonal directions are likely to be essentially independent (Preistley et al., 2007).

As shown in Fig. 6.1, five different bridge configurations were studied with different arrangements of column heights. For each configuration 3 different column diameters are considered (i.e., a total of 5 x 3=15 bridges). The 2006 Canadian Highway Bridge Design

Code (CHBDC) (CSA, 2006) classifies the importance of bridges in accordance with their performance requirements. “Emergency-route” bridges must be open to emergency vehicles immediately after the design earthquake. The CHBDC uses a response modification factor, R together with an importance factor, I. For single ductile reinforced concrete columns R is 3.0. For emergency-route bridges I is 1.5 and for other bridges I is 1.0. Based on the results obtained from the inelastic time history analyses of more than 600 bridge configurations designed based on the CHBDC, the use of a response modification factor, R, of 3 along with an importance factor, I, of 1.5 was found to be conservative for current seismic design practice (Tehrani, 2012). In order to reduce the conservatism by accounting for a larger R factor for the ductile bridge columns, the bridges in this study were also designed with R=5 and two cases were considered, one with I=1.5 (R/I=3.33) for emergency-route bridges and another case where I is taken as 1.0 (R/I = 5).

The design spectrum defined in the 2010 National Building Code of Canada (NBCC) (NRCC, 2010) rather than that of the CHBDC were used for the design of the bridges. It must be noted that the design spectra defined in NBCC correspond to 2% probability of exceedance in 50 years, while those defined in CHBDC correspond to 10% probability of exceedance in 50 years. It is expected that the design spectra defined in the NBCC be adopted for the next edition of the CHBDC. The bridges were designed for Vancouver assuming a site class C.

A computer program was developed to automatically generate the designs for the columns and the input files for the RUAUMOKO software (Carr, 2009) for different bridge configurations. The columns of the bridges were designed using the load combinations defined in the CHBDC based on the multi-mode elastic response analyses and the design spectra from the NBCC. For this purpose and also for the seismic performance evaluations a moment curvature analysis was carried out for each column and also the moment axial force interaction curves were determined. The columns were designed using capacity design principles and detailed for ductile response (CSA 2006).

In order to predict the ductility capacities, the confinement effects in the concrete core were considered using the confinement model by Mander et al. (1988).
The configurations and properties of the bridge structures studied are summarised in Tables 6.2 to 6.4. Where H_1, H_2 and H_3 are the heights of columns, D is the diameter of the columns, and R is the response modification factor. For the classification of regularity the provisions of the CHBDC (CSA 2006) were used except for configuration 4 which is actually regular for the transverse response. It is noted that the minimum amount of longitudinal reinforcement in a column is 0.8% which controls the amount of flexural reinforcement in columns with low seismic demands. The spiral confinement reinforcement ratio of 1.2% controlled the amount of transverse reinforcement in the plastic hinge regions of the columns. The spiral reinforcement consisted of 20 mm diameter bars spaced at 70 and 50 mm for column diameters of 1.5, 2.0 m, respectively and 25 mm diameter bars spaced at 70 mm for column diameter of 2.5 m.

Table 6.2. Summary of bridges with different configurations studied (a total of 30 bridges)

Bridge configuration	Regularity	H_1 (m)	H_2 (m)	H_3 (m)	D (m)	R/I
1	Regular - stiff columns	7	7	7	1.5, 2.0 and 2.5	3.3 and 5
2	Regular - more flexible columns	14	14	14	1.5, 2.0 and 2.5	3.3 and 5
3	Irregular bridge ("ramp")	7	14	21	1.5, 2.0 and 2.5	3.3 and 5
4	Regular bridge with flexible central column	7	14	7	1.5, 2.0 and 2.5	3.3 and 5
5	Highly irregular bridge	14	7	21	1.5, 2.0 and 2.5	3.3 and 5

Table 6.3. Periods (sec) and (%M at the fundamental period) for different bridge configurations studied in the case of a) R/I=3.33 and b) R/I=5

a)

Conf.	D= 1.5 m	D= 2 m	D= 2.5 m
1	1.09 (86%)	0.75 (86%)	0.57 (86%)
2	2.17 (86%)	1.75 (86%)	1.36 (87%)
3	1.65 (84%)	1.32 (79%)	1.13 (74%)
4	1.33 (84%)	0.96 (82%)	0.75 (78%)
5	1.28 (88%)	0.90 (90%)	0.72 (83%)

b)

Conf.	D= 1.5 m	D= 2 m	D= 2.5 m
1	1.17 (86%)	0.79 (86%)	0.57 (86%)
2	2.17 (86%)	1.75 (86%)	1.36 (87%)
3	1.75 (85%)	1.38 (81%)	1.16 (76%)
4	1.45 (85%)	1.03 (83%)	0.77 (79%)
5	1.41 (88%)	1.01 (90%)	0.79 (89%)

Table 6.4. Percentage of longitudinal reinforcement in the bridge columns C_1,C_2 and C_3 for different bridge configurations

	R/I= 3.33			R/I= 5		
Conf.	D= 1.5 m (C_1, C_2, C_3)	D= 2.0 m (C_1, C_2, C_3)	D= 2.5 m (C_1, C_2, C_3)	D= 1.5 m (C_1, C_2, C_3)	D= 2.0 m (C_1, C_2, C_3)	D= 2.5 m (C_1, C_2, C_3)
1	1.3%,1.5%,1.3%	1.0%,1.17%,1.0%	0.8%,0.8%,0.8%	0.8%,0.8%,0.8%	0.8%,0.8%,0.8%	0.8%,0.8%,0.8%
2	0.8%,0.8%,0.8%	0.8%,0.8%,0.8%	0.8%,0.8%,0.8%	0.8%,0.8%,0.8%	0.8%,0.8%,0.8%	0.8%,0.8%,0.8%
3	2.71%,0.8%,0.8%	2.04%,0.8%,0.8%	1.6%,0.8%,0.8%	1.33%,0.8%,0.8%	1.07%,0.8%,0.8%	0.88%,0.8%,0.8%
4	1.93%,0.8%,1.93%	1.3%,0.8%,1.3%	1.0%,0.8%,1.0%	0.8%,0.8%,0.8%	0.8%,0.8%,0.8%	0.8%,0.8%,0.8%
5	0.8%,2.92%,0.8%	0.8%,2.2%,0.8%	0.8%,1.71%,0.8%	0.8%,1.52%,0.8%	0.8%,1.22%,0.8%	0.8%,0.98%,0.8%

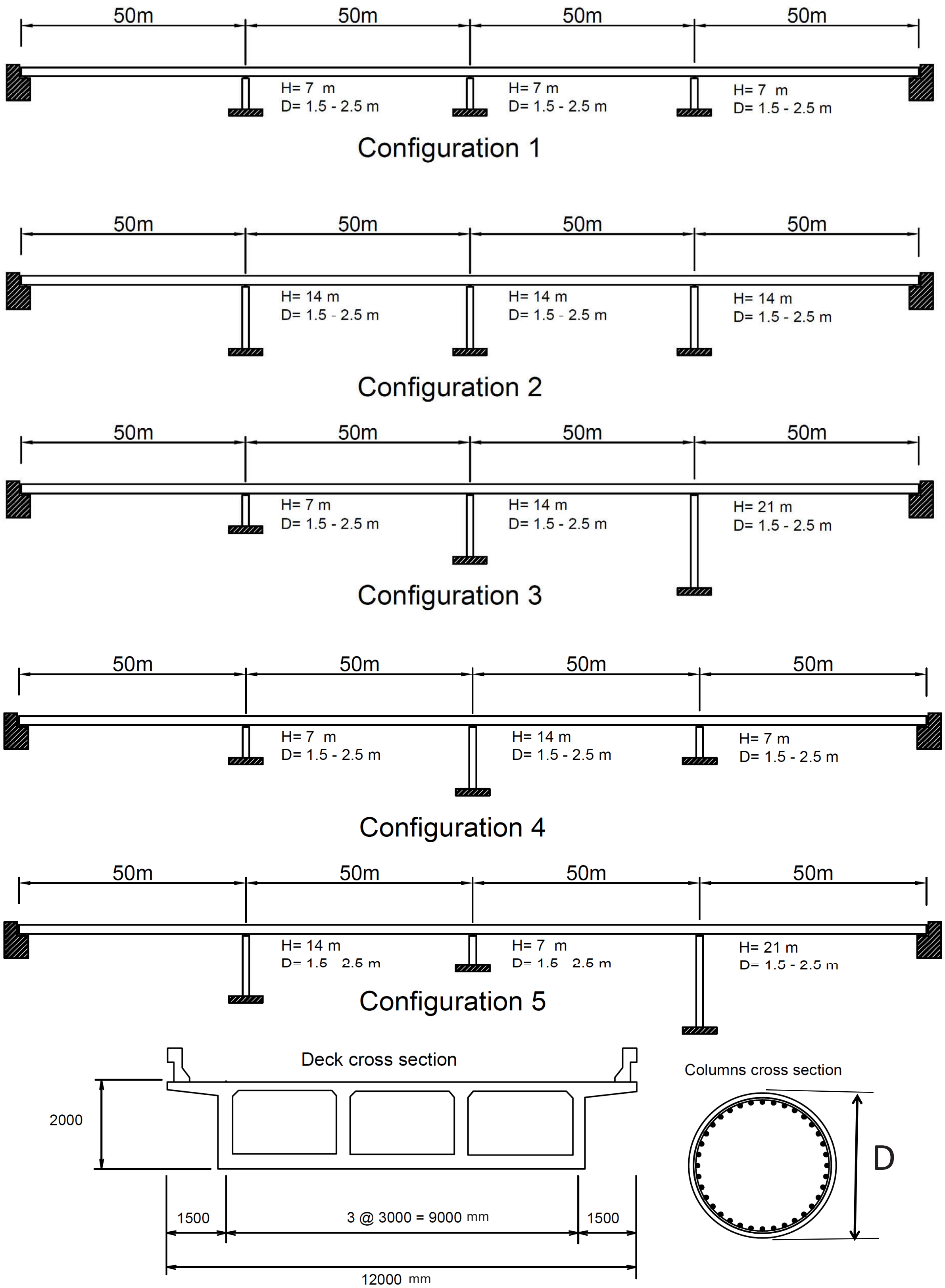

Fig. 6.1. Bridge configurations studied

6.8 Modelling of the bridges for IDA

In using IDA, the post-peak (i.e., cap point) response of structural elements should be included in modelling. The most important factors in structural modelling for IDA are the plastic rotation capacity, $\theta_{cap}{}^{p}$, and the post-capping rotation capacity, θ_{pc} (ATC-63, 2008). These parameters are used to define a component backbone curve, as shown in Fig. 6.2.

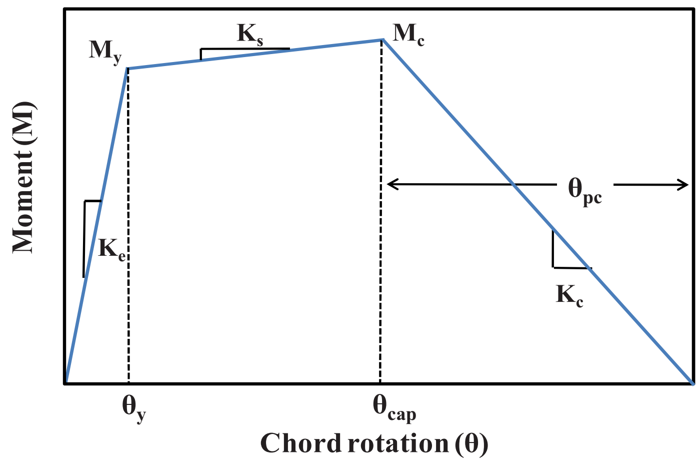

Fig. 6.2. Backbone curve parameters (adapted from ATC-63(2008))

A study by Berry and Eberhard (2007) provides some empirical equations to estimate the engineering demand parameters. These parameters include drift ratio, plastic rotation and strain in the longitudinal bars for circular bridge columns based on the properties of the columns including longitudinal and transverse steel ratio, axial load ratio, and geometry. In this research, the ultimate tensile strain in the steel bars corresponding to the bar buckling damage state from the empirical equations is used to compute the ultimate curvature of the columns and the corresponding drift and curvature ductility is defined as the point at which strength degradation begins (i.e., θ_{cap} in Fig. 6.2). Mackie and Stojadinovic (2007) provide an equation for estimating the drift beyond the peak load when the column reaches zero strength which was used in this research to define the post-capping stiffness, K_c. The modified Takeda hysteresis model (Otani, 1981) was used in this study to model the hysteretic behaviour of the RC columns using the Ruaumoko software (Carr, 2009). More details about the modelling parameters are available elsewhere (Tehrani, 2012).

The bridges under study were designed and detailed to meet the code requirements for ductile response, including capacity design concepts and adequate support lengths at the abutments. The ductile columns contained code-compliant spiral reinforcement to confine the concrete, avoid shear failure and to control buckling of the vertical reinforcing bars. For this continuous bridge, with all other failure modes avoided, the flexural response governs the response of the bridge and sidesway collapse is the governing collapse mechanism. The collapse prediction in this study is based on dynamic instability of the structures (Vamvatsikos and Cornell, 2002; ATC63, 2008).

6.9 Seismic hazard analysis

An updated seismic hazard model for western Canada, developed by Goda et al. (2010), was used to take advantage of new seismic data and seismological models to improve several aspects of the current Geological Survey of Canada model. Probabilistic seismic hazard analysis (PSHA) for Vancouver was carried out using the updated seismic hazard model based on Monte Carlo simulation by Goda et al. (2010). The assessment was based on the simulated seismic activities for 5 million years, and the considered annual non-exceedance probabilities range from 0.996 to 0.9999 (i.e., 10% to 0.5% probability of exceedance in 50 years). The deaggregation analysis is based on an "approximately equal criterion" (i.e., matching method) (Hong and Goda, 2006), where seismic events reaching a seismic intensity level between 90% and 110% of the target $S_a(T_n)$ value are used to produce deaggregation results. The deaggregation results for the mean epsilon values and the contributions of different event types are shown in Table 6.5. The results are based on the BA08 and Z06 GMPE which were used to compute the epsilon values in this study for the crustal and subduction earthquakes, respectively. The mean epsilon values from the seismic deaggregation are used in the epsilon-based record selection method and also in the prediction of the spectral shape factors (SSF, see Eq. [6.1]) based on the fundamental period of each bridge configuration. The percentage of contributions of each event type in the overall seismic hazard is used to determine the required number of records from each event type, when the results from different events are combined to estimate the overall collapse capacity due to all earthquake types.

Table 6.5. The deaggregation results for mean epsilon and percentage of contribution of different event types at 0.5% probability of exceedance in 50 years (using BA08 and Z06 GMPE).

	Percentage of contribution			Mean epsilon values		
	Crustal	Interface	Inslab	Crustal	Interface	Inslab
PGA	31%	4%	65%	1.40	2.31	1.76
T=0.2 sec	26%	7%	67%	1.28	2.23	1.87
T=0.5 sec	39%	27%	34%	1.49	1.79	1.82
T=1 sec	36%	34%	30%	1.66	1.38	1.85
T=2 sec	29%	48%	23%	1.71	1.24	2.67
T=3 sec	36%	54%	10%	1.72	1.15	2.17

6.10 Results obtained using different record sets and subsets

A fast IDA algorithm was used to predict the collapse capacity of the bridges. Fig. 6.3(a) shows an example of a full IDA curve carried out for one of the cases studied and the corresponding unmodified spectral accelerations obtained at different damage states. $S_a(T_1)$ is used as the intensity measure (IM) and the maximum drift ratio of columns is used as the damage measure (DM). The heavy lines in Fig. 3(a) show the IDA percentiles (median, 16% and 84%).The fast-IDA results for this case are also presented in Fig. 6.3(b) (see last row in table). The results obtained using the fast-IDA algorithm are the same as those obtained using a full IDA analysis at the collapse state. The minor differences are due to the precision of 0.02g accepted in the prediction of collapse capacity.

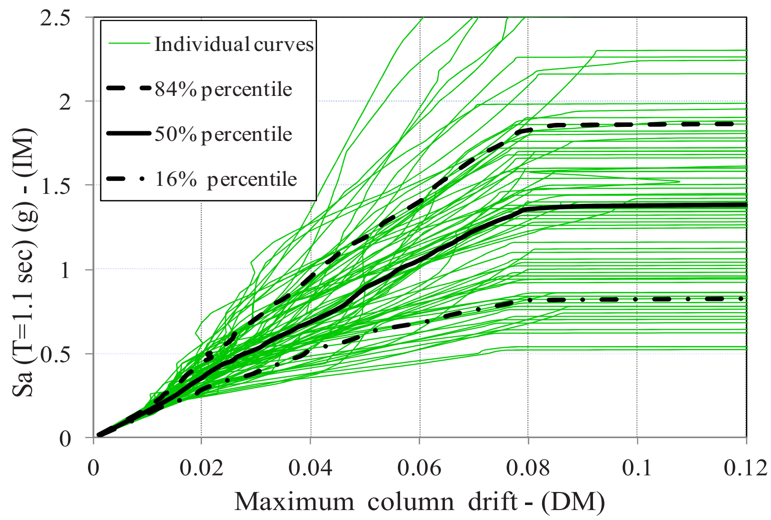

a)

78 Crustal records	IDA result percentiles (S_a (T_1))			
Damage states	Median	16%	84%	St Dev
Yielding	0.10	0.09	0.12	0.11
Cover Spalling	0.36	0.29	0.45	0.22
Bar buckling	1.03	0.68	1.37	0.37
Collapse	1.37	0.83	1.87	0.41
Collapse (Fast-IDA)	1.36	0.84	1.85	0.40

b)

Fig. 6.3. IDA results: a) full IDA curves for the bridge with configuration 1, D=1.5 m and R/I=3.3 using 78 crustal records (unmodified results) b) statistics of the IDA results for different damage states

Three different subsets of records were considered to include the three different earthquake types. Since a large number of records are available in each set (i.e., 78 records), it is possible to consider some different subsets of records. In this study 8 different subsets of records were considered. In each subset only the records with specific properties were considered. This involved selecting records with positive epsilon values, considering records requiring lower scale factors, removal of outliers and a combination of these parameters. To compute the modified collapse capacities, record-to-record variability, spectral shape factors, etc., for each subset only the records in that subset were considered. The details of different subsets considered are presented in Table 6.6.

Table 6.6. Different record subsets considered to compute the predicted median collapse capacity

Subset No.	1	2	3	4	5	6	7	8
Criteria	All records	Records with positive epsilon(T1)	All records with outliers removed	Records with positive epsilons and outliers removed	All records with lower scale factors	Records with lower scale factors and positive epsilon values	Records with lower scale factors and outliers removed	Records with lower scale factors and positive epsilon values and outliers removed

A summary of the results obtained using different record sets and subsets are shown in Tables 6.7 to 6.11. The results are given in terms of the modified median collapse capacities and the ratio of the obtained collapse margin ratio (CMR) to the acceptable collapse margin ratio ($CMR_{acceptable}$) assuming a 10% probability of collapse at the maximum considered earthquake level (i.e., 2% in 50 years). Direct comparison of the modified collapse capacities obtained for different configurations is not appropriate, since the fundamental periods of the structures in each configuration are different and consequently the seismic demands will be different for each configuration. To better compare the results from different configurations, the CMR/ $CMR_{acceptable}$ ratios are compared. The CMR includes the effects of different seismic demands and $CMR_{acceptable}$ includes the effects of different variability in the predictions of the collapse capacities using different sets and subsets.

In addition to these eight subsets, another subset was considered in which only the records with similar epsilon values to those obtained from the seismic deaggregations were considered (i.e., epsilon-based method). The results obtained using this subset is also shown in the tables which can be used to assess the predictions obtained using the spectral shape factors. For the case of some subsets for the inslab events there was an insufficient number of records, especially when the records with required lower scale factors were considered.

Table 6.7. Comparison of the median collapse capacity (g) and (CMR/ CMRacceptable) ratios using different subsets for configuration 1with R/I = 3.33 and a) D = 1.5 m and b) D = 2.5 m

a)

Modified median & ($CMR/CMR_{acceptable}$)	Crustal records	Interface records	Inslab records	All events
Subset 1	1.60 (2.34)	1.06 (1.14)	4.00 (3.59)	1.61 (1.57)
Subset 2	1.62 (2.38)	1.01 (1.05)	3.35 (3.43)	1.63 (1.64)
Subset 3	1.61 (2.41)	1.05 (1.16)	4.44 (4.27)	1.64 (1.59)
Subset 4	1.65 (2.48)	0.90 (0.97)	3.44 (3.88)	1.67 (1.74)
Subset 5	1.64 (2.40)	0.59 (0.75)	2.45 (2.85)	1.55 (1.74)
Subset 6	1.62 (2.38)	0.64 (0.81)	2.54 (3.17)	1.55 (1.77)
Subset 7	1.66 (2.48)	0.55 (0.74)	2.76 (3.24)	1.56 (1.70)
Subset 8	1.65 (2.48)	0.66 (0.90)	2.54 (3.17)	1.58 (1.81)
Epsilon-Based method	1.49 (2.34)	0.70 (0.73)	2.73 (3.38)	1.42 (1.58)

b)

Modified median & ($CMR/CMR_{acceptable}$)	Crustal records	Interface records	Inslab records	All events
Subset 1	2.75 (2.11)	2.93 (1.65)	7.11 (3.64)	3.45 (1.81)
Subset 2	2.75 (2.12)	2.82 (1.55)	6.02 (3.40)	3.46 (1.96)
Subset 3	2.77 (2.17)	2.85 (1.73)	7.13 (3.90)	3.40 (1.89)
Subset 4	2.78 (2.19)	2.75 (1.63)	6.11 (3.64)	3.39 (2.06)
Subset 5	2.71 (2.09)	2.22 (1.48)	4.49 (2.69)	3.17 (2.13)
Subset 6	2.74 (2.14)	2.10 (1.39)	4.67 (2.94)	3.17 (2.17)
Subset 7	2.73 (2.15)	2.04 (1.40)	4.49 (2.69)	3.26 (2.21)
Subset 8	2.76 (2.19)	2.04 (1.39)	4.67 (2.94)	3.18 (2.21)
Epsilon-Based method	2.99 (2.36)	2.38 (1.24)	5.68 (3.74)	2.70 (1.77)

Table 6.8. Comparison of the median collapse capacity (g) and (CMR/ CMRacceptable) ratios using different subsets and methods for configuration 2 (R/I = 3.3) and a) D = 1.5 m and b) D = 2.5 m

a)

Modified median & ($CMR/CMR_{acceptable}$)	Crustal records	Interface records	Inslab records	All events
Subset 1	1.37 (4.31)	1.01 (1.98)	3.74 (7.51)	1.30 (2.39)
Subset 2	1.43 (4.49)	0.96 (1.76)	2.99 (5.99)	1.36 (2.59)
Subset 3	1.35 (4.32)	0.89 (2.11)	3.52 (7.69)	1.20 (2.26)
Subset 4	1.39 (4.46)	0.85 (2.06)	3.04 (6.58)	1.25 (2.50)
Subset 5	1.32 (4.25)	0.47 (1.15)	2.72 (5.74)	1.05 (1.79)
Subset 6	1.32 (4.23)	0.49 (1.26)	2.22 (4.65)	1.00 (1.83)
Subset 7	1.32 (4.27)	0.47 (1.21)	2.77 (5.98)	1.04 (1.81)
Subset 8	1.31 (4.24)	0.47 (1.25)	2.22 (4.65)	0.98 (1.81)
Epsilon-Based method	1.38 (4.43)	0.75 (1.77)	1.84 (3.61)	1.03 (2.49)

b)

Modified median & ($CMR/CMR_{acceptable}$)	Crustal records	Interface records	Inslab records	All events
Subset 1	2.29 (3.69)	1.56 (1.97)	6.37 (6.59)	2.47 (2.53)
Subset 2	2.56 (4.15)	1.34 (1.57)	7.75 (8.32)	2.64 (2.69)
Subset 3	2.29 (3.75)	1.38 (1.87)	6.54 (7.52)	2.41 (2.55)
Subset 4	2.60 (4.27)	1.26 (1.62)	7.29 (8.93)	2.64 (2.84)
Subset 5	2.22 (3.63)	0.90 (1.29)	-	-
Subset 6	2.31 (3.83)	0.93 (1.35)	-	-
Subset 7	2.24 (3.70)	0.78 (1.23)	-	-
Subset 8	2.20 (3.71)	0.82 (1.38)	-	-
Epsilon-Based method	2.66 (4.76)	1.30 (1.66)	5.64 (6.68)	2.04 (2.51)

Table 6.9. Comparison of the median collapse capacity (g) and (CMR/ CMRacceptable) ratios using different subsets and methods for configuration 3 (R/I = 3.3) and a) D = 1.5 m and b) D = 2.5 m

a)

Modified median & (CMR/CMR$_{acceptable}$)	Crustal records	Interface records	Inslab records	All events
Subset 1	1.06 (2.21)	0.78 (1.21)	3.37 (4.36)	1.15 (1.49)
Subset 2	1.02 (2.21)	0.80 (1.19)	3.07 (4.72)	1.11 (1.46)
Subset 3	1.04 (2.20)	0.74 (1.28)	3.24 (4.60)	1.11 (1.49)
Subset 4	1.02 (2.20)	0.77 (1.31)	2.16 (3.82)	1.10 (1.73)
Subset 5	1.05 (2.19)	0.50 (0.88)	1.57 (2.53)	0.89 (1.36)
Subset 6	1.01 (2.18)	0.49 (0.91)	-	-
Subset 7	1.05 (2.19)	0.50 (0.89)	1.57 (2.53)	0.89 (1.36)
Subset 8	1.00 (2.16)	0.49 (0.91)	-	-
Epsilon-Based method	0.90 (2.02)	0.77 (1.15)	2.15 (2.90)	0.78 (1.33)

b)

Modified median & (CMR/CMR$_{acceptable}$)	Crustal records	Interface records	Inslab records	All events
Subset 1	1.86 (2.80)	1.19 (1.36)	4.38 (4.14)	1.86 (1.86)
Subset 2	1.87 (2.85)	1.19 (1.31)	3.84 (3.98)	1.88 (1.95)
Subset 3	1.91 (2.94)	1.17 (1.39)	4.78 (4.63)	1.94 (1.91)
Subset 4	1.92 (3.01)	1.18 (1.33)	3.68 (4.04)	1.89 (2.02)
Subset 5	1.87 (2.87)	0.73 (0.95)	1.57 (1.92)	1.59 (2.09)
Subset 6	1.90 (2.95)	0.77 (0.99)	2.10 (2.65)	1.82 (2.26)
Subset 7	1.89 (2.93)	0.68 (0.91)	1.35 (1.73)	1.55 (2.06)
Subset 8	1.93 (3.03)	0.77 (1.07)	2.10 (2.65)	1.81 (2.25)
Epsilon-Based method	1.88 (3.00)	0.77 (0.85)	4.06 (4.66)	1.44 (1.71)

Table 6.10. Comparison of the median collapse capacity (g) and (CMR/ CMRacceptable) ratios using different subsets and methods for configuration 4 (R/I = 3.3) and a) D = 1.5 m and b) D = 2.5 m

a)

Modified median & (CMR/CMR$_{acceptable}$)	Crustal records	Interface records	Inslab records	All events
Subset 1	1.56 (2.45)	1.08 (1.36)	4.51 (4.75)	1.69 (1.78)
Subset 2	1.77 (2.80)	0.90 (1.05)	5.00 (5.57)	1.85 (1.96)
Subset 3	1.50 (2.42)	1.02 (1.36)	4.67 (5.13)	1.68 (1.77)
Subset 4	1.76 (2.83)	0.89 (1.13)	4.62 (5.73)	1.81 (2.00)
Subset 5	1.61 (2.51)	0.66 (0.95)	1.16 (1.91)	1.40 (1.97)
Subset 6	1.74 (2.74)	0.65 (0.97)	-	-
Subset 7	1.64 (2.61)	0.61 (0.93)	1.16 (1.91)	1.40 (1.96)
Subset 8	1.63 (2.62)	0.62 (1.01)	-	-
Epsilon-Based method	1.60 (2.71)	0.86 (1.09)	3.17 (4.02)	1.39 (1.73)

b)

Modified median & (CMR/CMR$_{acceptable}$)	Crustal records	Interface records	Inslab records	All events
Subset 1	2.69 (2.41)	2.34 (1.62)	4.80 (3.53)	3.07 (2.27)
Subset 2	2.74 (2.50)	2.13 (1.39)	4.91 (4.04)	3.06 (2.34)
Subset 3	2.65 (2.45)	2.32 (1.67)	5.14 (3.85)	3.09 (2.29)
Subset 4	2.72 (2.56)	2.14 (1.46)	4.91 (4.04)	3.06 (2.40)
Subset 5	2.67 (2.47)	1.29 (1.08)	3.43 (2.31)	2.83 (2.30)
Subset 6	2.73 (2.58)	1.32 (1.09)	2.82 (2.21)	2.74 (2.29)
Subset 7	2.71 (2.53)	1.25 (1.10)	3.43 (2.31)	2.83 (2.29)
Subset 8	2.63 (2.55)	1.28 (1.15)	2.82 (2.21)	2.66 (2.26)
Epsilon-Based method	2.84 (2.71)	2.04 (1.30)	4.20 (3.62)	2.79 (2.11)

Table 6.11. Comparison of the median collapse capacity (g) and (CMR/ CMRacceptable) ratios using different subsets and methods for configuration 5 (R/I = 3.3) and a) D = 1.5 m and b) D = 2.5 m

a)

Modified median & ($CMR/CMR_{acceptable}$)	Crustal records	Interface records	Inslab records	All events
Subset 1	1.23 (1.91)	0.80 (1.00)	2.07 (2.64)	1.20 (1.52)
Subset 2	1.30 (2.05)	0.68 (0.79)	1.78 (2.58)	1.31 (1.71)
Subset 3	1.23 (1.94)	0.78 (1.03)	2.27 (2.96)	1.23 (1.53)
Subset 4	1.35 (2.15)	0.60 (0.75)	1.71 (2.60)	1.31 (1.81)
Subset 5	1.25 (1.94)	0.57 (0.79)	1.55 (2.04)	1.11 (1.42)
Subset 6	1.30 (2.05)	0.53 (0.72)	1.73 (2.61)	1.13 (1.53)
Subset 7	1.26 (2.00)	0.45 (0.66)	1.57 (2.09)	1.06 (1.34)
Subset 8	1.35 (2.15)	0.52 (0.71)	1.65 (2.66)	1.13 (1.54)
Epsilon-Based method	1.30 (2.18)	0.65 (0.83)	1.46 (2.36)	1.03 (1.27)

b)

Modified median & ($CMR/CMR_{acceptable}$)	Crustal records	Interface records	Inslab records	All events
Subset 1	2.25 (1.98)	1.93 (1.38)	3.49 (2.51)	2.49 (1.86)
Subset 2	2.24 (1.98)	1.81 (1.24)	3.09 (2.58)	2.44 (1.91)
Subset 3	2.19 (2.01)	1.82 (1.37)	3.81 (2.86)	2.47 (1.87)
Subset 4	2.24 (2.03)	1.81 (1.32)	2.85 (2.62)	2.35 (1.98)
Subset 5	2.29 (2.02)	1.40 (1.11)	3.11 (2.05)	2.28 (1.75)
Subset 6	2.25 (1.99)	1.28 (1.01)	2.96 (2.19)	2.23 (1.72)
Subset 7	2.22 (2.02)	1.23 (1.02)	3.11 (2.05)	2.21 (1.70)
Subset 8	2.24 (2.03)	1.24 (1.00)	3.10 (2.44)	2.19 (1.72)
Epsilon-Based method	2.31 (2.09)	1.64 (1.10)	2.91 (2.53)	2.23 (1.78)

As can be seen from the tables, the use of the simplified method for the crustal events for all the subsets of records studied resulted in similar predictions. This indicates that for this case the modified median collapse capacities were not sensitive to the subsets of the records used. On the other hand the predicted modified median collapse capacities for the subduction interface and the inslab events were similar within the first four subsets (subset 1 to 4) and within the second four subsets (subsets 5 to 8). However the results from subset 1 to 4 were somewhat different from those obtained using subset 5 to 8 in which only the records with required smaller scale factors were considered. This emphasizes the need to impose a limitation on the maximum allowable scale factors to avoid the results being biased and unrealistic. For these cases imposing this limitation decreased the predicted collapse capacity. This problem was found to be more important for the subduction earthquake records, while the collapse capacities obtained using the crustal records were less sensitive to the limitation on the scale factor. This may be due to the fact that a larger number of strong crustal records are available in the databases and hence smaller scale factors are required.

A comparison of the results obtained using the epsilon-based record selection method with those obtained using the simplified method (modifying the results using SSF factor) for the case of crustal events shows a very good agreement between the results even using different record subsets. As an example, for the case of configuration 1 with column diameters of 1.5 m the predicted median collapse capacity for crustal records using the simplified method varied between 1.60 g to 1.66 g for 8 subsets of records studied, the direct use of the epsilon-based method for this case resulted in a median collapse capacity of 1.49 g. For other cases shown in the tables even better agreement of the results are observed. In the epsilon-based method only the results from the records with similar epsilon values to the mean epsilon values obtained at the fundamental period of the structure from the seismic deaggregation were considered.

In the case of the subduction interface events the predicted median collapse capacity using the simplified method was between 0.9 g to 1.06 g using the subsets 1 to 4 of the records and for the subset 5 to 8 the predicted median varied between 0.59 g to 0.66 g. The direct use of the epsilon-based record selection method however results in a median collapse capacity of 0.70 g which is closer to the results obtained using subset 8 for this case. The results obtained for various configurations studied indicate that typically the use of subset 4 or 8 resulted in the predictions which were in better agreement with those obtained using the epsilon-based method. This is mainly because in these subsets only the records with positive epsilon values are considered which somewhat account for the spectral shapes effects.

It is interesting to note that considering the records which required lower scaling factors also reduced the record-to-record variability in the collapse capacity predictions. For example in the case of interface events the record-to-record variability was around 0.7 in subsets 1 to 4, while this variability reduced to around 0.5 to 0.6 in subsets 5 to 8. It must be noted that since both the median collapse capacity and record-to-record variability are important in the seismic performance evaluations, the use of the $CMR/ CMR_{acceptable}$ ratio (i.e. the ratio of the collapse margin ratio to the acceptable collapse margin ratio) can provide a better parameter for the purpose of comparing the results.

The predicted median collapse capacity for the inslab events varied between 3.35 g to 4.44 g in the subsets 1 to 4, and between 2.45 g to 2.76 g in subsets 5 to 8. The CMR/ $CMR_{acceptable}$ ratio varied between 3.43 to 4.27 in the subsets 1 to 4, and between 2.85 to 3.38 in the subsets 5 to 8. Similar high values of CMR and CMR/ $CMR_{acceptable}$ ratios obtained for other configurations studied. These high values of CMR/ $CMR_{acceptable}$ ratio indicate that the inslab events are the least critical case and the bridges are predicted to have high collapse margin ratios for inslab earthquakes.

Typically the interface record sets resulted in the lowest collapse capacity predictions for the bridges studied. However the difference between the results obtained using records from different earthquake types is different for each configuration studied. For some configurations the interface and crustal record sets resulted in similar collapse capacity predictions (e.g., configuration 1 with D=2.5 m) and for most of the configurations this difference was larger (e.g., configuration 3 with D=2.5 m). The results from the inslab record sets were not found to be critical for the cases considered in this study. Similar trends were observed for other configurations studied as can be seen in the tables.

6.11 Combining the results from different earthquake types

The collapse capacities for different event types (for all sets) were computed separately. In order to predict an average collapse capacity, the results from different events should be combined in proportion to the contribution of each earthquake type to the overall seismic hazard obtained from the seismic hazard deaggregation. This means that for example if many records with positive epsilon values are available in the crustal record set but fewer records with positive epsilon values are available in the interface and inslab record sets, then fewer crustal records were selected to maintain the ratio of the number of records proportional to the percentages of contribution of the event types. In such cases the priority in record selection was to the records with the closest epsilon values (at the fundamental period of the structure) to the mean epsilon values obtained from the seismic hazard deaggregation. In addition to the average median collapse capacity, logarithmic standard deviation of the collapse capacity can be directly computed in this method which represents the record-to-record variability in the collapse capacity predictions. It must be noted that the IDA results are combined for different subsets of records (i.e., 8 subsets were considered).

In order to combine the results from different events, the predicted collapse capacity of each record was modified by applying the SSF factor to the unmodified collapse capacity of the records. To do this, instead of using the average epsilon of records in Eq. [6.1], the epsilon value of each record at the fundamental period of the structure was used to predict the SSF for each record individually. It must be noted that for each earthquake type the GMPEs specific to that earthquake type were used to compute the epsilon values of the records and to predict the β_1 factors.

It is interesting to note that typically the median collapse capacities obtained by combining the effects of three earthquake types are close to the results obtained considering the crustal records alone. Although the median collapse capacities were similar, the record-to-record variability considering all the earthquake types was higher than that obtained considering only crustal events. This may indicate that the median collapse capacity of the structure could be predicted by considering only the crustal events. To account for the influence of different earthquake types, the record-to-record variability could be increased in the prediction of the acceptable collapse margin ratios and probability of collapse.

6.12 β_1 and SSF values using different sets and subsets of records

The use of the simplified method to modify the predicted collapse capacities for the effects of spectral shapes requires the β_1 factors to be computed. The β_1 factor shows how sensitive the collapse capacity predictions are to changes in ε (T_1) values. Larger values of β_1 indicate that the predictions are more sensitive to the spectral shape which is represented by the epsilon values at the fundamental period of the structure (i.e., ε (T_1)). The regression analysis method to compute the β_1 factors was described in Section 6.4.

For example in Fig. 6.4 the β_1 value from the regression analysis was calculated as 0.263 using 78 crustal records. The BA08 GMPE was used to compute ε (T_1).

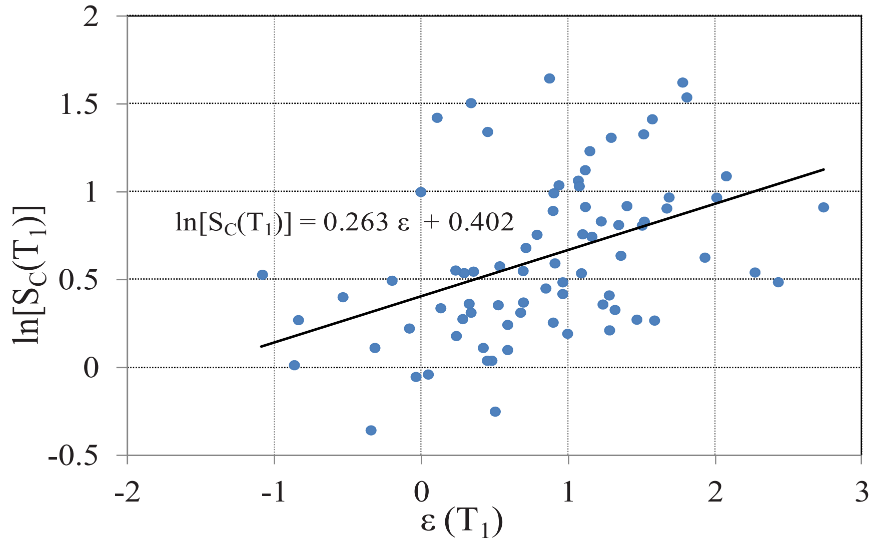

Fig. 6.4. Regression analysis to compute β_1 for the case of configuration 1 with D = 2 m using BA08 GMPE

The results obtained for the bridges studied indicate that although the calculated values of β_1 and SSF are different using different subsets of records, the predicted modified collapse capacities computed by applying the spectral shape factor (SSF) to the median collapse capacity of each subset, are similar. An example of the calculated β_1 and SSF factors for different subset of records and different earthquake types are shown in Table 6.12.

Results in this table also show the percentiles and standard deviations of the collapse capacities obtained using different record sets and subsets. As can be seen the variability of the results for the interface and inslab events were larger than that for the crustal events especially in subsets 1 to 4. However when only records with small scale factors were selected in subsets 5 to 8, the variability of the results from interface events became lower, but at the same time the median predicted collapse capacities also decreased.

Regression analyses were performed to obtain a simplified relationship between the β_1 factors and the period of the structures studied. The records in subset 3 (i.e., all the records with outliers removed) were used for this purpose. It must be noted that considering different subsets of records resulted in different β_1 factors.

Table 6.12**.** An example of Statistics of unmodified collapse capacity predictions for different earthquake types and for different subsets of records in each subset(Configuration 4, D = 2.5 m, and R/I = 3.33).

		IDA Percentiles (g) (Unmodified for the spectral shape effects)							
		50%	16%	84%	St Dev	Num. of Rec.	Mean ε (Records)	β_1	SSF
Subset 1	Crustal	2.26	1.61	4.20	0.47	78	0.84	0.24	1.19
	Interface	2.09	0.96	4.43	0.72	78	0.86	0.15	1.12
	Inslab	2.73	1.34	5.13	0.67	78	0.33	0.38	1.76
Subset 2	Crustal	2.40	1.64	4.27	0.45	68	1.03	0.24	1.14
	Interface	1.73	0.91	4.78	0.78	66	1.13	0.45	1.23
	Inslab	3.50	1.78	5.30	0.56	48	0.85	0.35	1.40
Subset 3	Crustal	2.22	1.59	3.98	0.44	75	0.85	0.25	1.20
	Interface	2.08	0.95	4.20	0.69	77	0.86	0.15	1.11
	Inslab	2.71	1.32	4.89	0.65	76	0.36	0.43	1.90
Subset 4	Crustal	2.34	1.63	4.00	0.42	65	1.04	0.29	1.16
	Interface	1.73	0.91	4.68	0.74	65	1.13	0.47	1.24
	Inslab	3.50	1.78	5.30	0.56	48	0.85	0.35	1.40
Subset 5	Crustal	2.18	1.54	3.89	0.44	71	0.91	0.30	1.22
	Interface	1.37	0.89	2.67	0.54	56	0.83	-0.08	0.94
	Inslab	1.81	0.85	4.29	0.75	17	0.62	0.52	1.89
Subset 6	Crustal	2.32	1.63	3.94	0.41	64	1.05	0.31	1.18
	Interface	1.28	0.84	2.69	0.55	50	1.00	0.06	1.03
	Inslab	2.15	1.31	4.72	0.61	13	1.05	0.35	1.31
Subset 7	Crustal	2.17	1.51	3.50	0.42	69	0.93	0.34	1.24
	Interface	1.36	0.87	2.61	0.49	54	0.83	-0.10	0.92
	Inslab	1.81	0.85	4.29	0.75	17	0.62	0.52	1.89
Subset 8	Crustal	2.26	1.63	3.50	0.38	62	1.04	0.29	1.17
	Interface	1.21	0.84	2.49	0.47	47	1.01	0.10	1.06
	Inslab	2.15	1.31	4.72	0.61	13	1.05	0.35	1.31

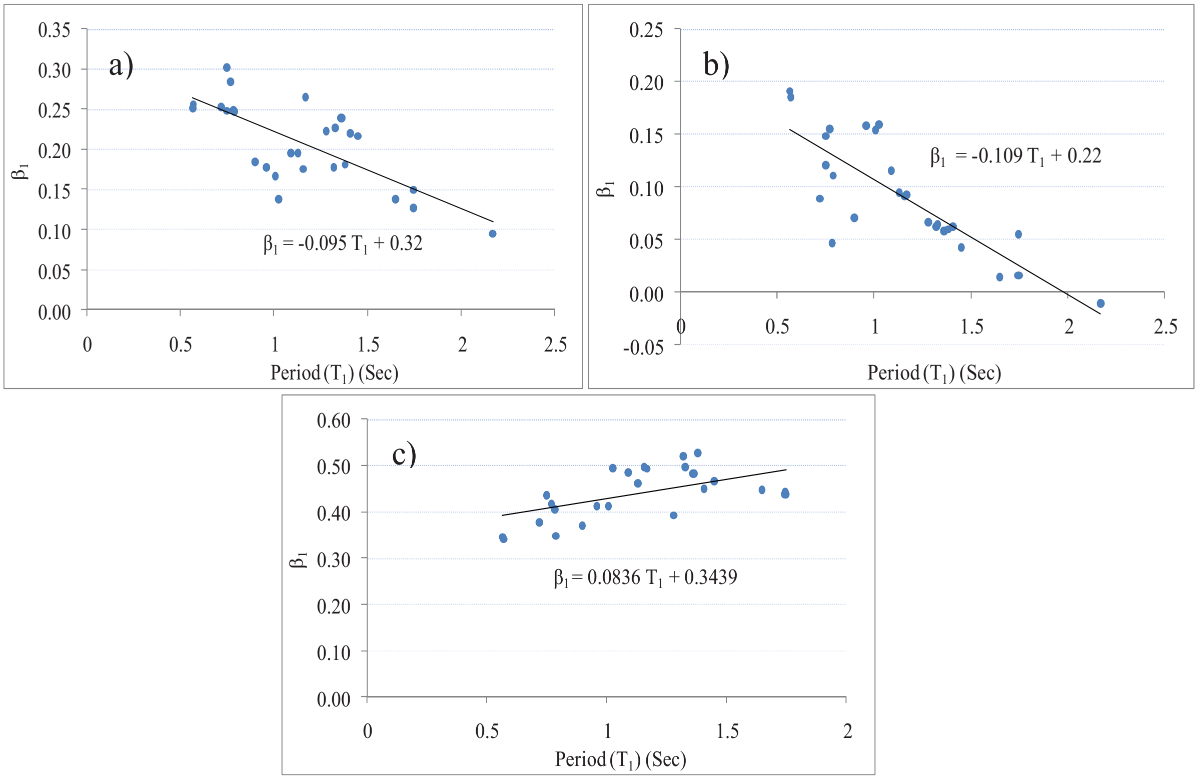

Fig. 6.5. Regression analysis for $\beta_1$and period (T_1) considering all records with removed outliers (i.e., subset 3) for a) crustal records, b) interface records and c) inslab records

As can be seen from Fig. 6.5(a) and (b), an increase in the period of a bridge results in a decrease in the β_1 factor. Each point in these figures represents the IDA results obtained for a specific bridge configuration subjected to 78 records. For the inslab events the $\beta_1$factors increased by increasing the period of the structure (see Fig. 6.5 (c)).

6.13 Effect of number of records (44 records vs 78 records)

For each earthquake type 78 records were used to perform the IDA and to compute the collapse capacities of the bridges. A comparison was made of the results obtained using 78 and 44 records for the bridge configurations designed using R=5 and I=1.5. Only the results computed using subset 3 (all records with outliers removed) will be studied here to facilitate the comparisons.

The results indicate that the differences in the unmodified collapse capacities are around 5% on average (except for inslab records which are not critical). A similar trend was observed in the modified collapse capacities and CMR/ $CMR_{acceptable}$ ratios. The modified median collapse capacities are given in Table 6.13.

Table 6.13. Comparison of the modified median collapse capacities obtained using 44 records and 78 records (in the parentheses) for different earthquake types and combined earthquake types

Modified median collapse capacity (g) using 44 records & (78 records)	*Crustal records*	*Interface records*	*Inslab records*	*Combined*
Configuration1 (D=1.5 m)	1.56 (1.61)	0.98 (1.05)	4.35 (4.44)	1.74 (1.64)
Configuration1 (D=2.0 m)	2.09 (2.12)	1.93 (1.83)	5.90 (6.33)	2.54 (2.51)
Configuration1 (D=2.5 m)	2.89 (2.77)	2.44 (2.85)	7.23 (7.13)	3.33 (3.40)
Configuration2 (D=1.5 m)	1.45 (1.35)	0.86 (0.89)	3.04 (3.52)	1.22 (1.20)
Configuration2 (D=2.0 m)	1.63 (1.71)	1.19 (1.21)	5.90 (4.99)	1.66 (1.61)
Configuration2 (D=2.5 m)	2.26 (2.29)	1.23 (1.38)	7.85 (6.54)	2.39 (2.41)
Configuration 3 (D=1.5 m)	1.04 (1.04)	0.70 (0.74)	4.23 (3.24)	1.07 (1.11)
Configuration 3 (D=2.0 m)	1.61 (1.45)	0.73 (0.98)	4.63 (4.40)	1.49 (1.49)
Configuration 3 (D=2.5 m)	1.62 (1.91)	1.14 (1.17)	4.65 (4.78)	1.83 (1.94)
Configuration 4 (D=1.5 m)	1.76 (1.50)	0.87 (1.02)	4.55 (4.67)	1.71 (1.68)
Configuration 4 (D=2.0 m)	2.03 (2.08)	1.38 (1.51)	4.42 (3.91)	2.26 (2.21)
Configuration 4 (D=2.5 m)	2.77 (2.65)	2.35 (2.32)	5.51 (5.14)	3.25 (3.09)
Configuration 5 (D=1.5 m)	1.34 (1.23)	0.61 (0.78)	2.30 (2.27)	1.23 (1.23)
Configuration 5 (D=2.0 m)	1.72 (1.76)	1.28 (1.19)	2.62 (2.84)	1.78 (1.74)
Configuration 5 (D=2.5 m)	2.28 (2.19)	1.81 (1.82)	4.17 (3.81)	2.67 (2.47)

The differences in the case of crustal records were in the range of 5%, while somewhat higher differences were observed in the case of subduction events. Nevertheless on average the differences were typically less than 15%. Results indicate that the interface and inslab events are more sensitive to the number of records used which is due to higher variability of responses due to such events.

6.14 Comparison of the bridge responses for different configurations

To investigate the influence of the regularity of the bridge structures on the overall seismic response and safety, the collapse margin rations were compared for the different bridges studied. The results obtained for the regular bridges and irregular bridges are compared (see Table 6.14). The results are based on subset 3 of the records. Because the inslab events were not critical only the results obtained from the crustal and interface events are presented.

Table 6.14**.** Modified and unmodified median collapse capacities and corresponding collapse margin ratios (CMR) and (CMR /CMRacceptable) using subset 3 of records. (D = 2 m, and R/I = 3.33)

		Median	CMR	Modified median	Modified CMR	β_{TOT}	$CMR_{acceptable}$	$CMR/CMR_{acceptable}$
Configuration 1 (D=2.0 m)	Crustal	1.71	3.53	2.12	4.37	0.61	2.18	2.00
	Interface	1.68	3.46	1.83	3.78	0.81	2.81	1.34
	Average	**1.69**	**3.49**	**1.98**	**4.07**	**0.71**	**2.50**	**1.67**
Configuration 2 (D=2.0 m)	Crustal	1.45	6.86	1.71	8.06	0.57	2.08	3.88
	Interface	1.20	5.66	1.21	5.73	0.75	2.60	2.21
	Average	**1.32**	**6.26**	**1.46**	**6.90**	**0.66**	**2.34**	**3.04**
Configuration 3 (D=2.0 m)	Crustal	1.21	4.34	1.45	5.19	0.60	2.15	2.41
	Interface	0.93	3.34	0.98	3.51	0.76	2.64	1.33
	Average	**1.07**	**3.84**	**1.21**	**4.35**	**0.68**	**2.40**	**1.87**
Configuration 4 (D=2.0 m)	Crustal	1.79	5.05	2.08	5.85	0.58	2.10	2.79
	Interface	1.33	3.75	1.51	4.25	0.86	3.01	1.41
	Average	**1.56**	**4.40**	**1.79**	**5.05**	**0.72**	**2.55**	**2.10**
Configuration 5 (D=2.0 m)	Crustal	1.52	3.88	1.76	4.49	0.57	2.08	2.16
	Interface	1.12	2.85	1.19	3.02	0.79	2.74	1.10
	Average	**1.32**	**3.37**	**1.47**	**3.76**	**0.68**	**2.41**	**1.63**

As can be seen in the table the modified collapse margin ratio is 3.76 for configuration 5, which is the most irregular bridge. This predicted value is smaller than those for the other configurations. Regular configurations 2 and 4 have average modified collapse margins of 6.9 and 5.05 respectively which are the largest CMR values obtained. For configuration 3, which represents a bridge ramp, the average CMR is 4.35 which is lower than those obtained for the regular configurations. It is noted that regular configuration 1 with stiff columns has relatively low collapse margin ratios. This is due to the increased demand in the middle column. This illustrates that in addition to the relative stiffness ratio of the columns along the bridge that the deflected shape is also important and should be addressed in the design of bridge structures. Hence the columns at the locations of maximum expected displacement demands (i.e., center of bridge for bridges with restrained abutment conditions and near the ends for bridges with free movements at the abutments) could result in lower safety margins. It should be noted however that for configuration 1, the design reinforcement ratio is around 1.17% in the central column, while for configuration 5 this ratio is around 2.2%. This resulted in the nominal moment strength of the central column in configuration 5 being about 50% greater than that of the column in configuration 1. However, due to the influence of irregularity on the seismic response, the collapse margin ratios are smaller for configuration 5.

Table 6.15. Modified and unmodified median collapse capacities and corresponding CMR and CMR /CMRacceptable using subset 3 of records. (D = 2.5 m, and R/I = 5)

		Median	CMR	Modified median	Modified CMR	β_{TOT}	$CMR_{acceptable}$	$CMR/CMR_{acceptable}$
Configuration 1 (D=2.5 m)	Crustal	2.42	4.06	2.83	4.74	0.59	2.13	2.22
	Interface	2.52	4.22	2.83	4.74	0.79	2.76	1.72
	Average	**2.47**	**4.14**	**2.83**	**4.74**	**0.69**	**2.45**	**1.97**
Configuration 2 (D=2.5 m)	Crustal	1.80	6.60	2.29	8.41	0.63	2.24	3.75
	Interface	1.32	4.85	1.38	5.08	0.78	2.71	1.87
	Average	**1.56**	**5.72**	**1.84**	**6.74**	**0.70**	**2.48**	**2.81**
Configuration 3 (D=2.5 m)	Crustal	1.38	4.53	1.62	5.33	0.60	2.17	2.46
	Interface	0.98	3.22	1.05	3.46	0.78	2.71	1.28
	Average	**1.18**	**3.87**	**1.34**	**4.40**	**0.69**	**2.44**	**1.87**
Configuration 4 (D=2.5 m)	Crustal	2.05	4.33	2.52	5.33	0.63	2.26	2.36
	Interface	1.88	3.98	2.12	4.48	0.82	2.88	1.56
	Average	**1.96**	**4.16**	**2.32**	**4.91**	**0.73**	**2.57**	**1.96**
Configuration 5 (D=2.5 m)	Crustal	1.51	3.29	1.81	3.94	0.59	2.14	1.84
	Interface	1.31	2.85	1.44	3.12	0.78	2.72	1.15
	Average	**1.41**	**3.07**	**1.62**	**3.53**	**0.69**	**2.43**	**1.49**

The results obtained for the case of different bridge configurations with D=2.5 and R/I=5 are shown in Table 6.15. The results in this case are interesting, since the minimum reinforcement requirements were controlling for most of the configurations so that the bridge columns had almost similar strengths. A comparison between the CMR values obtained for the regular and irregular bridges in this case can better present the effects of irregularity on the seismic behaviour of the bridges. For example, the CMR values obtained for the highly irregular bridge (i.e., configuration 5) is significantly lower than those obtained for the regular configurations 2, 4 and 1 which highlights the significance of regularity on the seismic response.

6.15 Comparing design using R/I=3.33 and R/I=5

The bridge structures were designed using two different R/I values of 3.33 and 5. While higher R/I values give lower seismic demands, for R/I=5 the minimum reinforcement limit of 0.8% was controlling in most cases and this resulted in strengths somewhat above the demand strength. In addition, the use of a higher R/I value in design will result in a more flexible bridge with lower seismic demands. As can be seen in Table 6.16, the use of R/I of 5 in design did not significantly reduce the predicted collapse margin ratios.

Table 6.16. Modified median collapse capacities and corresponding collapse margin ratios (CMR) using subset 3 of records for R/I=3.33 and R/I=5. (D = 2.0 m)

		R/I = 3.33			R/I = 5		
		Modified median	Modified CMR	$CMR/CMR_{acceptable}$	Modified median	Modified CMR	$CMR/CMR_{acceptable}$
Configuration 1 (D=2.0 m)	Crustal	2.12	4.37	2.00	1.97	4.23	1.95
	Interface	1.83	3.78	1.34	1.53	3.28	1.22
	Average	**1.98**	**4.07**	**1.67**	**1.75**	**3.75**	**1.58**
Configuration 2 (D=2.0 m)	Crustal	1.71	8.06	3.88	1.71	8.06	3.88
	Interface	1.21	5.73	2.21	1.21	5.73	2.21
	Average	**1.46**	**6.90**	**3.04**	**1.46**	**6.90**	**3.04**
Configuration 3 (D=2.0 m)	Crustal	1.45	5.19	2.41	1.26	4.67	2.21
	Interface	0.98	3.51	1.33	0.80	2.96	1.13
	Average	**1.21**	**4.35**	**1.87**	**1.03**	**3.81**	**1.67**
Configuration 4 (D=2.0 m)	Crustal	2.08	5.85	2.79	1.79	5.51	2.66
	Interface	1.51	4.25	1.41	1.33	4.10	1.37
	Average	**1.79**	**5.05**	**2.10**	**1.56**	**4.81**	**2.01**
Configuration 5 (D=2.0 m)	Crustal	1.76	4.49	2.16	1.31	3.99	1.94
	Interface	1.19	3.02	1.10	0.97	2.94	1.00
	Average	**1.47**	**3.76**	**1.63**	**1.14**	**3.47**	**1.47**

Table 6.16 compares the results for bridges designed with R/I values of 3.33 and 5. The results obtained for bridges with D=2.0 m is presented, while similar results observed for other cases. For configuration 2, because the minimum reinforcement requirement controlled the design for all of the columns for both cases of R/I equal to 3.33 and 5, the predicted results are similar. Based on the results obtained for all cases, a reduction of about 10 % to 15% in the collapse margin ratios was typically observed for the case of R/I= 5.

6.16 Conclusions

The seismic responses of bridges with 5 different configurations and having different column stiffnesses were studied using Incremental Dynamic Analysis (IDA). The influence of different earthquake types on the response was considered by using three different sets of records in IDA representing three different earthquake types. The conclusions from this study of bridges located in Vancouver are summarized below:

(1) The median collapse capacities where typically lower for the bridges when the subduction interface records were used in the IDA. This is likely due to different frequency contents and much longer duration of the interface events compared to the crustal events. It was found that the inslab events were not critical and resulted in higher median collapse capacities and collapse margin predictions. This may be due to the relatively long period of the 4-span bridge structures, while inslab events are usually more critical for structures with shorter periods.

(2) When the records were combined in proportional to the percentage of contribution of each of the three event types, it resulted in the average median collapse capacities being similar to those determined using the crustal records only. However the variability of the collapse capacity predictions was higher when the three different event types were considered. This may indicate that the crustal records could be used along with a modified record-to-record variability to include the effects of different event types in

seismic performance assessments. However, more research is however required to verify this.

(3) The use of the simplified method to account for the effects of spectral shapes typically resulted in predictions that were in good agreement with those obtained using the more complex epsilon-based record selection method which directly accounts for the spectral shapes.

(4) Considering only the records with lower scale factors at collapse reduced the variability in the collapse capacity predictions. The median collapse capacities obtained considering the lower scaling factors were generally lower than those obtained using higher scaling factors, particularly for interface and inslab events. Care must be taken to make sure that the results obtained are not biased due to the application of large scaling factors.

(5) The values of β_1 and SSF factors were computed using different subsets of records and for different earthquake types and simplified equations were derived to predict the β_1 values. It was found that although the predicted values of β_1 and SSF factors using different subsets of records were different, the application of these factors to the unmodified median collapse capacity of the corresponding subsets resulted in relatively similar modified median collapse capacities.

(6) The results from IDA for the different bridge configurations indicate that for irregular bridges the collapse margin ratios were lower than for regular bridges and the effects of irregularity were more pronounced as the force modification factor, R, increased.

Acknowledgements

The financial support provided by the Natural Sciences and Engineering Research Council of Canada for the Canadian Seismic Research Network is gratefully acknowledged. Ground motion data for Japanese earthquakes were obtained from the K-NET and KiK-NET databases at www.k-net.bosai.go.jp and www.kik.bosai.go.jp and other crustal ground motion data obtained from the PEER-NGA database available at http://peer.berkeley.edu. The Nisqually earthquake records were obtained through COSMOS virtual data center available at http://db.cosmos-eq.org. Data on Japanese earthquake records was provided by Katsuichiro Goda.

References

Please see the last section.

7 Conclusions

7.1 Summary and main conclusions

The conclusions from each manuscript were stated at the end of the chapters. The main conclusions from this thesis, based on studies of four-span reinforced concrete bridges located in Vancouver, are summarized as follows:

7.1.1 Conclusions regarding seismic response and evaluation of bridges with column stiffness irregularities

- The force-based design procedures of the 2006 CHBDC gives conservative designs due to the combined use of low R factors and the use of importance factors, even for irregular bridges.

- In the transverse direction, contrary to that in the longitudinal direction, the seismic behaviour is also affected by the position of columns along the length of the bridge and the superstructure stiffness properties. Such parameters are not currently considered in the definition of irregularity in the seismic codes.

- It was shown that exceeding a maximum column stiffness ratio of about 5 to 8 can cause significant concentration of ductility demand as well as deviation of the predicted non-linear response from the predicted elastic response.

- A superstructure to substructure stiffness ratio, RS, of less than 0.3 in the case of restrained movements at the abutments, and 0.8 in the case of free movements at the abutments may result in incorrect response predictions using elastic multi-mode analysis. Bridges with RS ratios greater than 1.0 typically had more uniform ductility demands in the columns, while bridges with RS values less than 1.0 may exhibit concentrations of seismic ductility demand in a few elements.

- While the column stiffness ratios and the superstructure to substructure stiffness ratios provide simple, practical means of identifying regularity, the DRMS index can also be used to choose an appropriate method of analysis. For bridges with restrained abutment conditions and with DRMS index values of less than 0.08 the results from the elastic and inelastic analyses were in good agreement.

- Based on the results obtained, for some irregular bridge configurations, the displacement envelopes were significantly different from the elastic and inelastic analysis; however due to high conservatism in the current CHBDC this did not lead to an unsafe design at least for the cases considered in this study. This problem may be more important if less conservative design approaches are used and when higher earthquake levels are considered.

- The seismic response and the maximum ductility demands in the longitudinal direction are controlled by the total stiffness of the substructure, the stiffness ratio of the columns, and the minimum aspect ratio of the columns. Seismic ductility demands in the longitudinal direction were correlated with the product of the total stiffness of the columns and the maximum stiffness ratio of the columns. This indicates that the ductility demands in bridge columns increase as the structural stiffness and stiffness irregularity increases.

- Analyses in the longitudinal direction of bridges demonstrated that the concentration of ductility demands increases significantly with an increase in the column stiffness ratio, K_{max}/K_{min}. An equation was developed to provide a means of estimating the ratio of the maximum to minimum ductility demands. This equation is useful for designers in determining the influence of the column stiffness irregularity on the concentration of the ductility demands.

- The influence of the abutments on the longitudinal seismic responses of bridges was studied. Up to an 80% decrease in seismic ductility demands were observed when the abutments were considered in the structural models. The reduction of ductility demand correlates with the ratio of the total stiffness of the columns and the effective stiffness of the abutments. The influence of the abutments was more pronounced for the bridges with more flexible columns and stiffer abutments.

- A dimensionless parameter was defined as $(\Delta D) / H^2$ (i.e., drift ratio divided by column aspect ratio) which provided an improved indicator of the structural damage compared to the conventional drift ratio (i.e., Δ / H). It was also demonstrated that normalizing the maximum ductility demands by the minimum aspect ratio of the columns significantly reduced the dispersions in the results.

- The seismic ductility demands to ductility capacity ratios were estimated for the combination of the seismic responses in the longitudinal and transverse directions. It was observed that the demand to capacity ratios were lower than 0.7 with the majority of the cases having values less than 0.5. These ratios decreased, when the influence of the abutments were considered in the seismic response. The range of demand to capacity ratios was quite high which indicate uneven safety margins for different bridges. Exceeding the maximum stiffness ratio of about 5.0 to 8.0 resulted in much larger demand to capacity ratios.

- CSA S6-06 requires elastic dynamic analysis for an emergency-route bridge in seismic performance zones 2 and higher if the bridge is irregular. This study indicates that elastic dynamic analysis is appropriate for irregular bridges in the longitudinal direction. However, nonlinear dynamic analysis would be required for such irregular bridges in the transverse direction in order to accurately predict the displacement envelope and the ductility demands.

7.1.2 Conclusions regarding the use of incremental dynamic analysis (IDA) for seismic analysis and evaluation of bridges

- The use of the UHS-based method resulted in very conservative predictions of collapse capacities which were significantly lower than those predicted using the epsilon-based method. The use of the CMS- or UHS-based methods generally underestimated the record-to-record variability compared to the epsilon-based record selection method.
- It was demonstrated that the IDA results can be sensitive to the choice of the record selection method. The epsilon-based method in all of the cases resulted in the highest prediction for the capacity of the structure. However more research is required to verify the reliability of this method for seismic evaluations, as it was found that the results can be sensitive to the number of records used. Furthermore, different sets of records with comparable mean epsilon values could result in somewhat different collapse capacity predictions. Increasing the number of records used in the IDA did not influence the results obtained using the CMS-based record selection methods. The use of different GMPEs for record selection did not significantly affect the results in IDA. The influence of the record selection methods was greater on the collapse capacity prediction than on the other damage states such as yielding and spalling.

- The CMS and the mean epsilon values were predicted using the matching method in seismic deaggregation. The use of the exceeding method for seismic deaggregation tended to overestimate the mean epsilon values and thus the collapse capacity of the structure.

- The median collapse capacities where typically lower for the bridges when the subduction interface records were used in the IDA. This is likely due to different frequency contents and much longer duration of the interface events compared to the crustal events. It was found that the inslab events were not critical and resulted in higher median collapse capacities and collapse margin predictions. This may be due to the relatively long period of the 4-span bridge structures, while inslab events are usually more critical for structures with shorter periods.

- When the records were combined in proportional to the percentage of contribution of each of the three event types, it resulted in the average median collapse capacities being similar to those determined using the crustal records only. It was also demonstrated that the average conditional mean spectrum for all earthquake types (i.e., CMS-All) was close to the CMS-Crustal and thus combining the effects of different seismic event types led to similar results as considering crustal events alone. However the variability of the collapse capacity predictions was higher when the three different event types were considered. This may indicate that the crustal records could be used along with a modified record-to-record variability to include the effects of different event types in the seismic performance assessments. More research is however required to verify this.
  The increased record-to-record variability due to considering different earthquake types has at least two outcomes: first, the IDA needs to be carried out using a larger number of records for a more precise prediction of the collapse capacity of the structure and second, the increased variability will increase the probability of collapse at the MCE level.

- The use of the simplified method to account for the effects of spectral shapes typically resulted in predictions that were in good agreement with those obtained using the more complex epsilon-based record selection method which directly accounts for the spectral shapes. The values of β_1 and spectral shape factors (SSF) were computed using different subsets of records and for different earthquake types and simplified equations were derived to predict the β_1 values. It was found that although the predicted values of β_1 and SSF factors using different subsets of records were different, the application of these factors to the unmodified median collapse capacity of the corresponding subsets resulted in similar modified median collapse capacities.

- The results from IDA for different bridge configurations indicate that for irregular bridges the collapse margin ratios were lower than for regular bridges and the effects of irregularity were more pronounced as the force modification factor, R, increased.

7.2 Future research

- This research focused on the irregularity of bridges due to different stiffnesses of columns. Similar studies can be conducted to study the influence of different span lengths, skewness and curvature of bridges accompanied with the irregular distribution of column stiffnesses.
- The behaviour of irregular bridges with different column stiffnesses in the near-field regions subjected to high velocity pulses needs to be studied.
- The analyses presented in Chapters 3 and 4 can be carried out using natural records matched to the conditional mean spectrum (CMS), rather than the UHS, for a more precise evaluation of the seismic performance of bridges.
- The seismic behaviour of irregular bridges was studied accounting for the maximum considered earthquake level (i.e., 2% probability of exceedance in 50 years). More studies can be carried out to study the seismic response of irregular bridges at different hazard levels such as that corresponding to a serviceability limit state.
- The effects of bidirectional excitation of ground motions could be studied directly by applying the pairs of ground motions simultaneously.
- A similar study needs to be carried out for case of older existing bridges with poor detailing. The effects of column stiffness irregularity are even more important for older bridges. This is because due to poor detailing, the concentration of ductility demands in the shortest column will result in degradation of the shear strength of the columns. On the other hand high shear forces are attracted in the shortest columns due to larger stiffness of columns. This may lead to brittle shear failure and catastrophic collapse of older bridges.

- In this study only columns with aspect ratios larger than 2.5 were considered (i.e., flexure dominant columns). Some studies could be carried out for columns with lower aspect ratios. The response of such columns is controlled by shear and more detailed nonlinear shear models should be incorporated in structural modelling. The shear-flexure interactions (especially in the case of older bridges) can also be studied.
- More research is needed on the applications of other methods of analysis including the single-mode-pushover, modal pushover analysis (as used in Appendix A) and adaptive pushover analyses in prediction of the seismic response of irregular bridges. Appropriate criteria for application of such analyses methods to irregular bridges are required.
- The use of direct displacement-based design approach (as discussed in Chapter 1) for the design of a wide range of irregular bridges can be studied and the results be compared with those obtained in this study using the force-based design approach. It is expected that the seismic performance of irregular bridges will be improved, when displacement-based design concepts are used.

7.3 Statement of original contributions

The original contributions in this thesis include:

- The seismic behaviour and safety margin of bridges with different stiffness ratio and with different modelling and design properties for a wide range of bridges with different column and superstructure stiffnesses was studied. Important aspects which influence the seismic behaviour of bridges were investigated and recommendations were made on suitable ranges of these parameters to improve the seismic performance of bridges.

- The results of elastic versus inelastic analysis were compared for bridges with different configurations and different parameters. The use of different regularity indices, proposed in the past, to predict the response of bridges were also evaluated and compared for a wide range of bridges. Recommendations were made for the improvement of the current CHBDC provisions to address the effects of irregularity in seismic analysis and design of bridges.

- The use of different record selection methodologies for the seismic performance evaluation of bridges using incremental dynamic analysis was studied. In addition, the effects of including the records from three different earthquake sources including subduction interface events, inslab events and crustal events, were investigated.

- The effects of epsilon and spectral shapes on the seismic performance assessment of bridges were studied for different damage states and for different earthquake types. The use of the Conditional Mean Spectrum (CMS) on the seismic evaluation of bridges was studied and the results were compared with the case of the conventional UHS-based method. The use of CMS for different event types and the average CMS for all event types in the seismic evaluation of bridges was also studied. The use of different ground motion prediction equations on the seismic performance assessment of bridges using conditional mean spectrum (CMS) was also investigated

- A large set of ground motion records for subduction earthquakes (i.e., interface and inslab) and crustal earthquakes were used for the seismic evaluation of different bridge configurations and the effects of using different subsets of records with specific properties in the seismic performance assessments were also studied. The use of three different earthquake types based on the seismic deaggregation results in seismic evaluation of different bridge configurations were studied and the results were compared with the case that only crustal events are considered (i.e., current design practice). Recommendations were made to include the effects of different event types in the seismic assessment of bridges.

- The ATC-63 (ATC, 2008) methodology was applied to bridge structures. The evaluation of damage states using different theoretical and experimental approaches were carried out and a backbone curve for the evaluation of the bridges using the IDA approach was defined.

- A comprehensive program was developed, as discussed in Appendix B, which is capable of design, modelling and evaluating the bridges for large parametric studies using a large number of ground motion records and by means of different methods of analysis. A large pool of ground motions (both artificial and natural records) were incorporated in the program. Furthermore, other programs were also developed as discussed in Appendices C to E for record selections using different methods, computing the CMS and the epsilon values and extracting the seismic deaggregation results.

Appendix A: Verification of the models, preliminary studies and other modelling details

The modelling details for bridges studied in this research are discussed in Chapters 3 and 5. This appendix provides further details concerning the modelling and verification of the results. In addition, some preliminary results obtained regarding the seismic response of irregular bridges with different column heights are presented.

A.1. Verifications of computer models

The lumped plasticity models, as discussed in Chapter 3, have been widely used in research and practice to predict the seismic response of structures. The application of these models along with appropriate hysteresis loop models can successfully predict the maximum displacement obtained during the seismic excitations which are in good agreement with the experimental results (e.g., Saiidi and Sozen, 1979; Otani, 1981; Calvi et al. 1994; Fischinger and Isacovic, 2003; Priestley et al., 1996 and 2007 and ATC-62, 2008). The recommendations by Priestley et al. (1996 and 2007) were used in this research for the prediction of the modelling parameters including plastic hinge lengths, strain penetration length, moment curvature idealization, etc.

Although the use of such models for prediction of the seismic response of structures are widely verified and used and are recommended by many seismic design codes (e.g., Caltrans (2006) and AASHTO Guidelines (2009)) for analysis and design of structures, an attempt is also made in this study to compare the numerical results with those obtained from experiments.

a) Cyclic tests of columns

The modified Takeda hysteresis model (Otani, 1981) was used in this study to model the behaviour of the RC columns using Ruaumoko software (Carr, 2009).This model has two main parameters, α and β, which control the unloading and the reloading stiffness, respectively. The parameter α is usually in the range of 0 to 0.5 and β varies between 0 and 0.6. Increasing the parameter α decreases the unloading stiffness and increasing the β parameter increases the reloading stiffness. Some researchers computed the mean values of α and β based on experiments, as 0.26 (Stdev=0.13) and 0.49 (Stdev=0.15), respectively (Mechakhchekh, 2008). Priestley et al. (2007) recommend using α=0.3 and β=0.6 for the case of well-detailed beams with no axial force (i.e., “Fat Takeda”). For the building and bridge columns the values of α =0.5 and β =0 is recommended (i.e., “Thin Takeda”).

Some reinforced concrete columns were tested by Benzoni and Priestley (1996). The experimental data from that study is available in the PEER structural database (Berry et al., 2004). The lumped plasticity models along with the modified Takdea hysteresis loop (Otani, 1981) were used to compare the experimental and numerical results. As shown in Fig. A.1a, the use of α=0.5 conservatively underestimate the unloading stiffness while the use of α=0.3, as shown in Fig. A.1b, can predict the unloading stiffness very well. It should be noted that the column tested by Benzoni and Priestley (1996) had a small percentage of longitudinal reinforcement (i.e., 0.5%) and small axial load ratio (i.e., 6%). This resulted in high pinching effects in the hysteresis behaviour. The effects of pinching on the overall response of structures with medium to long period ranges (e.g., the range of period of the bridges studied in this research) have been shown to be minimal (e.g., ATC-62, 2008). Where the effects of pinching are controlling, the SINA hysteresis loop model (Saiidi and Sozen, 1971) may be used to include the pinching effects (e.g., see Fig. A.1.c).

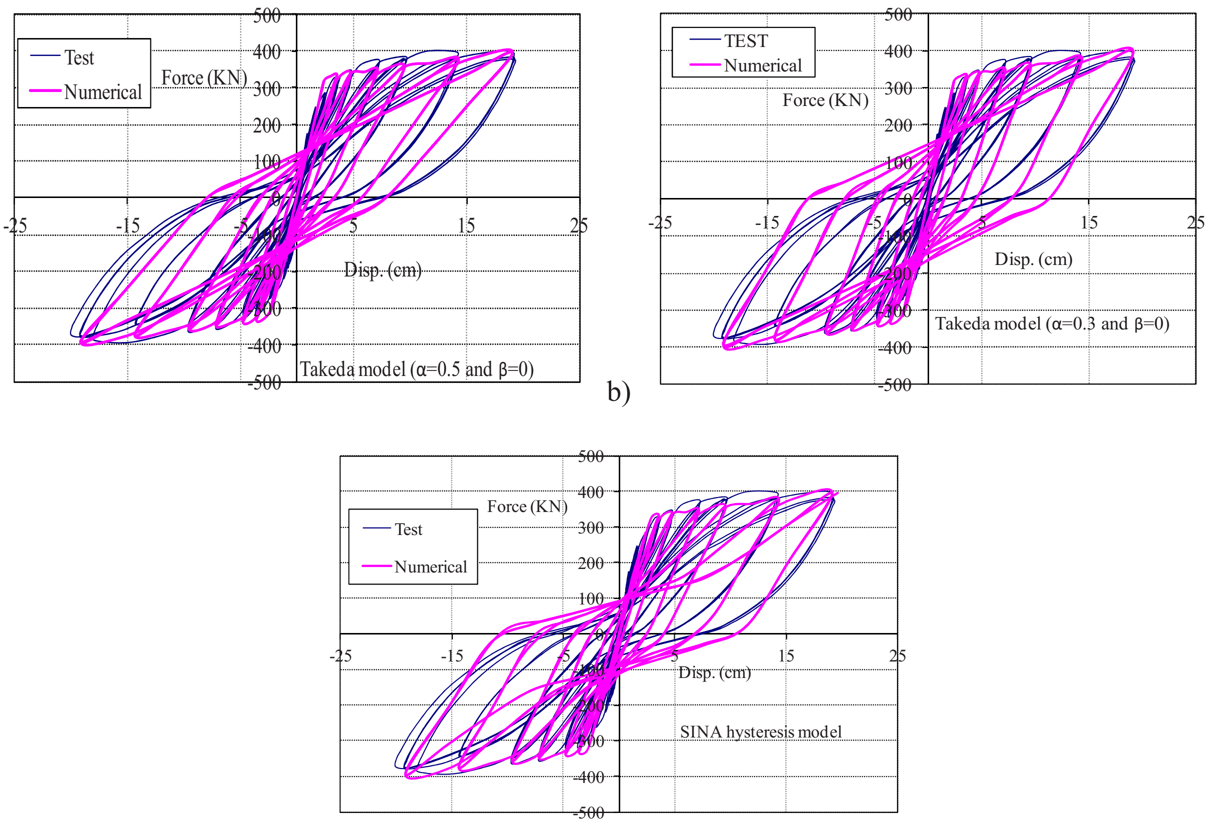

a) b) c)

Fig. A.1. The use of lumped plasticity model along with Takeda hysteresis model to predict the experimental results by Benzoni and Priestley (1996).

b) **Bridge tested in the European Laboratory for Structural Assessment (ELSA)**

In the framework of an integrated European programme of pre-normative research in support of Eurocode 8 (CEN, 2002), some bridge prototypes, representative of typical multi-span continuous deck motorway bridges, have been designed (Pinto et al., 1996) with different procedures for a PGA of 0.35g, in medium soil conditions (soil type B), applying the EC8 provisions. Corresponding large-scale (1:2.5) bridge models have then been constructed and tested in pseudo-dynamic fashion at the Joint Research Centre at Ispra (Italy) (Pinho, 2007).

The tested bridge model labelled as B213C in the experimental study by Pinto et al. (1996) will be considered to evaluate the predictions from the numerical models. The experimental data from this test was provided by the European Laboratory for Structural Assessment (ELSA). This bridge consists of three piers *5.6*, *2.8* and *8.4 m* high and a continuous deck with four identical *20 m* spans. The superstructure is restrained against the transverse movements at the ends, as shown in Fig. A.2, by means of the abutment shear keys. The deck-pier connections are assumed to be hinged (no transmission of moments). The piers have rectangular hollow sections with 160 mm wall thickness (Fig. A.2). The reinforcement layout of the pier models are shown in Fig. A.3. The cross sections of piers 1 and 3 in Fig. A.2, are shown in Fig. A.3 as section type 4 and the cross section of pier 2 is shown as section type 1. The mechanical characteristics of materials, pier and superstructure details and other required data are available by Pinho (2007) and Pinto et al. (1996).

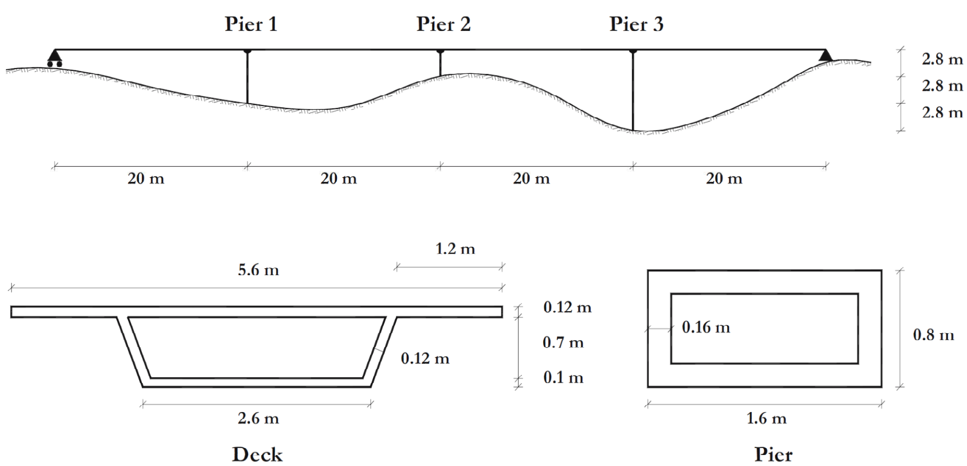

Fig. A.2. Bridge configuration and member cross sections of 1:2.5 scale model (from Pinho (2007))

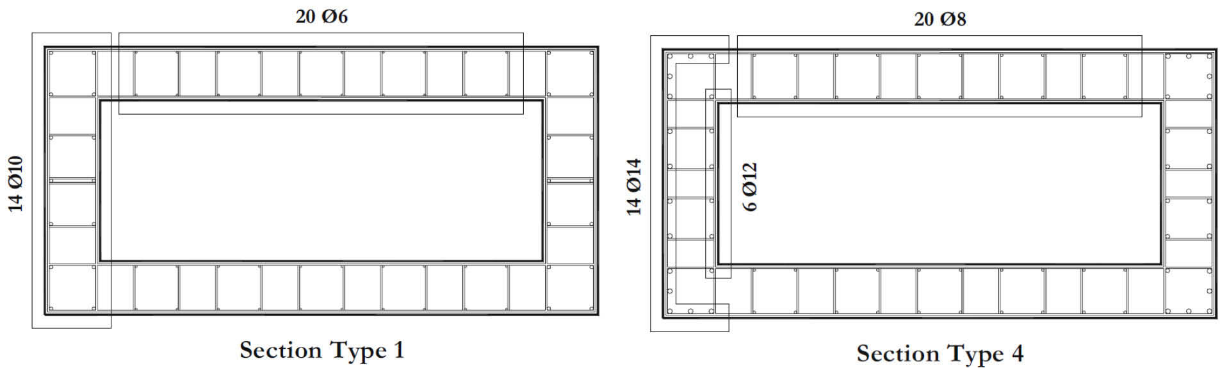

Fig. A.3. Reinforcement layout for columns (from Pinho (2007))

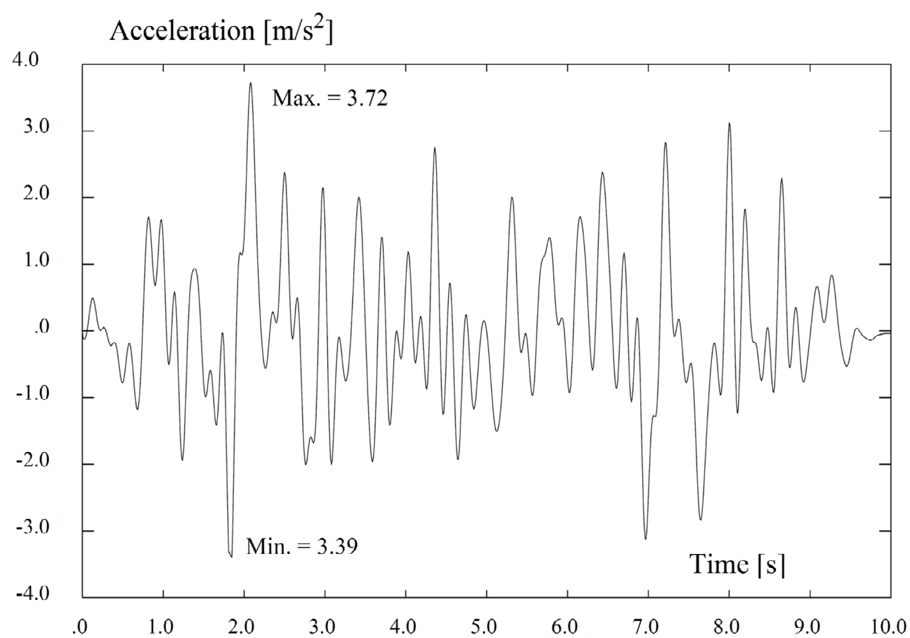

Fig. A.4. Acceleration history of the design earthquake (from Pinto et al. (1996))

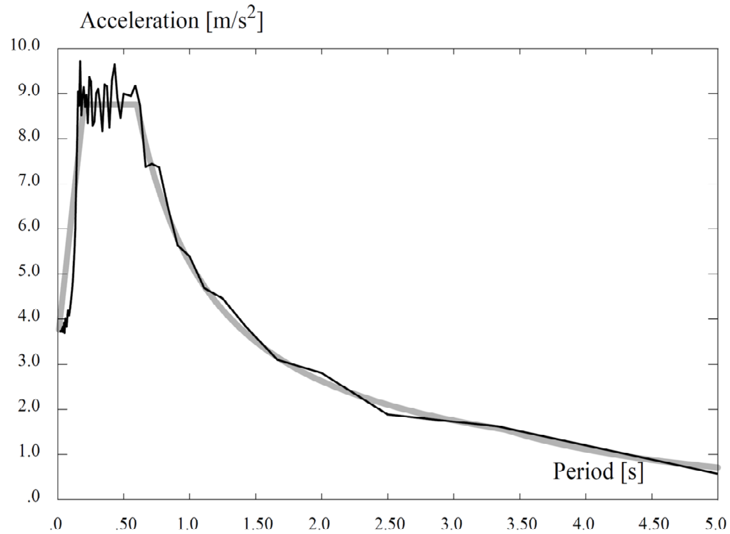

Fig. A.5. Design earthquake, corresponding response spectrum and EC8-Soil B spectrum (5% damping) (from Pinto et al. (1996))

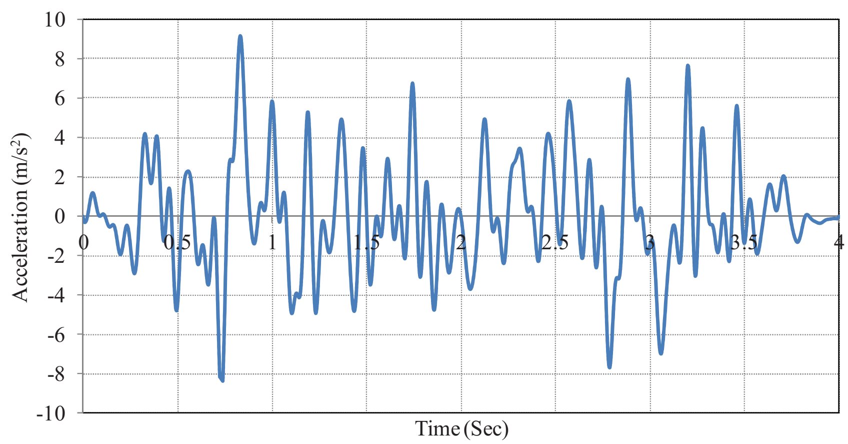

Fig. A.6. Acceleration history of the design earthquake applied to the (1:2.5) scale model

The details of the ground motion record used along with its response spectrum are shown in Fig. A.4 and Fig. A.5, respectively. The same record was used in this study to compare the numerical and experimental results. Fig. A.6 demonstrates the ground motion record which is applied to the bridge model. The application of the ground motion record in Fig. A.6 to the 1:2.5 scale model has the same effect as the application of the ground motion record in Fig. A.4 to the original bridge.

To further investigate the validity of the use of lumped plasticity models, an attempt is made to model this bridge in the RUAUMOKO program. First, the middle column was modelled and subjected to the reversed cyclic displacement pattern shown in Fig. A.7. The hysteresis loops from the numerical analysis are compared to those obtained from the test. As shown in Fig. A.8, the hysteresis loops can be predicted with reasonable approximation, when appropriate hysteresis parameters are adopted. The area of the hysteretic loops was computed to estimate the dissipated energy obtained from the test and the numerical results. The use of unloading stiffness parameter, α, of 0.0, 0.3, and 0.4 in the modified Takeda hysteresis model resulted in 0.91, 0.65, and 0.57 MN.m energy dissipation, respectively. The measured dissipated energy from the test was computed as 0.58 MN.m. This indicates that the use of α=0.4 is appropriate to estimate the total amount of energy dissipated through cyclic testing. Increasing the parameter α decreases the unloading stiffness and thus the area under the hysteresis loops.

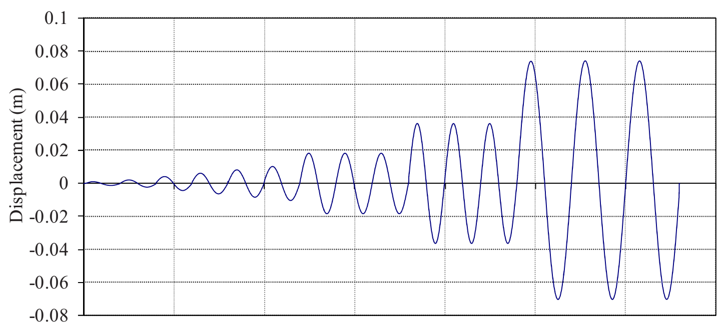

Fig. A.7. Displacement history used for reversed cyclic testing

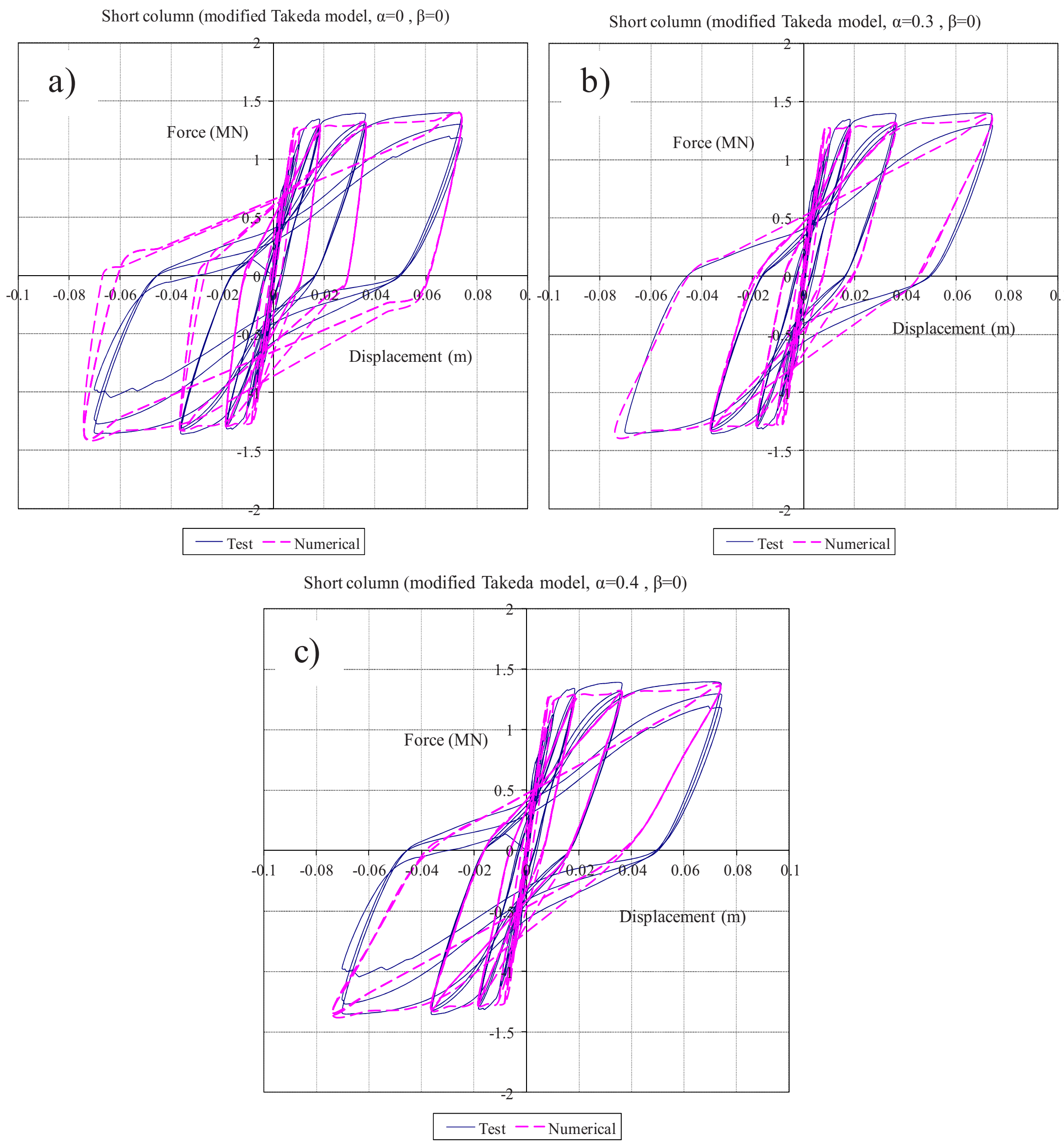

Fig. A.8. Comparison of the test results with the numerical predictions using the modified Takeda model with: a) α=0 and β=0; b) α=0.3 and β=0; c) α=0.4 and β=0

The bridge structure, shown in Fig. A.2, was modelled in the RUAUMOKO program. The detailed properties of the superstructure and substructure elements are described by Pinto et al. (1996) and Pinho (2007). The superstructure was modelled using elastic beam elements and the superstructure mass was lumped at the nodal points as shown in Fig. A.9. In addition, the mass of the columns were considered in the corresponding nodal points. Rigid elements were defined to model the superstructure depth. The heights of these elements were considered as half of the superstructure depth (see Fig. A.9). The columns were modelled using inelastic beam elements. The plastic hinge lengths and the strain penetration depths were computed using the equations given by Priestley et al. (2007) which are accepted for the bridges studied in this research. To consider the deformations due to bond slippage the strain penetration depth, L_{sp}, was considered in modelling the column heights as recommended by Priestley et al. (1996 and 2007). A Takeda hysteresis model with α=0.5 and β=0 (i.e., thin Takeda model) was used based on the recommendations by Priestley et al. (2007) for bridge columns.

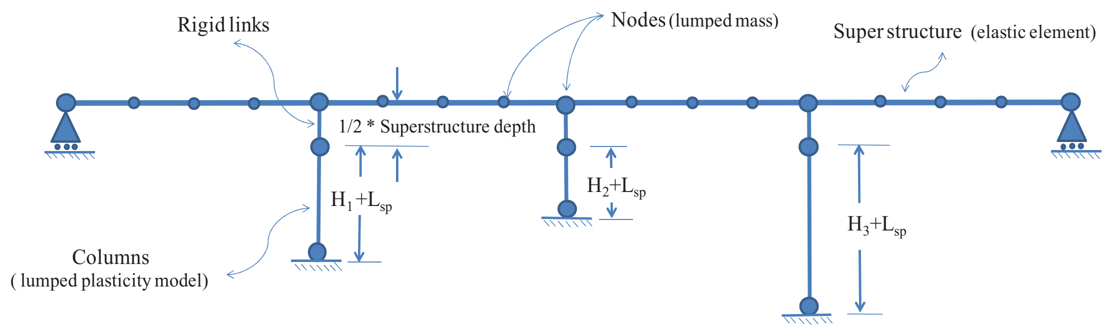

Fig. A.9. Schematic presentation of the structural modelling of the bridge in the RUAUMOKO program

The bridge was subjected to the design earthquake ground motion (as shown in Fig. A.6) and was also subjected to 1.2 times the design earthquake. The resulting displacements and shear forces of the columns are compared to those obtained in the tests as shown in Fig. A.10 to Fig. A.13. The results indicate that the computer models can predict the maximum displacements and shear forces reasonably well. The analytical models can be refined even more by incorporating the stiffness of the foundations of the columns and by refining the hysteresis parameters. Such refined models are out of the scope of this research. The recommendations made by Priestley et al. (2007) for modelling bridge structures provided sufficient accuracy in predicting the maximum displacement demands. Therefore these modelling assumptions were adopted for the seismic analysis and evaluation of the bridges in this research.

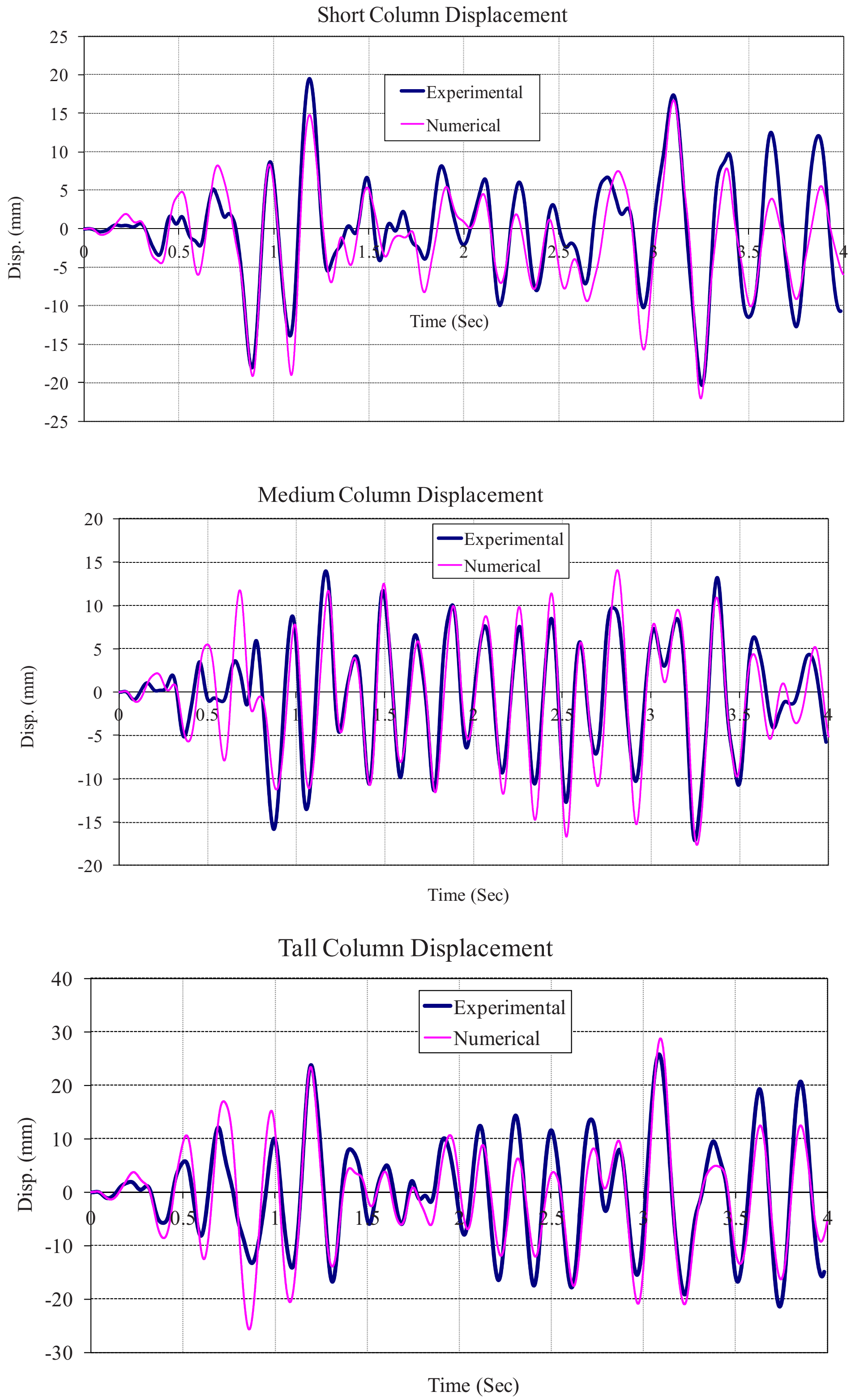

Fig. A.10. Comparison of the column displacements obtained using experimental data and numerical analysis for the design earthquake

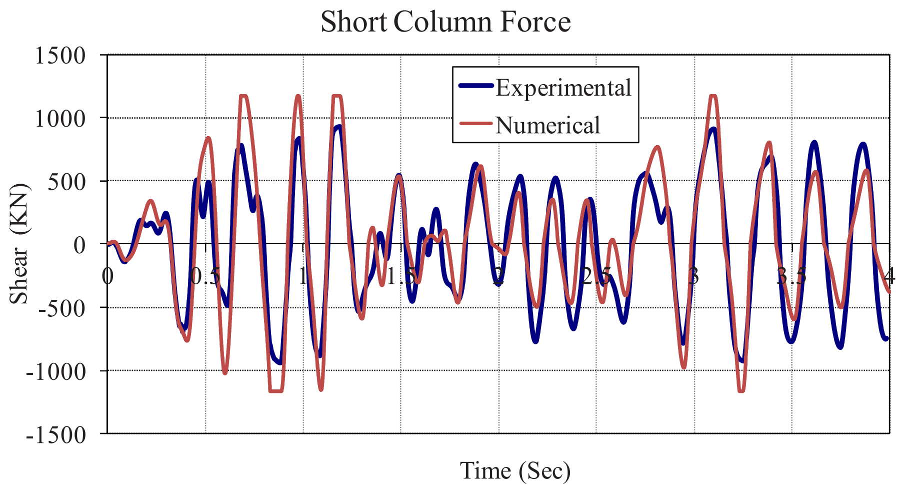

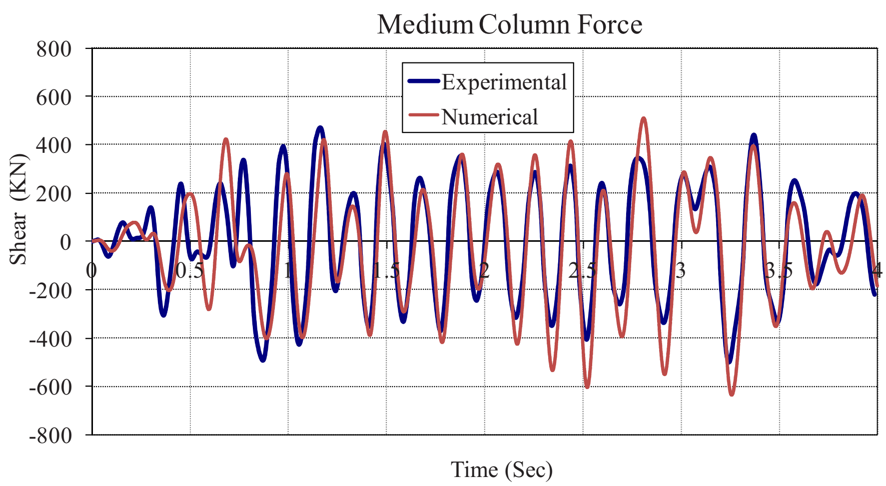

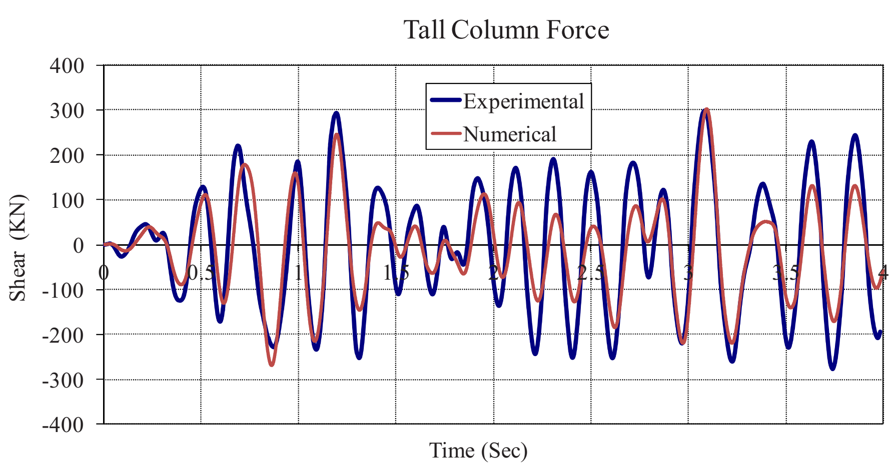

Fig. A.11. Comparison of the column shear forces obtained using experimental data and numerical analysis for the design earthquake

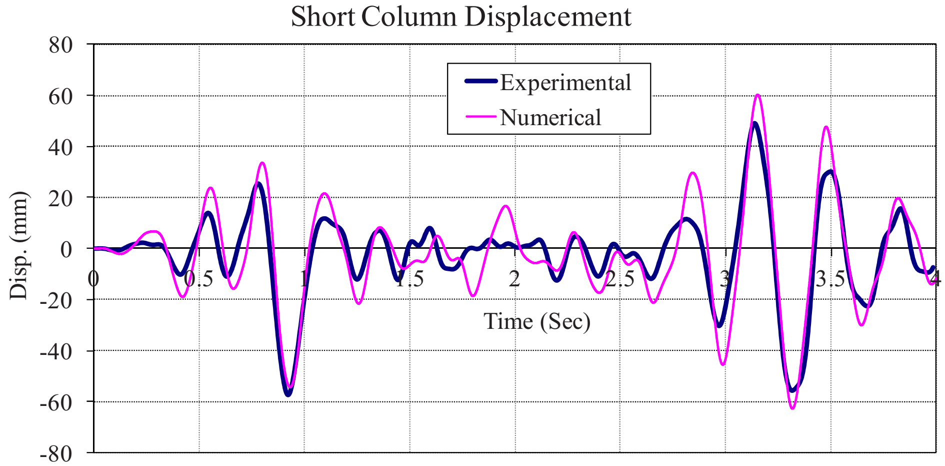

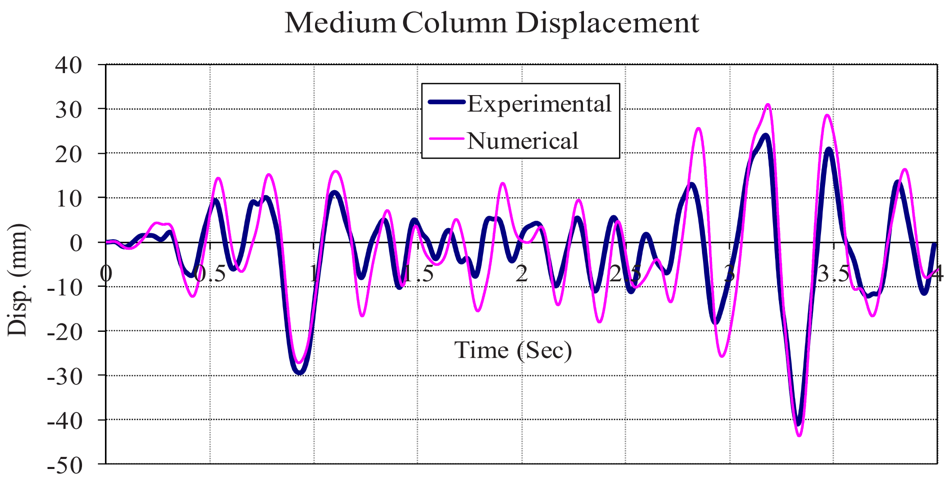

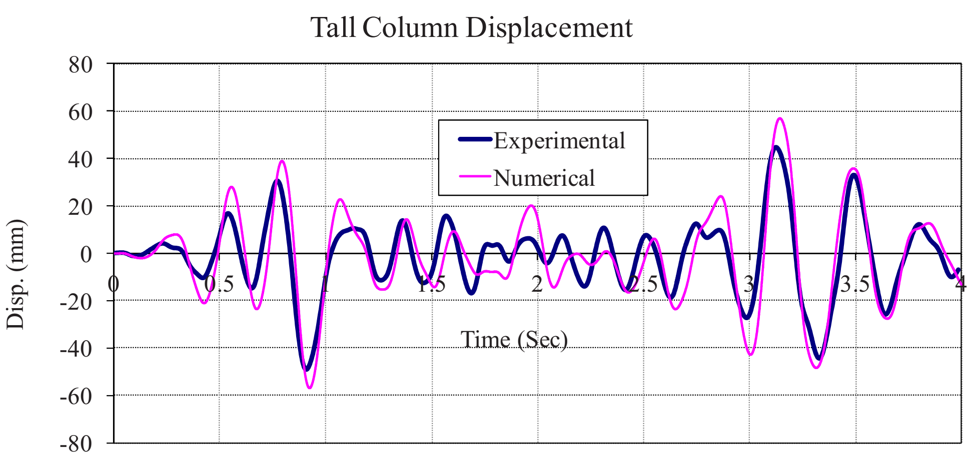

Fig. A.12. Comparison of the column displacements obtained using experimental data and numerical analysis for maximum earthquake (i.e., 1.2 * design earthquake)

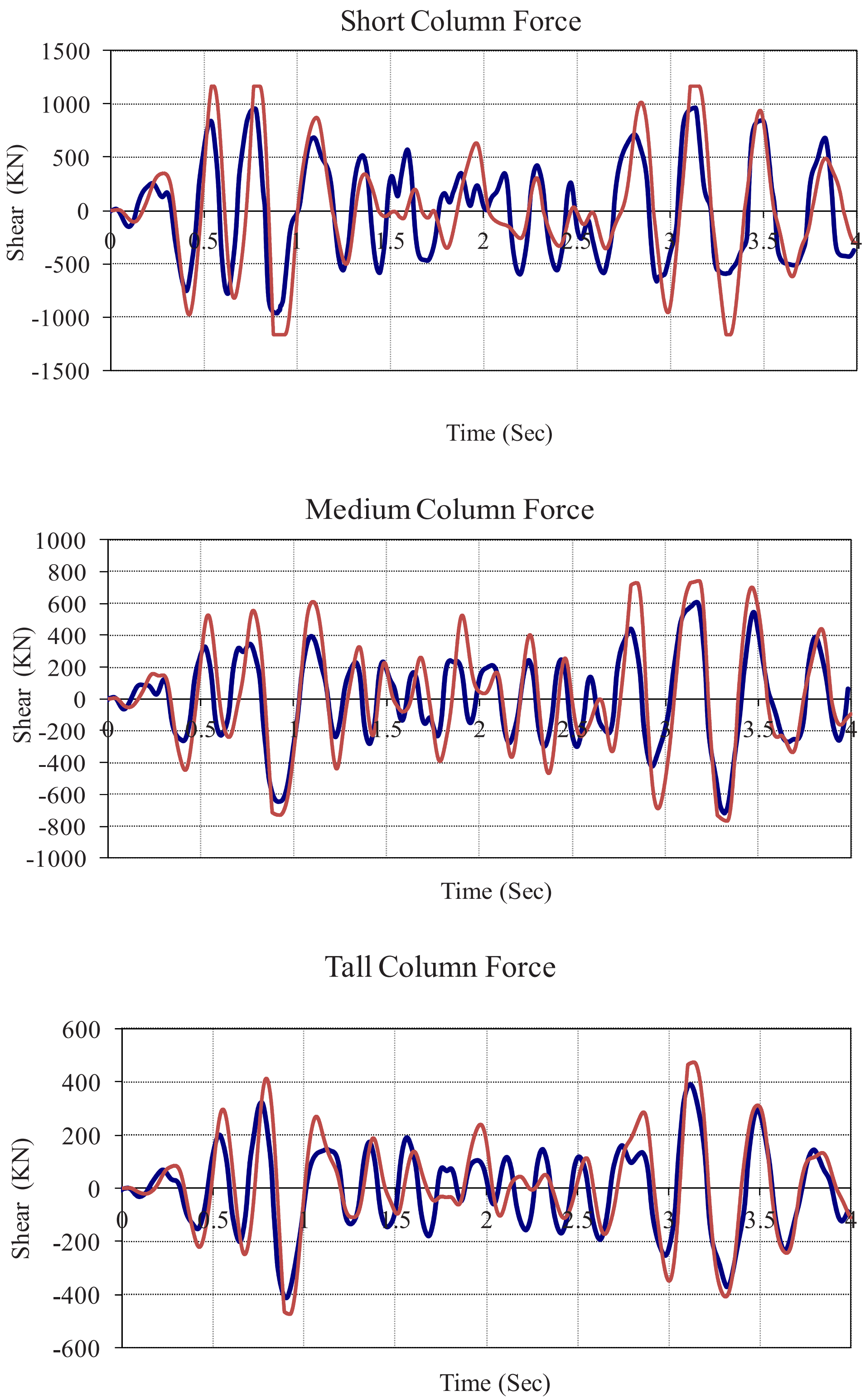

Fig. A.13. Comparison of the column shear forces obtained using experimental data and numerical analysis for maximum earthquake (i.e., 1.2 * design earthquake)

A.2. Shear deformations

The aspect ratios of columns considered in this research are larger than 2.8. When this ratio is more than 2.5 the column behaviour is governed by flexure and shear deformations are typically small. In addition, bridge columns were designed based on the new seismic design philosophy including capacity design. Therefore the significant amounts of confinement reinforcement required in columns will ensure a ductile flexural collapse mode. This means that the shear capacity of the columns are always higher than the corresponding shear developed in the columns due to formation of the plastic hinges in the columns.

To further investigate this issue and also the effects of strength degradation of concrete due to high flexural ductility demands in the plastic hinge regions, a study was carried out using Response-2000 software (Bentz, 2001). For this purpose a column with an aspect ratio of 2.5 was considered. This aspect ratio is equivalent to that of a 10 m long column with diameter of 2.0 m which is fixed at the ends. The column contained 3% longitudinal reinforcement and the corresponding required shear reinforcement (e.g., around 2%).

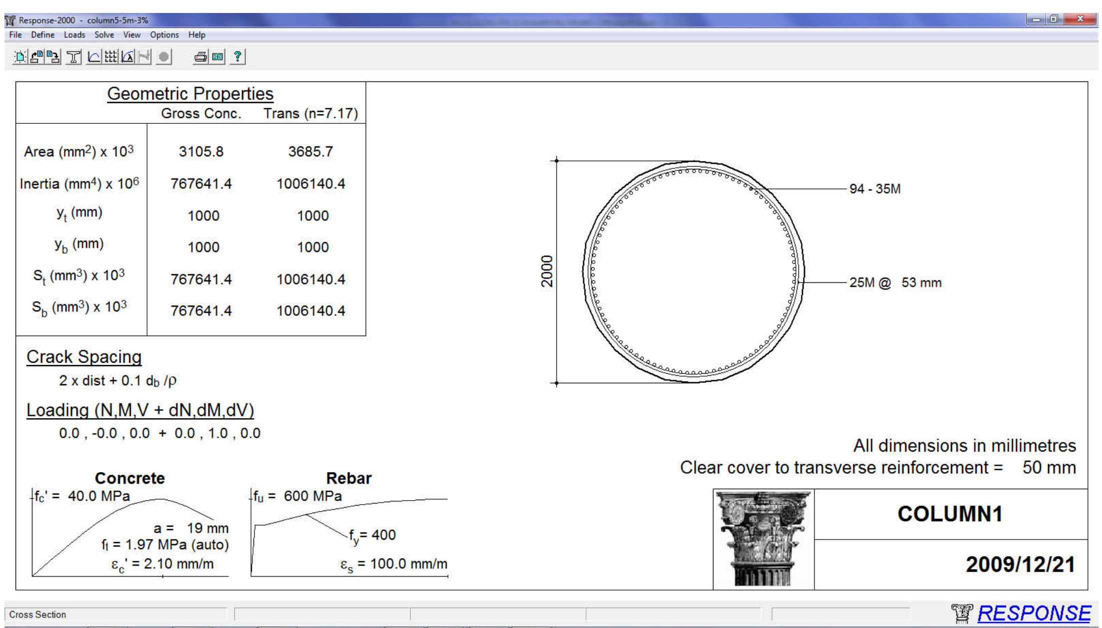

Fig.A.14. Cross section and properties of the column modelled in Response-2000

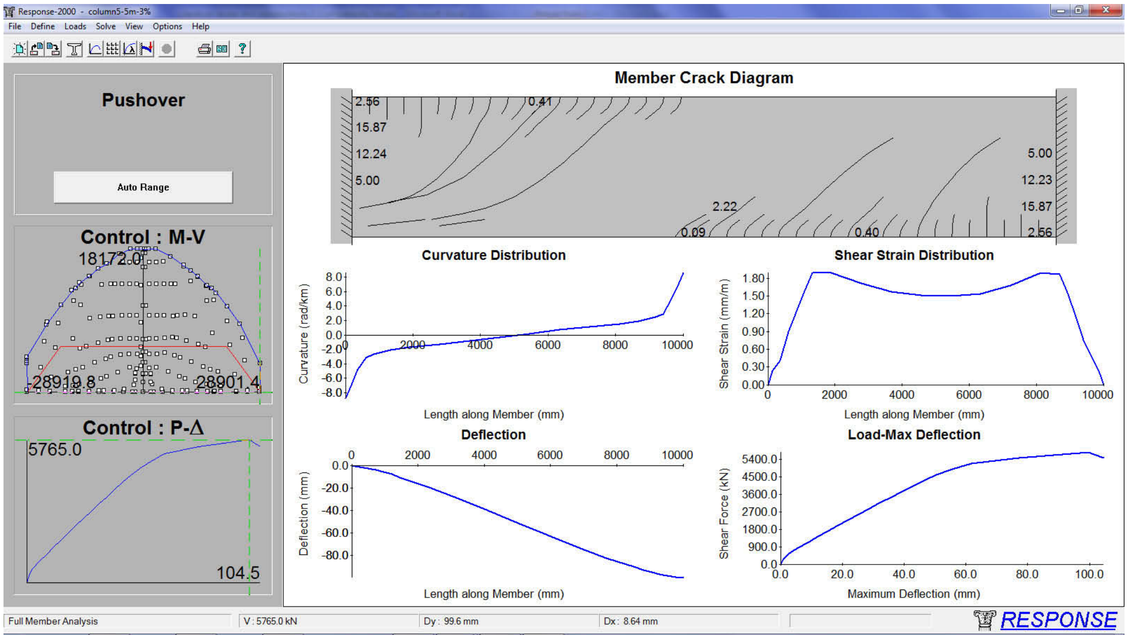

Fig. A.15. Example of the response of the column modelled in Response-2000

Fig. A.14 shows a sample model and Fig. A.15 demonstrates an example of the analysis results obtained in Response-2000. As can be seen from Fig. A.15, the Response-2000 program gives a relationship for the shear force-total displacement and it does not directly provide the shear force-shear displacement results. However the plots of the shear strain over the length of the column are given by the program. Therefore shear strain could be integrated over the length of the column to obtain the shear displacement corresponding to each load stage. There are several load stages and hence, the diagrams should be integrated for each load stage, in order to obtain the shear force shear displacement relationship (Patwardhan, 2005). These integrations were performed for different load stages and the results are shown in Fig. A.16. To include the effects of strength degradation of concrete due to high flexural ductility demands, the tension stiffening factor, f_t, in Response-2000 program was varied between 1 to 0. The tension stiffening effect represents the capacity of the intact concrete between cracks to continue to carry tensile stresses and offer stiffness. The results indicate that no shear failure occurs and that shear deformations are almost linear, before and after shear cracking, up to the ultimate deformation. The results indicate that in the case of this column with a small aspect ratio of 2.5, the shear deformations are less than 15% of the total deformation. The contribution of shear deformations is even smaller in columns having larger aspect ratios.

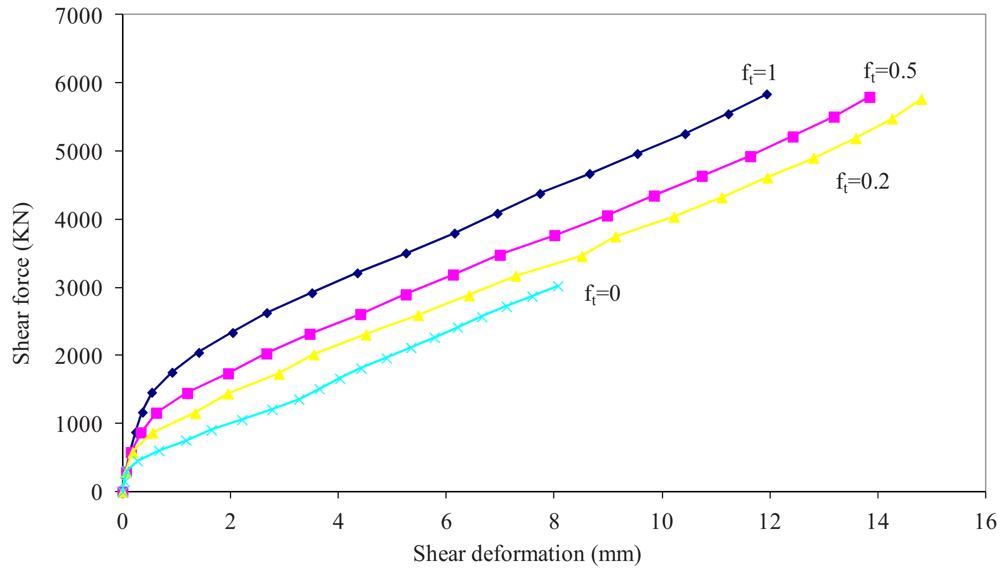

Fig. A.16. Shear force versus shear deformation for different tenstion stiffening factors, f_t.

Where column aspect ratios are smaller than 2.5, the shear deformations are important and should be included in structural modelling. AASHTO-Guidelines (2009) recommends using the effective shear area for ductile elements with aspect ratios lower than 2.5 (i.e., pier walls) according to Eq. [A.1].

[A.1] $$(GA)_{eff} = G_c A_v \frac{E_c I_{eff}}{E_c I_g}$$

Where $(GA)_{eff}$ is the effective shear stiffness, E_c is the modulus of elasticity of concrete, G_c is the shear modulus of concrete, A_v is the shear area, I_g is the gross moment of inertia, and I_{eff} is the effective moment of inertia of the reinforced concrete cross section (i.e., $E_c I_{eff} = M_n/\Phi_y$).

However the use of this equation is not mandatory for the columns with larger aspect ratios. This is because the shear deformations are not significant and are often negligible for bridge columns with aspect ratios larger than 2.5. In this research Eq. [A.**7.1**] was used to compute the shear stiffness of the columns. All bridge columns considered in this research had aspect ratios larger than 2.5. Deformations due to bond slippage at the column base were considered by incorporating the strain penetration length in plastic hinge length and length of columns, based on the recommendations by Priestley et al., (1996 and 2007).

A.3. Effect of irregularity due to different column heights on the seismic response of bridges (preliminary studies)

For the preliminary evaluations in this study and to demonstrate the research significance of this subject, the seismic responses of an irregular and a regular bridge were studied.
The bridges are straight continuous four-span bridges with span lengths of 50 m as shown in Fig. A.17.

The bridges were modelled in SAP2000 (Computers and Structures, 1999) as well as in RUAUMOKO (Carr, 2009). The bridges were designed using the 2006 CHBDC provisions in SAP2000 for the maximum zonal acceleration ratio of A=0.4 in the CHBDC provisions. This maximum zonal acceleration was chosen to carry out the preliminary studies. The importance factor of the bridges was considered as 1.0 and the site coefficient of S=1.2 for soil profile type II was used. The super structure mass was computed as 300 KN/m.

The seismic responses of bridges were evaluated using different methods of analysis including elastic response spectrum analysis, pushover analysis with uniform load pattern, modal pushover analysis and inelastic time history analysis. The bridges were studied for two cases of free and restrained transverse movements at the abutments.
The elastic response spectrum analysis and the pushover analyses were performed using SAP2000 software. The inelastic time history analysis was carried out using the

RUAUMOKO software. For the time-history analyses, 7 spectrum matched records were used. The records were matched to the design spectrum from the 2006 CHBDC provisions.

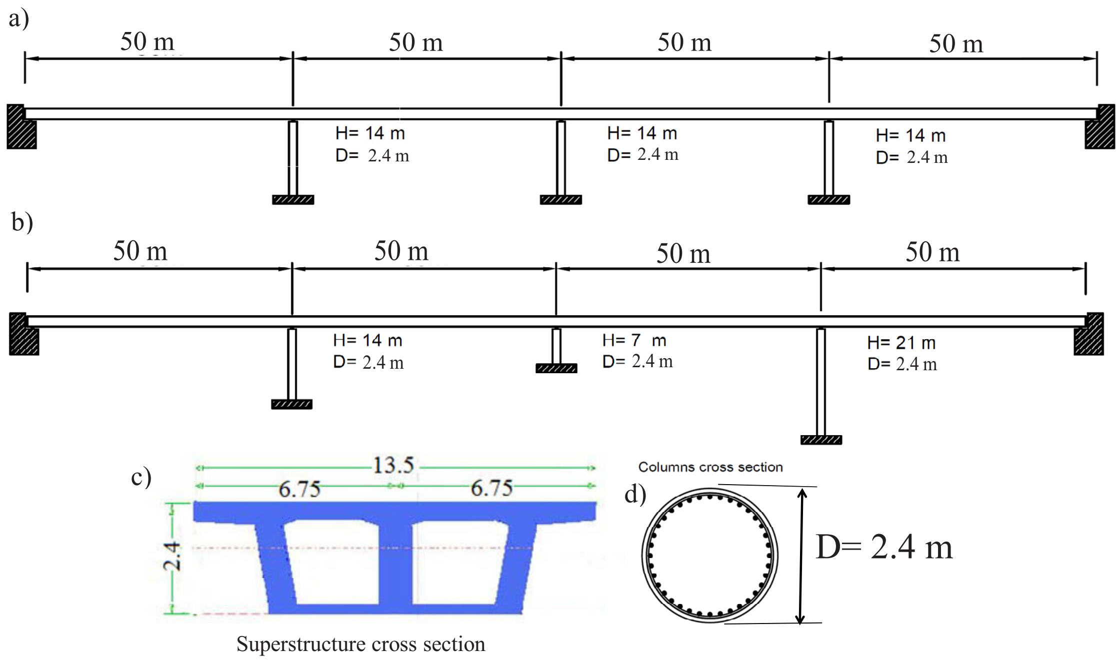

Fig. A.17. The properties of bridges studied: a) regular bridge, b) irregular bridge, c) superstructure cross section and d) columns cross section

For the modal pushover analyses (MPA) the response of the bridges in each mode was determined using the capacity-spectrum method as defined by the ATC-40 provisions (ATC-40, 1996). The capacity spectum method concept is shown in Fig. A.18 and an example of this method for the prediction of the seismic demands for two different modes are shown in Fig. A.19. The maximum drift ratio in the most critical bridge column was used to determine the responses using MPA as recommended by Kappos et al. (2004) and Paraskeva et al., (2006).

MPA is based on two principal simplifications. First, The coupling among modes is essentially neglected and second, it is assumed that the SRSS or CQC combination rules are valid.

MPA can be performed in following steps :

- Calculating the natural periods, T_n and modes, φ_n
- Performing separate pushover analyses for each mode using force distribution, $\mathbf{s}_n = \mathbf{m}\varphi_n$ (where $\mathbf{m}$ is the mass matrix)
- Predicting the earthquake displacement demands for each mode (e.g. using the capacity spectrum method)
- Combining the peak 'modal' responses using the SRSS or the CQC combination rule.

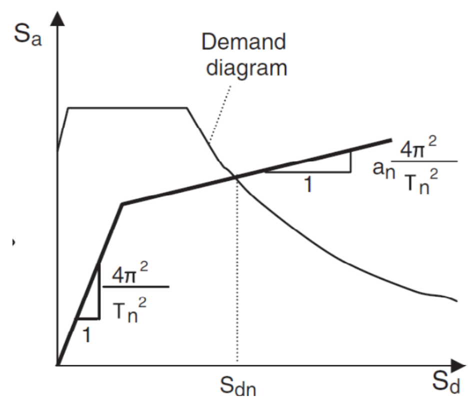

Fig. A.18. Application of the capacity spectrum method to determine the seismic demands (Paraskeva et al. (2006)).

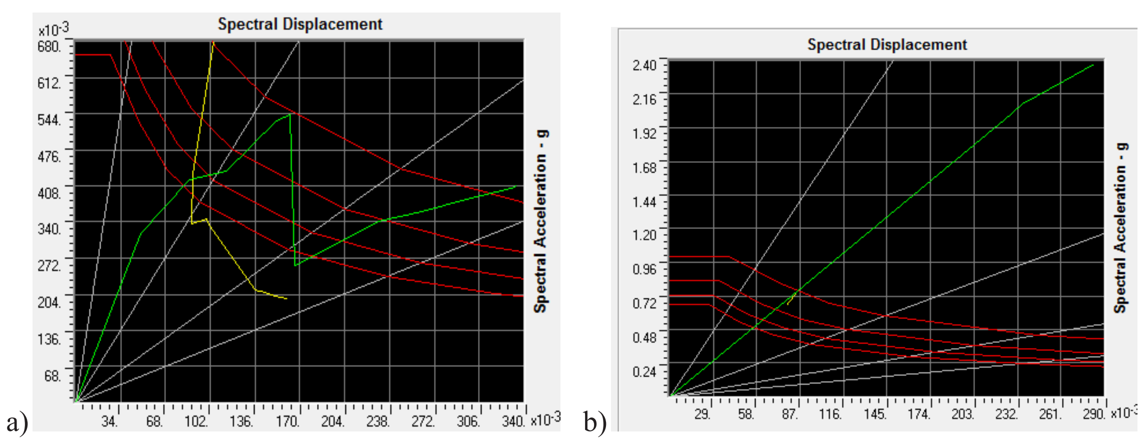

Fig. A.19. Examples of capacity-spectrum method used in SAP2000 to perform modal pushover analyses for: a) first mode (inelastic deformations); b) second mode (controlled by elastic deformations)

The seismic response predictions for the regular bridge with restrained transverse movements at the ends are shown in Fig. A.20 for different methods of analyses. As can be seen, the results from the elastic response spectrum analysis, inelastic time history analysis and the modal pushover analysis are in good agreement for this case. The results indicate that the pushover analysis using the uniform load pattern underestimates the maximum displacement demands. The similar results were observed for the case of the regular bridge with free movements at the abutments as shown in Fig. A.21.

For the irregular bridge two different superstructure stiffnesses were considered in the analyses. The superstructure transverse moment of inertia was considered as 140 m^4 (i.e., "rigid" superstructure) and 70 m^4 (i.e., flexible superstructure). The seismic response predictions for the two cases of rigid and flexible superstructures are shown in Fig. A.22 and Fig. A.23, respectively. In the case of a rigid superstructure (Fig. A.22) the predictions using different methods of analyses are in relatively good agreement, although the overall displacement envelope patterns are somewhat different from the different methods of analysis. On the other hand, in the case of a more flexible superstructure (Fig. A.23) the predictions from the inelastic and elastic analyses are significantly different. The displacement demands at the central column, which is the most critical column that controls the bridge response for this case, is significantly underestimated using the elastic response spectrum analysis method. Therefore using the response spectrum analysis, which is permitted in the current seismic codes for the design of such irregular bridges, can lead to unsafe designs. The predictions using the modal pushover analysis in this case are in good agreement with those obtained using the inelastic time history analysis.

The mode shapes of the irregular bridge with a flexible superstructure are compared with the mode shape of the bridge deck in Fig. A.24. As can be seen the mode shapes of the bridge resemble the displacement pattern obtained using the elastic analysis, while the mode shape of the bridge deck somewhat resembles the displacement envelopes obtained using the inelastic time history analysis. As the difference between the mode shapes of the bridge and mode shapes of the deck increases, the results from the elastic analyses differ more from the actual response of the bridge. That is why in most of the regularity indices the difference between the mode shapes of the bridge and deck are used to measure the degree of irregularity.

Similar results are observed for the case of the irregular bridge with free transverse movements at the abutments as shown in Fig. A.25. The use of the elastic response spectrum analysis underestimated the maximum displacement demand in the central critical column. Even the use of the modal pushover analysis did not significantly improve the predictions for this case.

Based on the preliminary results obtained, more research is needed to investigate the effects of different column heights, superstructure stiffness, and position of the columns on the seismic response of bridges. The comparisons of the inelastic and elastic responses for a wide range of bridge structures with different configurations can provide useful information to recognize the limitations of the elastic analyses and to improve the seismic design codes to better address such problems for analysis and design of bridges.

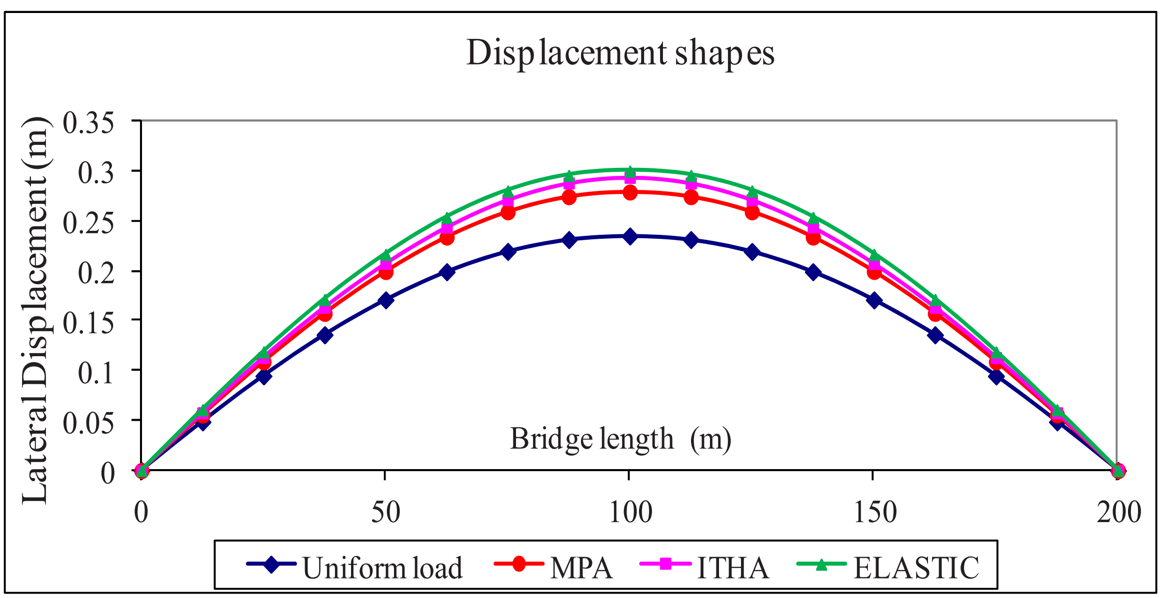

Fig. A.20. Seismic response predictions using different methods of analysis for the regular bridge with restrained transverse movements at the abutments.

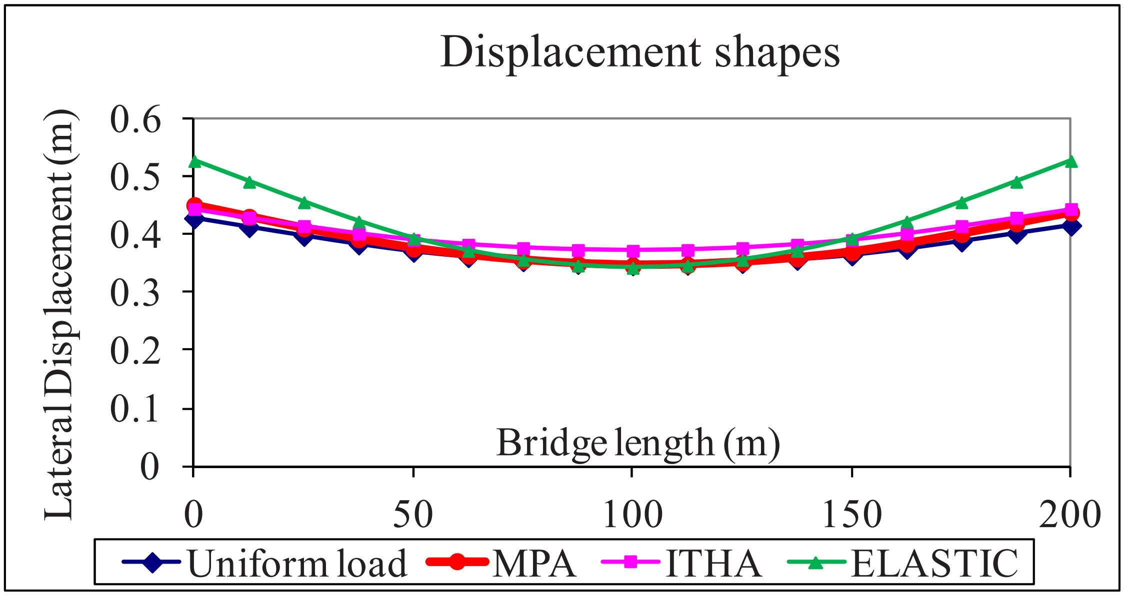

Fig. A.21. Seismic response predictions using different methods of analysis for the regular bridge with free transverse movements at the abutments.

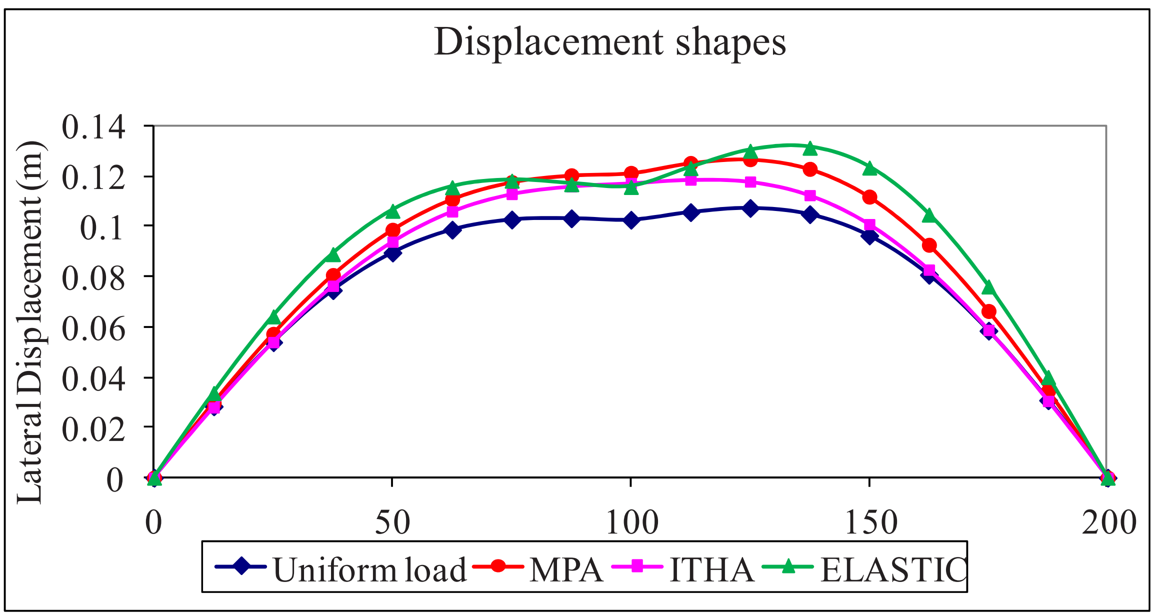

Fig. A.22. Seismic response predictions using different methods of analysis for the irregular bridge with a rigid superstructure and with restrained transverse movements at the abutments.

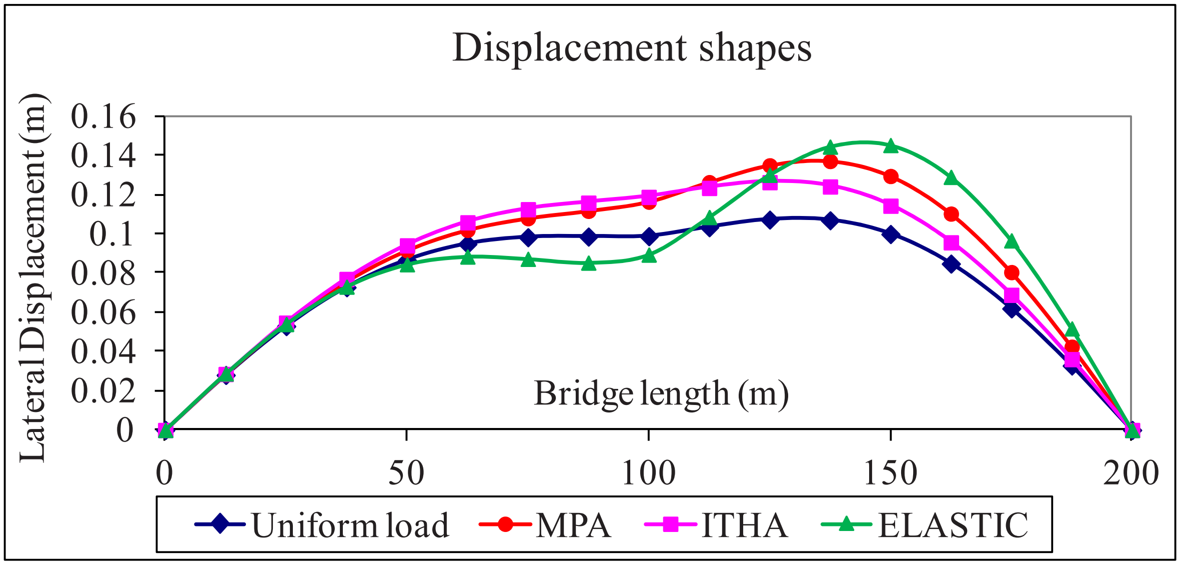

Fig. A.23. Seismic response predictions using different methods of analysis for the irregular bridge with a flexible superstructure and with restrained transverse movements at the abutments.

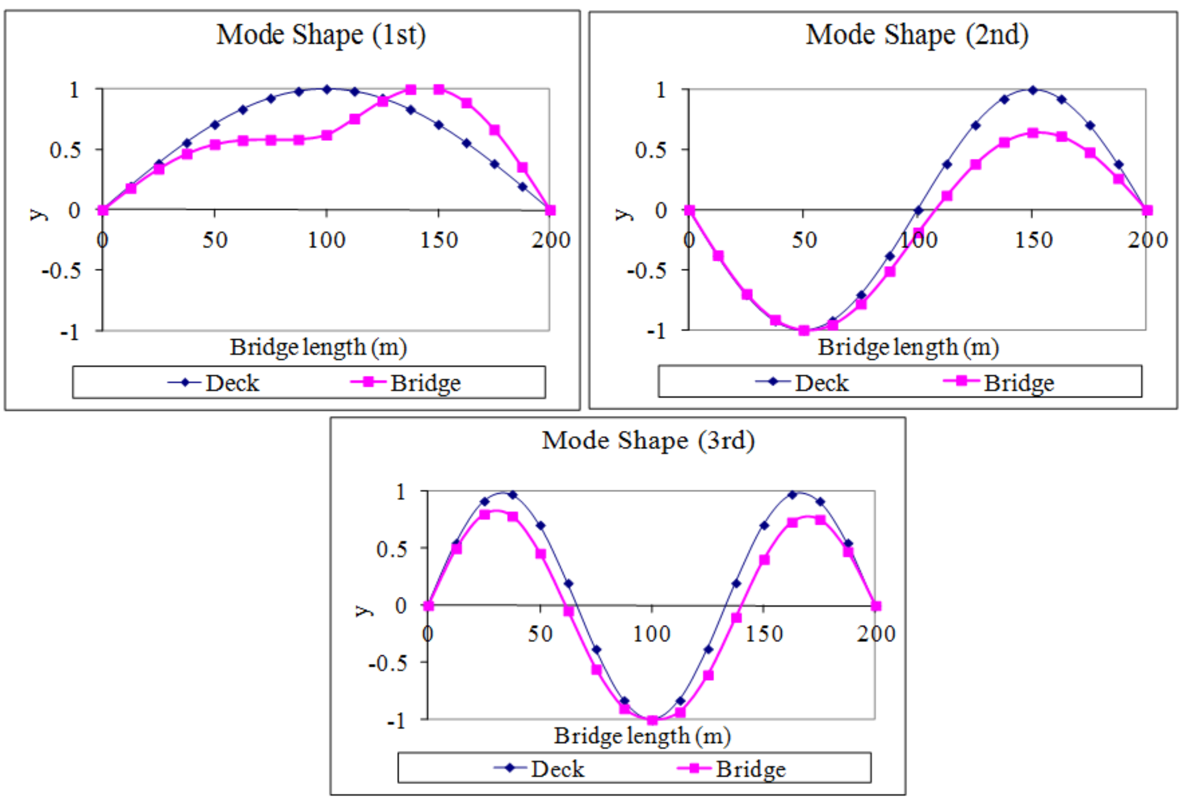

Fig. A.24. Comparison of the mode shapes of an irregular bridge with the mode shapes of the bridge deck for the first 3 modes.

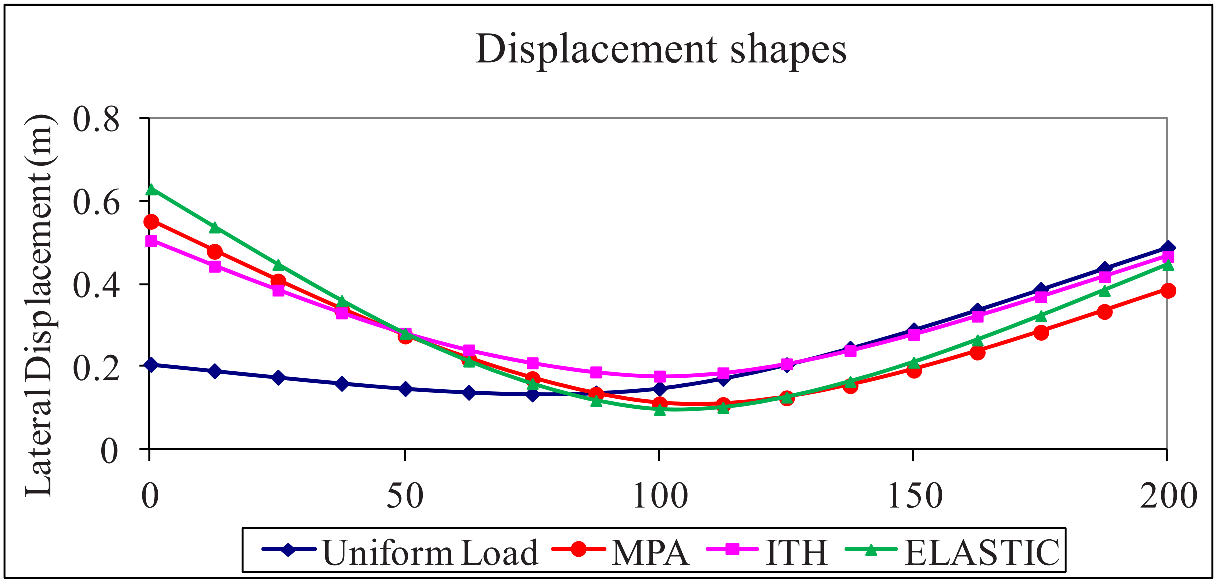

Fig. A.25. Seismic response predictions using different methods of analysis for the irregular bridge with a flexible superstructure and with free transverse movements at the abutments.

Appendix B: Computer program for designing, modelling, running the analyses, extracting and post processing the results

A comprehensive computer program was developed which is capable of designing and evaluating the bridges by means of elastic dynamic and inelastic dynamic analysis. The program is capable of automatically generating the input files and extracting all the required information for the seismic evaluations (according to the research objectives) using the RAUAMOKO program. Some of the main capabilities of the program are briefly as follows:

Main outputs and options available in the program:

- Computes the moment curvature and moment-axial force interaction diagrams considering the confinement effect due to the transverse reinforcement for the core concrete and considering unconfined concrete for the cover concrete.
- Designs the bridge columns for flexure and shear according to the 2006 CHBDC provisions by means of response spectrum analysis in the RAUAMOKO program and updates the design by updating the effective stiffnesses in several trials.
- Shear design is carried out based on the 2006 CHBDC provisions. The transverse steel ratios are determined to satisfy all requirements of the 2006 CHBDC provisions including the requirements for maximum factored shear forces, confinement in the plastic hinge regions, and the capacity design philosophy.
- Calculates the nodal points, elements, loads, masses, elastic and inelastic properties of the columns and ductility capacities at different damage states for modelling in the RAUAMOKO program automatically.
- Extracts the modal properties (see Figs. B.1 and B.2) and calculates several regularity indices to be used in the seismic evaluations. The program automatically recognizes the mode number and the type of the mode (i.e., torsional, transverse, longitudinal or vertical).

- Compares the displacements, drifts, curvatures and ductility demands and also the displacement envelopes from the elastic and inelastic time history analyses. The displacement envelopes from the elastic and inelastic analyses will be plotted automatically as shown in Fig. B.3. Displacements, drifts, ductility demands, and forces are extracted for all nodal points and column elements. The moment and shear forces in the superstructure elements are also extracted as shown in Figs.B4 and B.5.
- Calculates the mean or median responses for the desired number of records corresponding to two different levels of earthquakes for seismic performance evaluations.
- The mean or median values can be computed using either the maximum absolute values or the negative and positive displacement envelopes (see Priestley et al. (2007) for more details) to compute the average response of the structures subjected to a number of ground motion records.
- Calculates and compares the displacements and curvature demands to the corresponding ductility capacities calculated based on the maximum allowable strain in concrete or steel bar for different levels of damage and performance objectives corresponding to the earthquake level considered. The program also calculates the demand to capacity ratios to evaluate the available safety margins. The ductility capacities can be computed based on either theoretical or empirical methods in the program as discussed in Chapter 2.
- Performs incremental dynamic analysis (IDA) and evaluates the bridges based on the ATC-63 procedure. IDA can be performed using several algorithms including, regular IDA, time-effective IDA, fast IDA and also the method used by the ATC63 provisions. Such algorithms are discussed in Chapters 2 and 6.
- Summarises the results and develops of the IDA curves using linear interpolation. Computes the percentiles (i.e., 16%, 50%, and 84% percentiles) and predicts the collapse capacity of the structure for each record. Computes the capacity of the structure at different limit states or damage states including yielding, serviceability, cover spalling, bar buckling, bar fracture, and collapse. Different methods can be chosen in the program to predict the engineering demand parameters at different damage states (e.g., the method by Priestley et al, (2007) or the method by Berry and Eberhard (2007)). The median, percentiles and standard deviation at different damage states are computed. The IDA

cures are developed for different engineering demand parameters such as displacements, drifts, displacement ductility, curvature ductility, ductility demand to ductility capacity (i.e., D/C ratios) and inelastic rotation. Such IDA curves are developed for each bridge column separately and then the maximum drift ratio of all columns will be used to compute the IDA curves to represent the overall response of the bridge including the maximum response of all bridge columns.

- Computes the fragility curves based on the IDA results. The fragility curves are developed for various damage states (e.g., yielding, cover spalling, bar buckling and collapse).
- A large pool of records is incorporated in the program including the NGA databse records, K-KIK net records for subduction events, Atkinson records compatible with the NBCC spectra (Atkinson, 2009) and simulated records to match target spectra for different hazard levels for the cities of Vancouver and Montreal. The program is capable of scaling the records based on the method described by Atkinson (2009) to select the best records for the structural analysis (i.e., the records with better matching to the target spectrum and records that requires smaller scale factors) based on the fundamental period of the structure. The number of records from different record sets can be selected based on the seismic deaggregation results.
- The structural analyses can be carried out for the transverse or longitudinal bridge separately or the pairs of records can be applied in a 3D structural analysis. In the latter case, the program is also able to obtain the maximum radial displacements during the excitation.
- Options are available for the number of spans, number of nodes for each span (to capture the displacement of the superstructure), column heights for different columns, span lengths, abutment conditions, dead loads (i.e., structural mass), material properties, maximum and minimum reinforcement for design, concrete cover, bar diameters, strength factors Φ_s, and Φ_c for design, and etc.
- Options are available for force modification factors, R, in the longitudinal and transverse direction separately.
- Options are available to design the bridges based on either the NBCC or CHBDC design spectra and for Vancouver or Montreal.

- Options are available to compute the effective moment of inertia of columns based on different methods. This includes the iterative approach in which the bridge is designed in several trials. The column properties are updated in each trial and the structural analyses are performed using the updated column properties and new design forces are obtained until the required reinforcements are similar to those obtained in the last step.
- The abutment model by Aviram et al. (2008) is incorporated in the program to compute the stiffness and strength properties of the abutment components for modelling in the RUAUMOKO program.
- The program carries out pushover analysis for the bridges in RUAUMOKO and computes the yielding and ultimate displacements (based on the guidelines of the ASCE/SEI 41-06 provisions (ASCE, 2006)) for the obtained pushover curves for different columns and for different nodes as monitoring points for pushover. The ductility capacity of the structures is then determined. The pushover curves are converted to the S_a-S_d format as indicated in the ATC-40 (ATC, 1996) provisions.
- The program computes the collapse capacity of the bridges using different sets of records (e.g., three sets of records for crustal, interface and inslab earthquakes) and also using different subset of records (e.g., 8 different subsets as described in the thesis). The results can also be computed for a set of records with similar epsilon values to those from the seismic deaggregation (i.e., epsilon-based method). The program computes the mean epsilon values and percentages of contribution of different earthquake types at the selected hazard level (which can be set to 10%, 2% and 0.5% probability of exceedance in 50 years). The program performs regression analysis to compute the β_1 factor and the spectral shape factor (SSF). The IDA results then will be modified for the computed SSF values. The regression analyses are performed for three different earthquake types and different subsets of records separately. After computing the percentiles and the standard deviation of the IDA results, the results from different earthquake types are combined based on the seismic deaggregation results to compute the overall collapse capacity of the structure. The collapse margin ratios, acceptable collapse margin rations, mean epsilon values of the records are also computed by the program for this purpose.

- Subroutines are incorporated in the program to automatically perform large parametric studies using a large pool of records for inelastic time history analyses and for incremental dynamic analyses as demonstrated in the papers presented in this thesis which involved a large number of bridge structures and a large number of inelastic dynamic analyses.
- All important parameters from all of the analyses are extracted and stored in a file for comparison between different cases. All the results obtained for each structure is also stored in a file.

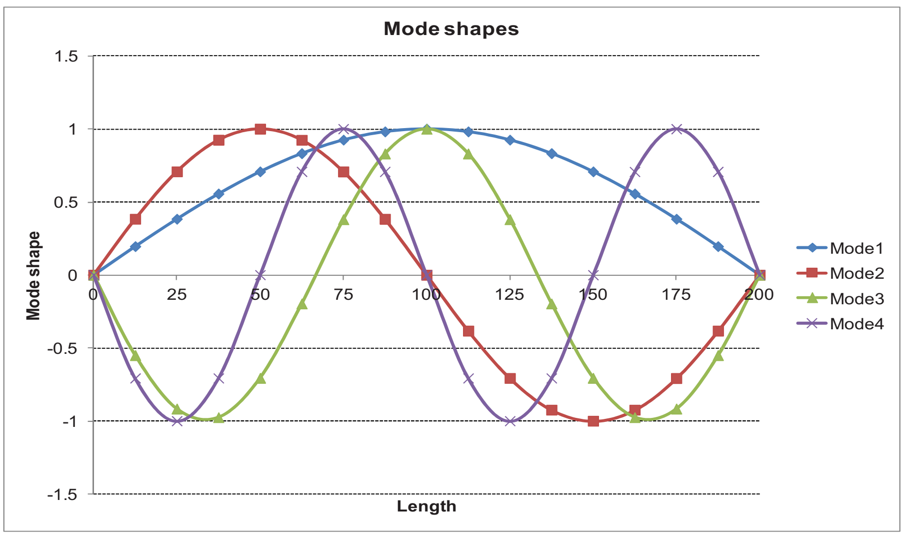

Fig.B.1. Extraction of the mode shapes of the bridges

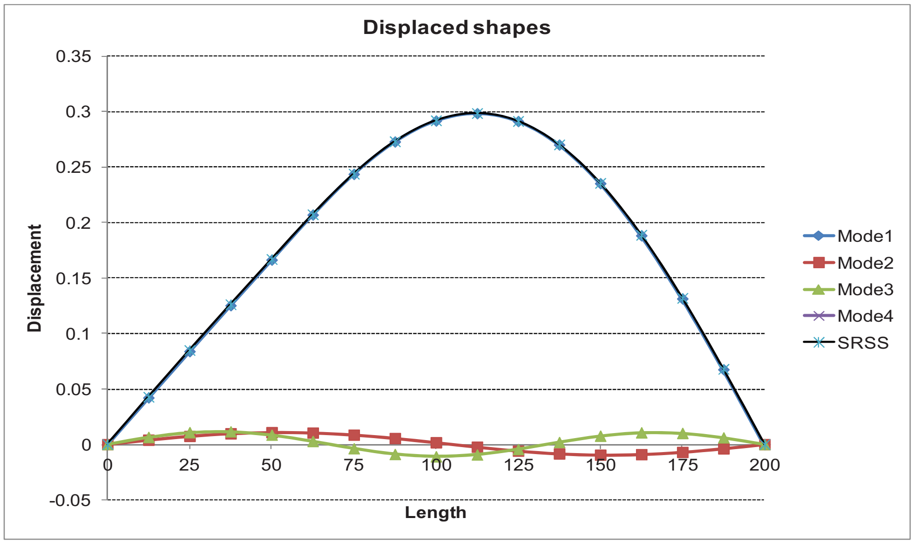

Fig.B.2. Modal displacements of the bridge

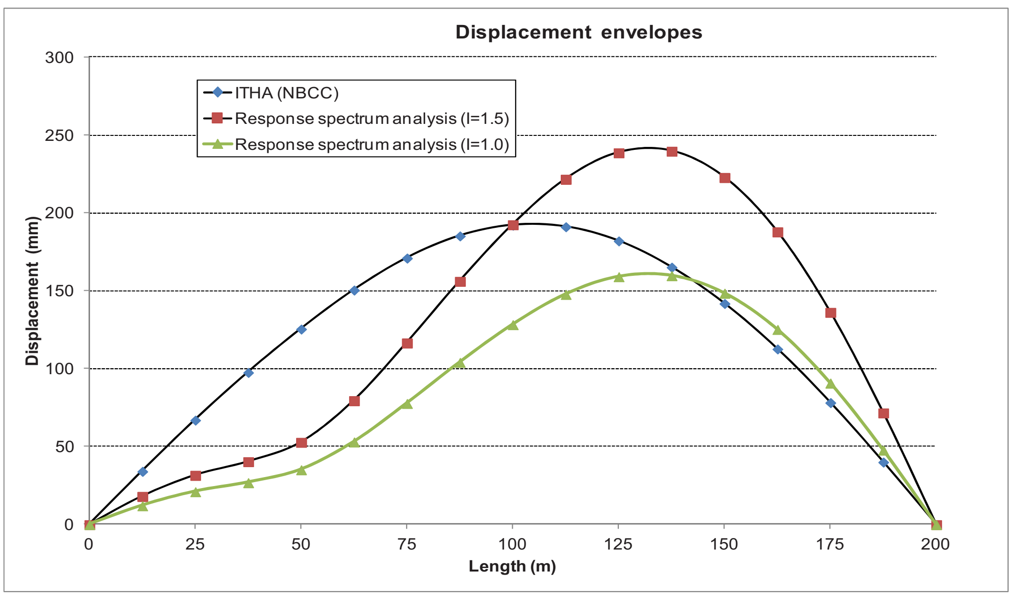

Fig.B.3. Comparison of the displacement envelopes predicted using elastic response spectrum and inelastic time history analyses.

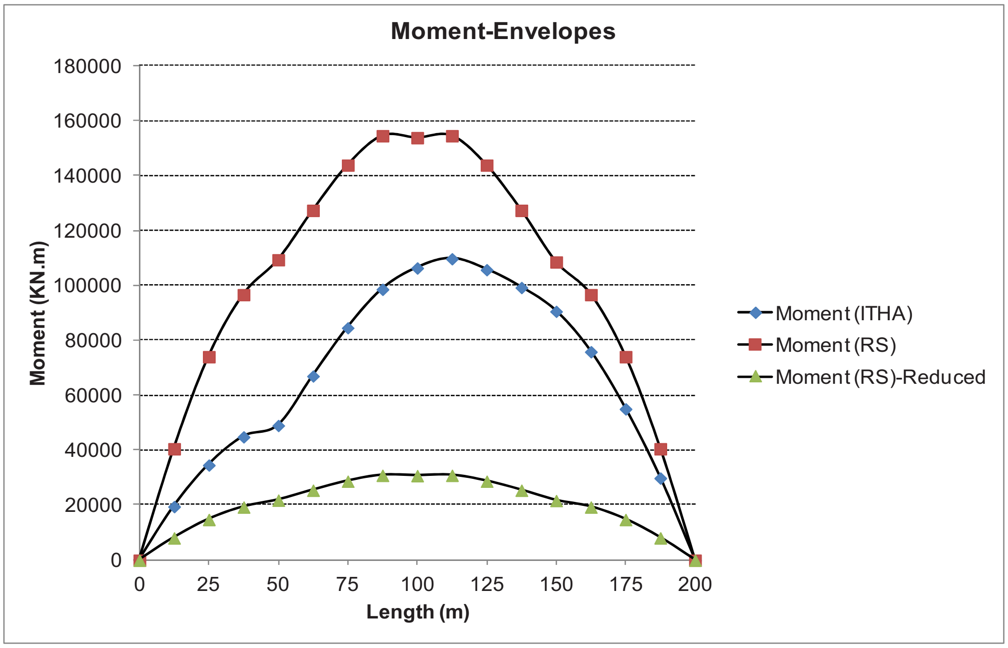

Fig.B.4. Comparison of the superstructure moment forces predicted using elastic response spectrum and inelastic time history analyses.

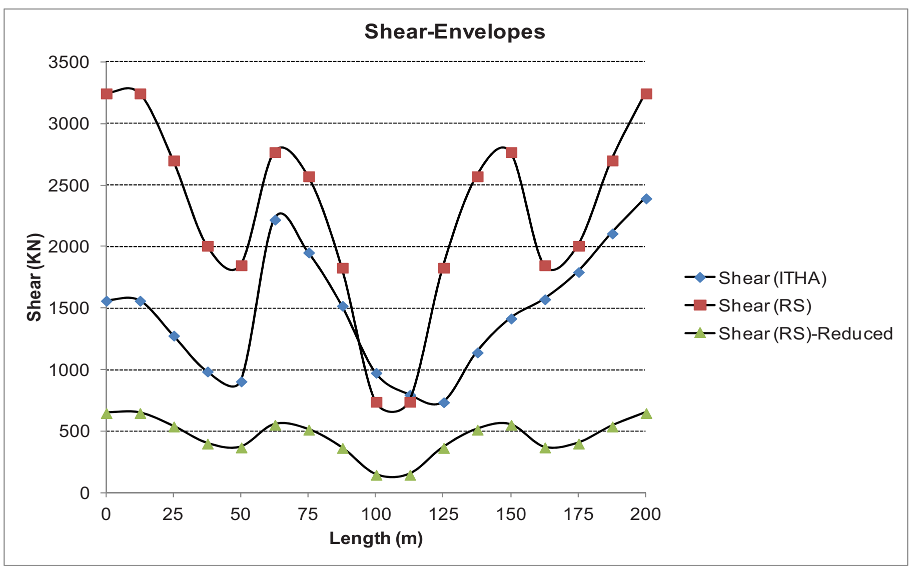

Fig.B.5. Comparison of the superstructure shear forces predicted using elastic response spectrum and inelastic time history analyses.

Appendix C: Probabilistic seismic hazard analysis and the program developed for seismic deaggregation

The main objective of the probabilistic seismic hazard analysis (PSHA) is to estimate the mean frequency per unit time or, alternatively, the probability in a given future time period that a specified level of some ground motion parameter will be exceeded at a site of interest. More formally, the PSHA methodology allows computation of the mean annual frequency of exceedance, γ, of a ground motion with amplitude, y, based on the aggregated hazard from N sources located at different distances and capable of generating events of different magnitudes (Bazzurro and Cornell, 1999). The standard formulation of probabilistic seismic hazard to calculate a frequency of exceedence, γ, of a ground motion amplitude, y, is given in Eq. [C.1] (McGuire 1995):

[C.1] $$\gamma(y) = \sum_i \nu_i \int\int f_M(m) f_R(r) P[Y > y \mid m, r]\, dm\, dr$$

where ν_i is the activity rate for source i *(e.g.,* the mean annual rate of occurrence of earthquakes generated by source i with magnitude greater than some specified lower bound), $f_M(m)$ is the magnitude probability density function which describes the frequency of occurrence of each event with magnitude m, and function $f_R(r)$ denotes the probability density function of distances, from the site, of the locations of earthquakes, given an earthquake occurring in a seismic source. P[Y>y| m, r] is the conditional probability that the ground motion amplitude exceeds the value of y given the magnitude, m, and distance, r. Assuming that ground motion amplitude y has a log-normal density function, ln(y) has a normal distribution function. Therefore the probability density function (pdf) of y, p(y) can be obtained using Eq. [C.2] and the cumulative distribution function (CDF), P(y), can be obtained using Eq. [C.3].

[C.2] $$p(y)=\frac{1}{\sigma\sqrt{2\pi}}e^{-(\ln(y)-g(m,r))^2/2\sigma}$$

[C.3] $$P(Y>y\mid m,r)=[1-\Phi(\frac{\ln(y)-g(m,r)}{\sigma})]$$

where g(m, r) and σ are the mean and standard deviation of ln(y) respectively, given by the attenuation relationship (i.e., ground motion prediction equation (GMPE)) .

The probability in the integrand of Eq. [C.1] can be expressed explicitly as a function of the ground-motion randomness ε, given (McGuire, 1995):

[C.4] $$\gamma(y)=\sum_i v_i\int\int\int f_M(m)f_R(r)f_\varepsilon(\varepsilon)\;P[Y>y\mid m,r,\varepsilon]dm\,dr\,d\varepsilon$$

[C.5] $$\varepsilon=\frac{\ln(y)-g(m,r)}{\sigma}$$

where ε is defined as the number of logarithmic standard deviations by which the logarithmic ground motion deviates from the median (Eq. [C.5]) and $f_\varepsilon(\varepsilon)$ = $(1/\sqrt{(2\pi)})\exp(-\varepsilon^2/2)$ represents the standardized Normal distribution. In this formulation, the probability P[Y>y| m, r, ε] is simply an indicator function which is zero if ln g(m, r, ε) from the attenuation function (i.e., GMPE) is less than ln(y), and 1 otherwise.

The physical image of earthquake scenarios in terms of magnitude and distance is lost in the highly integrated framework of the PSHA. For physical interpretation of the results from PSHA it is desirable to have the contribution of each earthquake scenarios with magnitude, M and distance, R to the overall seismic hazard obtained through the PSHA method. This can be achieved through the deaggregation of the probabilistic seismic hazard. The deaggregation of the hazard results by magnitude M, distance R, and ground-motion deviation ε is achieved by accumulating (by magnitude, distance, and ε) the annual frequencies of exceedence of the target ground-motion amplitude for each period, T, separately. Dividing these annual frequencies by the total hazard (the total annual frequency) gives the probability that, given an exceedence of that amplitude, it has been caused by a certain combination of M, R, and ε (McGuire, 1995).

For seismic deaggregations Eq. [C.6] is used instead of the indicator function (as discussed before), in order to derive the contributions to γ(y) by M, R, and ε:

$$[C.6] \qquad P[Y > y \mid m, r, \varepsilon] = \delta[\ln Y\ (m, r, \varepsilon) - \ln y\ ]$$

where δ is the Dirac delta function, which gives a probability of 1 at In *Y(m,* r, ε) = In(y) and zero otherwise (δ is used because the determination of *M-R-* ε sets that *equal* the target ground motion, not that *exceed* it, is sought). The formulations in Eqs. [C4] and [C.6] are used for deaggregation to derive the contributions to γ (y) by m, r, and ε (McGuire,1995).

Program developed for the seismic deaggregation ("Deaggregation calculator")

The probabilistic seismic hazard analyses (PSHA) for Vancouver and Montreal was carried out based on the updated seismic hazard model using the Monte Carlo simulations by Goda et al., (2010). For the purpose of this study, a program was developed to process the raw seismic hazard data provided by Goda et al., (2010).

The computer program was developed in visual basic to process the raw data and to compute the required information for deaggregation of the seismic hazard, mean magnitude, distance, and epsilon, contribution of different event types (i.e., crustal, interface, and inslab events).

The program is capable of performing the following tasks:

Inputs:

- Probability of exceedance: Any probability of exceedance, up to 0.5% in 50 years, can be considered.
- Bin sizes: The bin sizes for magnitude, M, Distance, R, and epsilon, ε, are given.
- The range of minimum to maximum desired magnitude, distance, and epsilon for deaggregations
- Site of interest: e.g., Vancouver or Montreal
- Data type: Data using an updated model by Goda et al. (2010) or data from the Geology Survey of Canada (GSC)) model can be used for the seismic deaggregation.
- Deaggregation type: Either matching method or exceeding method (Hong and Goda, 2006) can be used for the seismic deaggregation. If the matching method is chosen, the percentages above and below of the target value to match should be defined (e.g., 10% was considered for this study).
- Type of distance: Either hypocentral or extended distances (the distance type used in the GMPE (e.g., RRUP, RJB, etc.)) can be used.
- Vibration periods: The deaggregation can be carried out for spectral accelerations at different periods including PGA, Sa(0.2), Sa(0.5), Sa(1.0), Sa(2.0), and Sa(3.0).
- Event types: Four options in this case are available. The user can choose either any earthquake type (i.e., crustal, interface, and inslab) or all earthquake types. If individual earthquake type is chosen then the seismic deaggregation will be carried out only for the selected earthquake type. For example if the interface events are chosen, the mean magnitude, distance and epsilon only for this event type will be computed. If all earthquake types are chosen then the average mean magnitude, distance and epsilon for all earthquake types will be computed. Further, in the later case the percentage of contribution of each event type to the overall seismic hazard at different vibration periods can be computed.

- Selected GMPE: An option is available to choose the desired ground motion prediction equations (GMPE) to carry out the seismic deaggregation. Any number of GMPEs can be selected or alternatively all GMPEs used in the seismic hazard analyses can be used. For example the epsilon values from different GMPEs are somewhat different and specific GMPEs can be selected to derive epsilon values to be used in the epsilon-based record selection or prediction of the conditional mean spectrum.

Out puts:

The main output of the program is:

- Computing the seismic deaggregation for magnitude, distance and epsilon (i.e., the relative frequencies of each bin with specific M,R, and ε).
- Prediction of the mean values: The mean values of magnitude, M, distance, R, and epsilon, ε, for the input variables discussed before will be computed. In addition, the mode values of magnitude, distance and epsilon can be computed. The computation of mode values can be based on either the marginal probability functions of M, R, and ε separately, or they can be computed for the joint probabilities of M-R or M-R-ε. However the mode values were not required for the purpose of this study and were not reported.
- Prediction of the uniform hazard spectrum (UHS) : The UHS values for different periods and different probability of exceedances can be computed.
- Prediction of the percentages of contribution of each earthquake type on the overall seismic hazard
- Auto computation of the seismic deaggregation for different periods and different hazard levels: A subroutine was added to compute the deaggregations for a full range of periods and for different hazard levels and to print the results in the tables automatically.
- Development of the conditional mean spectrum (CMS): The CMS at any desired period for different earthquake types and different period ranges can be computed. For periods other than those used in the seismic hazard analysis (i.e., PGA, T=0.2, 0.5, 1, 2, 3) seismic deaggregation will be carried out two times for the lower and upper periods

and a linear interpolation is used to predict the deaggregation results for the period of interest. The computation of the CMS is carried out by computing a CMS for each bin and considering the relative frequency of each bin. The overall CMS will be computed by aggregating the CMS of each bin weighted by the relative frequency of that bin from the seismic deaggregation results. For the purpose of this study the CMS was calculated using certain GMPEs (i.e., BA08, Z06 and AB03). Although the other GMPEs are also incorporated in the program and the weighting factors can be assigned to compute the average CMS computed for different GMPEs, for the purpose of this study only the BA08, Z06 and AB03 GMPEs were fully verified and used.

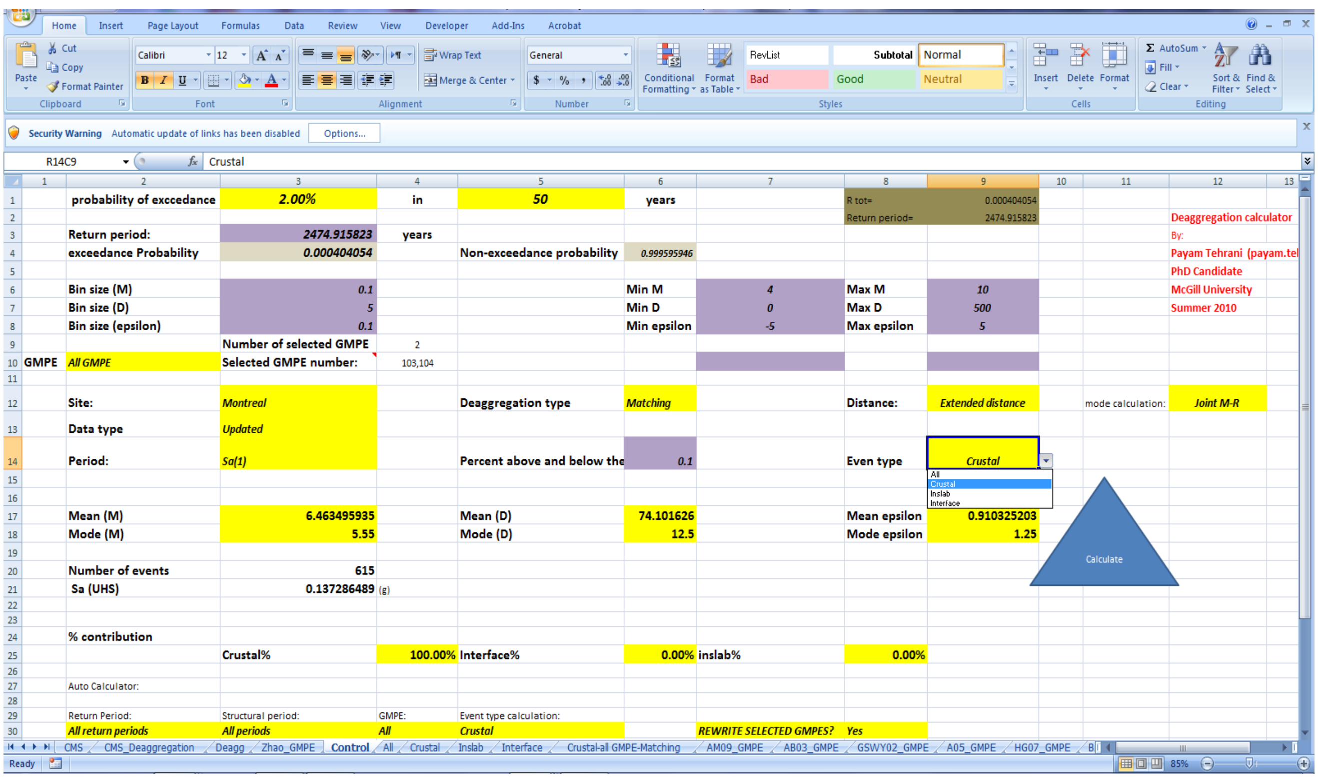

Fig. C.1. A view of the program developed for deaggregation of the seismic hazard data

Table C.1. Deaggregation results for all earthquake types using all GMPEs using exceeding method

PGA		Mean			Contribution %			
		M	D	ε	Crustal	Interface	Inslab	Sa (UHS)
10% in 50	Updated	6.78	69.15	1.29	33.6%	6.9%	59.5%	0.24
	GSC	6.29	72.43	1.68	12.3%	3.7%	84.0%	0.35
2% in 50	Updated	6.96	66.40	1.64	32.0%	5.4%	62.6%	0.49
	GSC	6.34	67.76	2.14	8.1%	1.9%	90.0%	0.68
0.5% in 50	Updated	7.06	66.16	1.94	30.3%	4.2%	65.5%	0.79
	GSC	6.38	65.74	2.51	4.4%	0.6%	95.0%	1.07

Sa(0.5)		Mean			Contribution %			
		M	D	epsilon	Crustal	Interface	Inslab	Sa (UHS)
10% in 50	Updated	7.10	74.77	1.28	43.5%	20.9%	35.5%	0.34
	GSC	6.62	77.38	1.54	16.9%	7.8%	75.3%	0.47
2% in 50	Updated	7.33	73.50	1.63	42.7%	24.8%	32.6%	0.75
	GSC	6.70	71.76	2.00	14.5%	5.7%	79.9%	0.96
0.5% in 50	Updated	7.43	70.20	1.90	48.7%	23.8%	27.5%	1.31
	GSC	6.71	68.13	2.41	12.2%	3.0%	84.8%	1.55

Sa(1)		Mean			Contribution %			
		M	D	epsilon	Crustal	Interface	Inslab	Sa (UHS)
10% in 50	Updated	7.31	83.91	1.21	40.4%	27.0%	32.6%	0.18
	GSC	6.79	81.52	1.50	23.0%	10.4%	66.7%	0.23
2% in 50	Updated	7.56	83.70	1.58	37.9%	34.2%	28.0%	0.43
	GSC	6.88	73.55	1.93	22.7%	9.5%	67.8%	0.45
0.5% in 50	Updated	7.64	80.78	1.91	44.5%	34.5%	21.0%	0.75
	GSC	6.91	65.46	2.24	24.2%	6.6%	69.3%	0.73

Sa(2)		Mean			Contribution %			
		M	D	epsilon	Crustal	Interface	Inslab	Sa (UHS)
10% in 50	Updated	7.52	94.37	1.13	35.7%	35.3%	29.1%	0.09
	GSC	6.86	83.66	1.57	37.2%	10.2%	52.5%	0.11
2% in 50	Updated	7.80	96.85	1.52	30.0%	46.5%	23.4%	0.23
	GSC	6.99	74.02	1.94	32.8%	12.2%	55.0%	0.22
0.5% in 50	Updated	7.96	98.48	1.84	30.7%	51.3%	18.0%	0.41
	GSC	7.07	66.41	2.22	34.3%	10.0%	55.7%	0.36

Sa(3)		Mean			Contribution %			
		M	D	epsilon	Crustal	Interface	Inslab	Sa (UHS)
10% in 50	Updated	7.62	99.23	1.07	37.2%	39.6%	23.3%	0.05
	GSC	6.77	98.53	1.57	0.0%	16.0%	84.0%	0.04
2% in 50	Updated	7.95	102.60	1.46	30.5%	53.8%	15.6%	0.13
	GSC	6.93	94.77	2.06	0.0%	18.2%	81.8%	0.09
0.5% in 50	Updated	8.05	100.17	1.76	36.7%	55.3%	8.0%	0.25
	GSC	6.97	91.48	2.46	0.0%	16.8%	83.2%	0.17

PGA		Mean			Contribution %			
		M	D	ε	Crustal	Interface	Inslab	Sa (UHS)
10% in 50	Updated	6.64	70.88	1.07	36.4%	7.7%	55.8%	0.24
	GSC	6.24	75.66	1.38	16.0%	4.7%	79.3%	0.35
2% in 50	Updated	6.88	67.61	1.40	33.3%	6.5%	60.2%	0.49
	GSC	6.29	68.41	1.85	10.9%	2.4%	86.6%	0.68
0.5% in 50	Updated	6.99	64.51	1.66	30.8%	4.0%	65.2%	0.79
	GSC	6.37	68.32	2.27	6.7%	0.9%	92.4%	1.07

Sa(0.5)		Mean			Contribution %			
		M	D	epsilon	Crustal	Interface	Inslab	Sa (UHS)
10% in 50	Updated	6.89	75.09	1.07	48.1%	15.8%	36.1%	0.34
	GSC	6.54	82.04	1.28	20.4%	8.2%	71.4%	0.47
2% in 50	Updated	7.21	73.80	1.45	40.9%	23.0%	36.1%	0.75
	GSC	6.68	75.79	1.73	13.8%	8.5%	77.7%	0.96
0.5% in 50	Updated	7.43	77.80	1.68	38.9%	27.4%	33.7%	1.31
	GSC	6.73	71.25	2.11	13.5%	5.3%	81.3%	1.55

Sa(1)		Mean			Contribution %			
		M	D	epsilon	Crustal	Interface	Inslab	Sa (UHS)
10% in 50	Updated	7.08	84.03	1.03	47.2%	19.4%	33.5%	0.18
	GSC	6.71	86.29	1.24	25.9%	10.0%	64.1%	0.23
2% in 50	Updated	7.47	83.90	1.33	37.9%	33.2%	28.9%	0.43
	GSC	6.86	77.42	1.63	23.4%	10.9%	65.7%	0.45
0.5% in 50	Updated	7.63	85.07	1.64	36.1%	34.3%	29.6%	0.75
	GSC	6.90	72.26	2.01	21.3%	9.0%	69.8%	0.73

Sa(2)		Mean			Contribution %			
		M	D	epsilon	Crustal	Interface	Inslab	Sa (UHS)
10% in 50	Updated	7.23	91.93	0.93	44.8%	22.9%	32.3%	0.09
	GSC	6.77	89.38	1.33	41.2%	9.2%	49.6%	0.11
2% in 50	Updated	7.73	98.23	1.30	29.1%	45.4%	25.5%	0.23
	GSC	6.91	79.10	1.71	34.3%	10.5%	55.2%	0.22
0.5% in 50	Updated	7.86	96.96	1.62	28.6%	48.4%	23.0%	0.41
	GSC	7.04	71.20	2.03	36.7%	12.2%	51.1%	0.36

Sa(3)		Mean			Contribution %			
		M	D	epsilon	Crustal	Interface	Inslab	Sa (UHS)
10% in 50	Updated	7.27	94.92	0.92	47.2%	23.1%	29.6%	0.05
	GSC	6.64	101.24	1.25	0.0%	13.3%	86.7%	0.04
2% in 50	Updated	7.85	104.58	1.26	29.4%	50.2%	20.4%	0.13
	GSC	6.86	97.15	1.79	0.0%	17.3%	82.7%	0.09
0.5% in 50	Updated	7.95	99.00	1.55	35.6%	54.2%	10.3%	0.25
	GSC	6.93	93.62	2.21	0.0%	18.4%	81.6%	0.17

Table C.2. Deaggregation results for all earthquake types using all GMPEs using matching method

PGA		Mean		Mean ε	
		M	D	All GMPEs	BA08 GMPE
10% in 50	Updated	6.41	16.04	1.22	1.34
	GSC	6.43	25.77	1.40	-
2% in 50	Updated	6.74	8.32	1.37	1.48
	GSC	6.59	15.52	1.71	-
0.5% in 50	Updated	6.96	4.67	1.58	1.74
	GSC	7.03	13.41	1.89	-

Sa(0.5)		Mean		Mean ε	
		M	D	All GMPEs	BA08 GMPE
10% in 50	Updated	6.58	24.57	1.26	1.35
	GSC	6.75	34.70	1.24	-
2% in 50	Updated	6.83	12.95	1.38	1.48
	GSC	6.90	20.38	1.37	-
0.5% in 50	Updated	7.04	8.11	1.54	1.64
	GSC	7.01	11.76	1.52	-

Sa(1)		Mean		Mean ε	
		M	D	All GMPEs	BA08 GMPE
10% in 50	Updated	6.76	30.71	1.31	1.41
	GSC	6.96	51.17	1.31	-
2% in 50	Updated	6.95	14.86	1.43	1.56
	GSC	7.07	33.32	1.49	-
0.5% in 50	Updated	7.10	8.96	1.65	1.79
	GSC	7.11	19.65	1.59	-

Sa(2)		Mean		Mean ε	
		M	D	All GMPEs	BA08 GMPE
10% in 50	Updated	6.90	35.96	1.32	1.47
	GSC	6.92	63.45	1.39	-
2% in 50	Updated	7.07	15.71	1.42	1.59
	GSC	7.03	39.29	1.57	-
0.5% in 50	Updated	7.19	7.66	1.55	1.80
	GSC	7.14	29.33	1.79	-

Sa(3)		Mean		Mean ε	
		M	D	All GMPEs	BA08 GMPE
10% in 50	Updated	6.97	40.55	1.31	1.39
	GSC	-	-	-	-
2% in 50	Updated	7.14	18.38	1.39	1.57
	GSC	-	-	-	-
0.5% in 50	Updated	7.24	9.86	1.45	1.47
	GSC	-	-	-	-

Table C.3. Deaggregation results for only crustal events using all GMPEs and BA08 GMPE using exceeding method

Table C.4. Deaggregation results for only crustal events using all GMPEs and BA08 GMPE using matching method

PGA		Mean		Mean ε	
		M	D	All GMPEs	BA08 GMPE
10% in 50	Updated	6.23	21.80	1.12	1.22
	GSC	6.34	34.42	1.29	-
2% in 50	Updated	6.59	12.00	1.27	1.40
	GSC	6.48	17.70	1.58	-
0.5% in 50	Updated	6.82	5.57	1.24	1.40
	GSC	6.82	14.55	1.74	-

Sa(0.5)		Mean		Mean ε	
		M	D	All GMPEs	BA08 GMPE
10% in 50	Updated	6.43	33.59	1.19	1.25
	GSC	6.66	48.19	1.24	-
2% in 50	Updated	6.69	19.31	1.38	1.53
	GSC	6.79	24.66	1.30	-
0.5% in 50	Updated	6.92	10.50	1.30	1.49
	GSC	6.92	15.55	1.29	-

Sa(1)		Mean		Mean ε	
		M	D	All GMPEs	BA08 GMPE
10% in 50	Updated	6.65	43.91	1.26	1.31
	GSC	6.87	64.27	1.21	-
2% in 50	Updated	6.85	21.58	1.30	1.47
	GSC	6.99	40.30	1.31	-
0.5% in 50	Updated	7.09	13.26	1.41	1.66
	GSC	7.12	30.11	1.47	-

Sa(2)		Mean		Mean ε	
		M	D	All GMPEs	BA08 GMPE
10% in 50	Updated	6.78	50.18	1.26	1.29
	GSC	6.83	76.57	1.23	-
2% in 50	Updated	6.98	24.94	1.41	1.60
	GSC	6.97	50.70	1.45	-
0.5% in 50	Updated	7.17	11.60	1.33	1.71
	GSC	7.09	38.88	1.72	-

Sa(3)		Mean		Mean ε	
		M	D	All GMPEs	BA08 GMPE
10% in 50	Updated	6.87	56.10	1.24	1.26
	GSC	-	-	-	-
2% in 50	Updated	7.09	31.48	1.44	1.51
	GSC	-	-	-	-
0.5% in 50	Updated	7.10	14.17	1.44	1.72
	GSC	-	-	-	-

Table C.5. Deaggregation results for only interface events using all GMPEs, AB03 and Z06 GMPE using exceeding method

PGA		Mean		Mean ε		
		M	D	All GMPEs	AB03 GMPE	Z06 GMPE
10% in 50	Updated	8.58	141.42	1.55	2.21	1.40
	GSC	8.15	142.50	1.77	-	-
2% in 50	Updated	8.64	141.09	2.25	3.15	2.18
	GSC	8.15	142.50	2.51	-	-
0.5% in 50	Updated	8.76	140.12	2.71	-	2.67
	GSC	8.15	142.50	3.05	-	-

Sa(0.5)		Mean		Mean ε		
		M	D	All GMPEs	AB03 GMPE	Z06 GMPE
10% in 50	Updated	8.56	141.84	1.11	1.11	0.99
	GSC	8.15	142.50	1.39	-	-
2% in 50	Updated	8.63	142.23	1.83	2.10	1.66
	GSC	8.15	142.50	2.15	-	-
0.5% in 50	Updated	8.64	141.11	2.40	2.81	2.18
	GSC	8.15	142.50	2.74	-	-

Sa(1)		Mean		Mean ε		
		M	D	All GMPEs	AB03 GMPE	Z06 GMPE
10% in 50	Updated	8.56	141.97	0.94	0.94	0.72
	GSC	8.15	142.50	1.29	-	-
2% in 50	Updated	8.62	141.32	1.60	1.76	1.31
	GSC	8.15	142.50	1.98	-	-
0.5% in 50	Updated	8.67	140.62	2.08	2.33	1.79
	GSC	8.15	142.50	2.53	-	-

Sa(2)		Mean		Mean ε		
		M	D	All GMPEs	AB03 GMPE	Z06 GMPE
10% in 50	Updated	8.55	142.02	0.80	0.79	0.59
	GSC	8.15	142.50	1.35	-	-
2% in 50	Updated	8.61	141.99	1.47	1.59	1.17
	GSC	8.15	142.50	2.04	-	-
0.5% in 50	Updated	8.67	140.81	1.90	2.21	1.63
	GSC	8.15	142.50	2.54	-	-

Sa(3)		Mean		Mean ε		
		M	D	All GMPEs	AB03 GMPE	Z06 GMPE
10% in 50	Updated	8.55	142.07	0.68	1.11	0.46
	GSC	-	-	-	-	-
2% in 50	Updated	8.63	141.68	1.41	2.02	1.06
	GSC	-	-	-	-	-
0.5% in 50	Updated	8.70	141.47	1.89	2.76	1.56
	GSC	-	-	-	-	-

Table C.6. Deaggregation results for only interface events using all GMPEs, AB03 and Z06 GMPE using matching method

PGA		Mean		Mean ε		
		M	D	All GMPEs	AB03 GMPE	Z06 GMPE
10% in 50	Updated	8.56	142.42	1.17	1.77	0.87
	GSC	8.15	142.50	1.37	-	-
2% in 50	Updated	8.61	140.15	1.93	3.15	1.77
	GSC	8.15	142.50	2.24	-	-
0.5% in 50	Updated	8.73	142.88	2.41	-	2.31
	GSC	8.15	142.50	2.88	-	-

Sa(0.5)		Mean		Mean ε		
		M	D	All GMPEs	AB03 GMPE	Z06 GMPE
10% in 50	Updated	8.53	141.98	0.55	0.42	0.33
	GSC	8.15	142.50	0.90	-	-
2% in 50	Updated	8.59	142.62	1.37	1.47	1.18
	GSC	8.15	142.50	1.84	-	-
0.5% in 50	Updated	8.62	141.89	2.00	2.26	1.79
	GSC	8.15	142.50	2.41	-	-

Sa(1)		Mean		Mean ε		
		M	D	All GMPEs	AB03 GMPE	Z06 GMPE
10% in 50	Updated	8.52	142.66	0.33	0.20	0.01
	GSC	8.15	142.50	0.81	-	-
2% in 50	Updated	8.59	142.08	1.21	1.19	0.82
	GSC	8.15	142.50	1.63	-	-
0.5% in 50	Updated	8.64	141.65	1.71	1.94	1.38
	GSC	8.15	142.50	2.25	-	-

Sa(2)		Mean		Mean ε		
		M	D	All GMPEs	AB03 GMPE	Z06 GMPE
10% in 50	Updated	8.49	142.12	0.10	-0.03	-0.25
	GSC	8.15	142.50	0.91	-	-
2% in 50	Updated	8.56	142.34	1.13	1.10	0.71
	GSC	8.15	142.50	1.62	-	-
0.5% in 50	Updated	8.61	141.43	1.62	1.84	1.24
	GSC	8.15	142.50	2.29	-	-

Sa(3)		Mean		Mean ε		
		M	D	All GMPEs	AB03 GMPE	Z06 GMPE
10% in 50	Updated	8.47	142.49	-0.01	0.48	-0.26
	GSC	8.15	142.50	0.65	-	-
2% in 50	Updated	8.57	142.11	1.01	1.60	0.58
	GSC	8.15	142.50	1.44	-	-
0.5% in 50	Updated	8.64	142.61	1.53	2.33	1.15
	GSC	8.15	142.50	1.97	-	-

Table C.7. Deaggregation results for only inslab events using all GMPEs, AB03 and Z06 GMPE using exceeding method

PGA		Mean		Mean ε		
		M	D	All GMPEs	AB03 GMPE	Z06 GMPE
10% in 50	Updated	6.77	68.29	1.29	1.20	1.32
	GSC	6.18	75.59	1.71	-	-
2% in 50	Updated	6.93	61.71	1.72	1.74	1.67
	GSC	6.28	70.39	2.17	-	-
0.5% in 50	Updated	7.00	57.23	2.06	2.21	1.96
	GSC	6.34	67.43	2.54	-	-

Sa(0.5)		Mean		Mean ε		
		M	D	All GMPEs	AB03 GMPE	Z06 GMPE
10% in 50	Updated	6.86	63.38	1.39	1.28	1.43
	GSC	6.43	79.51	1.63	-	-
2% in 50	Updated	6.99	55.24	1.79	1.76	1.78
	GSC	6.56	75.21	2.11	-	-
0.5% in 50	Updated	7.09	51.23	2.09	2.20	2.03
	GSC	6.61	72.78	2.53	-	-

Sa(1)		Mean		Mean ε		
		M	D	All GMPEs	AB03 GMPE	Z06 GMPE
10% in 50	Updated	6.95	63.76	1.30	1.14	1.49
	GSC	6.53	81.59	1.60	-	-
2% in 50	Updated	7.08	55.51	1.75	1.62	1.97
	GSC	6.64	76.08	2.07	-	-
0.5% in 50	Updated	7.12	49.93	2.17	1.98	2.45
	GSC	6.72	72.34	2.44	-	-

Sa(2)		Mean		Mean ε		
		M	D	All GMPEs	AB03 GMPE	Z06 GMPE
10% in 50	Updated	7.03	67.61	1.29	1.18	1.59
	GSC	6.57	85.00	1.75	-	-
2% in 50	Updated	7.14	57.93	1.75	1.68	2.06
	GSC	6.70	77.72	2.13	-	-
0.5% in 50	Updated	7.23	54.67	2.16	2.05	2.99
	GSC	6.83	73.38	2.43	-	-

Sa(3)		Mean		Mean ε		
		M	D	All GMPEs	AB03 GMPE	Z06 GMPE
10% in 50	Updated	7.07	69.29	1.36	1.22	1.67
	GSC	6.51	90.13	1.64	-	-
2% in 50	Updated	7.20	57.59	1.76	1.65	2.06
	GSC	6.66	84.14	2.12	-	-
0.5% in 50	Updated	7.28	55.63	2.30	2.24	2.47
	GSC	6.73	81.21	2.52	-	-

Table C.8. Deaggregation results for only inslab events using all GMPEs, AB03 and Z06 GMPE using matching method

PGA		Mean		Mean ε		
		M	D	All GMPEs	AB03 GMPE	Z06 GMPE
10% in 50	Updated	6.64	73.47	1.03	0.88	1.12
	GSC	6.11	79.37	1.40	-	-
2% in 50	Updated	6.86	65.67	1.41	1.34	1.41
	GSC	6.22	72.01	1.88	-	-
0.5% in 50	Updated	6.96	60.47	1.81	1.88	1.76
	GSC	6.32	71.05	2.30	-	-

Sa(0.5)		Mean		Mean ε		
		M	D	All GMPEs	AB03 GMPE	Z06 GMPE
10% in 50	Updated	6.78	70.60	1.13	1.01	1.17
	GSC	6.32	84.01	1.33	-	-
2% in 50	Updated	6.91	58.36	1.59	1.57	1.55
	GSC	6.50	76.81	1.80	-	-
0.5% in 50	Updated	7.04	52.94	1.85	1.83	1.82
	GSC	6.60	74.95	2.23	-	-

Sa(1)		Mean		Mean ε		
		M	D	All GMPEs	AB03 GMPE	Z06 GMPE
10% in 50	Updated	6.84	70.17	1.10	0.95	1.23
	GSC	6.42	85.63	1.32	-	-
2% in 50	Updated	7.00	57.61	1.53	1.34	1.77
	GSC	6.60	78.71	1.74	-	-
0.5% in 50	Updated	7.12	53.12	1.85	1.82	1.85
	GSC	6.67	74.77	2.15	-	-

Sa(2)		Mean		Mean ε		
		M	D	All GMPEs	AB03 GMPE	Z06 GMPE
10% in 50	Updated	6.95	75.42	1.06	0.91	1.40
	GSC	6.46	88.82	1.48	-	-
2% in 50	Updated	7.10	61.72	1.45	1.34	1.78
	GSC	6.64	83.12	1.89	-	-
0.5% in 50	Updated	7.13	56.29	1.99	1.79	2.69
	GSC	6.73	75.10	2.19	-	-

Sa(3)		Mean		Mean ε		
		M	D	All GMPEs	AB03 GMPE	Z06 GMPE
10% in 50	Updated	6.98	75.55	1.13	1.00	1.41
	GSC	-	-	-		-
2% in 50	Updated	7.15	63.71	1.60	1.47	2.06
	GSC	-	-	-	-	-
0.5% in 50	Updated	7.20	51.35	2.02	1.90	2.17
	GSC	-	-	-	-	-

Appendix D: Computer program for different record selection methods and predictions of CMS

A computer program was developed which is capable of selecting ground motion records using several record selection methodologies. The information for a large pool of records, compiled by combining the records from different sources including PEER-NGA, K-NET, KiK-NET, and COSMOS databases, was incorporated in the program. The records from three different earthquake types (i.e., crustal, interface, and inslab) are included.

The program inputs and options:

- Target period: The target period, T_1, is typically the fundamental period of the structure.
- Period range to match: If UHS-based or CMS-based record selection methods are selected, the minimum and maximum range of periods for spectrum matching should be assigned. This is typically taken as $0.2T_1$ to $2T_1$.
- Number of records: The number of required records to be selected are given
- Record type: Four options for record types are available including crustal, interface, inslab, and all types. For example if "inslab" is chosen, the program only selects the inslab records in the database and if "all" is selected, the program search all the database without any limitations on the earthquake type.
- Scaling option: The records can be selected with or without scaling. If scaling is enabled, a better matching will typically obtained and if scaling is disabled only original records will be used to match the target spectrum.
- Response matching option: An option is available to choose whether the geometric means of the pairs of the records spectra or the individual record spectra are used for spectrum matching.
- Database option: The data base can also be selected to determine whether the records should be searched within a specific database or all databases should be searched for record selection.

- Ranges of record parameters: Limitations on the minimum and maximum range of different record parameters including record magnitude, distance, shear wave velocity (V_{s30}), peak ground acceleration (PGA) and peak ground velocity (PGV) can be imposed.
- Based on the record selection method to be used, the results from the seismic deaggregation (which is computed using the deaggregation calculator program described in Appendix C) are given to the program. Such results include the UHS or CMS (including CMS-crustal, CMS-interface, CMS-inslab, and CMS-All), the contribution of each event types to the overall seismic hazard, the mean magnitude, distance and epsilon, for different event types.

The main functions of the program are summarized as follows:

Record selection methodologies:
The program can choose the desired number of records based on different methodologies including:

a) UHS-based and CMS-based record selection:

The uniform hazard spectrum (UHS) and conditional mean spectrum (CMS) are computed using the deaggreagtion calculator program (Appendix C) and the information will be given to this program. The records that most closely match the defined spectra over a range of periods (which is defined for the program) will be selected. The information of these records in addition to the response spectra and the average response spectra of the records will be determined.

b) Epsilon-based record selection:
The program can compute the epsilon values of the records at different periods using different GMPEs which will be used for the epsilon-based record selection.

c) MR-based record selection:
In this method the records with the closest magnitude and distance to the mean magnitude and distance from the seismic deaggregation will be selected.

d) All-based and event-based methods:

For record selection methods discussed, the selection can either be carried out using "All-based" procedure or "Event-based" procedure. For the "Event-based" procedure the number of records from each earthquake type will be proportional to the percentage of contribution of that event type to the overall seismic hazard and thus the record selection will be carried out for each event types separately and the required number of records will be selected for each earthquake types. In "All-based" procedure no limitation on the type of record is imposed and the records from all earthquake types can be selected.

Other outputs of the program:

a) The list of selected records and detailed information of records:
A list of the required number of records that match the criteria will be determined along with all required record data. The average response spectrum of the records will be calculated and the response spectrum of individual records will also be printed. If the scale factors are allowed the required scale factor for each record will be printed. In the epsilon-based record method the epsilon values of the records at the fundamental period and the average epsilon value of the record sets will be computed. The sum of the square errors (SSE) which denotes the error in matching will be computed for each record and the records will be sorted in the order of lowest to largest SSE.

b) Response spectrum of records:
A subroutine is incorporated which computes the elastic response spectra of the records for the desired period ranges and damping ratios.

c) Epsilon values of the records:
The epsilon values will be computed for each record at different vibration periods. The ground motion prediction equations (GMPE) specific for each event type are used to compute the epsilon values.

d) Changing the format of the records:

Some subroutines were incorporated to read the earthquake record files with different formats and convert it to the desirable formats or the formats compatible with the RUAUMOKO program. The format of records here is referred to the way the acceleration histories and time are written in the ground motion record file (e.g., Number of columns in each row, whether time steps are included or not, etc.)

e) Output for the RUAUMOKO program:

The selected records data will also be printed out in a format compatible with the RUAUMOKO program which will be used in the main program (Appendix B) for the structural analyses.

Appendix E: Dynaplot helper

After performing the nonlinear analyses using the RUAUMOKO program, it is very difficult to view the details of the analyses such as hysteresis loops of elements, displacement and force histories. To view such results from RUAUMOKO program one should use a program called Dynaplot (Carr, 2009). To do this the information of the structures and elements should be given to the program one by one which is very time consuming. Moreover, if any mistake occurs all the information should be given from the beginning. The use of such methods to control the accuracy of the structural analyses and hysteresis loops of elements can be extremely time consuming.

To facilitate the inspection of various parameters from the structural analyses, a computer code was developed which creates all the required input files for the Dynaplot software, execute the program, extract the results and show the results along with the graphs in excel sheets. Therefore the required analysis details can be viewed only by pressing the execute bottom in the program.

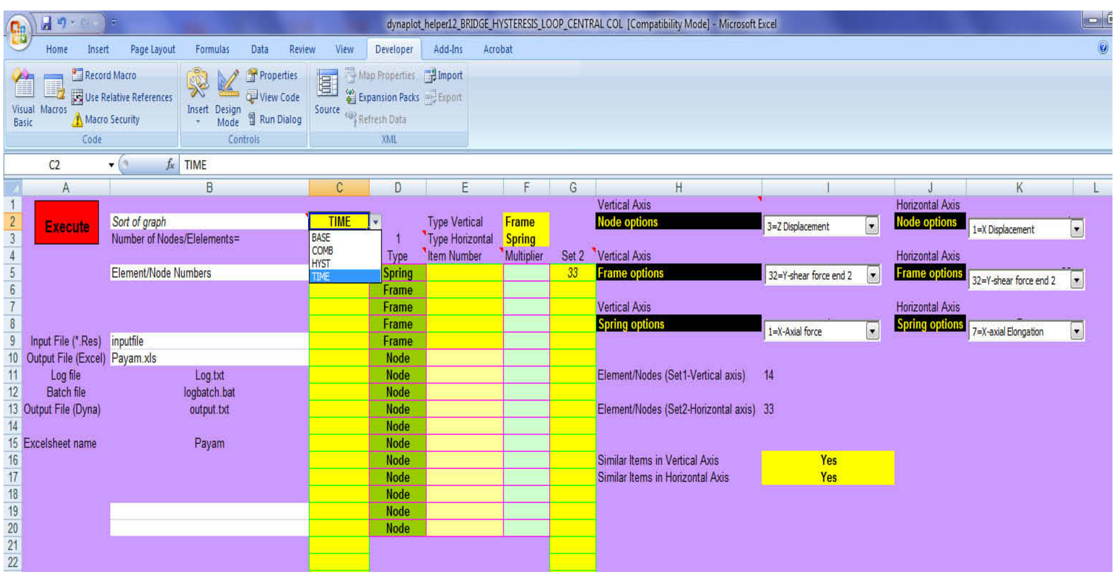

Fig. F.1. A view of the Dynaplot-helper program

Appendix F: Different earthquake types

In common practice for seismic assessment of the structures crustal earthquake records, such as those available in PEER-NGA database, are mainly used and little attention has been given to other earthquake types that can play an important role in seismic performance assessment of the structures located near subduction zones such as the Cascadia subduction zone. The Cascadia subduction zone extends from northern Vancouver island to northern California and separates the Juan de Fuca tectonic plate and the North America plates (see Fig. F.1). Major cities affected by this subduction zone include Vancouver and Victoria, British Columbia, Seattle, Washington, Portland, Oregon, and Sacramento California.

Seismic hazard for the Strait of Georgia region of British Columbia (including Vancouver, Victoria and a substantial fraction of B.C.'s population) comes from three sources of earthquakes as shown in Fig. F.2. These sources include the crustal seismicity in the North American plate, great earthquakes of the Cascadia subduction zone on the interface between the North American and subducting Juan de Fuca plate(i.e., subduction interface or subduction thrust earthquakes) and deep earthquakes within the subducting slab (i.e., inslab earthquakes). Therefore, in addition to the common crustal earthquakes, for a site located in Vancouver at least two other earthquake types resulting from the Cascadia subduction zone (i.e., interface and inslab earthquakes) should be considered in seismic hazard evaluations, structural analyses, and risk assessments.

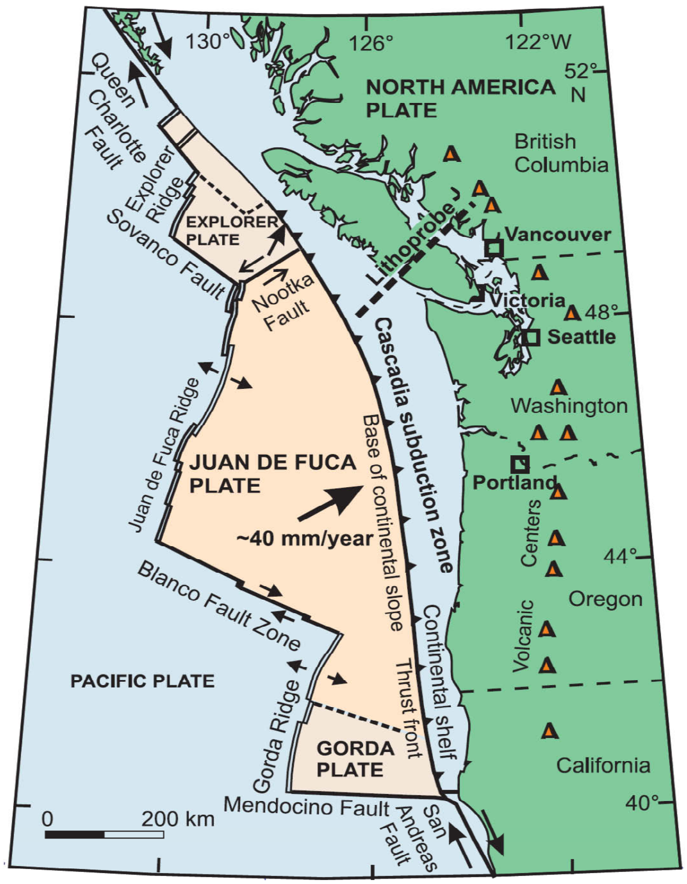

Fig. F.1. Juan de Fuca plate and Cascadia subduction zone (from Hyndman and Rogers, 2010)

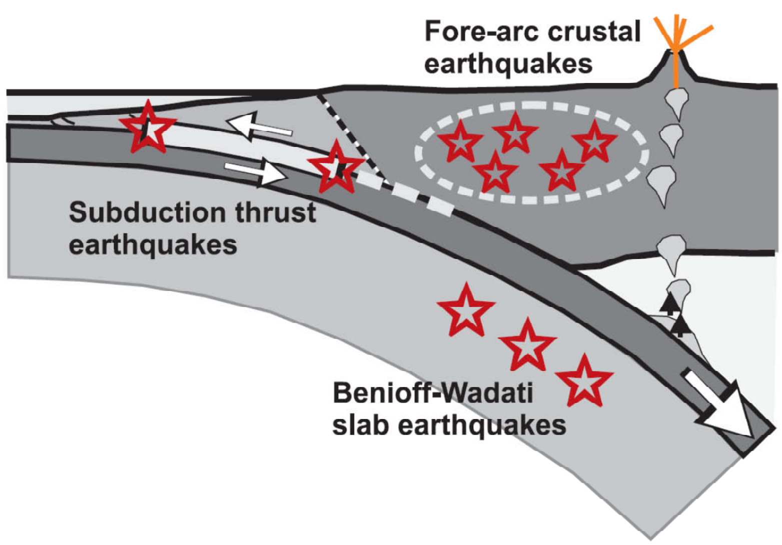

Fig. F.2. Three earthquake types of the Cascadia subduction zone (Hyndman and Rogers, 2010)

Interface earthquakes (also known as Megathrust and interplate earthquakes)

Interface (megathrust) earthquakes occur at subduction zones at destructive plate boundaries where one tectonic plate is forced under (subducts) another (at the interface of the tectonic plates) as shown in Fig. F.2 and Fig. F.3. The interface earthquakes are among the largest earthquakes possible in the world. The moment magnitudes of such earthquakes can exceed 9.0. All of the past earthquakes in the globe with magnitude of 9.0 and greater have been interface earthquakes and no other known tectonic activity can produce earthquakes with such large magnitudes.

It is recognized that the coast of British Columbia and the US pacific northwest has substantial earthquake hazard however until the mid 1980s the risk of great subduction interface (mega thrust) events was not appreciated, because no great earthquakes of this type was available in the written historical record. The evidence that there is indeed active subduction under thrusting was summarized by Riddihough and Hyndman (1976) and the case for great earthquakes was made more than 20 years ago (e.g, Heaton and Kanamori 1984; Heaton and Hartzell 1987; Rogers 1988). Although supporting data were limited, the accumulated evidence has left little doubt that great earthquakes and associated tsunamis have occurred many times in the past and that they will occur and produce damage in the future (Hyndman and Rogers, 2010).

Very few earthquakes of any size have been detected on the Cascadia subduction thrust. In general the lack of any subduction interface (thrust) earthquakes is not common. Most of the world's great earthquakes with magnitude of M>8 have occurred on subduction zone thrust faults, and most subduction zones have experienced historical great earthquakes. However some subduction zones that have had the largest earthquakes (e.g., M=9 Sumatra in 2004, Alaska in 1964, Chile in 1960, and Kamchatka in 1952) also have had very long time intervals between the events, while just a few small interface earthquakes occurred between these intervals.

For Cascadia, the written historical record is short, with only a little more than 200 years. This limited written history is in clear contrast to the detailed Japanese record of great subduction zone earthquakes and tsunami waves that extends back to the 7th century.

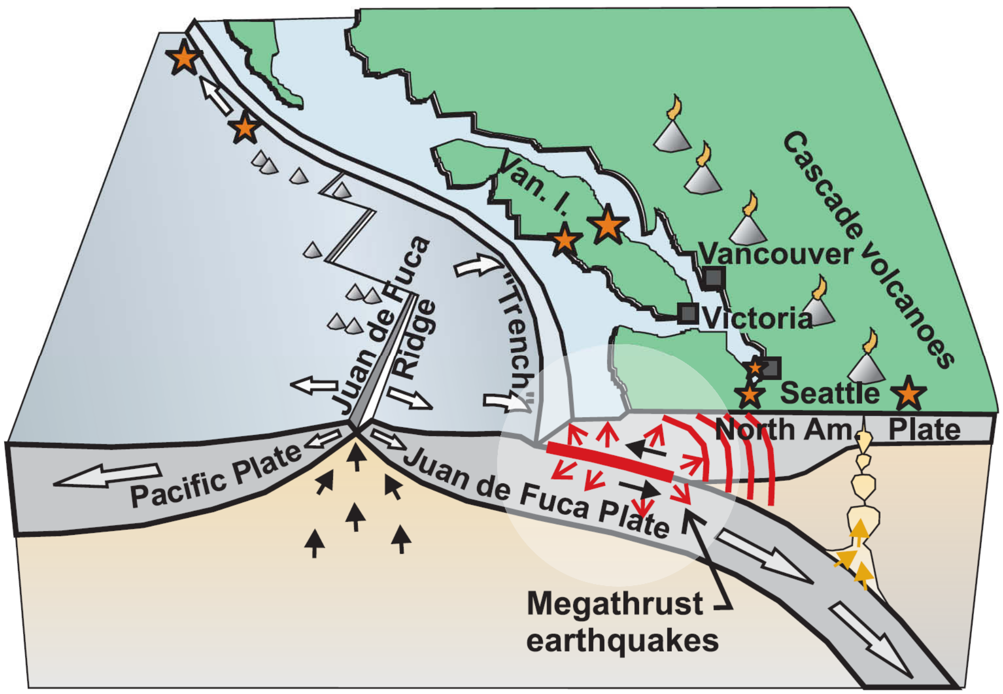

Fig. F.3. Schematic cross-section of the Cascadia subduction and megathrust (interface) earthquake zone and the epicentres of some larger historical earthquakes (Hyndman and Rogers, 2010).

There are three possible explanations for the lack of historical Cascadia great earthquakes:

(1) the Juan de Fuca plate is no longer converging and underthrusting North America
(2) Underthrusting is continuing, but it is accommodated by smooth stable sliding
(3) The thrust fault is completely locked with not enough motion to generate even small earthquakes.

Unlike the first two options, the third option implies that there is a potential for very large and damaging earthquakes that has not been included in hazard estimates until recently. Riddihough and Hyndman (1976) compiled a variety of evidence against the fist option (i.e., no convergence) indicating that there is ongoing convergence and underthrusting and since then the evidence has become conclusive. The debate over the second possibility, smooth aseismic underthrusting, continued until recently. Again the contrary evidence is now strong, especially from paleoseismicity, the traces of past great earthquakes preserved in the coastal and deep sea geological record and from measurements of present elastic strain building up in the continent near the coast. The observed deformation corresponds to that expected for a locked thrust fault.
Thus based on the available variety of evidence the third option has a strong possibility in which great earthquakes do occur, but the last one was more than 200 years ago, prior to the historical written record (Hyndman and Rogers, 2010).

The evidence based on the repeated sediment deposits on the floor of the Cascadia deep sea basin indicate that the most recent major event was about 300 years ago. The intervals for the last 13 events range mostly from about 300 to 900 years. This very long intervals between Cascadia events compared with most subduction zones means that there is large elastic strain build up and thus very large earthquake slip and large magnitude.
For the Cascadia subduction zone, the rate of convergence between the Juan de Fuca plate and North American plate is about 40 mm/year (Riddihough, 1984). This convergence represents an average rupture displacement of about 20m if the event interval is 500 years on average.

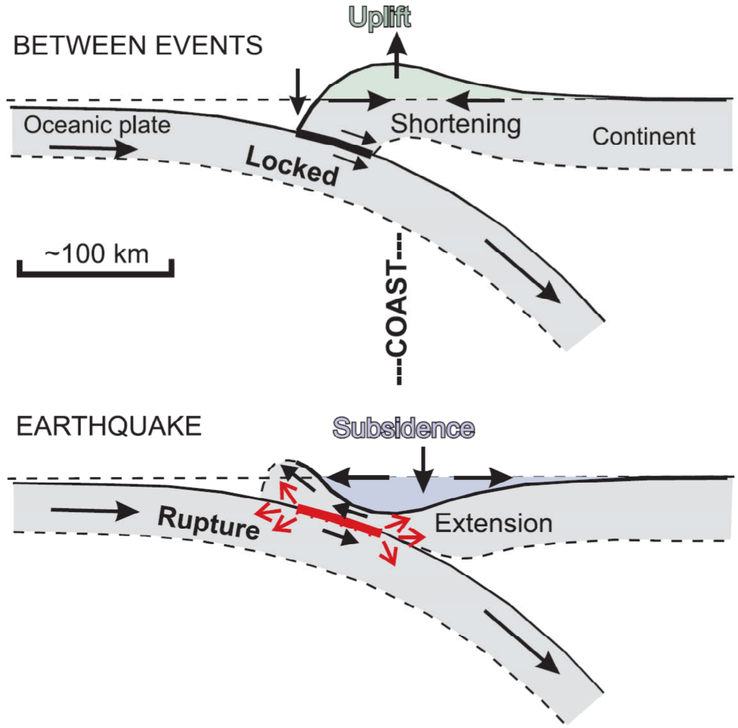

Fig.F.4. Simplified model of great earthquake elastic strain build up and release (Hyndman and Rogers, 2010)

In the simple subduction earthquake model, ongoing convergence drags down the seaward nose of the continent and causes an upward flexural bulge (Fig. F.4). There also is a region of crustal shortening (Fig. F.4). At the time of the earthquake, the edge of the continent springs back seaward and the bulge collapses downward. The abrupt coseismic uplift of the outer continental shelf and slope and subsidence near the coast are the main cause of the great tsunamis. The collapse of the flexural bulge causes the sudden coastal subsidence recorded in buried intertidal marshes (Hyndman and Rogers, 2010).

Inslab earthquakes (also known as intraplate, intraslab and Wadati-Benioff slab earthquakes)

There are two regions of observed deep seismicity in the Cascadia system: one just north of the Mendocino triple junction and another under the Puget lowlands/ Georgia Strait. Large intraslab earthquakes, by virtue of their frequency of occurrence, locations directly beneath population centers and source characteristics, represent a major earthquake hazard in the Cascadia subduction zone. Investigations to date of intraslab earthquake sources worldwide show that they tend to be enriched in high-frequency energy compared to nearby interplate thrust earthquakes (i.e., interface earthquakes) of comparable scalar seismic moment. Subduction in some particular regions, such as Mexico, Peru and Chile has produced many large (M>7.0–8.0) and very destructive slab earthquakes probably in the subducted slab mantle. These events are sometimes exceptionally enriched in high-frequency energy, a factor that contributes to their destructiveness. These unusual regions may involve down dip changes in the sign of slab curvature (implied by their flat-slab geometry that occurs in some of those localities). The normal-faulting focal mechanisms of these events are consistent with reverse-curvature flexure in the slab mantle but the physical mechanisms for faulting in such settings are not known (Kirby et al., 2002).

Inslab earthquakes (earthquakes within the subducting Juan de Fuca plate) also make a major contribution to seismic hazard for the Strait of Georgia region of British Columbia. Key knowledge of in-slab earthquakes needed to improve seismic hazard estimates for southwestern British Columbia includes the constraints on the spatial distribution, rate and maximum size of the earthquakes, the ground motions to be expected, the nature of the earthquake sources and the structure and properties of the lithosphere through which the waves propagate (Adams and Halchuk, 2002). Relatively little knowledge is available about this type of earthquake.

In Canada’s fourth generation seismic hazard model (see Adams et al., 1999a, 1999b and 2000), these earthquakes dominate the hazard despite their greater depth, firstly because they occur at a rate up to five-fold higher per unit area than the shallower crustal earthquakes, and secondly, because their predicted shaking is stronger than crustal events of the same size (Adams and Halchuk, 2002).

The largest historical inslab event occurred in 1949, of moment magnitude about 6.9. Compared with recent earthquakes, almost nothing is known about the rupture parameters of this earthquake, such as its depth extent, fault length or stress drop. Some geophysical constraints such as temperature in the slab are believed to limit the thickness of brittle rock thus restricting fault width; larger earthquakes therefore require greater fault lengths or greater slip (or both). The GSC model currently allows an upper bound magnitude of 7.3 for Puget Sound (with an uncertainty range of 7.1–7.6), presuming that a future large earthquake could extend deeper into the slab, or have larger displacement, or rupture a longer fault. In 1997, the USGS adopted an upper bound magnitude of 7.0. Because of the high rate for these large earthquakes, their contribution to the total seismic hazard is not trivial (for the GSC's results, about 14–24% of the seismic hazard, dependent on model, comes from earthquakes larger than the 1949 one) (Adams and Halchuk, 2002).

Different assumptions were adopted by the USGS in 1997 and the GSC in 1994–1999 and resulted in different estimates of seismic hazard for the U.S. and Canadian territory overlying these inslab earthquakes. This indicates that the knowledge about this earthquake type needs to be improved.

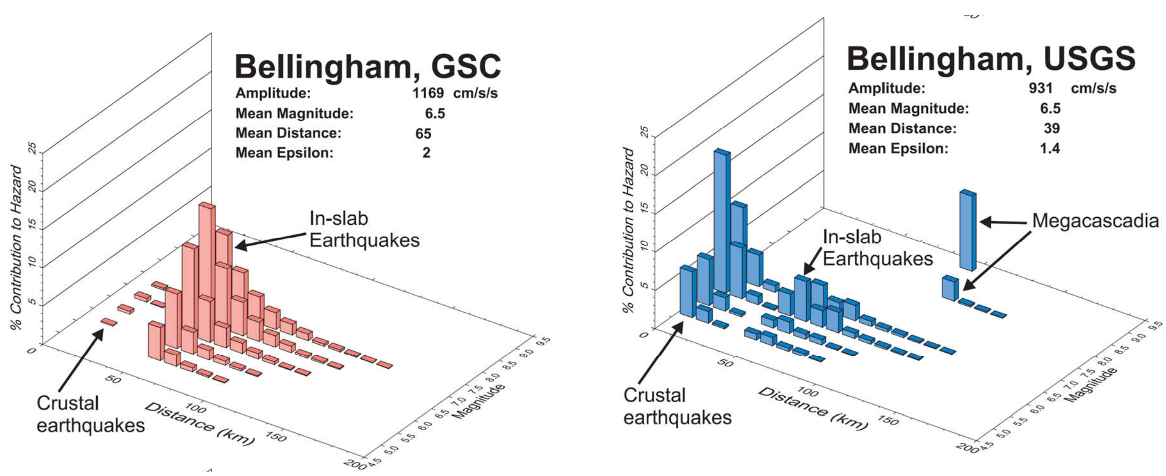

Fig. F.5. Seismic hazard deaggregations of 0.2 second spectral acceleration values at 2%/50 years for Bellingham show the GSC results are dominated by the contribution from in-slab earthquakes, unlike the 1997 USGS results (Adams and Halchuk (2002)).

The seismic hazard analyses by Goda et al., (2010) using updated seismic data indicates that the significance of the interface earthquakes are underestimated by the current model of the Geological Survey of Canada (e.g., see the deaggregation results given in Appendix C) and this event type contributes significantly to the overall seismic hazard at medium to long period ranges.

Appendix G: Detailed information of the ground motion records used

NO.	Eq. Name	Record ID	Event ID	Type	Mag. (M)	Epicentral Dist. (Km)	Focal depth	V_{s30}	PGA	PGV	Database
1	Northridge	953	127	Crustal	6.69	17.15	17.5	356	0.46	54	NGA
2	Northridge	960	127	Crustal	6.69	12.44	17.5	309	0.44	45	NGA
3	Duzce, Turkey	1602	138	Crustal	7.14	12.04	10	326	0.72	59	NGA
4	Hector Mine	1787	158	Crustal	7.13	11.66	5	685	0.31	34	NGA
5	Imperial Valley	169	50	Crustal	6.53	22.03	9.96	275	0.28	28	NGA
6	Imperial Valley	174	50	Crustal	6.53	12.45	9.96	196	0.37	37	NGA
7	Kobe, Japan	1111	129	Crustal	6.9	7.08	17.9	609	0.49	36	NGA
8	Kobe, Japan	1116	129	Crustal	6.9	19.15	17.9	256	0.23	34	NGA
9	Kocaeli, Turkey	1158	136	Crustal	7.51	15.37	15	276	0.32	54	NGA
10	Kocaeli, Turkey	1148	136	Crustal	7.51	13.49	15	523	0.17	28	NGA
11	Landers	900	125	Crustal	7.28	23.62	7	354	0.21	38	NGA
12	Landers	848	125	Crustal	7.28	19.74	7	271	0.35	32	NGA
13	Loma Prieta	752	118	Crustal	6.93	15.23	17.48	289	0.48	34	NGA
14	Loma Prieta	767	118	Crustal	6.93	12.82	17.48	350	0.47	42	NGA
15	Manjil, Iran	1633	144	Crustal	7.37	12.56	19	724	0.52	47	NGA
16	Superstition Hills	721	116	Crustal	6.54	18.2	9	192	0.29	43	NGA
17	Superstition Hills	725	116	Crustal	6.54	11.16	9	207	0.37	32	NGA
18	Cape Mendocino	829	123	Crustal	7.01	14.33	9.6	312	0.44	45	NGA
19	Chi-Chi, Taiwan	1244	137	Crustal	7.62	9.96	6.76	259	0.39	91	NGA
20	Chi-Chi, Taiwan	1485	137	Crustal	7.62	26	6.76	705	0.47	39	NGA
21	San Fernando	68	30	Crustal	6.61	22.77	13	316	0.20	18	NGA
22	Friuli, Italy	125	40	Crustal	6.5	15.82	5.1	425	0.34	26	NGA
23	Northridge	1003	127	Crustal	6.69	27.01	17.5	309	0.45	35	NGA
24	Northridge	1077	127	Crustal	6.69	26.45	17.5	336	0.58	32	NGA
25	Northridge	952	127	Crustal	6.69	18.36	17.5	546	0.51	34	NGA
26	Imperial Valley	162	50	Crustal	6.53	10.45	9.96	231	0.24	19	NGA
27	Imperial Valley	189	50	Crustal	6.53	9.64	9.96	339	0.38	23	NGA
28	Kobe, Japan	1107	129	Crustal	6.9	22.5	17.9	312	0.27	22	NGA
29	Kobe, Japan	1106	129	Crustal	6.9	0.96	17.9	312	0.71	78	NGA
30	Landers	864	125	Crustal	7.28	11.03	7	379	0.26	35	NGA
31	Loma Prieta	783	118	Crustal	6.93	74.26	17.48	249	0.28	42	NGA
32	Loma Prieta	776	118	Crustal	6.93	27.93	17.48	371	0.28	45	NGA
33	Loma Prieta	777	118	Crustal	6.93	27.6	17.48	199	0.23	42	NGA
34	Loma Prieta	778	118	Crustal	6.93	24.82	17.48	216	0.28	40	NGA
35	Superstition Hills	728	116	Crustal	6.54	13.03	9	194	0.21	27	NGA
36	Chi-Chi, Taiwan	1524	137	Crustal	7.62	45.18	6.76	447	0.53	56	NGA
37	Chi-Chi, Taiwan	1506	137	Crustal	7.62	19.02	6.76	401	0.21	56	NGA
38	Chi-Chi, Taiwan	1595	137	Crustal	7.62	9.96	6.76	259	0.39	72	NGA
39	Chi-Chi, Taiwan	1182	137	Crustal	7.62	9.77	6.76	438	0.36	52	NGA

Table. G.1. Details of the 39 pairs of ground motions from crustal earthquakes

No.	Record ID	Event ID	Type	Mag. (M)	Epicentral Dist. (Km)	Focal depth	V_{s30}	PGA	PGV	Record file name	Database
1	27538	368	Inslab	6.8	111.88	120	390	0.85	23	IWTH020807240026.NS(EW)	K-KIK
2	27548	368	Inslab	6.8	117.20	120	368	0.71	21	IWTH120807240026.NS(EW)	K-KIK
3	27539	368	Inslab	6.8	108.12	120	733	0.52	14	IWTH030807240026.NS(EW)	K-KIK
4	27451	368	Inslab	6.8	114.01	120	392	0.48	16	IWT0070807240026.NS(EW)	K-KIK
5	27557	368	Inslab	6.8	109.86	120	521	0.47	17	IWTH210807240026.NS(EW)	K-KIK
6	27545	368	Inslab	6.8	112.09	120	967	0.48	12	IWTH090807240026.NS(EW)	K-KIK
7	9815	184	Inslab	7	68.78	71	456	0.74	31	IWTH040305261824.NS(EW)	K-KIK
8	9697	184	Inslab	7	63.77	71	392	0.80	19	IWT0070305261824.NS(EW)	K-KIK
9	9813	184	Inslab	7	117.21	71	390	0.75	19	IWTH020305261824.NS(EW)	K-KIK
10	9839	184	Inslab	7	53.87	71	934	0.74	13	MYGH030305261824.NS(EW)	K-KIK
11	9837	184	Inslab	7	58.16	71	670	0.72	15	IWTH270305261824.NS(EW)	K-KIK
12	9841	184	Inslab	7	103.06	71	305	0.61	25	MYGH050305261824.NS(EW)	K-KIK
13	9831	184	Inslab	7	79.59	71	521	0.58	20	IWTH210305261824.NS(EW)	K-KIK
14	6301	141	Inslab	6.8	69.64	51	469	0.60	24	HRS0090103241528.NS(EW)	K-KIK
15	6494	141	Inslab	6.8	45.57	51	362	0.52	15	EHMH050103241528.NS(EW)	K-KIK
16	6306	141	Inslab	6.8	58.31	51	247	0.41	33	HRS0140103241528.NS(EW)	K-KIK
17	6510	141	Inslab	6.8	72.32	51	487	0.46	16	HRSH030103241528.NS(EW)	K-KIK
18	6267	141	Inslab	6.8	46.89	51	268	0.39	25	EHM0030103241528.NS(EW)	K-KIK
19	20480	294	Inslab	6	52.26	52	282	0.15	13	CHB0100504110722.NS(EW)	K-KIK
20	19650	285	Inslab	6.2	79.79	50	272	0.14	10	HKD0680501182309.NS(EW)	K-KIK
21	WA: Olympia, WSDOT Test Lab	Nisqually	Inslab	6.8	55.50	52.4	187	0.24	19	20010228_1.corrected.0730a_a.smc (0730c)	cosmos
22	Seattle, WA Seatac Airport FS	Nisqually	Inslab	6.8	69.27	52.4	347	0.16	15	20010228_1.corrected.1421a_a.smc (1421c)	cosmos
23	27550	368	Inslab	6.8	108.95	120	816	0.40	13	IWTH140807240026.NS(EW)	K-KIK
24	27554	368	Inslab	6.8	109.02	120	892	0.39	14	IWTH180807240026.NS(EW)	K-KIK
25	27463	368	Inslab	6.8	108.19	120	367	0.35	21	IWT0190807240026.NS(EW)	K-KIK
26	27544	368	Inslab	6.8	119.26	120	305	0.35	15	IWTH080807240026.NS(EW)	K-KIK
27	27460	368	Inslab	6.8	108.08	120	439	0.36	14	IWT0160807240026.NS(EW)	K-KIK
28	9840	184	Inslab	7	64.68	71	850	0.59	16	MYGH040305261824.NS(EW)	K-KIK
29	9816	184	Inslab	7	63.91	71	429	0.55	15	IWTH050305261824.NS(EW)	K-KIK
30	9836	184	Inslab	7	86.50	71	371	0.51	20	IWTH260305261824.NS(EW)	K-KIK
31	9833	184	Inslab	7	63.95	71	923	0.48	14	IWTH230305261824.NS(EW)	K-KIK
32	9828	184	Inslab	7	78.84	71	892	0.46	13	IWTH180305261824.NS(EW)	K-KIK
33	6270	141	Inslab	6.8	38.10	51	258	0.40	20	EHM0070103241528.NS(EW)	K-KIK
34	6311	141	Inslab	6.8	43.35	51	211	0.37	21	HRS0190103241528.NS(EW)	K-KIK
35	6278	141	Inslab	6.8	59.69	51	280	0.29	30	EHM0150103241528.NS(EW)	K-KIK
36	6493	141	Inslab	6.8	46.06	51	254	0.33	21	EHMH040103241528.NS(EW)	K-KIK
37	WA: West Seattle; F S 29	Nisqually	Inslab	6.8	74.82	52.4	328	0.15	15	20010228_1.corrected.1416a_a.smc (1416c)	cosmos
38	WA: Bremerton; Fire Station	Nisqually	Inslab	6.8	69.33	52.4	463	0.18	12	20010228_1.corrected.1422a_a.smc (1422c)	cosmos
39	WA: Gig Harbor Fire Station	Nisqually	Inslab	6.8	56.19	52.4	416	0.11	12	20010228_1.corrected.0725a_a.smc (0725c)	cosmos

Table. G.2. Details of the 39 pairs of ground motions from subduction inslab earthquakes

NO.	Record ID	Event ID	Type	Mag. (M)	Epicentral Dist. (Km)	Focal depth	V_{s30}	PGA	PGV	Record file name	Data base
1	19085	276	Interface	7	79.98	48	326	0.665	24.60	KSRH060411290332.NS (.EW)	K-KIK
2	19004	276	Interface	7	93.02	48	311	0.342	20.18	HKD0800411290332.NS (.EW)	K-KIK
3	19002	276	Interface	7	73.08	48	243	0.296	24.19	HKD0780411290332.NS (.EW)	K-KIK
4	11026	194	Interface	7.9	119.95	42	213	0.568	36.60	KSRH100309260450.NS (.EW)	K-KIK
5	11025	194	Interface	7.9	62.65	42	230	0.387	60.15	KSRH090309260450.NS (.EW)	K-KIK
6	11020	194	Interface	7.9	110.04	42	250	0.501	29.72	KSRH030309260450.NS (.EW)	K-KIK
7	11019	194	Interface	7.9	73.17	42	219	0.396	45.67	KSRH020309260450.NS (.EW)	K-KIK
8	19266	278	Interface	6.7	58.62	46	213	0.390	19.30	KSRH100412062315.NS (.EW)	K-KIK
9	19262	278	Interface	6.7	87.85	46	326	0.386	16.03	KSRH060412062315.NS (.EW)	K-KIK
10	19192	278	Interface	6.7	59.53	46	282	0.320	14.27	HKD0710412062315.NS (.EW)	K-KIK
11	21598	301	Interface	7.1	97.14	42	859	0.380	13.28	MYGH110508161146.NS (.EW)	K-KIK
12	21597	301	Interface	7.1	115.52	42	348	0.358	13.31	MYGH100508161146.NS (.EW)	K-KIK
13	21471	301	Interface	7.1	115.21	42	284	0.260	14.21	MYG0130508161146.NS (.EW)	K-KIK
14	552	12	Interface	6.7	59.03	39	217	0.207	14.82	MYZ0139610192344.NS (.EW)	K-KIK
15	556	12	Interface	6.7	77.94	39	348	0.181	14.32	MYZ0179610192344.NS (.EW)	K-KIK
16	4409	99	Interface	6.2	21.01	15	258	0.188	14.72	TKY0100007011602.NS (.EW)	K-KIK
17	757	17	Interface	6.7	39.99	35	217	0.171	15.04	MYZ0139612030718.NS (.EW)	K-KIK
18	169	Tohoku	Interface	9	83.70	24	463	1.748	70.90	MYG0041103111446.NS (.EW)	K-KIK
19	175	Tohoku	Interface	9	71.00	24	436	0.960	44.43	MYG0121103111446.NS (.EW)	K-KIK
20	237	Tohoku	Interface	9	69.14	24	418	0.906	56.84	TCG0141103111446.NS (.EW)	K-KIK
21	304	Tohoku	Interface	9	93.91	24	487	0.869	35.62	FKSH101103111446.NS2 (.EW)	K-KIK
22	128	Tohoku	Interface	9	52.32	24	399	0.778	30.49	IBR0061103111446.NS (.EW)	K-KIK
23	18995	276	Interface	7	49.15	48	282	0.343	14.33	HKD0710411290332.NS (.EW)	K-KIK
24	19083	276	Interface	7	66.74	48	189	0.276	27.10	KSRH040411290332.NS (.EW)	K-KIK
25	19089	276	Interface	7	50.80	48	213	0.322	17.89	KSRH100411290332.NS (.EW)	K-KIK
26	19084	276	Interface	7	92.82	48	389	0.331	15.82	KSRH050411290332.NS (.EW)	K-KIK
27	19081	276	Interface	7	94.44	48	219	0.254	26.41	KSRH020411290332.NS (.EW)	K-KIK
28	11075	194	Interface	7.9	57.68	42	353	0.465	29.97	TKCH080309260450.NS (.EW)	K-KIK
29	11028	194	Interface	7.9	148.64	42	315	0.493	23.34	NMRH020309260450.NS (.EW)	K-KIK
30	11024	194	Interface	7.9	79.56	42	204	0.420	35.90	KSRH070309260450.NS (.EW)	K-KIK
31	10796	194	Interface	7.9	73.16	42	437	0.359	44.94	HKD0840309260450.NS (.EW)	K-KIK
32	19199	278	Interface	6.7	80.28	46	243	0.266	16.58	HKD0780412062315.NS (.EW)	K-KIK
33	21468	301	Interface	7.1	96.84	42	303	0.238	15.56	MYG0100508161146.NS (.EW)	K-KIK
34	21473	301	Interface	7.1	117.12	42	240	0.206	14.74	MYG0150508161146.NS (.EW)	K-KIK
35	370	Tohoku	Interface	9	74.46	24	574	0.687	46.01	TCGH131103111446.NS2 (.EW)	K-KIK
36	323	Tohoku	Interface	9	62.49	24	450	0.672	27.09	IBRH151103111446.NS2 (.EW)	K-KIK
37	168	Tohoku	Interface	9	66.35	24	494	0.625	28.47	MYG0031103111446.NS (.EW)	K-KIK
38	167	Tohoku	Interface	9	56.45	24	505	0.651	23.94	MYG0021103111446.NS (.EW)	K-KIK
39	232	Tohoku	Interface	9	78.41	24	492	0.382	58.94	TCG0061103111446.NS (.EW)	K-KIK

Table. G.2. Details of the 39 pairs of ground motions from subduction interface earthquakes

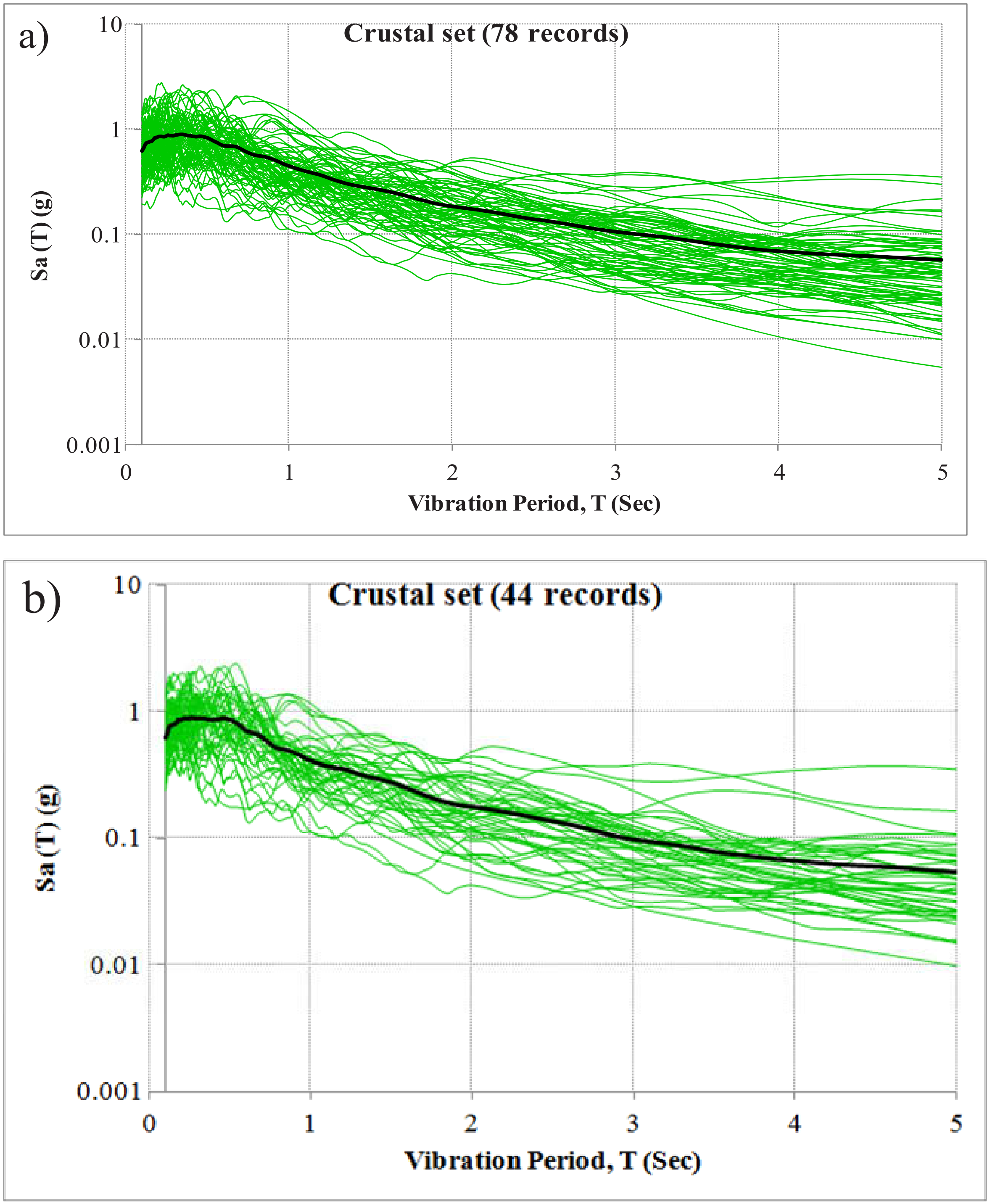

Fig. G.1. Response spectra for the crustal record set and the average response spectrum for a) 78 records b) 44 records

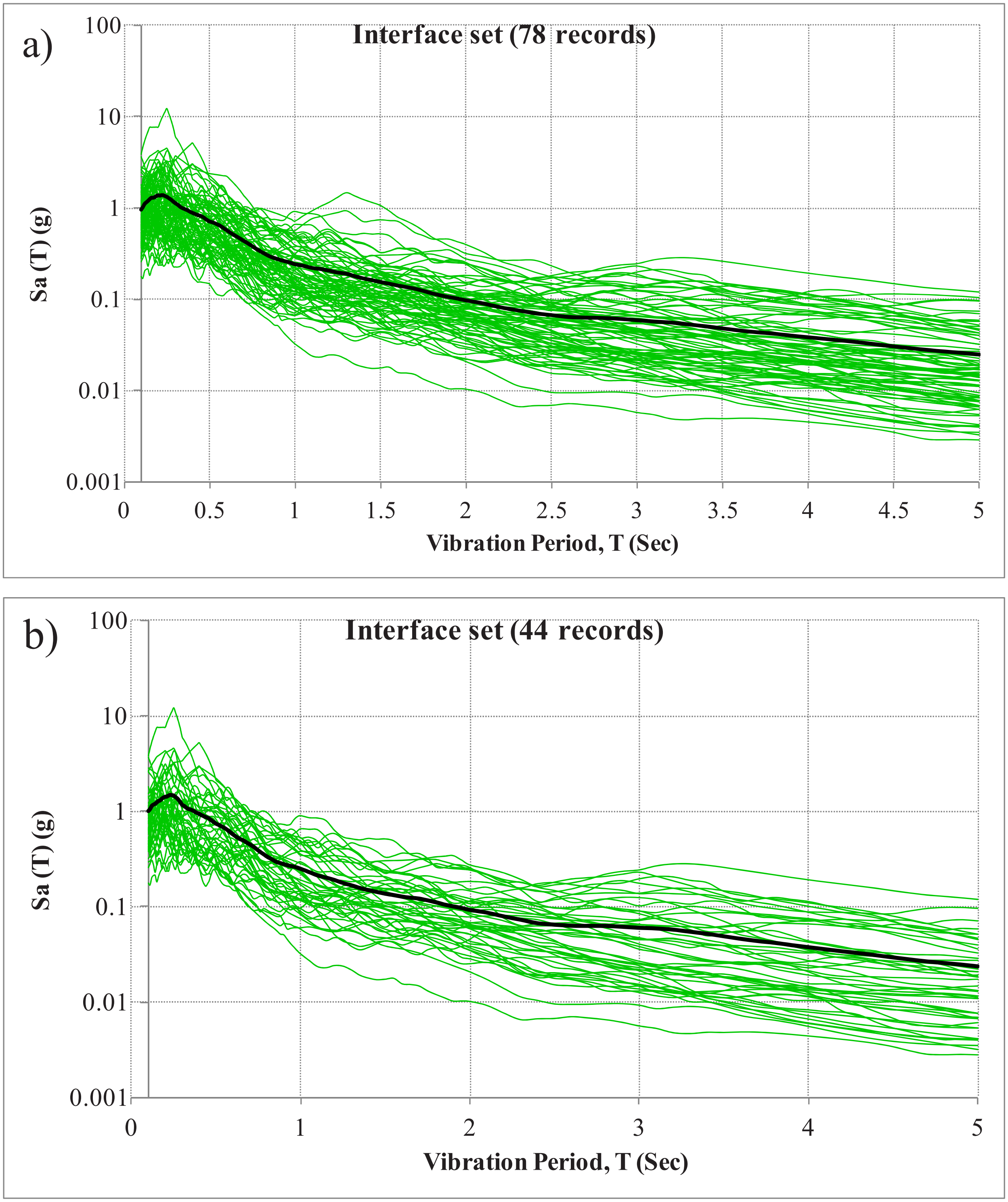

Fig. G.2. Response spectra for the interface record set and the average response spectrum for a) 78 records b) 44 records

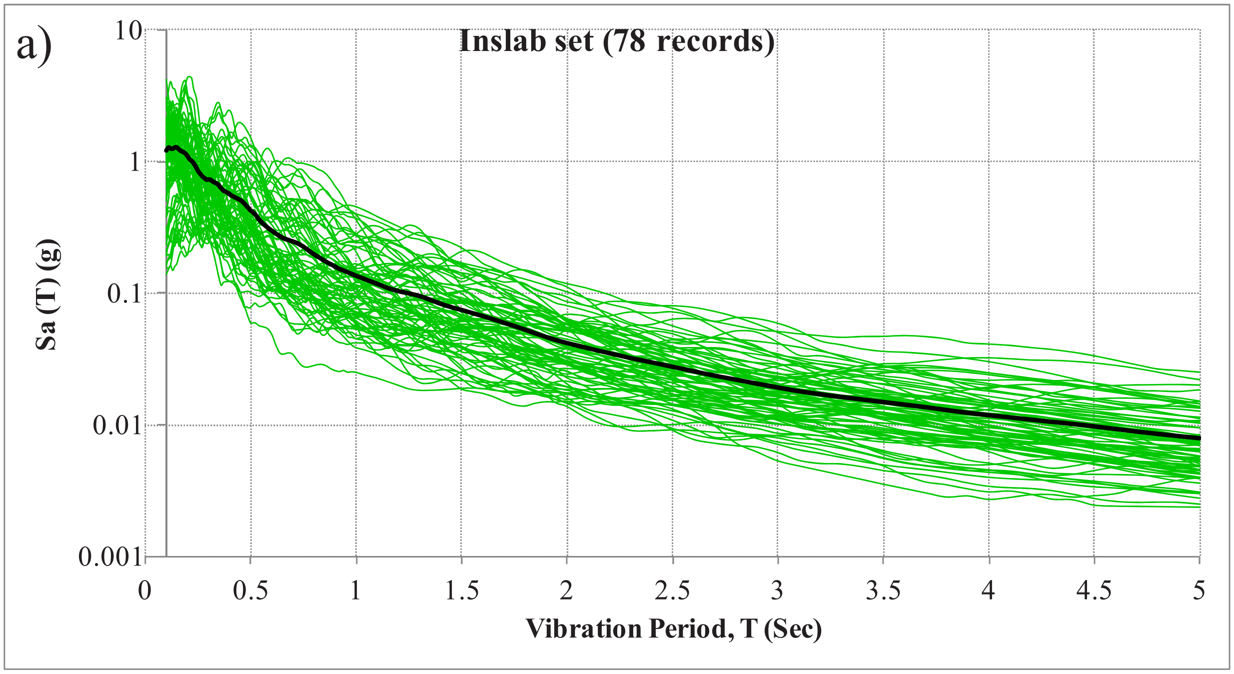

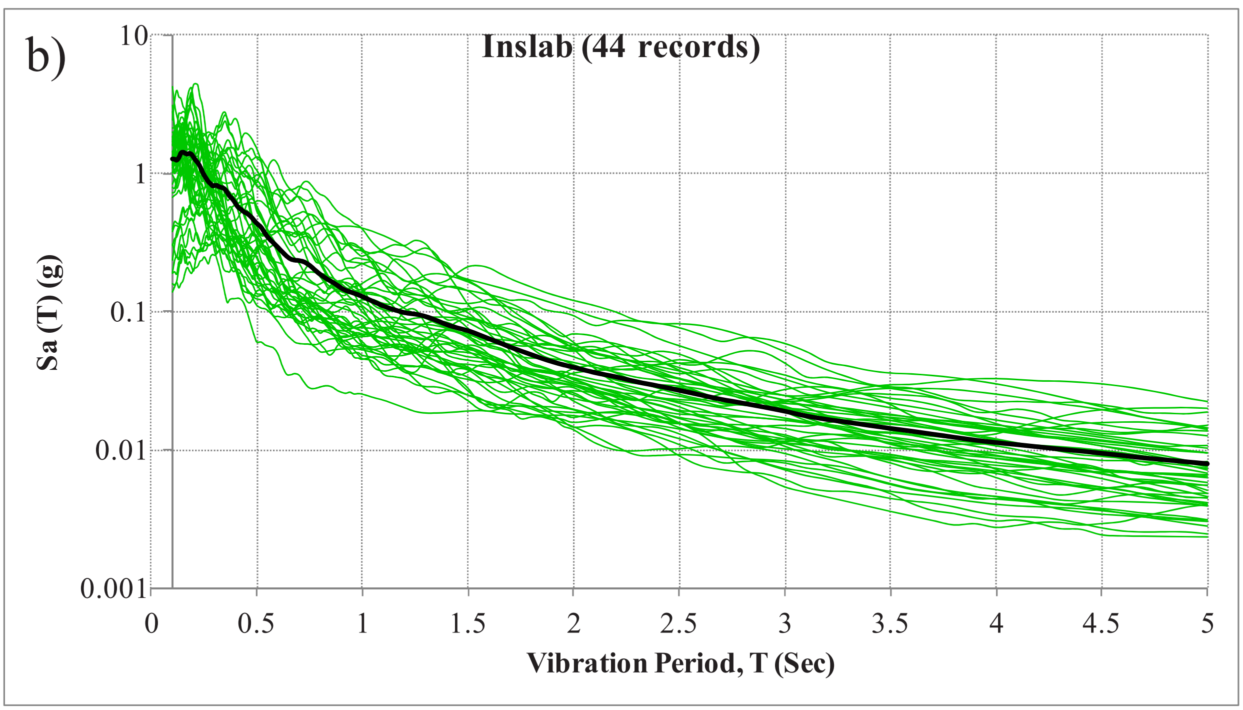

Fig. G.3. Response spectra for the inslab record set and the average response spectrum for a) 78 records b) 44 records

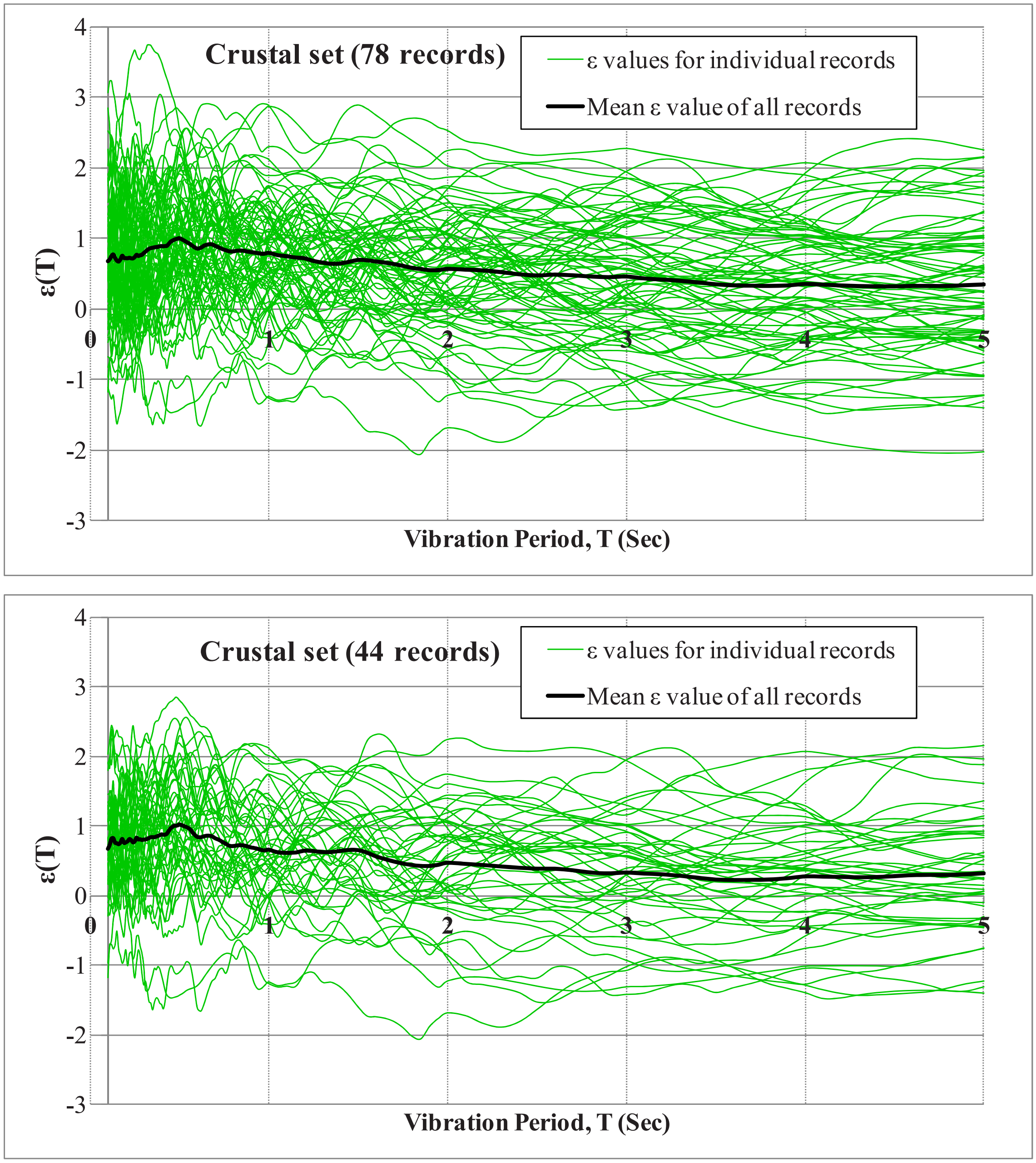

Fig. G.5. ε(T) for the crustal record set and mean ε(T) for 78 records (top) and 44 records (bottom) (ε values computed using the BA08 GMPE).

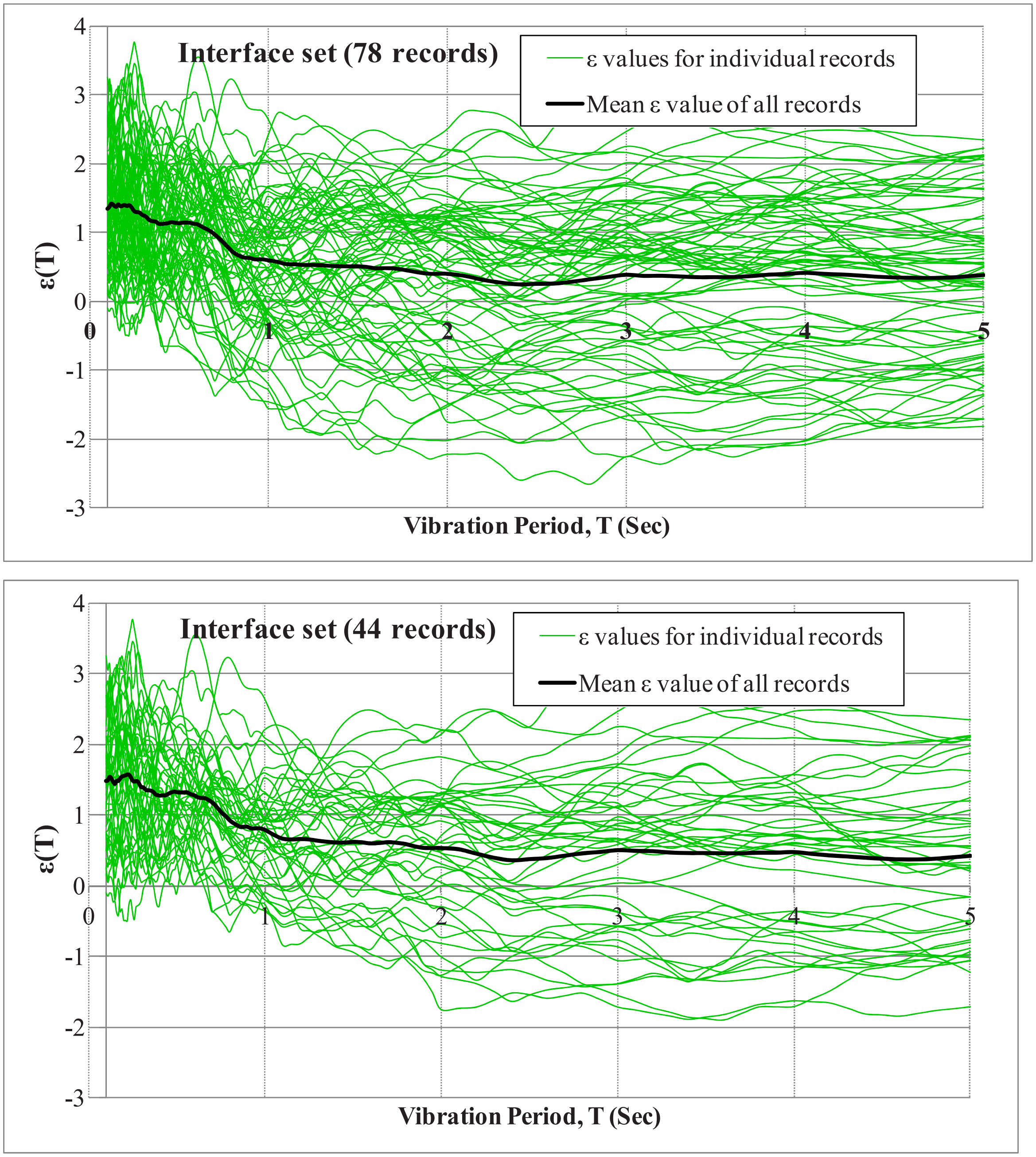

Fig. G.5. ε(T) for the interface record set and mean ε(T) for 78 records (top) and 44 records (bottom) (ε values computed using the Z06 GMPE).

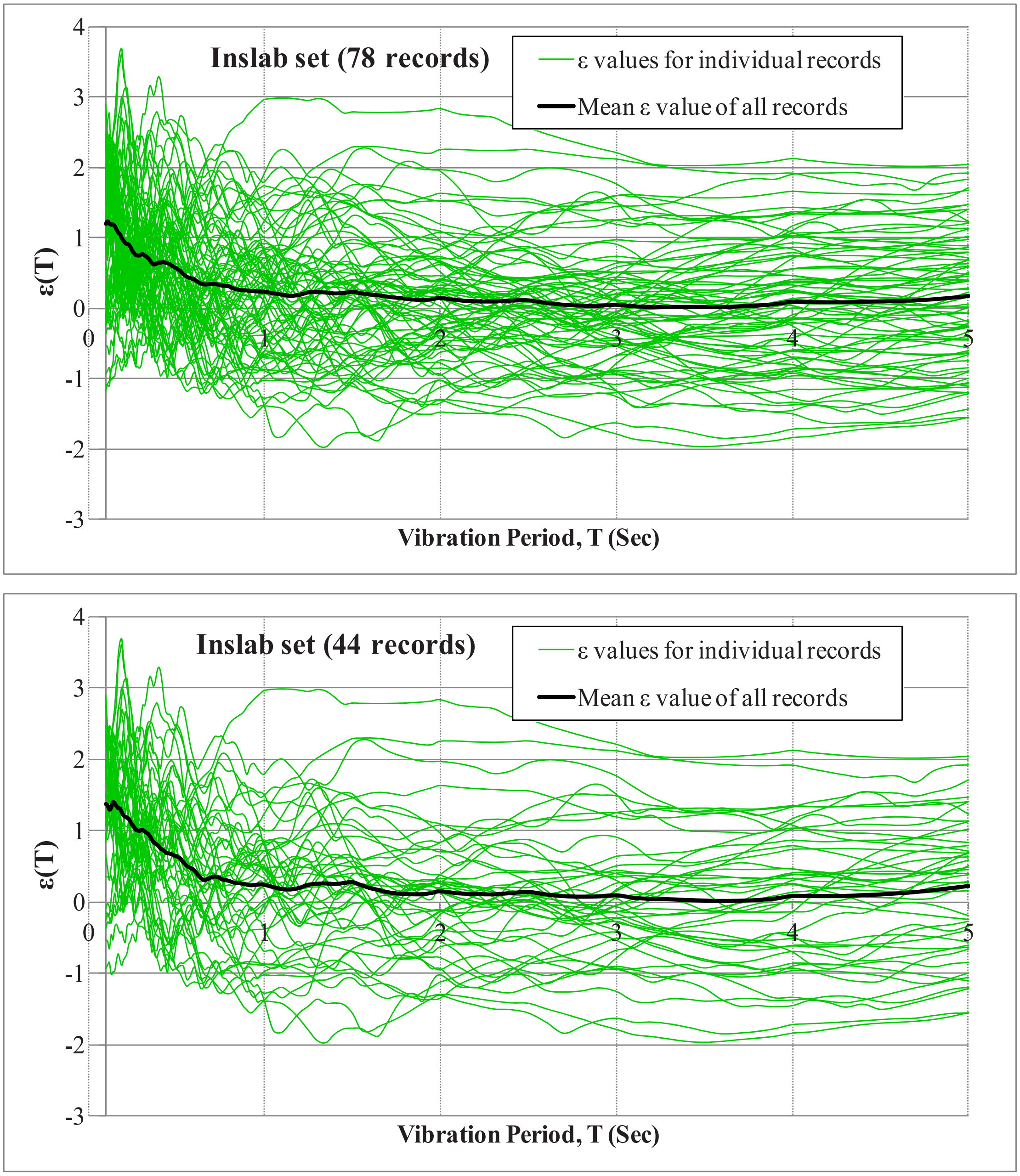

Fig. G.6. ε(T) for the inslab record set and mean ε(T) for 78 records (top) and 44 records (bottom) (ε values computed using the Z06 GMPE).

Appendix H: Pushover analysis of the bridge in Chapter 5

Nonlinear static analysis (pushover) can provide some general information about the seismic capacity of structures and is widely used for the case of buildings. However for bridges pushover analysis must be carried out with caution especially when higher mode effects are important or the structure is highly irregular. For such cases, the use of modal pushover (Chopra and Goel, 2002) and adaptive pushover analysis seems to provide a better prediction of the seismic response of the structure (Isakovic and Fischinger, 2006). For the bridge structure under study, an adaptive pushover analysis was performed to provide general information of the seismic behaviour including overall ductility capacity and over-strength factor. The "adaptive pushover" analysis uses an updated stiffness calculated for each load step. The initial load pattern was based on the fundamental mode and during the analysis this pattern was updated in each step based on the stiffness and mode shape in that step. The pushover curve shows the shear force of columns versus the drift ratio of the central column (i.e., the critical column). The total elastic shear force of columns using response spectrum analysis was 13000 kN, and by applying a response modification factor of 3 in design according to the 2006 CHBDC, the total design shear force is reduced to 4333 kN for the columns. The maximum shear force from pushover analysis (V_{max}) was found 6140 kN as shown in Fig. H.1. Thus the over-strength factor defined as a ratio of the maximum shear force to the design shear force, is 6140/4333 =1.42.

To evaluate the structural collapse ductility, the procedure defined by ASCE/SEI 41-06 (ASCE, 2006), which was used by the ATC-63 provisions, was utilized here. For this purpose, the effective yield displacement (Δ_y) and the ultimate displacement (Δ_{ult}), defined at the point of 20% strength loss, was calculated as 33(mm) and 420 (mm), respectively from the pushover analysis and the displacement at which strength degradation starts was 260 mm. The structural collapse ductility, μ_c, is Δ_{ult}/Δ_y =420/33 = 12.8. The ductility at the point of strength degradation is about 8.0.

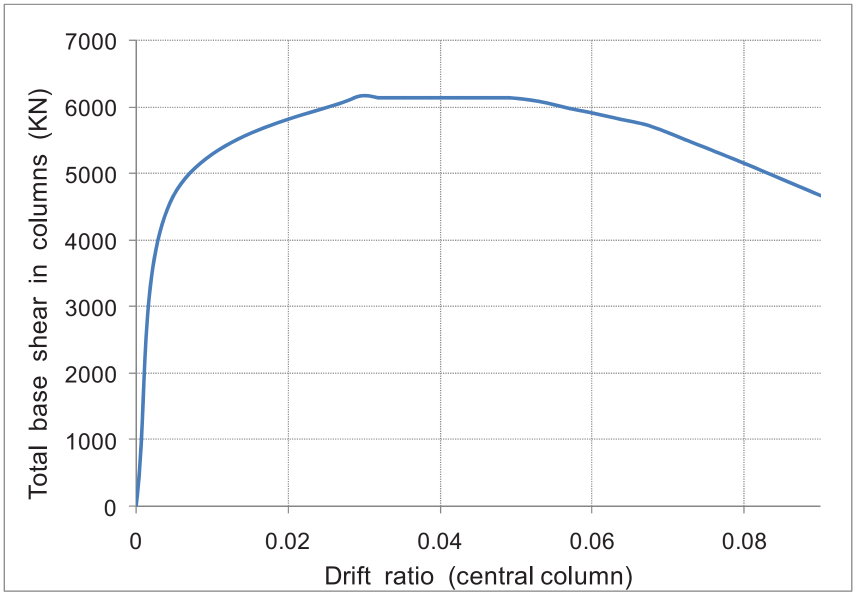

Figure H.1. Pushover analysis of the bridge

Appendix I: Some of the results from Chapter 6

In Chapter 6 the IDA method was applied (using a large record set) to evaluate the seismic response of 30 bridges with different configurations designed using different force modification factors. The detailed results from all 30 cases are available in tables. However due to space limitations only the results obtained for the configurations 4 and 5 with column diameters of D=2.0 m, designed using a force modification factor of R=5 are presented as examples.

Also the bridge structure studied in Chapter 5 was subjected to the large record sets considered in Chapter 6 and the detailed results for this bridge for the case of the restrained transverse movements at the abutments are also presented in this appendix.

The details of the ground motion record sets are given in Appendix G for 39 pairs of ground motions (i.e., 78 horizontal components) for each earthquake type. The record numbers in the tables are consistent with those given in Appendix G, considering that 39 pairs of records have 78 horizontal components. In the tables, CMR is the collapse margin ratio and ACMR is the required collapse margin ratio for 10% probability of collapse in MCE level (i.e., acceptable collapse margin ratio). More details concerning the computation of CMR are available in Chapters 2, 5 and 6.
The standard deviation of the IDA results given in the tables represents the record-to-record variability, β_{RTR}. The total uncertainty, β_{TOT}, reported in the tables includes all sources of uncertainty as discussed in more details in Chapter 2.
The criteria for the subsets of records (i.e., case 1 to 8 in the tables) are given in Chapter 6.

	Collapse Capacities (g)				Collapse Capacities (g)		
Record number	Crustal records set	Interface records sets	Inslab records set	Record number	Crustal records set	Interface records sets	Inslab records set
1	1.98	0.44	3.28	41	1.40	1.29	8.65
2	1.72	0.49	2.89	42	1.23	1.72	5.96
3	1.05	0.51	1.51	43	2.30	1.23	1.43
4	2.92	0.66	2.55	44	3.25	1.98	3.15
5	1.80	0.83	2.47	45	2.87	1.82	4.32
6	4.70	1.13	3.67	46	2.19	2.09	3.14
7	2.74	0.47	3.10	47	0.99	0.64	1.93
8	1.61	0.44	2.14	48	1.56	0.88	1.11
9	0.87	0.79	4.73	49	1.65	0.80	2.54
10	1.30	0.70	5.84	50	2.17	0.57	1.87
11	0.82	0.59	1.65	51	2.65	0.47	1.24
12	1.17	0.52	1.74	52	1.29	0.45	2.60
13	1.19	0.59	0.59	53	2.02	1.19	0.81
14	1.15	0.51	0.99	54	1.43	1.79	0.89
15	1.45	0.76	7.31	55	1.30	0.56	4.10
16	1.41	0.55	9.57	56	1.67	0.53	3.08
17	1.08	0.64	0.82	57	2.96	0.64	0.53
18	1.09	0.45	0.98	58	3.84	0.65	0.70
19	1.60	4.86	1.77	59	1.88	0.63	2.57
20	0.69	2.88	1.26	60	1.32	0.65	1.23
21	1.26	0.34	0.43	61	1.97	1.92	5.46
22	1.58	0.41	0.45	62	2.13	1.51	3.92
23	2.61	0.63	3.68	63	2.10	1.18	1.30
24	2.25	0.53	4.36	64	1.99	1.08	1.09
25	1.98	1.83	1.72	65	1.74	2.38	5.17
26	2.30	1.62	0.81	66	1.94	4.04	4.56
27	2.05	5.06	3.18	67	0.95	3.57	3.02
28	0.85	3.06	2.56	68	2.06	4.69	5.17
29	1.22	1.76	0.56	69	1.51	2.06	4.23
30	1.09	2.73	0.61	70	2.10	1.97	3.76
31	1.13	1.86	3.07	71	1.85	1.32	0.64
32	0.57	4.62	2.47	72	1.56	2.09	0.51
33	1.74	4.05	6.21	73	1.14	1.18	10.05
34	1.28	4.63	3.56	74	0.99	1.85	5.35
35	2.12	1.21	2.46	75	0.94	0.90	8.07
36	3.87	0.87	2.12	76	1.22	1.46	4.30
37	1.04	3.16	5.36	77	2.48	1.22	1.06
38	1.25	3.67	7.88	78	0.95	1.63	0.76
39	1.70	1.66	10.92	Median	1.61	1.18	2.57
40	2.36	4.08	12.54	St dev	0.41	0.74	0.85

Table I.1. Collapse capacity of the bridge (configuration 4, D=2.0 m and R/I= 5) for 78x3=234 records from three earthquake types.

		Percentiles							
		50%	16%	84%	St Dev	Num.	Mean ε (Records)	β_1	SSF
Case 1	Crustal	1.61	1.09	2.30	0.41	78	0.78	0.157	1.148
	Interface	1.18	0.53	2.83	0.74	78	0.59	0.146	1.121
	Inslab	2.57	0.84	5.36	0.85	78	0.22	0.440	2.064
Case2	Crustal	1.58	1.08	2.26	0.41	69	0.95	0.268	1.208
	Interface	0.98	0.51	3.52	0.81	58	1.00	0.465	1.192
	Inslab	3.15	1.60	5.96	0.69	49	0.76	0.260	1.337
Case3	Crustal	1.59	1.09	2.21	0.35	74	0.78	0.138	1.129
	Interface	1.18	0.53	2.67	0.73	77	0.60	0.159	1.131
	Inslab	2.56	0.83	5.33	0.84	77	0.25	0.494	2.230
Case4	Crustal	1.56	1.08	2.16	0.34	65	0.96	0.259	1.198
	Interface	0.88	0.51	3.08	0.78	56	1.03	0.602	1.234
	Inslab	3.16	1.69	6.02	0.66	48	0.77	0.199	1.245
Case5	Crustal	1.57	1.07	2.21	0.40	74	0.83	0.215	1.194
	Interface	0.79	0.51	1.79	0.59	57	0.46	-0.106	0.908
	Inslab	0.70	0.51	2.38	0.72	15	0.17	0.669	3.109
Case6	Crustal	1.57	1.07	2.20	0.40	68	0.95	0.266	1.207
	Interface	0.65	0.48	1.58	0.61	41	0.89	0.206	1.106
	Inslab	1.99	1.02	3.00	0.58	8	0.97	0.805	2.068
Case7	Crustal	1.56	1.08	2.13	0.34	70	0.84	0.199	1.178
	Interface	0.73	0.51	1.64	0.51	54	0.46	-0.110	0.904
	Inslab	0.70	0.51	2.38	0.72	15	0.17	0.669	3.109
Case8	Crustal	1.56	1.08	2.13	0.33	64	0.96	0.257	1.196
	Interface	0.64	0.47	1.22	0.46	38	0.92	0.395	1.200
	Inslab	1.99	1.02	3.00	0.58	8	0.97	0.805	2.068

Table I.2. Percentiles of unmodified collapse capacity, β_{RTR}, β_1 factor and spectral shape factor (SSF) predicted for different earthquake types and for different subsets of records in each set (Configuration 4, D = 2.0 m and R/I = 5).

		Median	CMR	Modified median	Modified CMR	β_{TOT}	ACMR	CMR/ACMR
Case 1	Crustal	1.61	4.94	1.84	5.67	0.61	2.17	2.61
	Interface	1.18	3.64	1.33	4.08	0.87	3.04	1.34
	Inslab	2.57	7.90	5.30	16.30	0.96	3.42	4.76
	Average	1.74	5.35	2.68	8.24	0.81	2.84	2.90
Case 2	Crustal	1.58	4.84	1.90	5.85	0.60	2.17	2.70
	Interface	0.98	3.01	1.17	3.59	0.92	3.26	1.10
	Inslab	3.15	9.69	4.21	12.95	0.83	2.88	4.49
	Average	1.83	5.63	2.33	7.15	0.79	2.76	2.59
Case 3	Crustal	1.59	4.88	1.79	5.51	0.57	2.07	2.66
	Interface	1.18	3.62	1.33	4.10	0.86	3.00	1.37
	Inslab	2.56	7.88	5.71	17.56	0.96	3.40	5.16
	Average	1.73	5.32	2.78	8.56	0.80	2.79	3.07
Case 4	Crustal	1.56	4.81	1.87	5.76	0.56	2.06	2.80
	Interface	0.88	2.70	1.08	3.33	0.90	3.17	1.05
	Inslab	3.16	9.73	3.94	12.11	0.80	2.77	4.37
	Average	1.80	5.52	2.21	6.78	0.76	2.66	2.55
Case 5	Crustal	1.57	4.83	1.87	5.76	0.60	2.16	2.67
	Interface	0.79	2.44	0.72	2.21	0.74	2.59	0.85
	Inslab	0.70	2.16	2.19	6.73	0.85	2.98	2.26
	Average	1.05	3.21	1.57	4.81	0.73	2.55	1.89
Case 6	Crustal	1.57	4.83	1.89	5.82	0.60	2.16	2.70
	Interface	0.65	2.01	0.72	2.22	0.76	2.64	0.84
	Inslab	1.99	6.13	4.12	12.68	0.73	2.56	4.95
	Average	1.38	4.23	2.14	6.58	0.70	2.44	2.69
Case 7	Crustal	1.56	4.80	1.84	5.66	0.56	2.05	2.75
	Interface	0.73	2.25	0.66	2.03	0.68	2.39	0.85
	Inslab	0.70	2.16	2.19	6.73	0.85	2.98	2.26
	Average	1.02	3.14	1.53	4.71	0.70	2.44	1.93
Case 8	Crustal	1.56	4.80	1.87	5.74	0.56	2.04	2.81
	Interface	0.64	1.97	0.77	2.36	0.64	2.28	1.04
	Inslab	1.99	6.13	4.12	12.68	0.73	2.56	4.95
	Average	1.37	4.21	2.15	6.61	0.64	2.28	2.90

Table I.3. Modified and unmodified median collapse capacities and corresponding collapse margin ratios (CMR) and acceptable CMR (ACMR) (Configuration 4, D = 2.0 m and R/I = 5).

	Unmodified				Modified			
	Median	*16% Percentile*	*84% Percentile*	*St Dev.*	*Median*	*16% Percentile*	*84% Percentile*	*St Dev.*
Subset 1	1.72	0.76	3.67	0.74	1.98	1.04	4.78	0.83
Subset 2	1.80	0.82	3.90	0.76	1.96	1.08	4.81	0.76
Subset 3	1.70	0.78	3.38	0.73	1.95	1.01	4.46	0.84
Subset 4	1.75	0.81	3.67	0.75	1.91	1.12	4.35	0.72
Subset 5	1.25	0.56	2.16	0.65	1.92	0.65	3.51	0.73
Subset 6	1.61	0.64	2.40	0.61	1.90	0.65	3.20	0.72
Subset 7	1.25	0.56	2.16	0.63	1.90	0.65	3.31	0.72
Subset 8	1.61	0.64	2.40	0.61	1.90	0.65	3.20	0.71

Table I.4. Unmodified and modified collapse capacities for the combined records from 3 event types (configuration 4, D = 2.0 m and R/I = 5).

	Number of records							
	Crustal	*Interface*	*Inslab*	*Beta total*	*CMR*	*Modified CMR*	*Acceptable CMR*	*CMR/A CMR*
Subset 1	78	75	64	0.94	5.29	6.10	3.35	1.82
Subset 2	59	57	49	0.88	5.52	6.04	3.09	1.95
Subset 3	74	71	60	0.95	5.21	6.00	3.40	1.77
Subset 4	57	56	47	0.85	5.37	5.87	2.96	1.98
Subset 5	19	18	16	0.85	3.85	5.90	2.98	1.98
Subset 6	11	10	9	0.85	4.96	5.83	2.97	1.96
Subset 7	19	18	16	0.85	3.85	5.85	2.96	1.98
Subset 8	11	10	9	0.84	4.96	5.83	2.95	1.98

Table I.5. Number of records in each subset and the computed CMR, ACMR, and total uncertainty (configuration 4, D = 2.0 m and R/I = 5)

	Unmodified				Modified			
	Median	*16% Percentile*	*84% Percentile*	*St Dev.*	*Median*	*16% Percentile*	*84% Percentile*	*St Dev.*
Subset 1	1.45	0.64	2.45	0.62	1.69	0.73	2.89	0.61
Subset 2	1.51	0.64	2.80	0.65	1.65	0.81	3.06	0.61
Subset 3	1.43	0.65	2.30	0.60	1.67	0.75	2.62	0.59
Subset 4	1.40	0.64	2.39	0.63	1.74	0.80	2.70	0.55
Subset 5	1.28	0.63	2.10	0.57	1.40	0.56	2.29	0.63
Subset 6	1.22	0.55	2.18	0.63	1.43	0.63	2.29	0.62
Subset 7	1.25	0.60	1.99	0.53	1.36	0.53	2.05	0.59
Subset 8	1.22	0.54	1.99	0.57	1.41	0.65	1.98	0.52

Table I.6. Unmodified and modified collapse capacities for the combined records from 2 event types (excluding inslab events) (configuration 4, D = 2.0 m and R/I = 5)

	Number of records							
	Crustal	*Interface*	*Inslab*	β_{TOT}	*CMR*	*Modified CMR*	*ACMR*	*CMR/ACMR*
Subset 1	78	75	0	0.76	4.46	5.21	2.65	1.97
Subset 2	59	58	0	0.75	4.63	5.09	2.63	1.94
Subset 3	74	71	0	0.74	4.41	5.13	2.58	1.99
Subset 4	57	56	0	0.71	4.31	5.34	2.49	2.15
Subset 5	58	57	0	0.77	3.94	4.29	2.68	1.60
Subset 6	42	41	0	0.76	3.76	4.41	2.66	1.66
Subset 7	55	54	0	0.74	3.85	4.17	2.59	1.61
Subset 8	39	38	0	0.69	3.74	4.34	2.41	1.80

Table I.7. Number of records in each subset and the computed CMR, ACMR, and total uncertainty for the case inslab events are excluded (configuration 4, D = 2.0 m and R/I = 5)

	Percentiles				Num. of records							Mean epsilon of records		
Earthquake type	50%	16%	84%	St-Dev	Crustal	Interface	Inslab	β_{TOT}	CMR	ACMR	CMR/ACMR	Crustal	Interface	Inslab
CRUSTAL	1.90	1.39	2.66	0.32	28	-	-	0.55	5.83	2.03	2.88	1.42	-	-
INTERFACE	1.16	0.54	3.08	0.76	-	32	-	0.88	3.56	3.10	1.15	-	1.25	-
INSLAB	3.15	2.48	5.73	0.54	-	-	15	0.70	9.69	2.46	3.93	-	-	1.35
ALL EVENTS	1.64	0.64	3.57	0.74	18	17	15	0.87	5.05	3.04	1.66	1.52	1.34	1.35
ALL EVENTS (No Inslab)	1.70	0.64	2.81	0.65	28	27	-	0.79	5.21	2.75	1.90	1.42	1.20	-

Table I.8. Results from the epsilon-based method including the collapse capacity statistics and number of records from each set (configuration 4, D = 2.0 m and R/I = 5)

Modified median & (CMR/ACMR)	Crustal records	Interface records	Inslab records	Combined events	Combined (no inslab records)
Subset 1 (simplified method)	1.84 (2.61)	1.33 (1.34)	5.30 (4.76)	1.98 (1.82)	1.69 (1.97)
Subset 2 (simplified method)	1.90 (2.70)	1.17 (1.10)	4.21 (4.49)	1.96 (1.95)	1.65 (1.94)
Subset 3 (simplified method)	1.79 (2.66)	1.33 (1.37)	5.71 (5.16)	1.95 (1.77)	1.67 (1.99)
Subset 4 (simplified method)	1.87 (2.80)	1.08 (1.05)	3.94 (4.37)	1.91 (1.98)	1.74 (2.15)
Subset 5 (simplified method)	1.87 (2.67)	0.72 (0.85)	2.19 (2.26)	1.92 (1.98)	1.40 (1.60)
Subset 6 (simplified method)	1.89 (2.70)	0.72 (0.84)	4.12 (4.95)	1.90 (1.96)	1.43 (1.66)
Subset 7 (simplified method)	1.84 (2.75)	0.66 (0.85)	2.19 (2.26)	1.90 (1.98)	1.36 (1.61)
Subset 8 (simplified method)	1.87 (2.81)	0.77 (1.04)	4.12 (4.95)	1.90 (1.98)	1.41 (1.80)
Epsilon-Based method	1.90 (2.88)	1.16 (1.15)	3.15 (3.93)	1.64 (1.66)	1.70 (1.90)

Table I.9. Comparison of the median collapse capacity and CMR/ACMR ratios using different subsets and methods (configuration 4, D = 2.0 m and R/I = 5)

	Collapse Capacities (g)				Collapse Capacities (g)		
Record number	Crustal records set	Interface records sets	Inslab records set	Record number	Crustal records set	Interface records sets	Inslab records set
1	1.54	0.31	2.97	41	0.99	0.86	4.63
2	1.22	0.37	2.19	42	1.19	1.53	4.07
3	0.70	0.37	1.08	43	1.64	0.91	1.04
4	2.38	0.51	1.58	44	2.13	1.87	2.26
5	1.35	0.64	1.83	45	1.99	1.29	4.15
6	2.76	0.93	2.63	46	1.60	1.71	2.19
7	1.85	0.35	1.53	47	0.61	0.46	1.65
8	0.95	0.32	1.84	48	1.16	0.68	0.84
9	0.75	0.58	4.46	49	1.19	0.50	1.60
10	0.98	0.54	4.55	50	1.43	0.47	0.99
11	0.63	0.42	1.23	51	1.86	0.36	0.99
12	0.79	0.39	1.26	52	0.89	0.36	1.92
13	0.91	0.42	0.41	53	1.55	0.89	0.63
14	0.91	0.36	0.71	54	1.09	1.16	0.74
15	1.01	0.58	9.34	55	0.91	0.50	3.46
16	1.05	0.39	7.42	56	1.12	0.42	2.77
17	0.86	0.55	0.66	57	2.16	0.42	0.41
18	0.79	0.42	1.08	58	2.70	0.46	0.55
19	1.21	3.87	1.27	59	1.29	0.43	1.86
20	0.58	2.08	1.05	60	0.95	0.51	0.95
21	0.81	0.24	0.42	61	1.55	0.95	4.47
22	1.08	0.31	0.41	62	1.51	1.11	3.21
23	2.14	0.42	3.10	63	1.59	0.87	1.25
24	1.52	0.37	3.12	64	1.47	0.76	0.82
25	1.36	1.46	1.35	65	1.33	1.47	4.15
26	1.12	1.19	0.75	66	1.17	2.68	3.63
27	1.32	3.27	6.59	67	0.72	2.70	2.02
28	0.66	2.09	2.41	68	1.64	3.93	2.72
29	0.98	1.30	0.48	69	1.13	1.93	2.96
30	0.85	1.98	0.54	70	1.33	1.48	2.23
31	0.79	1.54	2.01	71	1.45	1.08	0.54
32	0.42	3.30	1.52	72	1.14	1.70	0.45
33	1.21	2.90	5.45	73	0.85	0.70	6.16
34	1.00	3.33	5.19	74	0.79	1.34	4.40
35	1.49	1.07	1.85	75	0.79	0.72	4.52
36	1.86	0.65	1.51	76	1.04	1.13	3.17
37	0.85	2.17	3.73	77	1.88	0.77	0.78
38	1.10	2.42	5.31	78	0.74	0.99	0.55
39	1.35	0.99	8.35	Median	1.15	0.86	1.86
40	1.56	1.75	9.13	St dev	0.37	0.73	0.84

Table I.10. Collapse capacity of the bridge (configuration 5, D=2.0 m and R/I= 5) for 78x3=234 records from three earthquake types.

		Percentiles							
		50%	16%	84%	St Dev	Num.	Mean ε (Records)	β_1	SSF
Case 1	Crustal	1.15	0.79	1.63	0.37	78	0.79	0.156	1.145
	Interface	0.86	0.40	1.96	0.73	78	0.60	0.140	1.115
	Inslab	1.86	0.72	4.47	0.84	78	0.23	0.347	1.755
Case2	Crustal	1.14	0.79	1.60	0.37	69	0.96	0.240	1.181
	Interface	0.72	0.38	2.16	0.78	58	1.00	0.471	1.195
	Inslab	2.10	1.02	4.54	0.73	48	0.78	0.353	1.462
Case3	Crustal	1.14	0.79	1.59	0.34	75	0.81	0.166	1.151
	Interface	0.86	0.39	1.92	0.72	77	0.61	0.154	1.126
	Inslab	1.85	0.71	4.45	0.83	77	0.25	0.411	1.931
Case4	Crustal	1.14	0.80	1.60	0.34	67	0.97	0.222	1.164
	Interface	0.68	0.37	2.09	0.76	57	1.02	0.557	1.223
	Inslab	2.10	1.02	4.54	0.73	48	0.78	0.353	1.462
Case5	Crustal	1.14	0.79	1.60	0.37	76	0.83	0.198	1.177
	Interface	0.64	0.37	1.49	0.65	63	0.55	0.071	1.061
	Inslab	0.76	0.45	2.01	0.64	26	0.23	0.539	2.399
Case6	Crustal	1.14	0.79	1.60	0.37	69	0.96	0.240	1.181
	Interface	0.54	0.37	1.30	0.67	45	1.01	0.528	1.218
	Inslab	1.26	0.69	2.11	0.57	17	0.79	0.579	1.852
Case7	Crustal	1.13	0.79	1.58	0.34	73	0.86	0.209	1.182
	Interface	0.58	0.37	1.39	0.60	61	0.49	-0.038	0.967
	Inslab	0.74	0.44	1.88	0.61	25	0.21	0.518	2.345
Case8	Crustal	1.14	0.80	1.60	0.34	67	0.97	0.222	1.164
	Interface	0.51	0.37	1.08	0.61	42	1.04	0.650	1.246
	Inslab	1.26	0.69	2.11	0.57	17	0.79	0.579	1.852

Table I.11. Percentiles of unmodified collapse capacity, β_{RTR}, β_1 factor and spectral shape factor (SSF) predicted for different earthquake types and for different subsets of records in each set. (Configuration 5, D = 2.0 m and R/I = 5)

		Median	CMR	Modified median	Modified CMR	β_{TOT}	ACMR	CMR/ACMR
Case 1	Crustal	1.15	3.49	1.31	4.00	0.58	2.11	1.90
	Interface	0.86	2.63	0.96	2.94	0.86	3.00	0.98
	Inslab	1.86	5.66	3.26	9.93	0.95	3.39	2.93
	Average	1.26	3.83	1.77	5.38	0.80	2.79	1.93
Case 2	Crustal	1.14	3.47	1.35	4.10	0.58	2.11	1.94
	Interface	0.72	2.19	0.86	2.62	0.90	3.16	0.83
	Inslab	2.10	6.40	3.07	9.35	0.86	3.00	3.12
	Average	1.28	3.89	1.69	5.14	0.78	2.73	1.88
Case 3	Crustal	1.14	3.47	1.31	3.99	0.56	2.06	1.94
	Interface	0.86	2.61	0.97	2.94	0.84	2.95	1.00
	Inslab	1.85	5.64	3.58	10.89	0.94	3.33	3.27
	Average	1.25	3.82	1.86	5.67	0.79	2.74	2.07
Case 4	Crustal	1.14	3.47	1.33	4.04	0.56	2.05	1.97
	Interface	0.68	2.08	0.84	2.54	0.88	3.09	0.82
	Inslab	2.10	6.40	3.07	9.35	0.86	3.00	3.12
	Average	1.27	3.85	1.67	5.09	0.77	2.69	1.89
Case 5	Crustal	1.14	3.46	1.34	4.07	0.58	2.11	1.93
	Interface	0.64	1.96	0.68	2.08	0.79	2.76	0.75
	Inslab	0.76	2.31	1.82	5.53	0.78	2.71	2.04
	Average	0.86	2.60	1.25	3.82	0.72	2.51	1.52
Case 6	Crustal	1.14	3.47	1.35	4.10	0.58	2.11	1.94
	Interface	0.54	1.64	0.66	2.00	0.80	2.80	0.71
	Inslab	1.26	3.82	2.32	7.08	0.72	2.53	2.80
	Average	0.97	2.94	1.40	4.25	0.71	2.47	1.72
Case 7	Crustal	1.13	3.45	1.34	4.08	0.56	2.06	1.99
	Interface	0.58	1.76	0.56	1.71	0.75	2.62	0.65
	Inslab	0.74	2.25	1.73	5.27	0.76	2.63	2.00
	Average	0.83	2.51	1.19	3.61	0.69	2.42	1.49
Case 8	Crustal	1.14	3.47	1.33	4.04	0.56	2.05	1.97
	Interface	0.51	1.56	0.64	1.94	0.76	2.65	0.73
	Inslab	1.26	3.82	2.32	7.08	0.72	2.53	2.80
	Average	0.96	2.91	1.38	4.21	0.68	2.40	1.75

Table I.12. Modified and unmodified median collapse capacities and corresponding collapse margin ratios (CMR) and acceptable CMR (ACMR). (Configuration 5, D = 2.0 m and R/I = 5)

	Unmodified				Modified			
	Median	*16% Percentile*	*84% Percentile*	*St Dev.*	*Median*	*16% Percentile*	*84% Percentile*	*St Dev.*
Subset 1	1.21	0.57	2.69	0.73	1.45	0.77	3.02	0.80
Subset 2	1.24	0.60	2.71	0.74	1.44	0.82	3.22	0.76
Subset 3	1.19	0.58	2.43	0.72	1.45	0.80	3.16	0.81
Subset 4	1.21	0.58	2.69	0.74	1.41	0.84	3.16	0.74
Subset 5	0.98	0.42	1.69	0.62	1.33	0.50	2.38	0.67
Subset 6	1.04	0.42	1.86	0.62	1.25	0.49	2.43	0.68
Subset 7	0.98	0.42	1.63	0.61	1.35	0.47	2.31	0.67
Subset 8	1.04	0.42	1.86	0.62	1.25	0.51	2.42	0.67

Table I.13. Unmodified and modified collapse capacities for the combined records from 3 event types (configuration 5, D = 2.0 m and R/I = 5)

	Number of records							
	Crustal	*Interface*	*Inslab*	β_{TOT}	*CMR*	*Modified CMR*	*ACMR*	*CMR/A CMR*
Subset 1	78	75	64	0.92	3.68	4.41	3.24	1.36
Subset 2	58	56	48	0.88	3.78	4.37	3.10	1.41
Subset 3	75	71	61	0.93	3.64	4.43	3.28	1.35
Subset 4	58	56	48	0.87	3.70	4.31	3.04	1.41
Subset 5	31	30	26	0.81	2.98	4.04	2.82	1.43
Subset 6	20	19	17	0.81	3.18	3.81	2.84	1.34
Subset 7	30	29	25	0.81	2.98	4.10	2.81	1.46
Subset 8	20	19	17	0.81	3.18	3.80	2.81	1.35

Table I.14. Number of records in each subset and the computed CMR, ACMR, and total uncertainty (configuration 5, D = 2.0 m and R/I = 5)

	Unmodified				Modified			
	Median	*16% Percentile*	*84% Percentile*	*St Dev.*	*Median*	*16% Percentile*	*84% Percentile*	*St Dev.*
Subset 1	1.06	0.50	1.86	0.60	1.18	0.54	2.09	0.59
Subset 2	1.06	0.47	1.91	0.62	1.19	0.63	2.00	0.58
Subset 3	1.05	0.50	1.74	0.59	1.18	0.54	2.01	0.57
Subset 4	1.03	0.46	1.81	0.61	1.21	0.63	1.94	0.54
Subset 5	0.98	0.44	1.58	0.58	1.12	0.49	1.78	0.58
Subset 6	0.98	0.42	1.64	0.62	1.11	0.56	1.85	0.54
Subset 7	0.96	0.45	1.54	0.55	1.10	0.42	1.64	0.59
Subset 8	0.95	0.42	1.55	0.60	1.10	0.57	1.51	0.48

Table I.15. Unmodified and modified collapse capacities for the combined records from 2 event types (excluding inslab events) (configuration 5, D = 2.0 m and R/I = 5)

	Number of records							
	Crustal	*Interface*	*Inslab*	β_{TOT}	*CMR*	*Modified CMR*	*ACMR*	*CMR/ACMR*
Subset 1	78	74	0	0.74	3.23	3.59	2.60	1.38
Subset 2	60	58	0	0.73	3.22	3.63	2.54	1.43
Subset 3	75	71	0	0.73	3.19	3.59	2.54	1.41
Subset 4	59	57	0	0.70	3.12	3.68	2.46	1.50
Subset 5	65	63	0	0.73	2.98	3.41	2.56	1.33
Subset 6	47	45	0	0.70	2.98	3.39	2.46	1.38
Subset 7	63	61	0	0.74	2.94	3.34	2.57	1.30
Subset 8	43	42	0	0.65	2.89	3.34	2.31	1.44

Table I.16. Number of records in each subset and the computed CMR, ACMR, and total uncertainty for the case inslab events are excluded (configuration 5, D = 2.0 m and R/I = 5)

	Percentiles				Num. of records							Mean epsilon of records		
Earthquake type	50%	16%	84%	St-Dev	Crustal	Interface	Inslab	β_{TOT}	CMR	ACMR	CMR/ ACMR	Crustal	Interface	Inslab
CRUSTAL	1.35	0.98	1.88	0.31	26	-	-	0.55	4.11	2.01	2.04	1.42	-	-
INTERFACE	0.67	0.37	2.10	0.76	-	32	-	0.88	2.06	3.10	0.66	-	1.20	-
INSLAB	2.23	1.54	4.51	0.59	-	-	15	0.74	6.79	2.58	2.64	-	-	1.35
ALL EVENTS	1.11	0.51	2.70	0.69	18	17	15	0.82	3.37	2.86	1.18	1.56	1.34	1.35
ALL EVENTS (No Inslab)	1.15	0.45	2.09	0.66	26	24	-	0.80	3.50	2.77	1.26	1.42	1.23	-

Table I.17. Results from epsilon-based method including collapse capacity statistics and number of records from each set (configuration 5, D = 2.0 m and R/I = 5)

Modified median & (CMR/ACMR)	Crustal records	Interface records	Inslab records	Combined events	Combined (no inslab records)
Subset 1 (simplified method)	1.31 (1.90)	0.96 (0.98)	3.26 (2.93)	1.45 (1.36)	1.18 (1.38)
Subset 2 (simplified method)	1.35 (1.94)	0.86 (0.83)	3.07 (3.12)	1.44 (1.41)	1.19 (1.43)
Subset 3 (simplified method)	1.31 (1.94)	0.97 (1.00)	3.58 (3.27)	1.45 (1.35)	1.18 (1.41)
Subset 4 (simplified method)	1.33 (1.97)	0.84 (0.82)	3.07 (3.12)	1.41 (1.41)	1.21 (1.50)
Subset 5 (simplified method)	1.34 (1.93)	0.68 (0.75)	1.82 (2.04)	1.33 (1.43)	1.12 (1.33)
Subset 6 (simplified method)	1.35 (1.94)	0.66 (0.71)	2.32 (2.80)	1.25 (1.34)	1.11 (1.38)
Subset 7 (simplified method)	1.34 (1.99)	0.56 (0.65)	1.73 (2.00)	1.35 (1.46)	1.10 (1.30)
Subset 8 (simplified method)	1.33 (1.97)	0.64 (0.73)	2.32 (2.80)	1.25 (1.35)	1.10 (1.44)
Epsilon-Based method	1.35 (2.04)	0.67 (0.66)	2.23 (2.64)	1.11 (1.18)	1.15 (1.26)

Table I.18. Comparison of the median collapse capacity and CMR/ACMR ratios using different subsets and methods (configuration 5, D = 2.0 m and R/I = 5)

	Collapse Capacities (g)				Collapse Capacities (g)		
Record number	Crustal records set	Interface records sets	Inslab records set	Record number	Crustal records set	Interface records sets	Inslab records set
1	1.00	0.55	2.17	41	0.67	1.46	3.02
2	0.88	0.77	3.57	42	1.26	2.06	3.00
3	1.34	0.52	1.63	43	1.50	1.80	1.83
4	3.37	1.15	1.30	44	3.27	1.86	3.43
5	1.25	1.69	2.23	45	2.31	1.44	2.71
6	1.09	1.66	2.91	46	2.15	1.55	1.25
7	1.05	0.88	1.20	47	1.07	1.40	1.15
8	0.67	0.82	1.39	48	1.57	1.73	1.06
9	1.84	0.84	5.39	49	0.90	1.12	2.33
10	1.14	0.64	2.56	50	1.97	0.64	1.43
11	0.84	0.53	0.86	51	2.95	0.39	1.43
12	1.49	0.68	1.10	52	0.94	0.59	1.36
13	2.31	0.75	0.62	53	1.82	0.96	1.78
14	3.55	0.77	0.48	54	2.25	1.26	1.67
15	1.57	0.82	6.27	55	1.35	0.94	2.89
16	2.58	0.49	3.29	56	0.84	0.87	2.89
17	1.13	0.45	0.88	57	2.26	0.77	0.47
18	0.84	0.62	1.16	58	2.36	0.74	0.44
19	1.35	9.94	0.68	59	2.11	0.74	2.34
20	1.00	5.29	0.61	60	2.04	0.66	1.50
21	1.07	0.55	0.52	61	1.32	2.01	1.40
22	0.79	0.53	0.75	62	1.54	1.96	1.64
23	3.30	0.49	2.65	63	1.11	2.06	0.50
24	4.50	0.59	2.19	64	1.39	1.71	0.35
25	1.55	1.67	1.99	65	1.35	1.30	4.10
26	4.50	2.85	1.44	66	1.00	1.18	2.85
27	2.62	4.29	2.00	67	1.70	3.54	3.15
28	0.77	3.33	1.98	68	1.58	4.99	2.82
29	2.29	2.65	0.59	69	1.03	3.21	6.55
30	0.83	3.27	0.53	70	1.03	3.74	3.34
31	1.09	1.66	3.40	71	1.39	2.22	0.83
32	0.66	1.60	2.90	72	1.26	1.55	0.63
33	1.36	3.00	2.55	73	1.74	1.01	1.20
34	1.31	3.87	1.76	74	1.25	1.59	1.71
35	1.17	1.01	2.02	75	1.48	1.80	1.29
36	1.41	1.50	2.91	76	0.86	1.94	0.95
37	1.41	1.22	2.44	77	1.84	0.77	1.13
38	0.73	1.61	0.89	78	1.72	0.75	0.92
39	2.06	2.44	2.55	**Median**	**1.37**	**1.35**	**1.69**
40	1.98	2.42	2.03	**St dev**	**0.52**	**0.75**	**0.65**

Table I.19. Collapse capacity of the bridge in Chapter 5 (H=5m and D=1.5m) for 78x3=234 records from three earthquake types.

		Percentiles							
		50%	16%	84%	St Dev	Num.	Mean ε (Records)	β_1	SSF
Case 1	Crustal	1.37	0.91	2.28	0.45	78	0.89	0.257	1.189
	Interface	1.35	0.64	2.58	0.68	78	0.96	0.087	1.059
	Inslab	1.69	0.78	2.91	0.66	78	0.35	0.335	1.644
Case2	Crustal	1.41	1.00	2.31	0.44	71	1.02	0.258	1.148
	Interface	1.15	0.61	2.91	0.72	67	1.21	0.339	1.149
	Inslab	2.02	1.20	3.00	0.50	51	0.82	0.126	1.135
Case3	Crustal	1.35	0.90	2.13	0.40	74	0.88	0.249	1.184
	Interface	1.28	0.64	2.42	0.62	76	0.95	0.070	1.048
	Inslab	1.67	0.82	2.90	0.62	75	0.37	0.410	1.822
Case4	Crustal	1.39	0.95	2.20	0.39	67	1.03	0.266	1.152
	Interface	1.13	0.60	2.77	0.68	66	1.21	0.343	1.151
	Inslab	2.03	1.27	2.95	0.41	48	0.80	0.037	1.039
Case5	Crustal	1.37	0.91	2.28	0.45	78	0.89	0.257	1.189
	Interface	1.20	0.63	2.04	0.59	72	0.91	0.019	1.013
	Inslab	1.36	0.59	2.96	0.72	47	0.51	0.497	1.930
Case6	Crustal	1.41	1.00	2.31	0.44	71	1.02	0.258	1.148
	Interface	0.96	0.59	2.06	0.62	61	1.18	0.268	1.124
	Inslab	1.90	1.10	3.16	0.57	32	1.05	0.237	1.202
Case7	Crustal	1.35	0.90	2.13	0.40	74	0.88	0.249	1.184
	Interface	1.18	0.62	2.00	0.57	71	0.89	-0.024	0.983
	Inslab	1.39	0.61	2.92	0.71	44	0.48	0.557	2.124
Case8	Crustal	1.39	0.95	2.20	0.39	67	1.03	0.266	1.152
	Interface	0.95	0.59	2.04	0.61	60	1.19	0.301	1.137
	Inslab	1.98	1.18	3.19	0.52	31	1.06	0.213	1.178

Table I.20. Percentiles of unmodified collapse capacity, β_{RTR}, β_1 factor and spectral shape factor (SSF) predicted for different earthquake types and for different subsets of records in each set (bridge in Chapter 5 (H=5m and D=1.5m)).

		Median	CMR	Modified median	Modified CMR	β_{TOT}	ACMR	CMR/ACMR
Case 1	Crustal	1.37	2.69	1.63	3.20	0.63	2.25	1.43
	Interface	1.35	2.65	1.43	2.80	0.81	2.83	0.99
	Inslab	1.69	3.32	2.78	5.46	0.80	2.78	1.97
	Average	1.47	2.88	1.94	3.80	0.74	2.59	1.47
Case 2	Crustal	1.41	2.77	1.62	3.18	0.63	2.23	1.42
	Interface	1.15	2.26	1.32	2.59	0.85	2.97	0.87
	Inslab	2.02	3.96	2.29	4.50	0.67	2.36	1.91
	Average	1.53	3.00	1.75	3.42	0.71	2.50	1.37
Case 3	Crustal	1.35	2.65	1.60	3.14	0.60	2.15	1.46
	Interface	1.28	2.50	1.34	2.62	0.77	2.67	0.98
	Inslab	1.67	3.28	3.04	5.97	0.77	2.67	2.24
	Average	1.43	2.81	1.98	3.89	0.71	2.48	1.57
Case 4	Crustal	1.39	2.73	1.60	3.15	0.59	2.14	1.47
	Interface	1.13	2.22	1.30	2.56	0.81	2.84	0.90
	Inslab	2.03	3.97	2.10	4.13	0.60	2.17	1.90
	Average	1.52	2.97	1.67	3.28	0.67	2.36	1.39
Case 5	Crustal	1.37	2.69	1.63	3.20	0.63	2.25	1.43
	Interface	1.20	2.36	1.22	2.39	0.74	2.57	0.93
	Inslab	1.36	2.67	2.62	5.15	0.85	2.97	1.73
	Average	1.32	2.58	1.82	3.58	0.74	2.58	1.39
Case 6	Crustal	1.41	2.77	1.62	3.18	0.63	2.23	1.42
	Interface	0.96	1.88	1.08	2.11	0.76	2.65	0.80
	Inslab	1.90	3.73	2.29	4.49	0.72	2.53	1.77
	Average	1.43	2.81	1.67	3.27	0.70	2.46	1.33
Case 7	Crustal	1.35	2.65	1.60	3.14	0.60	2.15	1.46
	Interface	1.18	2.31	1.16	2.27	0.72	2.53	0.90
	Inslab	1.39	2.74	2.96	5.81	0.84	2.92	1.99
	Average	1.31	2.58	1.90	3.73	0.72	2.51	1.48
Case 8	Crustal	1.39	2.73	1.60	3.15	0.59	2.14	1.47
	Interface	0.95	1.86	1.08	2.11	0.75	2.62	0.81
	Inslab	1.98	3.88	2.33	4.57	0.69	2.42	1.89
	Average	1.45	2.83	1.68	3.29	0.68	2.38	1.38

Table I.21. Modified and unmodified median collapse capacities and corresponding collapse margin ratios (CMR) and acceptable CMR (ACMR) (bridge in Chapter 5 (H=5m and D=1.5m)) .

	Unmodified				Modified			
	Median	*16% Percentile*	*84% Percentile*	*St Dev.*	*Median*	*16% Percentile*	*84% Percentile*	*St Dev.*
Subset 1	1.44	0.79	2.89	0.60	1.84	0.93	3.52	0.63
Subset 2	1.60	0.85	2.90	0.59	1.83	0.96	3.22	0.58
Subset 3	1.43	0.82	2.65	0.56	1.84	0.94	3.46	0.62
Subset 4	1.58	0.87	2.83	0.53	1.76	0.96	2.94	0.52
Subset 5	1.35	0.69	2.55	0.61	1.76	0.88	3.06	0.62
Subset 6	1.66	0.83	2.94	0.58	1.83	0.89	3.05	0.59
Subset 7	1.33	0.71	2.32	0.59	1.78	0.91	3.04	0.61
Subset 8	1.63	0.88	2.89	0.54	1.79	0.94	2.87	0.56

Table I.22. Unmodified and modified collapse capacities for the combined records from 3 event types (bridge in Chapter 5 (H=5m and D=1.5m))

	Number of records							
	Crustal	*Interface*	*Inslab*	β_{TOT}	*CMR*	*Modified CMR*	*ACMR*	*CMR/A CMR*
Subset 1	78	63	66	0.78	2.83	3.61	2.70	1.34
Subset 2	60	48	51	0.73	3.15	3.59	2.56	1.40
Subset 3	74	59	62	0.77	2.81	3.60	2.68	1.35
Subset 4	56	45	48	0.68	3.09	3.45	2.40	1.44
Subset 5	55	44	47	0.76	2.64	3.45	2.66	1.30
Subset 6	37	30	32	0.74	3.26	3.58	2.57	1.39
Subset 7	51	41	44	0.76	2.61	3.50	2.65	1.32
Subset 8	36	29	31	0.71	3.20	3.51	2.49	1.41

Table I.23. Number of records in each subset and the computed CMR, ACMR, and total uncertainty (bridge in Chapter 5 (H=5m and D=1.5m))

	Unmodified				Modified			
	Median	*16% Percentile*	*84% Percentile*	*St Dev.*	*Median*	*16% Percentile*	*84% Percentile*	*St Dev.*
Subset 1	1.35	0.77	2.44	0.59	1.62	0.84	2.69	0.58
Subset 2	1.40	0.77	2.61	0.60	1.70	0.92	2.81	0.58
Subset 3	1.31	0.75	2.29	0.54	1.56	0.81	2.53	0.53
Subset 4	1.35	0.77	2.31	0.55	1.61	0.88	2.55	0.52
Subset 5	1.32	0.75	2.26	0.54	1.55	0.77	2.50	0.55
Subset 6	1.33	0.76	2.30	0.55	1.55	0.87	2.52	0.53
Subset 7	1.26	0.75	2.06	0.51	1.51	0.76	2.32	0.51
Subset 8	1.32	0.77	2.15	0.52	1.55	0.89	2.37	0.49

Table I.24. Unmodified and modified collapse capacities for the combined records from 2 event types (excluding inslab events) (bridge in Chapter 5 (H=5m and D=1.5m))

	Number of records							
	Crustal	*Interface*	*Inslab*	*Beta total*	*CMR*	*Modified CMR*	*Acceptable CMR*	*CMR/A CMR*
Subset 1	78	62	0	0.73	2.64	3.18	2.55	1.25
Subset 2	71	57	0	0.73	2.75	3.34	2.55	1.31
Subset 3	74	59	0	0.69	2.58	3.05	2.43	1.26
Subset 4	67	53	0	0.69	2.65	3.15	2.42	1.30
Subset 5	78	62	0	0.71	2.58	3.04	2.47	1.23
Subset 6	71	57	0	0.69	2.61	3.04	2.42	1.25
Subset 7	74	59	0	0.68	2.47	2.96	2.40	1.24
Subset 8	67	53	0	0.66	2.58	3.03	2.33	1.30

Table I.25. Number of records in each subset and the computed CMR, ACMR, and total uncertainty for the case inslab events are excluded (bridge in Chapter 5 (H=5m and D=1.5m))

	Percentiles				Num. of records							Mean epsilon of records		
Earthquake type	50%	16%	84%	St-Dev	Crustal	Interface	Inslab	β_{TOT}	CMR	ACMR	CMR/ ACMR	Crustal	Interface	Inslab
CRUSTAL	1.74	1.09	2.34	0.42	41	-	-	0.61	3.40	2.20	1.55	1.37	-	-
INTERFACE	1.18	0.62	2.99	0.74	-	45	-	0.86	2.31	3.03	0.76	-	1.43	-
INSLAB	2.26	1.38	3.36	0.47	-	-	18	0.65	4.43	2.29	1.94	-	-	1.56
ALL EVENTS	1.71	1.09	3.54	0.58	21	17	18	0.73	3.35	2.56	1.31	1.45	1.59	1.56
ALL EVENTS (No Inslab)	1.60	0.83	2.92	0.58	41	32	-	0.73	3.15	2.56	1.23	1.37	1.59	-

Table I.26. Results from epsilon-based method including collapse capacity statistics and number of records from each set (studied bridge (H=5m and D=1.5m))

Modified median & (CMR/ACMR)	Crustal records	Interface records	Inslab records	Combined events	Combined (no inslab records)
Subset 1 (simplified method)	1.63 (1.43)	1.43 (0.99)	2.78 (1.97)	1.84 (1.34)	1.62 (1.25)
Subset 2 (simplified method)	1.62 (1.42)	1.32 (0.87)	2.29 (1.91)	1.83 (1.40)	1.70 (1.31)
Subset 3 (simplified method)	1.60 (1.46)	1.34 (0.98)	3.04 (2.24)	1.84 (1.35)	1.56 (1.26)
Subset 4 (simplified method)	1.60 (1.47)	1.30 (0.90)	2.10 (1.90)	1.76 (1.44)	1.61 (1.30)
Subset 5 (simplified method)	1.63 (1.43)	1.22 (0.93)	2.62 (1.73)	1.76 (1.30)	1.55 (1.23)
Subset 6 (simplified method)	1.62 (1.42)	1.08 (0.80)	2.29 (1.77)	1.83 (1.39)	1.55 (1.25)
Subset 7 (simplified method)	1.60 (1.46)	1.16 (0.90)	2.96 (1.99)	1.78 (1.32)	1.51 (1.24)
Subset 8 (simplified method)	1.60 (1.47)	1.08 (0.81)	2.33 (1.89)	1.79 (1.41)	1.55 (1.30)
Epsilon-Based method	1.74 (1.55)	1.18 (0.76)	2.26 (1.94)	1.71 (1.31)	1.60 (1.23)

Table I.27. Comparison of the median collapse capacity and CMR/ACMR ratios using different subsets and methods (studied bridge (H=5m and D=1.5m))

References

AASHTO, Guide specifications for LRFD seismic bridge design. 2009., Subcommittee T-3 for Seismic Effects on Bridges, American Association of State Highway and Transportation Officials, Washington D.C.

AASHTO. 2004. AASHTO LRFD Bridge Design Specifications American Association of State Highway and Transportation Officials, Washington, D.C.

Abrahamson, N.A., and Silva, W.J. 1997. Empirical response spectral attenuation relations for shallow crustal earthquake. Seismological Research Letters, 68 (1): 94-126.

Adams, J., and Halchuk, S. 2003. Fourth generation seismic hazard maps of Canada: values for over 650 Canadian localities intended for the 2005 National Building Code of Canada. Open-File 4459, Geological Survey of Canada, Ottawa, Canada.

Adams, J., and Halchuk,S. 2002., Knowledge of inslab earthquakes needed to improve seismic hazard estimates for southwestern British Columbia, The Cascadia subduction zone and related subduction systems. U.S. Geological Survey Open-File Report 02–328 Geological Survey of Canada Open File 4350.

Adams, J., Halchuk, S., and Weichert, D.H. 2000., Lower probability hazard, better performance? Understanding the shape of the hazard curves from Canada’s Fourth Generation seismic hazard results, Paper 1555, 12th World Conference on Earthquake Engineering, Auckland, 30th January–4th February 2000, 8 pp.

Adams, J., Weichert, D.H., and Halchuk, S. 1999a. Trial seismic hazard maps of Canada 1999: 2%/50 year values for selected Canadian cities, 107 pp., Geological Survey of Canada Open File 3724.

Adams, J., Weichert, D.H., and Halchuk, S. 1999b. Lowering the probability level—fourth generation seismic hazard results for Canada at the 2% in 50 year probability level, in Proceedings 8th Canadian Conference on Earthquake Engineering, Vancouver 13–16th June 1999, pp. 83–88.

Antoniou, S., Rovithakis, A., and Pinho, R. 2002. Development and verification of a fully adaptive pushover procedure. Paper No. 822. Proceedings of the 12th European Conference on Earthquake Engineering, London, U.K.

ASCE 7-05. 2005. Minimum design loads for buildings and other structures. American Society of Civil Engineers (ASCE), Reston, Virginia.

ASCE/SEI 41-06. 2006. Seismic rehabilitation of existing buildings. American Society of Civil Engineers (ASCE), Reston, Virginia.

ATC-40 .1996. Seismic evaluation and retrofit of concrete buildings. Applied Technology Council (ATC). Redwood City, CA.

ATC-62. 2008. Effects of strength and stiffness degradation on seismic response, ATC-62/FEMA P440A, prepared by the Applied Technology Council for the Federal Emergency Management Agency, Applied Technology Council, Redwood City, California.

ATC-63. 2008. Quantification of building seismic performance factors, ATC-63 Project Report - 90% Draft, prepared by the Applied Technology Council for the Federal Emergency Management Agency, Applied Technology Council, Redwood City, California.

Atkinson, G.M., and Boore, D.M. 2003. Empirical ground-motion relations for subduction-zone earthquakes and their application to Cascadia and other regions. Bull. Seism. Soc. Am., 93: 1703-1729.

Atkinson, G.M., and Goda, K. 2011. Effects of seismicity models and new ground-motion prediction equations on seismic hazard assessment for four Canadian cities. Bulletin of the Seismological Society of America, 101 (1): 176-189.

Aviram, A., Mackie, K.R., and Stojadinovic, B. 2008. Effect of abutment modeling on the seismic response of bridge structures. Earthquake Eng & Eng Vibration, 7(4): 395-402.

Aydinoglu, M.N. 2004. An improved pushover procedure for engineering practice: incremental response spectrum analysis IRSA. Proceedings of the International Workshop: Performance-Based Seismic Design Concepts and Implementation, Bled, Slovenia, 345–356.

Baker, J.W. 2011. The conditional mean spectrum: A tool for ground motion selection, Journal of Structural Engineering, 137 (3): 322-331.

Baker, J.W., and Cornell, C.A. 2005, Vector-valued ground motion intensity measures for probabilistic seismic demand analysis, Report #150, John A. Blume Earthquake Engineering Center, Stanford, CA .

Baker, J.W., and Cornell, C.A. 2006a. Spectral shape, epsilon and record selection. Earthquake Engineering& Structural Dynamics, 34(10):1193-1217.

Baker, J.W., and Cornell, C.A. 2006b. Correlation of response spectral values for multicomponent ground motions. Bulletin of the Seismological Society of America, 96 (1): 215-227.

Baker, J.W., and Cornell, C.A. 2006c. Which Spectral Acceleration Are You Using? Earthquake Spectra, 22(2): 293–312.

Baker, J.W., and Cornell, C.A. 2008. Vector-valued intensity measures incorporating spectral shape for prediction of structural response. Journal of Earthquake Engineering, 12 (4): 534-554.

Bazzurro, P., and Cornell, C.A. 1999. Disaggregation of seismic hazard. Bulletin of the Seismological Society of America, 89(2): 501-520.

Benjamin, J.R., and Cornell, C.A. 1970. Probability, statistics and decision for civil engineers. New York: McGraw-Hill.

Bentz, E. 2001. Response-2000, Shell-2000, Triax-2000, Membrane-2000: User Manual, Department of Civil Engineering, University of Toronto, Toronto, Ontario, Canada.

Berry, M., Parrish, M., and Eberhard, M. 2004. PEER Structural Performance Database User's Manual. (www.ce.washington.edu/~peera1), Pacific Earthquake Engineering Research Center, University of California, Berkeley, Calif.

Berry, M.P., and Eberhard, M.O. 2007. Performance modeling strategies for modern reinforced concrete bridge columns. PEER-2007/07, Pacific Earthquake Engineering Research Center, University of California- Berkeley, Berkeley, Calif.

Boore, D.M., and Atkinson, G.M. 2008. Ground-motion prediction equations for the average horizontal component of PGA, PGV, and 5%-damped PSA at spectral periods between 0.01 s and 10.0 s, Earthquake Spectra, 24 (1): 99-138.

Botero, J.C.A. 2004. Displacement-based design of continuous concrete bridges under transverse seismic excitation. Master thesis, European School for Advanced Studies in Reduction of Seismic Risk (ROSE School), Pavia, Italy.

Bracci, J.M., Kunnath, S.K., and Reinhorn, A.M. 1997. Seismic performance and retrofit evaluation for reinforced concrete structures. Journal of Structural Engineering (ASCE), 123(1):3–10.

Broderick, B.M., and Elnashai, A.S. 1995. Analysis of the failure of Interstate 10 freeway ramp during the Northridge earthquake of 17 January 1994, Earthquake Engineering & Structural Dynamics, 24(2): 189-209.

Caltrans. 2006. Seismic Design Criteria. California Department of Transportation, California.

Caltrans. 2011. Bridge memo to designers. California Department of Transportation. Available from: http://www.dot.ca.gov/hq/esc/techpubs/manual/bridgemanuals/bridge-memo-to-designer/bmd.html [accessed Sep. 2011].

Calvi, G.M., Elnashai, S.A., and Pavese, A. 1994. Influence of regularity on the response of RC bridges, Second International Workshop on Seismic Design of Bridges, Queenstown, New Zealand, pp. 80-89.

Calvi, G.M., and Kingsley, G.R. 1995. Displacement-based seismic design of multi-degree of freedom bridge structures. Earthquake Engineering and Structural Dynamics, 24: 1247-1266.

Calvi, G.M., and Pavese, A. 1997. Conceptual design of isolation systems for bridge structures. Journal of Earthquake Engineering, 1(1): 193-218.

Calvi, G.M., and Pinto, P.E. 1996. Experimental and numerical investigations on the seismic response of bridges and recommendations for code provisions. ECOESJIPREC8 Report No 4, LNEC. Lisbon.

Carr, A. 2009. RUAUMOKO, a computer program for Inelastic Dynamic Analysis. Department of Civil Engineering, University of Canterbury, New Zealand.

CEN. 2005. Eurocode 8: Design of structures for earthquake resistance, part2: Bridges, EN 1998-2-2005, Comité Européen de Normalization, Brussels, Belgium.

CSA. 2006. CAN/CSA-S6-06 Canadian Highway Bridge Design Code (CHBDC) and commentary. Canadian Standards Association (CSA), Mississauga, ON.

Chen, W.F. and Duan, L. 2000. Bridge Engineering Handbook, CRC Press LLC.

Chopra, A.K., and Goel, R.K. 2002. A modal pushover analysis procedure for estimating seismic demands for buildings. Earthquake Engineering and Structural Dynamics, 31(3): 561–582.

Chopra, A.K., and Goel, R.K. 2004. A modal pushover analysis procedure to estimate seismic demands for unsymmetric-plan buildings. Earthquake Engineering and Structural Dynamics, 33(8):903–927.

Computers and Structures Inc. 1999. SAP2000: Three dimensional static and dynamic finite element analysis and design of structures. Computers and Structures Inc. Berkeley, CA.

Cornell, C.A., and Krawinkler, H. 2000. Progress and challenges in seismic performance assessment. PEER Center News; 3(2):1–2 URL http://peer.berkeley.edu/news/2000spring/performance.html (accessed: Jan, 2012).

Cornell, C.A., Jalayer, F., Hamburger, R.O., and Foutch, D.A. 2002. The probabilistic basis for the 2000 SAC/FEMA steel moment frame guidelines. ASCE Journal of Structural Engineering, 128 (4): 526–533.

Dhakal, R.P., and Mander J.B. 2006. Financial risk assessment methodology for natural hazards. Bulletin of the New Zealand Society of Earthquake Engineering, 39(2): 91-105.

Dutta, A., and Mander, J.B. 1998. Seismic fragility analysis of highway bridges, Proceedings of the INCEDE-MCEER Center-to-Center Workshop on Earthquake Engineering Frontiers in Transportation Systems, Tokyo, Japan, pp. 311-325.

Dwairi, H., and Kowalsky, M. 2006. Implementation of inelastic displacement patterns in direct displacement-based design of continuous bridge structures. Earthquake Spectra, 22(3): 631-662.

Elwood, K. 2004. Modeling failures in existing reinforced concrete columns. Canadian Journal of Civil Engineering, 31:846–859

Ewins, D.J. 2000. Modal testing: theory, practice and application, 2nd Ed., Research Studies Press, Baldock, UK.

Fardis, M.N., and Biskini, D.E. 2003. Deformation capacity of RC members, as controlled by flexure or shear. Otani Symposium. 511- 530.

FEMA-356. 2000. Prestandard and commentary for the seismic rehabilitation of buildings, American Society of Civil Engineers (ASCE). Washington, DC.

FEMA-350. 2000. Recommended seismic design criteria for new steel moment-frame buildings, SAC Joint Venture, Federal Emergency Management Agency, Washington, DC.

Fischinger, M., Beg D., Isakovic, T., Tomazevic, M., Zarnic, R. 2004. Performance based assessment from general methodologies to specific implementations. International Workshop on PBSD, Bled, Slovenia; 293–308 (published in PEER Report 2004-05 (UC Berkeley)).

Fischinger, M., Isakovic, T., and Fajfar, P. 1997, Seismic analysis of viaduct structures- Which method to choose?, Seismic design methodologies for the next generation of codes, Fajfar and Krawinkler (eds), Balkema, Rotterdam.

Fischinger, M., and Isakovic,T., 2003. Inelastic Seismic analysis of reinforced concrete viaducts, Structural Engineering International, 13(2): 111-118.

Goda, K., and Atkinson, G.M. 2011. Seismic performance of wood-frame houses in south-western British Columbia. Earthquake Engineering and Structural Dynamics, 40 (8): 903-924.

Goda, K., and Atkinson, G.M. 2009. Probabilistic characterization of spatially-correlated response spectra for earthquakes in Japan. Bull.Seism. Soc. of Am., 99 (5): 3003- 3020.

Goda, K., Hong, H.P., and Atkinson, G.M. 2010. Impact of using updated seismic information on seismic hazard in western Canada. Canadian Journal of Civil Engineering, 37 (4): 562-575.

Goel, R., and Chopra, A.K. 2004. Extension of modal pushover analysis to compute member forces. Earthquake Spectra, 21(1):125–139.

Goel, R.K., and Chopra, A. 1997. Evaluation of bridge abutment capacity and stiffness during earthquakes. Earthquake Spectra, 13(1): 1-23.

Gulkan, P., and Sozen, M. 1974. Inelastic response of reinforced concrete structures to earthquake motions, ACI Journal, 71: 604-610.

Gupta, B., and Kunnath, S.K. 2000. Adaptive spectra-based pushover procedure for seismic evaluation of structures. Earthquake Spectra, 16(2):367–392.

Haselton, C., Liel, A., Lange, S.T., and Deierlein, G.G. 2007. Beam- column element model calibrated for predicting flexural response leading to global collapse of RC frame buildings. Pacific Earthquake Engineering Research Center 2007/03, University of California, Berkeley.

Haselton, C.B., and Baker, J.W. 2006. Ground motion intensity measures for collapse capacity prediction: Choice of optimal spectral period and effect of spectral shape. 8th National Conference on Earthquake Engineering, San Francisco, California.

Haselton, C.B., and Deierlein, G.G. 2007. Assessing seismic collapse safety of modern reinforced concrete moment-frame buildings. PEER Report 2007/08, Pacific Engineering Research Center, University of California, Berkeley, California.

Haselton, C.B., Baker, J.W., Liel, A.B., and Deierlein, G.G. 2011. Accounting for ground-motion spectral shape characteristics in structural collapse assessment through an adjustment for epsilon', ASCE J. Struct. Eng., 137 (3), 332.

HAZUS. 1999. Earthquake loss estimation methodology, Technical Manual, National Institute of Building Sciences for the Federal Emergency Management Agency.

Heaton, T.H., and Hartzell, S.H. 1987. Earthquake hazards on the Cascadia subduction zone. Science, 236: 162–168.

Heaton, T.H., and Kanamori, H. 1984. Seismic potential associated with subduction in the northwestern United States. Bulletin of the Seismological Society of America, 74: 933–944.

Hong, H.P., and Goda, K. 2006. A comparison of seismic-hazard and risk deaggregation. Bulletin of the Seismological Society of America, 96 (6): 2021-2039.

Hyndman, R.D., and Rogers, G.C. 2010. Great earthquakes on Canada's west coast: a review, Can. J. Earth Sci., 47(5): 801–820 .

Ibarra, L.F., Medina, R.A., and Krawinkler, H. 2005. Hysteretic models that incorporate strength and stiffness deterioration. Earthquake Engineering and Structural Dynamics, 34 (11):1489-1511.

Isakovic, T., and Fischinger, M. 2006. Higher modes in simplified inelastic seismic analysis of single column bent viaducts. Earthquake Engineering and Structural Dynamics, 35(1): 95-114.

Isakovic, T., Pompeyo, M., Lazaro, N., and Fischinger, M. 2008. Applicability of pushover methods for the seismic analysis of single-column bent viaducts. Earthquake Eng. Struct. Dynamics, 37(8):1185–1202.

Jalayer, F., and Cornell, C.A. 2003. A technical framework for probability-based demand and capacity factor (DCFD) seismic formats. PEER-2003/08, Pacific Earthquake Engineering Research Center, University of California- Berkeley, Berkeley, CA.

Jones, M.H., Salama, A.E., and Dreher, S.T. 2001. BART SFO extension aerial guideways: Using nonlinear analysis to control and minimize seismic damage, Journal of Bridge Engineering, 6 (6): 451-460.

Kappos, A., Paraskeva, T., and Sextos, A. 2004. Seismic assessment of a major bridge using modal pushover analysis and dynamic time-history analysis. Advances in Computational and Experimental Engineering and Science; 673–680.

Kappos, A.J., Manolis, G.D., and Moschonas, I.F. 2002. Seismic assessment and design of R/C bridges with irregular configuration, including SSI effects, Engineering Structures, 24 (10):1337–1348.

Kirby, S., Wang, K., and Dunlop, S. 2002. The Cascadia subduction zone and related subduction systems, U.S. Geological Survey Open-File Report 02–328 Geological Survey of Canada Open File 4350.

Kowalsky, M.J. 1997. Direct displacement-based design: A seismic design methodology and its application to concrete bridges, PhD thesis, University of California, San Diego.

Kowalsky, M.J. 2002. A displacement-based design approach for the seismic design of continuous concrete bridges," Earthquake Enginieering and Structural Dynamics, Vol. 31, pp. 719-747.

Liel, A.B., Haselton, C.B., and Baker, J.W. 2009. Incorporating modelling uncertainties in the assessment of seismic collapse risk of buildings. Structural Safety, 31 (2): 197-211.

Luco, N., and Bazzurro, P. 2007. Does amplitude scaling of ground motion records result in biased nonlinear structural drift responses?. Earthquake Engineering & Structural Dynamics, 36(13): 1813-1835.

Maalek, S., Akbari, R., and Maheri, M.R. 2009. The effect of higher modes on the regularity of single-column-bent highway viaducts. Bridge Structures, 5(1): 29–43.

Mackie, K.R. and Stojadinovic, B. 2003. Seismic demands for performance-based design of bridges. PEER-2003/16, Pacific Earthquake Engineering Research Center, University of California- Berkeley, Berkeley, Calif.

Mackie, K.R. and Stojadinovic, B. 2007. R-factor parameterized bridge damage fragility curves. Journal of Bridge Engineering, 12(4): 500–510.

Mander, J.B, Priestley, M.J.N., and Park, R. 1988. Theoretical stress-strain model for confined concrete. ASCE Journal of Structural Engineering, 114(8): 1804-1826.

Mander, J.B., Dhakal, R., Mashiko, N., and Solberg, K. 2007. Incremental dynamic analysis applied to seismic financial risk assessment of bridges. Engineering Structures, 29(10): 2662-2672.

Maroney, B.H., and Chai, Y.H. 1994. Bridge abutment stiffness and strength under earthquake loadings. Proceedings, 2nd international workshop on the seismic design of bridges, Queenstown, New Zealand.

McGuire, R.K. 1995. Probabilistic seismic hazard analysis and design earthquakes: Closing the loop. Bull. Seism. Soc. Am., 85: 1275-1284.

Mechakhchekh, A. 2008. Seismic risk analysis of bridge structural systems. PhD thesis, City University of New York, NY.

Megally, S.H., Seible, F., Bozorgzadeh, A., Restrepo, J., and Silva, P.F. 2003. Response of sacrificial shear keys in bridge abutments to seismic loading. Proceedings of the FIB Symposium on Concrete Structures in Seismic Regions, Athens, Greece.

Mitchell, D., Bruneau, M., Williams, M., Anderson, D., Saatcioglu, M., and Sexsmith, R. 1995. Performance of bridges in the 1994 Northridge earthquake, Can. J. Civ. Eng., 22(2): 415-427.

National Research Council of Canada (NRCC). 2010. National Building Code of Canada (NBCC). Ottawa, Ontario.

Otani, S. 1981. Hysteresis model of reinforced concrete for earthquake response analysis. Journal of Fac. of Eng., Univ. of Tokyo, Series B, XXXVI-11(2): 407-441.

Pangiotakos, T.B., and Fardis, M.N. 2001. Deformations of reinforced concrete members at yielding and ultimate, ACI Structural Journal, 98(2): 135-148.

Paraskeva ,T. S., Kappos, A. J., and Sextos, A. G. 2006. Extension of modal pushover analysis to seismic assessment of bridges, Earthquake Engng Struct. Dyn, 35:1269–1293.

Patwardhan,C. 2005. Shear strength and deformation modelling of reinforced concrete columns. Master thesis, The Ohio State University.

Paultre, P., and Légeron, F. 2008. Confinement reinforcement design for reinforced concrete columns. ASCE, Journal of Structural Engineering, 134(5): 738-749.

Pinho, R. 2007. Nonlinear dynamic analysis of structures subjected to seismic action. Advanced Earthquake Engineering Analysis, Pecker, A. ed., Springer, NY.

Pinho, R., Antoniou, S., Casarotti, C., and Lopez, M. 2005. A displacement-based adaptive pushover for assessment of buildings and bridges. NATO International Workshop on Advances in Earthquake Engineering for Urban Risk Reduction, Istanbul, Turkey.

Pinho, R., Casarotti, C., Antoniou S. 2007. A comparison of single-run pushover analysis techniques for seismic assessment of bridges. Earthquake Engineering and Structural Dynamics, 36(10): 1347-1362.

Pinto, A.V., Verzeletti, G., Pegon, P., Magonette, G., Negro, P., and Guedes, J., 1996. Pseudo- Dynamic Testing of Large- Scale R/ C Bridges, Report EUR 16378, Ispra (VA), Italy.

Priestley, M.J.N. 1993. Myths and fallacies in earthquake engineering – Conflicts between design and reality. Bulletin NZ National Society for Earthquake Engineering, 26 (3): 328-341.

Priestley, M.J.N., and Benzoni, G. 1996. Seismic performance of circular columns with low longitudinal reinforcement ratios, ACI Structural Journal, 93(4): 474-485.

Priestley, M.J.N., Calvi, G.M. and Kowalsky, M.J. 2007. Direct displacement based design of structures, IUSS Press, Pavia, Italy.

Priestley, M.J.N., Seible, F., and Calvi, G.M. 1996. Seismic design and retrofit of bridges, John Wiley and Sons, New York.

Restrepo, J.C.O. 2006. Displacement-Based Design of Continuous Concrete Bridge under Transverse Seismic Excitation. . Master thesis, European School for Advanced Studies in Reduction of Seismic Risk (ROSE School), Pavia, Italy.

Riddihough, R.P. 1984. Recent movements of the Juan de Fuca plate system. Journal of Geophysical Research, 89: 6980–6994.

Riddihough, R.P., and Hyndman, R.D. 1976. Canada's active western margin - the case for subduction. Geoscience Canada, 3: 269–278.

Rogers, G.C. 1988. An assessment of the megathrust earthquake potential of the Cascadia subduction zone. Canadian Journal of Earth Sciences, 25: 844–852.

Saiidi, M., and Sozen, M.A. 1979. Simple and complex models for nonlinear seismic response of reinforced concrete structures.' Rep. No. UILU-ENG-79-2013, Struct. Res. Series No. 465, Univ. of Illinois, Urbana, Ill.

Saiidi, S., Moore, R.T., and Itani, A. 2001. Seismic performance of reinforced concrete bridges with unconventional configuration, ACI Structural Journal, 98(5): 717-126.

Sasaki, K.K., Freeman, S.A., Paret, T.F. 1998. Multimode pushover procedure (MMP)—a method to identify the effects of higher modes in a pushover analysis. Proceedings of the 6th US National Conference on Earthquake Engineering, Seattle; Paper No. 271.

Shome, N. and Cornell, C.A. 1999. Probabilistic seismic demand analysis of non-linear structures. Report No.RMS-35, RMS Program, Stanford University, Stanford.

Tehrani, P. 2012. Seismic analysis and behaviour of continuous reinforced concrete bridges. PhD thesis, Department of Civil Engineering, McGill University, Montreal.

Tehrani, P., and Mitchell, D. 2012a. Effects of column and superstructure stiffness on the seismic response of bridges in the transverse direction. Canadian. Journal of Civil Engineering (in press).

Tehrani, P., and Mitchell, D. 2012b. Seismic response of bridges subjected to different earthquake types using IDA. Submitted to Journal of Earthquake Engineering.

Tehrani, P., and Mitchell, D. 2012c. Effects of Column Stiffness Irregularity on the Seismic Response of Bridges in the Longitudinal Direction, submitted to Canadian. Journal of Civil Engineering.

Tehrani, P., and Mitchell, D. 2012d. Incremental dynamic analysis applied to seismic performance and risk assessment of RC bridges, Submitted to Seismic Risk Analysis and Management of Civil Infrastructure Systems, Editors: Tesfamariam, S., and Goda, K. Woodhead Publishing Limited.

Tehrani, P., Goda, K., Mitchell, D., Atkinson, G.M., and Chouinard, L. E. 2012. Effects of different record selection methods and earthquake types on the transverse response of bridges. Submitted to Journal of Earthquake Engineering and Structural Dynamics.

Vamvatsikos, D., and Cornell, C.A. 2004. Applied incremental dynamic analysis. Earthquake Spectra, 20(2): 523–553.

Vamvatsikos, D., and Cornell, C.A. 2002. Incremental dynamic analysis, Earthquake Engineering and Structural Dynamics, 31 (3): 491-514.

Vamvatsikos, D., and Cornell, C.A. 2005. Developing efficient scalar and vector intensity measures for IDA capacity estimation by incorporating elastic spectral shape information. Earthquake Engineering and Structural Dynamics, 34 (13): 1573-1600.

Vamvatsikos, D., and Cornell, C.A. 2006, Direct estimation of the seismic demand and capacity of oscillators with multi-linear static pushovers through Incremental Dynamic Analysis. Earthquake Engineering and Structural Dynamics, 35(9): 1097-1117.

Vanmarcke, E. H. and Gasparini, D.A. 1976. Simulated earthquake motions compatible with prescribed response spectra, Research report R76-4, Dept. of Civil Engineering, Massachusetts Inst. of Technology, Cambridge.

Veneziano, D. 2005. Probability and statistics in engineering, Lecture notes, MIT Course Number: 1.151, available online at http://ocw.mit.edu.

Zareian, F. 2006. Simplified performance-based earthquake engineering, PhD Dissertation, Department of Civil and Environmental Engineering, Stanford University.

Zareian, F., and Krawinkler, H. 2007. Assessment of probability of collapse and design for collapse safety. Earthquake Engineering and Structural Dynamics, 36 (13): 1901-1914.

Zhao, J.X., Zhang, J., Asano, A., Ohno, Y., Oouchi, T., Takahashi, T., Ogawa, H., Irikura, K., Thio, H.K., Somerville, P.G., and Fukushima, Y. 2006 Attenuation relations of strong ground motion in Japan using site classification based on predominant period. Bulletin of the Seismological Society of America 96(3): 898-913.